VOLUME 111 NUMBER 3

THE ASTROPHYSICAL JOURNAL

AN INTERNATIONAL REVIEW OF SPECTROSCOPY AND ASTRONOMICAL PHYSICS

MAY 1950

THE UNIVERSITY OF CHICAGO PRESS
CHICAGO, ILLINOIS, U.S.A.

May 1950 Vol. 111, No. 3

THE ASTROPHYSICAL JOURNAL

AN INTERNATIONAL REVIEW OF SPECTROSCOPY AND ASTRONOMICAL PHYSICS

The Astrophysical Journal is published bimonthly by the University of Chicago at the University of Chicago Press, 5750 Ellis Avenue, Chicago, Illinois, during July, September, November, January, March, and May. ¶The subscription price is $12.00 a year; the price of single copies is $2.00. Orders for service of less than a full year will be charged at the single-copy rate. ¶Postage is prepaid by the publishers on all orders from the United States and its possessions. No extra charge for countries in the Pan American Postal Union. ¶Postage is charged extra as follows: for Canada and Newfoundland, 42 cents on annual subscriptions (total $12.42); on single copies, 7 cents (total $2.07); for all other countries in the Postal Union, 96 cents on annual subscriptions (total $12.96), on single copies 16 cents (total $2.16). ¶Patrons are requested to make all remittances payable to The University of Chicago Press, in United States currency or its equivalent by postal or express money orders or bank drafts.

The following is an authorized agent:

For the British Empire, except North America and Australasia: The Cambridge University Press, Bentley House, 200 Euston Road, London, N.W. 1, England. Prices of yearly subscriptions and of single copies may be had on application.

Claims for missing numbers should be made within the month following the regular month of publication. The publishers expect to supply missing numbers free only when losses have been sustained in transit, and when the reserve stock will permit.

Business correspondence should be addressed to The University of Chicago Press, Chicago 37, Illinois.

Communications for the editors and manuscripts should be addressed to: W. W. Morgan, Editor of THE ASTROPHYSICAL JOURNAL, Yerkes Observatory, Williams Bay, Wisconsin.

Line drawings and photographs should be made by the author, and all marginal notes such as co-ordinates, wave lengths, etc., should be included in the cuts. It will not be possible to set up such material in type.

One copy of the corrected galley proof should be returned as soon as possible to the editor, Yerkes Observatory, Williams Bay, Wisconsin. Authors should take notice that the manuscript will not be sent to them with the proof.

The cable address is "Observatory, Williamsbay, Wisconsin."

The articles in this journal are indexed in the *International Index to Periodicals*, New York, N.Y.

Applications for permission to quote from this journal should be addressed to The University of Chicago Press, and will be freely granted.

Notice to subscribers: If you change your address, please notify us and your local postmaster immediately. The post office does not forward second-class mail.

Entered as second-class matter, July 31, 1930, at the Post-Office at Chicago, Ill., under the Act of March 3, 1879. Acceptance for mailing at special rate of postage provided for in United States Postal Act of October 3, 1917, Section 1103, amended February 28, 1925.

THE ASTROPHYSICAL JOURNAL

An International Review of Spectroscopy and Astronomical Physics

FOUNDED IN 1895 BY GEORGE E. HALE AND JAMES E. KEELER

VOLUME 111

JANUARY–MAY, 1950

THE UNIVERSITY OF CHICAGO PRESS
CHICAGO, ILLINOIS

CAMBRIDGE UNIVERSITY PRESS, LONDON

PUBLISHED JANUARY, MARCH, MAY, 1950

COMPOSED AND PRINTED BY THE UNIVERSITY OF CHICAGO PRESS
CHICAGO, ILLINOIS, U.S.A.

CONTENTS

NUMBER 1

NUMBER 2

NUMBER 3

THE ASTROPHYSICAL JOURNAL

AN INTERNATIONAL REVIEW OF SPECTROSCOPY AND ASTRONOMICAL PHYSICS

VOLUME 111 MAY 1950 NUMBER 3

32 CYGNI AS AN ECLIPSING BINARY

DEAN B. MCLAUGHLIN

University of Michigan Observatory

Received January 26, 1950

ABSTRACT

Spectrograms taken between November 1.1 and 9.0, 1949, U.T., show the absence of the early-type member of the composite spectrum of 32 Cygni (K5, A). Emergence probably began some hours before November 10.0. Atmospheric eclipse effects similar to those of ζ Aurigae were observed until December 25.0. The K line of *Ca* II was the last to disappear. A nearly grazing total eclipse of about 20 days' duration is suggested. The depth of the *Ca* II atmosphere considerably exceeds the radius of the K5 star, which is assumed to be $200\odot$, about equal to the primary of ζ Aurigae. The period is 1140.7 days (Hoffleit), and $a \sin i$ for the K star is about 2.5×10^8 km, according to Cannon's orbit and K. O. Wright's unpublished material. Approximate dimensions of the system are computed.

The long-period spectroscopic binary 32 Cygni has a spectrum that is a composite of class K5 and an uncertain subdivision of class A. It is one of several such objects that have been under observation at Ann Arbor for several years. The eclipse was detected when the absence of the early-type spectrum was noticed on a spectrogram taken by D. H. Clements, November 1.1, 1949, U.T. A confirmatory plate was obtained by Marilyn Mears and the writer, on November 4.1. In addition to announcement through the usual channels, telegrams were sent to several observatories on November 9. That evening E. B. Weston obtained two plates that, at first sight, seemed not to differ from those of a few preceding days; but closer examination now suggests that emergence had begun. Many more plates were obtained for several weeks after that date.

The following paragraphs contain a preliminary description based on visual inspection of the plates with the Hartmann spectrocomparator. All the spectrograms were taken with the two-prism spectrograph and 12-inch camera, dispersion 38 A/mm at $H\gamma$, and 24 A/mm at K. All are calibrated for spectrophotometry. Typical spectrograms are reproduced in Figures 1 and 2.

THE COMPOSITE SPECTRUM

The best spectrogram far from eclipse was obtained on July 13.3, 1949, U.T. Strong lines of the K-type spectrum are prominent as far into the ultraviolet as the exposure extends (about λ 3700). Evidence of the Balmer lines of the early-type star is inconclusive. Broadly winged lines could be effectively obscured by superimposed features of the K-type spectrum, but no line is clearly visible at $H\iota$, where such interference is least. The

filling-in of metallic lines by the early-type continuum is very marked in the ultraviolet and is appreciable even at $H\gamma$, though relatively inconspicuous to the longward of 4227 *Ca* I. The K line is not completely filled in; a diffuse minimum of radiation is perceptible at that position. Central emission is conspicuous, about 2 A wide, with a very fine central reversal.

Dr. K. O. Wright, of the Dominion Astrophysical Observatory, kindly sent copies of microphotometer tracings that show the K line outside eclipse. These show appreciable variations of the central emission structure. Visual inspection of Ann Arbor plates shows probable changes that may be due in part to shifting of the line of the companion across that of the primary; but no conclusions can be drawn as yet.

THE SPECTRUM DURING TOTAL ECLIPSE

Between November 1.1 and 9.0, U.T., nine spectrograms were obtained on six nights. The spectrum is that of a supergiant star of class K5. It matches almost perfectly the spectrum of ζ Aurigae during totality. However, the following differences are apparent: (1) the line 4078 *Sr* II is stronger in 32 Cygni; (2) the *Fe* I lines 4045, 4064, and 4072 appear sharper in 32 Cygni; (3) 32 Cygni has more conspicuous central emission in H and K of *Ca* II. During the interval, no change whatever was noted. It is therefore concluded that the eclipse was total rather than deep partial.

ATMOSPHERIC ECLIPSE EFFECTS

The changes that occurred during emergence of the early-type star from behind the atmosphere of the K-type star will be described from day to day in this section. The first four figures of all Julian dates are omitted for brevity. Phases are referred to tentative dates of mid-eclipse, computed from the formula:

$$\text{Min.} = \text{JD } 2411547.5 + 1140.7E\,,$$

which depends mainly upon the recent eclipse and the early Harvard spectra as reported by Miss Hoffleit.[1]

November 10.0, 1949, U.T. (JD 230.5). Phase 10 days.—Slight but distinct changes suggest the beginning of emergence. Increases of strength of absorption are evident at *Ti* II 3900 and 3913, *Mg* I 3838, and $H\zeta$ and are suspected at *Sr* II 4078 and a number of lines of *Fe* I. Conspicuous increase has occurred in a blend at λ 3941.

November 14.0–14.1 (JD 234.5–.6). Phase 14 days.—A great change has occurred. Numerous lines of weak and moderate intensity are now filled in by the continuum of the early-type star. All the more conspicuous lines of *Fe* I remain strong, indicating that the companion is still behind the strata in which they are absorbed. *Ti* II 3900 and 3913 and *Sr* II 4078 are conspicuously strengthened. The *Ca* I line 4227 and the *Fe* I lines 4045–4072 are definitely sharper than during totality. H and K *Ca* II are about 5 A wide and very strong, with fairly definite edges. The extreme wings are filled in. The blend at λ 3941 is much weaker. The spectrum resembles that of ζ Aurigae at fourth contact, but *Ti* II 3900 and 3913 are weaker than in that star, and hydrogen lines are much less conspicuous.

November 15.1 (JD 235.6). Phase 15 days.—One plate was obtained through openings in clouds. Changes during 24 hours are very slight. The H and K lines are a little less wide (about 4 A), and partial resolution of H and $H\epsilon$ is suspected.

November 20.0–20.1 (JD 240.5–.6). Phase 20 days.—For the first time since the emergence, strong exposure was obtained beyond λ 3800. The H and K lines have narrowed to 2 A width and appear black, with very sharp edges and no trace of outer wings. They are three to four times as strong as the lines of Vega. H and $H\epsilon$ are distinctly resolved.

[1] *Harvard Announcement Card* 1046.

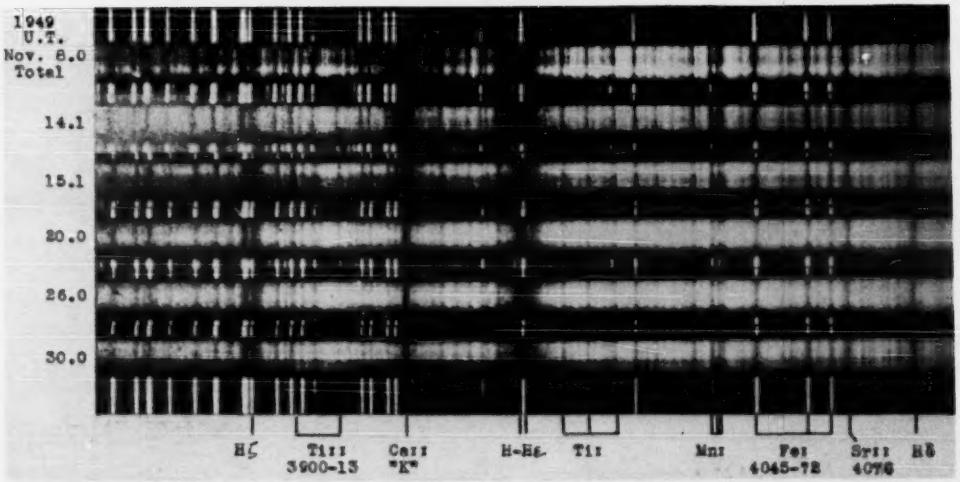

FIG. 1.—Spectra of 32 Cygni, λλ 3850–4110

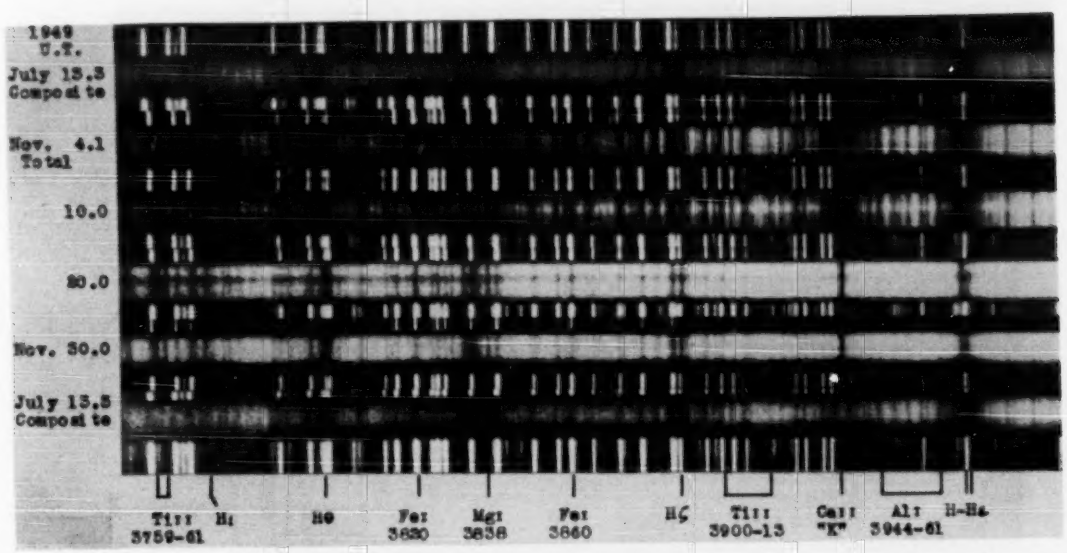

FIG. 2.—Spectra of 32 Cygni, λλ 3750–4000

"Filling-in" has begun to be noticeable at the *Fe* I lines 4045–4072. Some others, e.g., 3820 and 3860, have not yet weakened perceptibly, while a third set, including *Fe* I 3878, the four lines 3920–3930, and the *Al* I resonance lines 3944 and 3961, have become filled in to the same extent as in the normal composite spectrum. The resonance line *Ca* I 4227 is remarkably sharp, as compared with the strongly winged line of either the pure K5 spectrum or the composite spectrum. $H\zeta$ is a strong, rather sharp line, while $H\theta$ and $H\eta$ are conspicuous and have slightly diffuse edges. $H\iota$ is rather weak and a little diffuse, and the higher Balmer lines are obscured by blending with lines of the K5 star. The *Ti* II pair 3900 and 3913 are now weaker, but *Ti* II 3759 and 3761 are very strong. The *Mg* I line 3838 is strong and sharp.

November 22.0 (JD 242.5). Phase 22 days.—Changes in two days are slight. *Ca* I 4227 and *Sr* II 4078 and 4215 have probably begun to fill in. The *Fe* I group 4045, etc., is filled in as much as in the normal composite spectrum.

November 23.0 (JD 243.5). Phase 23 days.—The *Fe* I lines 3820 and 3860 are definitely weaker. There are no other changes.

November 24.0 (JD 244.5). Phase 24 days.—Changes are very slight. *Sr* II 4078, *Fe* I 3820 and 3860, and *Ca* I 4227 now appear as in the normal composite spectrum. H and K remain as wide and as strong as on November 20.

November 26.0 (JD 246.5). Phase 26 days.—H and K are definitely narrower, about 1.5 A in width. K shows indications of structure. The longward edge is strong and definite; the shortward edge appears a little weaker, as if a less intense absorption line were blended on that side.

November 30.0–30.1 (JD 250.5–.6). Phase 30 days.—Strong exposure was obtained beyond λ 3800 for the first time since November 23. H and K have become narrow lines, about as strong as in the spectrum of Vega. K clearly has a weaker companion blended with it on the shortward side. The center of the blend is in the position of the center of the wider K line as seen on preceding dates; that is, the narrow line is displaced in the positive direction relative to the center of the former wide line. $H\epsilon$ and $H\zeta$ are strong and sharp, but much less strong than in ζ Aurigae at a corresponding phase. $H\eta$ and $H\theta$ are strong with diffuse edges, while $H\iota$ is weak and sharp. The *Ti* II lines 3759 and 3761 remain very strong, though diminished since November 23. *Mg* I 3838 is weaker but still conspicuous.

December 3.0 (JD 253.5). Phase 33 days.—The shortward component of K has now disappeared; the longward is undiminished. The *Ti* II pair at 3760 is slightly weaker, and *Mg* I 3838 is probably due wholly to the K5 spectrum. $H\epsilon$ and $H\zeta$ are unchanged.

December 5.0, 10.0, 14.0, 25.0 (JD 255.5–275.5). Phases 35–55 days.—The K line gradually weakens until, on the last plate, its estimated intensity is half that of the line in the spectrum of Vega. The *Ti* II pair at 3760 no longer show appreciable intensification.

January 8.0, 1950 (JD 289.5). Phase 69 days.—The K line is gone.

MOUNT WILSON COUDÉ SPECTROGRAMS

Through the courtesy of Dr. I. S. Bowen and Dr. P. W. Merrill, four coudé spectrograms were loaned to the writer. These have dispersion 10 A/mm and show an enormous amount of fine detail. They are here discussed separately in order to avoid interruption of continuity of the low-dispersion record. One plate, taken on August 5.3, 1944, U.T., shows the normal composite spectrum.

November 11.2, 1949, U.T. (JD 231.7). Phase 11 days.—Compared with the normal composite spectrum, this plate shows great strengthening of all the strong lines. Especially outstanding are *Sr* II 4078 and the *Ti* II pair 3759 and 3761. A multitude of weak lines is intensified only slightly or not at all. The emergence of the early-type star was evidently well under way.

November 12.1 (JD 232.6). Phase 12 days.—There have been no conspicuous changes.

The *Ti* II pair 3900 and 3913 have definitely strengthened, and some weak lines have weakened further.

November 14.1 (JD 234.6). Phase 14 days.—Some of the fainter lines have weakened further. All the conspicuous lines of *Fe* I are fully as strong as on the previous plate. The pairs of *Ti* II lines at 3900, 3913, and 3759, 3761, are much strengthened, and appreciable intensification has occurred at $H\theta$ and $H\iota$. The wings of the K line are less broad than formerly, but still about 4 A wide.

OBSERVATIONS NEAR PREVIOUS ECLIPSES

July 6.3, 1940 (JD 9816.8). Phase 18 days.—The spectrum has the normal composite appearance, except for a strong narrow K line, about equal to that of Vega.

August 8.1, 1940 (JD 9849.6). Phase 51 days.—This plate differs from the previous one only in the K line, which is weaker but still conspicuous and very sharp.

July 31.1, 1943 (JD 0936.6). Phase −3 days.—The spectrum is underexposed at K, but the high contrast in the region λλ 4000–4200 shows that the eclipse was certainly total.

September 11.2, 1943 (JD 0978.7). Phase 39 days.—The K line is sharp and a little stronger than that of Vega. H and $H\epsilon$ are resolved. Otherwise the spectrum has the normal composite appearance.

July 23.2, 1946 (JD 2024.7). Phase −56 days.—A trace of a sharp K line is just suspected.

October 27.1, 1946 (JD 2120.6). Phase 40 days.—The K line is strong and sharp, perhaps half the intensity of the line in Vega.

COMPARISON WITH ζ AURIGAE

The spectrograms of 32 Cygni have been compared directly with those of ζ Aurigae during the eclipse of 1947–1948. In spite of the close similarity of the spectra of the primary stars of the two systems, the atmospheric eclipse effects differ, both in the relative intensities of lines and in rates of change.

The most outstanding difference is in the strength of the hydrogen lines. In ζ Aurigae the atmospheric eclipse components were very strong as far out as $H\lambda$. In 32 Cygni even the $H\iota$ line was rather weak. This difference may be due mainly to the different spectral types of the secondary stars, whose radiation may be chiefly responsible for excitation of hydrogen atoms.

The *Ti* II lines 3900 and 3913 were much weaker in 32 Cygni than in ζ Aurigae, though the pair 3759 and 3761 were about equally strong in both stars. The *Ca* II and *Mg* I lines were fairly comparable in the two stars.

The spectral changes of 32 Cygni from November 14 to November 30 were about equivalent to those of ζ Aurigae between January 22.3 and 26.2, 1948. The rates of change were thus in the ratio 1:4. The changes between November 10 and 14 suggest that the emergence (third to fourth contact) lasted 4 days, as contrasted with about 1 day in ζ Aurigae. On the other hand, the duration of totality was certainly less in 32 Cygni, perhaps less than 20 days, as against 38 days in ζ Aurigae. The differences can be partly harmonized by the hypothesis that the eclipse of ζ Aurigae is nearly central, while that of 32 Cygni is almost a grazing one. The long duration of strong *Ca* II lines, however, requires that the ionized calcium atmosphere of the K-type star extend above the photosphere much more than one stellar radius.

RADII, LUMINOSITIES, AND MASSES

Only a rough picture of the system can be calculated from available data. We assume the K5 star to be approximately equal in radius to the primary of the ζ Aurigae system; specifically, we adopt $R_K = 200\ \odot$. From the appearance of the composite spectrum, as

well as from Gaposchkin's estimate[1] of the range of variation, we estimate that the A-type companion is 2 mag. fainter photographically. According to Miss Hoffleit, the early Harvard spectra define the period as about 1140.7 days. Dr. K. O. Wright kindly communicated a plot of Victoria measures of velocity, which shows that the eccentricity is probably greater than that given by Cannon,[2] but $a \sin i$ is not greatly altered and is approximately 2.5×10^8 km. For the mass ratio we adopt two alternative values, 2.0 and 2.5. The resulting quantities are tabulated below. This star is not a favorable case for

DIMENSIONS OF THE SYSTEM 32 CYGNI

Mass Ratio	2.0	2.5
Mass of primary star, m_K	9.0 ⊙	15.0 ⊙
Mass of secondary star, m_A	4.5 ⊙	6.0 ⊙
Radius of primary star, R_K	200 ⊙	200 ⊙
Radius of secondary star, R_A	5 ⊙	5 ⊙
Absolute magnitudes (photo):		
Primary star, M_K	−3	−3
Secondary star, M_A	−1	−1
Mean separation of centers, $a_K + a_A$	7.6×10^8 km	8.8×10^8 km
Inclination of orbit, i	80°	81°.5
Parallax, p''	0".0025	0".0025

observation of an astrometric orbit.

The writer here records his appreciation of the kindness of Dr. I. S. Bowen and Dr. P. W. Merrill, who made possible the use of the Mount Wilson coudé plates; and of Dr. K. O. Wright, who communicated unpublished data. A number of the Ann Arbor spectrograms were obtained by Edwin B. Weston, Donald H. Clements, Robert Seall, and Marilyn Mears.

[1] *Pub. Dom. Obs. Ottawa*, **4**, 151, 1918.

THE STRUCTURE OF THE WOLF-RAYET ECLIPSING VARIABLE V 444 CYGNI*

GERALD E. KRON AND KATHERINE C. GORDON
Lick Observatory, University of California
Received February 1, 1950

ABSTRACT

A light-curve at λ 7200 made photoelectrically in the years 1943 and 1946 is presented. A solution for elements from our original light-curve at λ 4500 and from the new curve is given. This solution indicates that the Wolf-Rayet component consists of a small opaque core, of effective temperature 80,000° K, surrounded by a contiguous thick envelope that is luminous and semitransparent, whose luminosity is a function of wave length. This structure is inclosed by a second much larger envelope, which is inferred to be composed effectively of free electrons. The evidence indicates that the electron envelope must be a relatively thin, hollow shell, probably detached from the inner structure. The optical properties of the electron envelope are independent of wave length. Absolute dimensions and temperatures are given for the various components of the system. The distance is found to be 1500 parsecs after correction for space absorption by means of the color excesses of near-by stars observed by Stebbins, Huffer, and Whitford. Various unconventional features of V 444 Cygni are discussed.

I. INTRODUCTION

The Wolf-Rayet eclipsing variable V 444 Cygni = HD 193576 has received so much attention from astronomers in recent years that a repetition of introductory remarks to precede an additional paper seems unnecessary. E. S. Keeping[1] has presented an excellent summary of the significant contributions to our knowledge of this star, as well as new spectrographic data. Further investigation of the physical properties of the system of V 444 Cygni is now justified by the determination of a light-curve in the red, the details of which are presented here.

Up to the present time, quantitative analysis of V 444 has depended principally upon Gaposchkin's light-curve,[2] O. C. Wilson's velocity-curve,[3] and our light-curve at λ 4500[4]. Wilson's observations yielded physical data regarding the absolute dimensions of the system, and our light-curve led to the conclusion that one or both of the components must be surrounded by a thick atmosphere.[5, 6] The results indicated that a second light-curve, in another wave length, would contribute greatly to our knowledge of the properties of the thick atmosphere and possibly would add sufficiently to our knowledge to enable us to make estimates of physical dimensions—a difficult task because of the unconventional shapes of both minima of the light-curve at λ 4500.

II. THE OBSERVATIONS

TECHNIQUE

Observations of V 444 Cygni with the refrigerated infrared photoelectric photometer containing a Western Electric type D-97087 photoelectric cell were begun in 1943. Properties of this photometer have been described elsewhere in the literature.[7, 8]

* *Contributions from the Lick Observatory*, Ser. II, No. 29.

[1] *Pub. Dom. Ap. Obs., Victoria*, **7**, 349, 1947.
[2] *Pub. A.A.S.*, **10**, 52, 1940.
[3] *Ap. J.*, **91**, 379, 1940.
[4] *Ap. J.*, **97**, 311, 1943.
[5] *Ibid.*, p. 322.
[6] Kopal, *Ap. J.*, **100**, 205, 1944.
[7] *Lick Obs. Bull.*, **19**, 53, 1939 (No. 499).
[8] *Ap. J.*, **96**, 174, 1942; *Lick Obs. Contr.*, Ser. II, No. 5.

The effective wave length of the combination cell and 2-mm Schott OG1 filter was about λ 7200. The spectral region in which the observations were made was very wide: λ 5300 to beyond λ 10,000, a circumstance made necessary by the faintness of V 444 Cygni. On September 12, 1946, a new photocell, type CE 23D, was substituted for the D-97087 because it could be used without refrigeration.

A total of 954 observations was made with the 36-inch refractor, about a quarter of them in 1943 and the remainder during 1946. Fundamental data concerning the variable star and comparison stars are given in Table 1.

TABLE 1

DATA FOR V 444 CYG AND COMPARISON STARS

STAR	HD NUMBER	1900 POSITION		MAGNITUDE HD (PTM.)	SPECTRAL CLASS, HD
		R.A.	Dec.		
Check star *a*	193182	$20^h 13^m.8$	$+39° 16'$	$6^m.56$	A0
Comparison	193514	20 15.5	+38 57	7.29*	O8k
V 444 Cygni	193576	20 15.8	+38 25	8.04	WN5.5, O6†
Check star *b*	193634	20 16.2	+38 1	7.6	B8

* Our measures against four other stars show this magnitude should be corrected by about +0.2.
† C. S. Beals.

All observations at phases near or in minima are listed in Table 2, where successive columns give the heliocentric Julian date, the heliocentric phase in days computed from the formula

$$T = \text{JD } 2428771.379 + 4^d.21238E,$$

and the observed magnitude difference corrected to the zenith, in the sense of comparison star *minus* variable star. Table 3 gives the results of all observations made between minima, and they offer clear evidence of intrinsic variability in either V 444 Cygni or the comparison star, HD 193514. No systematic difference between the observations made with the CE 23D(f) cell, beginning at JD 2432076.758, and those made with the D-97087 could be found; it may be assumed, then, that the effective wave lengths of both cells are nearly the same.

INTRINSIC VARIABILITY

In 1947 the comparison star was checked on eight nights for variability against HD 193182 (check star *a*) with a multiplier phototube, our 1P21(a), and 1 mm of Corning 3385 filter glass, attached to the 12-inch refractor. The mean magnitude difference, in the sense of comparison *minus* check star *a*, at λ 5000 was found to be $+0.976 \pm 0.002$, with a range from +0.965 to +0.990 mag. On any one night the difference did not vary from the mean difference by more than 2.2 times the probable error of a single night's mean. We concluded from these results that the intrinsic variation arises in the system of V 444 Cygni.

In 1949 we attempted to study further the shape of the light-curve between minima. Although the project was not realized, we obtained even more impressive evidence of the intrinsic variability of the binary system by simultaneous magnitude-difference measures with the comparison star and check star *b*. The range in brightness of the variable star outside minima on three nights was 0.065 mag., while the range in the differences between the other two stars was 0.025 mag. The intrinsic variations in the light of V 444

TABLE 2

PHOTOELECTRIC OBSERVATIONS OF V 444 CYGNI MINIMA, λ 7200

Obs. No.	JD 243+	Heliocentric Phase (Days)	Δm
1	0942.692	1.937	−0.517
	.701	1.946	.516
	.709	1.954	.543
	.717	1.962	.567
5	.724	1.969	.538
	.732	1.977	.535
	.742	1.987	.551
	.749	1.994	.605
	.757	2.002	.638
10	.763	2.008	.604
	.771	2.016	.604
	.777	2.022	.623
	.859	2.104	.661
	.867	2.112	.640
15	.875	2.120	.636
	.885	2.130	.647
	.895	2.140	.638
	.906	2.151	.586
	.913	2.158	.564
20	.919	2.164	.556
	.927	2.172	.541
	.938	2.183	.567
	.946	2.191	.592
	.957	2.202	.550
25	0944.691	3.936	.519
	.699	3.944	.530
	.707	3.952	.542
	.714	3.959	.564
	.721	3.966	.530
30	.729	3.974	.564
	.735	3.980	.532
	.742	3.987	.561
	.749	3.994	.584
	.757	4.002	.547
35	.767	4.012	.540
	.773	4.018	.540
	.853	4.098	.687
	.861	4.106	.704
	.868	4.113	.692
40	.878	4.123	.725
	.885	4.130	.693
	.893	4.138	.716
	.900	4.145	.692
	.907	4.152	.716
45	.914	4.159	.716
	.920	4.165	.721
	.928	4.173	.678
	.936	4.181	.744
	.943	4.188	−0.708
50	0944.950	4.195	−0.706
	.961	4.206	.692
	.970	0.003	.680
	.979	0.012	.697
	0946.696	1.729	.496
55	.703	1.736	.519
	.711	1.744	.511
	.717	1.750	.474
	.725	1.758	.492
	.732	1.765	.462
60	.739	1.772	.482
	.745	1.778	.484
	.752	1.785	.471
	.761	1.794	.448
	.843	1.876	.482
65	.851	1.884	.480
	.858	1.891	.470
	.865	1.898	.458
	.872	1.905	.456
	.880	1.913	.479
70	.889	1.922	.460
	.898	1.931	.496
	.906	1.939	.464
	.912	1.945	.493
	.918	1.951	.492
75	.926	1.959	.502
	.933	1.966	.517
	.940	1.973	.532
	.947	1.980	.523
	.955	1.988	.526
80	0948.684	3.717	.469
	.692	3.725	.452
	.698	3.731	.443
	.705	3.738	.466
	.711	3.744	.479
85	.720	3.753	.479
	.726	3.759	.488
	.734	3.767	.467
	.741	3.774	.462
	.748	3.781	.476
90	.756	3.789	.465
	.852	3.885	.468
	.863	3.896	.462
	.871	3.904	.496
	.881	3.914	.500
95	.889	3.922	.510
	.898	3.931	.498
	.906	3.939	.524
	.919	3.952	.484
	.929	3.962	−0.526
100	0948.943	3.976	−0.535
	.955	3.988	.538
	.965	3.998	.562
	.974	4.007	.562
	.984	4.017	.580
105	0961.723	4.119	.679
	.741	4.137	.687
	.747	4.143	.692
	.755	4.151	.748
	0963.876	2.059	.621
110	.887	2.070	.615
	.892	2.075	.609
	.900	2.083	.631
	.909	2.092	.665
	.917	2.100	.613
115	.927	2.110	.630
	0965.683	3.866	.516
	.690	3.873	.532
	.697	3.880	.488
	.705	3.888	.493
120	.733	3.916	.514
	.741	3.924	.505
	.748	3.931	.520
	0972.665	2.424	.444
	.675	2.434	.456
125	.683	2.442	.458
	.691	2.450	.440
	.700	2.459	.438
	.712	2.471	.445
	.721	2.480	.466
130	.774	2.533	.467
	.785	2.544	.454
	.795	2.554	.464
	0974.663	0.209	.549
	.673	0.219	.514
135	.680	0.226	.526
	.689	0.235	.538
	.707	0.253	.524
	.715	0.261	.523
	.765	0.311	.500
140	.775	0.321	.449
	.782	0.328	.507
	.790	0.336	.494
	.835	0.381	.488
	.843	0.389	.476
145	.852	0.398	.460
	.859	0.405	.447
	.874	0.420	.453
	.882	0.428	.450
	0976.661	2.207	−0.530

TABLE 2—*Continued*

Obs. No.	JD 243+	Helio-centric Phase (Days)	Δm	Obs. No.	JD 243+	Helio-centric Phase (Days)	Δm	Obs. No.	JD 243+	Helio-centric Phase (Days)	Δm
150...	0976.669	2.215	−0.533	200...	1768.667	2.286	−0.492	250...	2031.755	4.206	−0.716
	.677	2.223	.530		.675	2.294	.470		.760	4.211	.748
	.684	2.230	.515		1985.940	0.515	.487		.765	0.004	.750
	.697	2.243	.520		.948	0.523	.500		.771	0.010	.736
	.705	2.251	.501		2001.841	3.779	.506		.775	0.014	.713
155...	.712	2.258	.470	205...	.850	3.788	.478	255...	.781	0.020	.722
	.739	2.283	.452		.857	3.795	.503		.786	0.025	.730
	.771	2.315	.462		.867	3.805	.491		.805	0.044	.729
	.780	2.324	.473		.900	3.838	.496		.812	0.051	.731
	.787	2.331	.438		.909	3.847	.489		.817	0.056	.740
160...	.794	2.338	.410	210...	2006.863	0.376	.495	260...	.821	0.060	.724
	.803	2.347	.424		.869	0.382	.471		.825	0.064	.680
	.811	2.355	.405		.880	0.393	.465		.830	0.069	.727
	.826	2.370	.438		.886	0.399	.499		.845	0.084	.716
	.834	2.378	.405		.893	0.406	.519		.851	0.090	.716
165...	.845	2.389	.417	215...	.910	0.423	.510	265...	.855	0.094	.713
	.854	2.398	.450		.917	0.430	.508		.887	0.126	.638
	.863	2.407	.464		.924	0.437	.513		.891	0.130	.643
	.872	2.416	.432		.935	0.448	.474		.896	0.135	.648
	0978.667	0.001	.693		.941	0.454	.483		.901	0.140	.640
170...	.677	0.011	.691	220...	.948	0.461	.501	270...	.905	0.144	.633
	.695	0.029	.706		.954	0.467	.497		.911	0.150	.646
	.702	0.036	.700		.961	0.474	.494		.915	0.154	.618
	.709	0.043	.723		2027.829	0.280	.570		.920	0.159	.629
	.741	0.075	.684		.834	0.285	.560		.925	0.164	.636
175...	.771	0.105	.644	225...	.838	0.289	.543	275...	.931	0.170	.625
	.780	0.114	.625		.856	0.307	.523		.935	0.174	.606
	.789	0.123	.622		.862	0.313	.492		.940	0.179	.570
	.795	0.129	.590		.867	0.318	.483		.944	0.183	.582
	.804	0.138	.579		.895	0.346	.515		.950	0.189	.556
180...	.811	0.145	.564	230...	.899	0.350	.547	280...	.954	0.193	.576
	.821	0.155	.579		.905	0.356	.483		.960	0.199	.554
	.829	0.163	.524		.909	0.360	.513		.965	0.204	.571
	.839	0.173	.530		.915	0.366	.479		.969	0.208	.580
	.847	0.181	.540		.920	0.371	.495		.973	0.212	.564
185...	.854	0.188	.507	235...	.924	0.375	.454	285...	2035.773	4.012	.541
	.863	0.197	.532		.931	0.382	.485		.777	4.016	.536
	.871	0.205	.503		.935	0.386	.486		.781	4.020	.539
	0999.676	4.160	.705		.941	0.392	.511		.787	4.026	.578
	.721	4.205	.709		.945	0.396	.496		.799	4.038	.566
190...	.729	0.001	.726	240...	.950	0.401	.445	290...	.805	4.044	.608
	.739	0.011	.751		.956	0.407	.508		.809	4.048	.557
	.748	0.020	.729		.961	0.412	.459		.813	4.052	.610
	.755	0.027	.747		.965	0.416	.449		.816	4.055	.578
	.762	0.034	.716		.971	0.422	.502		.831	4.070	.625
195...	.771	0.043	.693	245...	2031.727	4.178	.728	295...	.836	4.075	.600
	.780	0.052	.697		.733	4.184	.713		.840	4.079	.618
	.789	0.061	.682		.739	4.190	.720		.844	4.083	.588
	.796	0.074	.676		.743	4.194	.740		.849	4.088	.637
	.808	0.086	−0.652		.749	4.200	−0.730		.868	4.107	−0.678

TABLE 2—*Continued*

Obs. No.	JD 243+	Heliocentric Phase (Days)	Δm	Obs. No.	JD 243+	Heliocentric Phase (Days)	Δm	Obs. No.	JD 243+	Heliocentric Phase (Days)	Δm
300	2035.872	4.111	−0.690	350	2052.773	4.162	−0.708	400	2071.697	2.024	−0.582
	.877	4.116	.646		.785	4.174	.710		.701	2.028	.572
	.882	4.121	.698		.790	4.179	.721		.705	2.032	.589
	.889	4.128	.663		.794	4.183	.726		.709	2.036	.584
	.894	4.133	.628		.798	4.187	.732		.712	2.039	.584
305	.899	4.138	.694	355	.802	4.191	.694	405	.716	2.043	.621
	.903	4.142	.703		.813	4.202	.697		.731	2.058	.608
	.909	4.148	.694		.817	4.206	.734		.735	2.062	.588
	.915	4.154	.706		.821	4.210	.708		.739	2.066	.620
	.920	4.159	.658		.825	0.002	.714		.743	2.070	.608
310	.926	4.165	.694	360	2058.691	1.656	.412	410	.749	2.076	.610
	.932	4.171	.696		.695	1.660	.429		.770	2.097	.642
	.937	4.176	.670		.699	1.664	.426		.774	2.101	.633
	.943	4.182	.744		.703	1.668	.436		.778	2.105	.612
	.950	4.189	.738		.707	1.672	.443		.783	2.110	.606
315	.959	4.198	.724	365	.711	1.676	.446	415	.787	2.114	.624
	.964	4.203	.707		.715	1.680	.439		.792	2.119	.611
	.969	4.208	.751		.719	1.684	.447		.797	2.124	.638
	.974	0.000	.777		.735	1.700	.446		.812	2.139	.608
	.983	0.009	.759		.739	1.704	.415		.815	2.142	.627
320	2037.760	1.786	.489	370	.744	1.709	.430	420	.820	2.147	.631
	.764	1.790	.476		.749	1.714	.446		.825	2.152	.626
	.769	1.795	.453		.753	1.718	.444		.839	2.166	.594
	.773	1.799	.473		.768	1.733	.445		.844	2.171	.564
	.777	1.803	.458		.773	1.738	.428		.848	2.175	.606
325	.781	1.807	.448	375	.776	1.741	.460	425	.852	2.179	.578
	.785	1.811	.438		.780	1.745	.440		.858	2.185	.586
	.793	1.819	.448		.805	1.770	.435		.863	2.190	.584
	.797	1.823	.466		.809	1.774	.445		.869	2.196	.564
	.801	1.827	.462		.813	1.778	.430	2075.682		1.797	.477
330	.805	1.831	.442	380	.817	1.782	.442	430	.685	1.800	.475
	.810	1.836	.442		.821	1.786	.446		.690	1.805	.454
	2040.671	0.485	.466		.825	1.790	.440		.695	1.810	.496
	2052.685	4.074	.626		.829	1.794	.436		.699	1.814	.460
	.690	4.079	.610		.835	1.800	.433		.704	1.819	.472
335	.695	4.084	.637	385	.838	1.803	.440	435	.708	1.823	.466
	.699	4.088	.592		.843	1.808	.450		.719	1.834	.462
	.703	4.092	.636		.847	1.812	.458		.724	1.839	.475
	.707	4.096	.644		.853	1.818	.436		.728	1.843	.486
	.711	4.100	.628		.858	1.823	.425		.732	1.847	.472
340	.715	4.104	.669	390	.863	1.828	.441	440	.754	1.869	.460
	.719	4.108	.670		.868	1.833	.426		.759	1.874	.470
	.724	4.113	.655		.873	1.838	.449		.763	1.878	.449
	.728	4.117	.638		.877	1.842	.439		.769	1.884	.466
	.732	4.121	.666		.881	1.846	.443		.773	1.888	.470
345	.749	4.138	.690	395	2071.665	1.992	.552	445	.777	1.892	.461
	.753	4.142	.676		.669	1.996	.532		.781	1.896	.456
	.758	4.147	.691		.673	2.000	.540		.786	1.901	.493
	.762	4.151	.678		.677	2.004	.526		.792	1.907	.483
	.767	4.156	−0.702		.682	2.009	−0.568		.796	1.911	−0.467

TABLE 2—*Continued*

Obs. No.	JD 243+	Helio-centric Phase (Days)	Δm	Obs. No.	JD 243+	Helio-centric Phase (Days)	Δm	Obs. No.	JD 243+	Helio-centric Phase (Days)	Δm
450...	2075.800	1.915	-0.472	495...	2088.802	2.280	-0.487	540...	2107.640	0.057	-0.679
	.807	1.922	.474		.806	2.284	.480		.644	0.061	.702
	.811	1.926	.483		.810	2.288	.479		.682	0.098	.677
	.814	1.929	.489		.814	2.292	.465		.684	0.100	.650
	.818	1.933	.475		.817	2.295	.482		.689	0.105	.644
455...	.824	1.939	.474	500...	.821	2.299	.467	545...	.694	0.110	.636
	.828	1.943	.478		.824	2.302	.477		.698	0.114	.634
	.833	1.948	.503		2090.648	4.126	.663		.700	0.116	.639
	.837	1.952	.470		.652	4.130	.713		.707	0.123	.646
	.844	1.959	.537		.655	4.133	.693		.710	0.126	.632
460...	.848	1.963	.514	505...	.660	4.138	.713	550...	.714	0.130	.622
	.852	1.967	.505		.663	4.141	.721		.719	0.135	.604
	.857	1.972	.510		.668	4.146	.721		.723	0.139	.603
	.862	1.977	.511		.679	4.157	.728		.727	0.143	.630
	.867	1.982	.521		.683	4.161	.718		.742	0.158	.590
465...	2088.652	2.130	.667	510...	.686	4.164	.753	555...	.746	0.162	.594
	.656	2.134	.640		.690	4.168	.714		.750	0.166	.557
	.660	2.138	.636		.694	4.172	.718		.754	0.170	.578
	.664	2.142	.652		.720	4.198	.726		.758	0.174	.579
	.668	2.146	.620		.724	4.202	.750		.762	0.178	.592
470...	.672	2.150	.610	515...	.728	4.206	.745	560...	.766	0.182	.560
	.682	2.160	.601		.732	4.210	.751		.771	0.187	.581
	.685	2.163	.612		.736	0.002	.717		.774	0.190	.577
	.689	2.167	.633		.740	0.006	.739		.778	0.194	.565
	.694	2.172	.625		.743	0.009	.736		.783	0.199	.537
475...	.697	2.175	.607	520...	.748	0.014	.748	565...	.786	0.202	.565
	.724	2.202	.604		.752	0.018	.764		2117.671	1.662	.448
	.728	2.206	.568		.757	0.023	.760		.675	1.666	.443
	.732	2.210	.573		.762	0.028	.762		.681	1.672	.442
	.736	2.214	.550		.766	0.032	.758		.683	1.674	.470
480...	.740	2.218	.535	525...	.770	0.036	.768	570...	.688	1.679	.481
	.744	2.222	.564		.774	0.040	.786		.693	1.684	.456
	.748	2.226	.501		.777	0.043	.731		.705	1.696	.470
	.752	2.230	.550		.781	0.047	.758		.709	1.700	.449
	.755	2.233	.544		.785	0.051	.764		.712	1.703	.452
485...	.760	2.238	.546	530...	.790	0.056	.752	575...	.717	1.708	.469
	.763	2.241	.520		.794	0.060	.744		.722	1.713	.462
	.768	2.246	.498		.798	0.064	.720		2122.652	2.431	.469
	.772	2.250	.509		.801	0.067	.736		.657	2.436	.468
	.775	2.253	.518		.806	0.072	.745		.661	2.440	.501
490...	.780	2.258	.523	535...	.810	0.076	.689	580...	.666	2.445	.478
	.784	2.262	.488		.812	0.078	.710		.670	2.449	.479
	.788	2.266	.493		.817	0.083	.681		.674	2.453	.448
	.793	2.271	.502		.821	0.087	.689		.678	2.457	-0.460
	.798	2.276	-0.300		2107.637	0.053	-0.698				

Cygni may be correlated with spectrophotometric peculiarities pointed out by C. S. Beals.[9]

At the time that we published the light-curve at λ 4500 we knew that these data, too, seemed to indicate some kind of variation, but, because the war made early publication desirable and because of unfamiliarity with the precision to be expected, we decided to present the observations without a check on the comparison star and to place the ob-

TABLE 3

OBSERVATIONS BETWEEN MINIMA, λ 7200

JD 243+	Mean Heliocentric Phase (Days)	Mean Magnitude Difference	Probable Error of Mean	No. of Observations
0941.752–0.776	1.008	−0.497	±0.0066	4
0943.711– .761	2.981	.471	.0015	8
0945.701– .768	0.767	.468	.0036	8
0947.715– .763	2.771	.442	.0037	6
0962.710– .916	1.016	.454	.0024	17
0964.706– .926	3.021	.455	.0025	20
1773.623– .705	3.070	.446	.0024	11
1779.665– .715	0.668	.395	.0031	7
2003.841– .927	1.606	.453	.0031	11
2005.839– .926	3.607	.462	.0028	11
2013.740– .938	3.137	.471	.0026	30
2019.724– .909	0.675	.473	.0028	29
2040.697– .826	0.570	.473	.0018	27
2041.671– .779	1.543	.459	.0023	19
2047.684– .784	3.334	.464	.0023	20
2076.662– .728	2.810	.451	.0040	13
2076.758– .812	2.900	.475	.0022	13
2083.774– .839	1.497	.448	.0024	17
2087.682– .824	1.236	.446	.0021	28
2108.677– .777	1.143	.398	.0019	25
2117.647– .667	1.648	.482	.0046	6
2121.658– .720	1.468	.461	.0025	17
2135.621– .669	2.787	.444	.0048	12
2139.613–0.659	2.565	−0.471	±0.0034	12

served variations in the category of observational error. The reasonably certain knowledge that we are now dealing with an intrinsic variation of V 444 Cygni itself makes a re-examination of the λ 4500 data necessary; for there exists a possibility of greatly improving the precision of the light-curve. The observations between minima for the light-curves in both colors are shown schematically in Figure 1. The phases covered during one night's observing are indicated by the widths of the rectangles, while the heights correspond to twice the probable error of the mean magnitude difference. Phases between secondary and primary minimum have been "reflected" about the primary minimum. The original 1940 observations between minima have been given a correction of −0.010 mag. The large dispersion in magnitude differences compared with the night-to-night probable errors is striking.

Observations within minima for both light-curves were examined for the effects of intrinsic variability by plotting them year by year. Examination of these plots made

[9] *M.N.*, **104**, 215, 1944.

plain the existence on certain nights of displacements in magnitude that were the result of intrinsic variation alone and that were definitely distinguishable from possible phase variations. These displacements were measured, and, in forming the normal points, the affected observations were corrected by these amounts. The displacements are listed as

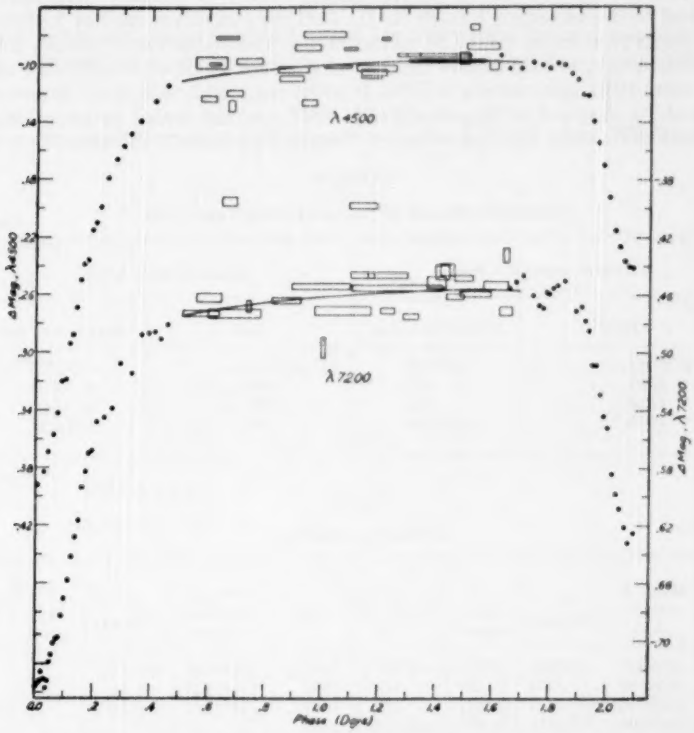

FIG. 1.—Photoelectric observations of V 444 Cygni at λ 4500 and λ 7200. Dots are the mean of ten observations reflected about the mid-point of each minimum. The mid-point of primary minimum is 0.000 day; that of secondary minimum is 2.100 days. Corrections for intrinsic variability and yearly changes in Δm, as described in the text, are included. Each rectangle indicates observations made during one night between minima. The width of the rectangles indicates the phases covered; their height is equal to twice the probable error of the night mean. The curves are freehand estimates of the light-curve between minima, upon which the rectification procedure is based.

corrections in Table 4. Care was taken that these corrections should not introduce phase displacements, and, when there was any doubt, the observations were used without modification. The difficulty in separating phase displacements from magnitude displacements within minima is very great, and this fact accounts for the absence of small corrections in Table 4. Small errors doubtless exist, but they cannot be positively identified as of one type or the other.

PHASE DISPLACEMENTS

When the observations at λ 4500 were published, a remark was made concerning the peculiar shape of the secondary minimum. The weight of the data contained in the two light-curves now indicates that the mean curve was distorted in shape by a large phase-

shift that took place in the time of secondary minimum between the years 1940 and 1942. An analysis of shifts in time of minima based on the comparison of observations made in more than one wave length can be criticized because the possibility exists that the shifts may be a function of wave length. Therefore, in 1946, contemporaneous with the 1946 red observations, the position of the descending branch of primary minimum on JD 2432073 and of the ascending branch on JD 2432086 was determined at λ 4500 with a 1P21 multiplier photometer on the 36-inch refractor. The mid-phase of primary minimum was at +0.015 day, in satisfactory agreement with the value of +0.011 day obtained from the mean 1946 light-curve at λ 7200. It seems reasonably safe, then, to assume that the phase-shifts observed in the minima of V 444 Cygni are caused by something about the star itself and not by the comparison of observations made at different wave lengths.

TABLE 4

CORRECTIONS FOR INTRINSIC LIGHT-VARIATION

Observations at λ 4500		Observations at λ 7200	
Date	Correction to Δm	Date	Correction to Δm
JD 2430544	+0m010	JD 2432058	−0m015
0599	+ .020	2088	+ .010
0603	− .020	2090	+ .018
0649	+0.010	2107	−0.020

TABLE 5

PHASES OF MINIMA

Year	Mean JD of Observation	I_1 (Primary)	I_2 (Secondary)	$(I_2-I_1)-P/2$	Year	Mean JD of Observation	I_1 (Primary)	I_2 (Secondary)	$(I_2-I_1)-P/2$
1940	2429880	−0d005	2d080:	−0d021:	1947	2432448	+0.02	.....	.....
1942	2430580	.000	2.100	− .006	1949	2433122	− .02	.....	.....
1943	2430960	− .019	2.082	− .005	1949	2433182	+0.02	.....	.....
1946	2432060	+0.011	2.108	−0.009					

Mean light-curves were formed for 1940, 1942, 1943, and 1946. The phases of minima were measured and are tabulated in Table 5. To this list we may add more recent determinations: in 1947[10] and 1949. The 1949 results are the mean of observations at λ 4300 and λ 5200. The change in phase between the two nights on which the primary minimum was observed is conspicuous.

The data in Table 5 show, from the last column, that mid-secondary occurs slightly earlier than midway between primary minima, an indication of the presence of a small orbital eccentricity. The longitude of periastron from these photometric measures does not agree with those from solutions of spectrographic data analyzed by Keeping,[1] but the point is a minor one in the general theory of the physical nature of the system of V 444 Cygni. The third and fourth columns contain the data necessary for correcting the light-curves from the various years, so that they may be combined into homogeneous mean curves. The conspicuous nature of the phase-shifts is best illustrated by Figure 2, which shows a plot of some of the data from which Table 5 was derived. The observations at

[10] W. A. Hiltner, *Ap. J.*, **110**, 95, 1949.

λ 4500, listed in *Ap. J.*, **97**, 313, 1943, Tables 2 and 3, were also computed from the epoch JD 2428771.379, and not from JD 2428771.335, as erroneously given on page 312. All data in Table 5 have therefore been derived from the same, correct epoch.

NORMAL POINTS

The observations within minima for each year were combined into normal points after having been made homogeneous by the application of corrections in magnitude (Table 4)

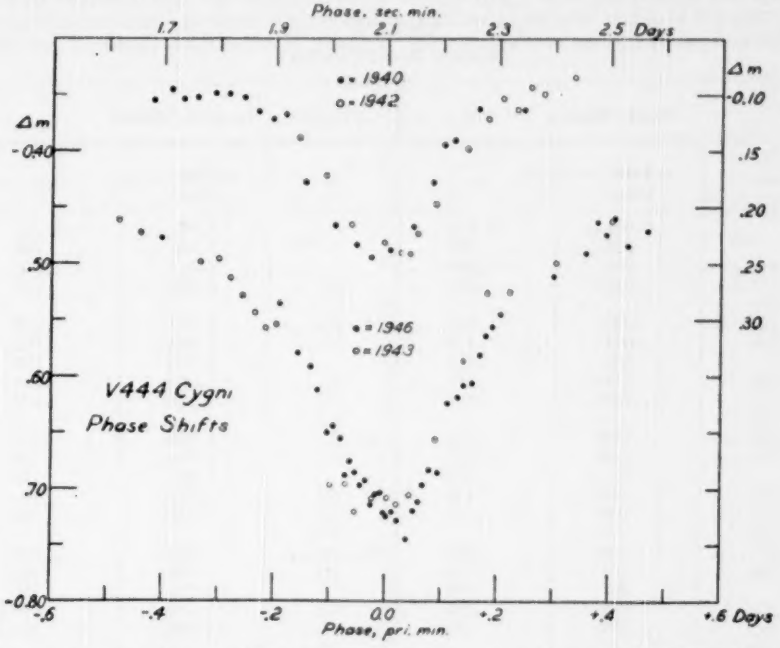

FIG. 2.—Examples of phase-shifts in minima based upon the ephemeris T = JD 2428771.379 + $4^d.21238E$. Each dot and circle represents the mean of five observations. The upper curve is the secondary minimum, the lower curve the primary minimum.

and in phase (Table 5). The minima were tested for asymmetry by reflecting the normal points about the mid-points of the respective minima. No asymmetry beyond that attributable to observational error was noted.

At this point the observations falling within minima had been condensed into four sets of preliminary normal points, two for each color. The next step was to combine these into two sets (one for each color) by removal of the small annual systematic differences in magnitude. The 1940 primary observations were corrected by −0.006 mag., and the 1940 secondary observations by −0.020 mag. A correction of −0.016 mag. was applied to the 1943 observations of primary minimum; no correction was found necessary for the secondary-minimum observations. The preliminary normal points, having served their purpose in aiding investigation of asymmetry and of systematic differences, were then abandoned. The individual observations within minima for both colors thus corrected were reflected about their respective mid-points (0.000 day for primary and 2.100 days

for secondary) and were combined into final normal points having ten observations each. The resulting values are given in Tables 6 and 7 and are plotted against phase in Figure 1.

RECTIFICATION

As may be seen in Figure 1, there appears to be a certain amount of re-radiation effect near secondary minimum. Without inquiring into the physical process involved, we felt that a rectification procedure should be applied to the light-curves before making a solution for the elements. Rectification of the λ 4500 observations was carried out by Rus-

TABLE 6

NORMAL POINTS, λ 4500

Primary Minimum			Secondary Minimum		
No.	Phase (Days)	Δm	No.	Phase (Days)	Δm
1	0.008	−0.392	1	2.091	−0.241
	.029	.383		2.076	.240
	.044	.369		2.062	.236
	.062	.357		2.046	.226
5	.077	.342	5	2.029	.215
	.092	.320		2.008	.192
	.106	.319		1.986	.170
	.119	.294		1.968	.154
	.130	.288		1.951	.139
10	.142	.268	10	1.931	.121
	.156	.250		1.914	.120
	.167	.239		1.895	.110
	.181	.236		1.872	.106
	.196	.215		1.847	.100
15	.210	.208	15	1.824	.099
	.223	.199		1.797	.102
	.247	.179		1.770	.100
	.276	.166		1.739	.098
	.299	.157		1.697	.102
20	.324	.148	20	1.656	.102
	.358	.139		1.624	−0.093
	.411	.125			
	0.453	−0.114			

sell's method[11] on the basis of the freehand curve drawn through the observations between minima, as shown in Figure 1. The poorer quality of the observations at λ 7200 did not seem to justify such an elaborate procedure. The light-intensity values were rectified by means of the formula

$$l_r = l \div (1.009 - 0.011 \cos\theta - 0.005 \cos 2\theta),$$

which was derived in the usual fashion from the lower freehand curve shown in Figure 1. For the λ 4500-curve the coefficient of cos θ was found to be −0.009, and the coefficient of cos 2θ, −0.004. The "rectified" normal points are given in Tables 8 and 9 in terms of sin θ, where θ is the phase angle, and of light-loss, $1 - l$. Because of their inferior qual-

[11] *Ap. J.*, **104**, 153, 1946.

ity and to facilitate computation by reducing the number of normals to be represented, each two normal points of Table 7 were combined into one twenty-point normal in Table 9.

III. ANALYSIS OF THE LIGHT-CURVES

As stated in the preliminary report[12] and confirmed by Hiltner,[10] there seems to be no fundamental difference between the shapes of the primary minimum in ultraviolet, blue, and red light within the precision of the observations. The results, therefore, offer observational evidence that the large envelope surrounding the W component has optical absorption that is independent of wave length from the ultraviolet region of the spectrum to the red. Z. Kopal and Martha B. Shapley[13] have shown that neutral absorption will be

TABLE 7

NORMAL POINTS, λ 7200

PRIMARY MINIMUM			SECONDARY MINIMUM		
No.	Phase (Days)	Δm	No.	Phase (Days)	Δm
1	0.003	−0.732	1	2.093	−0.625
	.011	− .730		2.075	− .632
	.017	− .728		2.062	− .621
	.023	− .722		2.045	− .608
5	.031	− .727	5	2.032	− .598
	.038	− .733		2.019	− .584
	.044	− .728		2.002	− .552
	.050	− .715		1.990	− .544
	.056	− .710		1.978	− .529
10	.063	− .702	10	1.965	− .509
	.072	− .699		1.950	− .509
	.080	− .698		1.939	− .485
	.090	− .683		1.925	− .478
	.100	− .671		1.912	− .468
15	.113	− .658	15	1.892	− .471
	.125	− .642		1.853	− .450
	.137	− .628		1.828	− .453
	.149	− .617		1.813	− .455
	.162	− .584		1.800	− .459
20	.175	− .583	20	1.790	− .458
	.185	− .570		1.778	− .469
	.197	− .568		1.764	− .467
	.213	− .548		1.743	− .460
	.239	− .545		1.708	− .446
25	.267	− .539	25	1.680	− .451
	.294	− .508		1.660	−0.455
	.334	− .515			
	.367	− .488			
	.393	− .487			
30	.414	− .486			
	.435	− .491			
	0.460	−0.481			

[12] *A.J.*, **52**, 154, 1947.

[13] *Ap. J.*, **104**, 160, 1946.

one of the properties of an envelope that is a highly ionized gas, in which free electrons far outnumber the stripped nuclei. Such an envelope will be called an "electron atmosphere" in the remaining part of this paper. This envelope causes distortion of the primary minimum by partial absorption of light from the O component, although radiation from it is undetectable at secondary minimum when the Wolf-Rayet component is behind the O-type component. Russell, however, has shown that the secondary mini-

TABLE 8

RECTIFIED NORMAL POINTS OF PRIMARY AND SECONDARY MINIMA, λ 4500

Primary Minimum					Secondary Minimum				
Normal Point No.	sin θ	1 − l	O − C		Normal Point No.	sin θ	1 − l	O − C	
			$k_c = 0.225$	$k_c = 0.45$				Disk Hypothesis	Ring Hypothesis
1	0.012	0.214	−0.002	+0.002	1	0.013	0.121	−0.0021	−0.0022
	.043	.208	− .005	− .001		.036	.121	− .0001	.0000
	.066	.198	− .010	− .004		.057	.117	− .0001	− .0001
	.092	.189	− .011	− .005		.081	.110	− .0003	.0000
5	.115	.179	− .013	− .003	5	.106	.100	+ .0001	+ .0002
	.137	.163	− .020	− .007		.137	.082	− .0016	− .0011
	.158	.162	− .013	+ .004		.169	.063	− .0011	− .0002
	.176	.143	− .021	− .004		.196	.050	+ .0032	+ .0042
	.193	.140	− .019	+ .005		.220	.036	+ .0033	+ .0043
10	.210	.125	− .021	+ .001	10	.250	.021	− .0009	− .0010
	.231	.110	− .025	− .002		.274	.020	+ .0033	+ .0024
	.246	.102	− .027	.000		.301	.011	− .0004	− .0011
	.267	.100	− .021	+ .011		.334	.006	+ .0001	+ .0023
	.288	.083	− .029	+ .006		.368	.002	+ .0002	+ .0006
15	.308	.077	− .028	+ .008	15	0.400	0.000	0.0000	0.0000
	.326	.070	− .027	+ .006					
	.360	.056	− .027	.000					
	.400	.043	− .023	− .002					
	.431	.036	− .019	− .002					
20	.465	.030	− .013	− .001					
	.509	.021	− .007	− .001					
	.576	.012	+ .002	+ .003					
	0.626	0.001	−0.001	−0.002					

mum, too, is not purely a geometrical eclipse,[14] although the degree of distortion is much less than that of the primary minimum.

In view of these factors, it was decided to start an analysis of the light-curve by determining geometrical elements from the secondary minimum[15] alone and to base the whole geometrical analysis upon the observations at λ 4500 because of their superior accuracy. But a solution for the elements of an eclipsing variable star with partial eclipses is indeterminate from one minimum, unless further information regarding the properties of the star is available. Fortunately, C. S. Beals[16] has determined the light-ratio of the O com-

[14] *Ap. J.*, **100**, 213, 1944.

[15] Cf. Kopal, *Ap. J.*, **100**, 208, 1944.

[16] *M.N.*, **104**, 205, 1944.

ponent to the W component, and his work provides the additional data necessary for a determinate solution for the orbital elements. Russell[14] has already given an analysis of the effects on the geometrical elements of errors in the light-ratio for V 444 Cygni.

An examination of the secondary minimum shows that the distortion is in the presence of "wings" like those in the primary minimum, only of smaller amplitude. We postulate that the wings are formed either (1) by the absorbing effect of a tenuous atmosphere surrounding the O component or (2) by the eclipse of a luminous, halo-like structure surrounding the W component. In this paper we devote detailed attention only to the second of these two hypotheses because we believe it is the more reasonable of the two. If the W core is enveloped by a scattering atmosphere, it is reasonable to suppose that light from the core will be scattered *into* the observer's line of sight, as well as *out* of it. This

TABLE 9

NORMAL POINTS AND RESIDUALS, λ 7200

PRIMARY MINIMUM			SECONDARY MINIMUM		
sin θ	1 − l	O − C	sin θ	1 − l	O − C
0.0104	+0.205	−0.001	0.0239	+0.145	0.000
.0298	+ .200	− .004	.0692	+ .134	.000
.0514	+ .204	+ .003	.1110	+ .115	+ .001
.0700	+ .198	+ .003	.1545	+ .080	− .003
.0886	+ .186	− .003	.1906	+ .054	.000
.1132	+ .180	+ .002	.2299	+ .036	+ .009
.1412	+ .165	+ .004	.2676	+ .015	− .003
.1766	+ .144	+ .003	.3328	+ .002	− .004
.2116	+ .121	+ .002	.4050	− .003	− .003
.2487	+ .094	− .003	0.4393	+0.001	+0.001
.2810	+ .079	+ .001			
.3308	+ .059	− .002			
.4062	+ .041	− .002			
.4992	+ .021	− .002			
.5661	+ .008	− .003			
0.6190	+0.010	−0.006			

phenomenon is responsible for the well-known "street-light-in-a-fog" effect and could cause a luminous halo around the W core.[17]

Furthermore, we must, if possible, seek some region in which the bright bands associated with the Wolf-Rayet spectrum can be generated. Whichever hypothesis is justified in the end, it is clear that a solution based upon the second will furnish a structure which may be useful later in explaining some of the physical phenomena associated with the Wolf-Rayet component.

Preliminary attempts to fit the secondary minimum by the usual methods of analysis indicated that the region from $\sin\theta = 0.00$ to $\sin\theta = 0.24$ could be fitted with remarkable accuracy, provided that no attempt was made to fit the wings, which extend from about $\sin\theta = 0.24$ to $\sin\theta = 0.40$. On the other hand, a few simple changes made possible an almost perfect fit of the wings if a fit of the section of the light-curve from $\sin\theta = 0.00$ to $\sin\theta = 0.24$ were neglected. This suggested at once the possibility of actually fitting the entire curve on the basis of the W component, consisting of a bright core surrounded by a symmetrical luminous region of lower surface brightness, and sub-

[17] L. Spitzer has independently reached this same conclusion (private communication).

sequent derivation of elements. No methods of dealing with the eclipse of a composite body had hitherto been worked out, so we were forced to develop one which would make the best possible use of the excellent theory and tables now available for the solution of normal eclipsing variable stars.

Throughout the following analysis, we have adopted the simplifying assumption that all composite parts of the system of V 444 Cygni are spherically symmetrical. Naturally, when a system of spherical eclipsing bodies is treated by accepted methods of analysis, the computer is dealing not with three-dimensional objects but with their plane projections. It is therefore to be understood that in the following treatment of this problem we deal with fictitious plane projections of the real three-dimensional objects. The distinction is indicated by our nomenclature, except in the case of the W core, which is called the "core" at all times.

DISK HYPOTHESIS

The standard symbols and formulae for the solution of eclipsing binary systems have been modified for the present composite model. In the first solution for secondary minimum, where for the W component the variation in surface brightness with radius is as shown in Figure 3, *a*, we have the following symbols:

k_c ..... Ratio of radii, W core to O star
k_d ..... Ratio of W luminous disk to O star
θ_c ..... Phase angle (true anomaly) at beginning of core eclipse
θ_d ..... Phase angle at beginning of disk eclipse
L_o ..... Light of O star
L_w ..... Light of W star = L_c (light of core) + L_d (light of disk)
$1 - \lambda_c$ ..... Light-loss of W core at conjunction
$1 - \lambda_d$ ..... Light-loss of W disk at conjunction
i ..... Orbital inclination
r_o ..... Radius of O star in terms of relative orbit

$$a_{0c} = \frac{1 - \lambda_c}{L_c}, \tag{1}$$

$$a_{0d} = \frac{1 - \lambda_d}{L_d}. \tag{2}$$

The fundamental equations for the elements of an eclipsing binary system may be written as follows:

$$\sin^2 \theta_c \sin^2 i + \cos^2 i = r_o^2 (1 + k_c p_c)^2 \tag{3}$$

and

$$\sin^2 \theta_d \sin^2 i + \cos^2 i = r_o^2 (1 + k_d p_d)^2, \tag{4}$$

for the core and disk, respectively, at the beginning of their eclipse. At conjunction, these reduce to

$$\cos^2 i = r_o^2 (1 + k_c p_{0c})^2, \tag{5a}$$

$$\cos^2 i = r_o^2 (1 + k_d p_{0d})^2. \tag{5b}$$

For any composite light-curve the starting point of the analysis is

$$k_c p_{0c} = k_d p_{0d}. \tag{6}$$

Our solution depends upon the following numerical data:

$$a) \qquad \frac{L_o}{L_w} = \frac{5}{1},$$

from Beals's spectrographic data. When expressed in decimal fractions for the purpose of computation, $L_e = 0.8333$ and $L_w = 0.1667$.

$$b) \qquad (1 - \lambda_e) + (1 - \lambda_d) = 0.1235 ,$$

from the depth of our light-curve. Of necessity, the solution is a series of approximations by the trial-and-error method. This series is begun with the following preliminary elements:

a) $\sin \theta_e = 0.24$ from preliminary experiment with our light-curve
b) $\sin \theta_d = 0.40$ from our light-curve
c) $k_e = 0.20$ from Russell's solution

Plainly, there is no possibility of determining a darkening coefficient for the W core, owing to the difficulty of finding such subtle quantities from a light-curve that is greatly distorted by other physical effects. Because the W core is a hot, early-type object, we

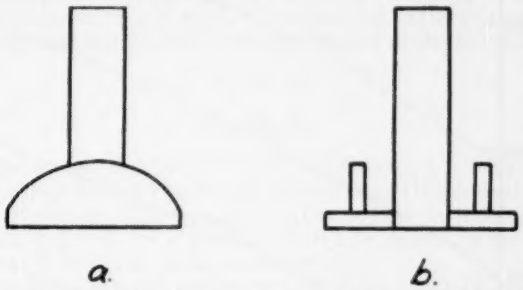

FIG. 3.—In these diagrams, which refer only to the luminous portion of the W-star, ordinates are proportional to surface brightness. The boundary lines above the base horizontal line would represent the variation in surface brightness across a diameter of the star if a direct-intensity trace could be made. The horizontal and vertical lines within the boundary are included to show how the several parts of the two models contribute to the total intensity, according to the analysis in the text.

assume for it a darkening coefficient of zero. The physical nature of the disk precludes the use of the limb-darkening conception in its intended form; however, the disk hypothesis is more successful for a light-distribution that decreases radially outward in intensity than for uniform illumination of the disk. The "darkened" tables provide a means for computing light-curves for disks with intensity falling off toward the edge, and we found by trial that the best fit was obtained by employing the tables for a limb-darkening coefficient of 0.8. Thus the W disk apparently has a light-distribution somewhat like that of a strongly limb-darkened star, though, of course, we do not wish thereby to convey the impression that the physical processes responsible for the two kinds of darkened limbs are at all similar. The tables referred to above, from which one obtains values of p, α, and k_d, are those of W. Zessevitch[18] and J. E. Merrill.[19]

It seems worth while to present the analytical procedure in some detail, inasmuch as it may be helpful to other investigators of nongeometrical eclipsing systems. For V 444 Cygni we begin with the assumption that $k_e = 0.2$ and, after finding reasonable fits to the light-curve on this basis, proceed to make solutions for $k_e = 0.175$ and 0.225. We first choose some arbitrary values of L_e and $1 - \lambda_e$, guided by the shape of the light-curve, which indicates approximately reasonable limits. It is convenient to pick a value of L_e and to compute α_{0e} from equation (1) for a few values of $1 - \lambda_e$. Then, for another value

[18] *Bull. Inst. Astr. Acad. Sci. URSS*, No. 50, 1940.

[19] Copy of unpublished data, courtesy of Princeton University.

of L_e we find values of $1 - \lambda_e$ corresponding to the same values of α_{0e} as for the first L_e. Several more such sets of $1 - \lambda_e$ and L_e may be computed later when one has a better idea of their probable range. If one has, as in the present case, a preliminary, fixed value of $\sin \theta_e$, then i and r_0 depend only on p_{0e} and hence on α_{0e}, since i and r_0 are found by solving equations (3) and (5a) simultaneously. In equation (3) $p_e = 1.0$ by definition.

In order to compute light-curves, we must also determine k_d. An approximate value for it may be found by solving equation (4), substituting several values of i and r_0, and letting $\sin \theta_d = 0.40$ as determined from the light-curve. In the present case, for $k_e = 0.2$, k_d has a small range around 0.65; if $\sin \theta_d$ is increased to 0.41, then k_d will be about 0.70. We may now narrow our range of possible combinations of $1 - \lambda_e$ and L_e by considering them functions of α_{0e}. Or, if we reason backward, since $\sin \theta_d$ is about 0.4, k_d is about 0.65 for certain i and r_0 values and hence for certain values of α_{0e}. We may limit our comput-

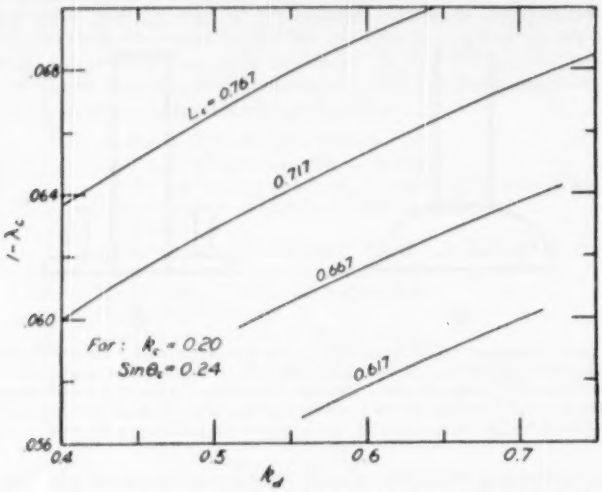

FIG. 4.—Example of curves prepared to aid in obtaining a physically consistent solution of the secondary minimum on the basis of the disk hypothesis.

ing to those values of $1 - \lambda_e$ and L_e which yield $k_d > 0.63$ and < 0.72. To each set of $1 - \lambda_e$ and L_e there are corresponding values of $1 - \lambda_d$ and L_d to equal the known total light and total light-loss of the W component. For these, values of α_{0d} are determined by equation (2). We find p_{0e} from Zessevitch's tables and compute $k_e p_{0e}$. We then look up, in Merrill's tables for 0.8 darkening, values of k_d and p_{0d} corresponding to α_{0d} to satisfy equation (6). Thus we have values of k_d of physically real significance for each set of $1 - \lambda_e$ and L_e. Because it is time-consuming in preliminary solutions to interpolate in Merrill's tables for nontabulated values of k_d, one may avoid this by plotting values of $1 - \lambda_e$ against k_d for the various sets of L_e, as shown in Figure 4. From the plot we can read the values of $1 - \lambda_e$ which correspond to $k_d = 0.65$ for each value of L_e.

The foregoing results now enable one to compute families of light-curves for values of $1 - \lambda_e$ and L_e based upon the same set of values, k_e, k_d, and $\sin \theta_e$. For each light-curve we compute $k_e p_{0e}$ and substitute it in equation (7) below, obtained by dividing equation (3) by equation (5a):

$$\sin^2 \theta_e \tan^2 i + 1 = \frac{(1 + k_e)^2}{(1 + k_e p_{0e})^2}.$$

From equation (7) we obtain $\tan^2 i$ and thus $\cos^2 i$, and, by substitution of this value and $k_e p_{0e}$ in equation (5*a*), we solve for $\frac{2}{0}$. An exact value of sin θ_d is found from equation (4) divided by equation (5*a*) that reduces to the form

$$\sin^2 \theta_d = \frac{[(1 + k_d)^2/(1 + k_e p_{0e})^2] - 1}{\tan^2 i}, \tag{8}$$

in which the terms $(1 + k_e p_{0e})^2$ and $\tan^2 i$ have already been determined.

We now proceed by means of equation (9), below, to compute preliminary light-curves, assuming convenient, arbitrary values of sin θ but including sin θ_d, and sin θ_e, and sin $\theta = 0.0$:

$$\sin^2 \theta \sin^2 i + \cos^2 i = r_0^2 (1 + kp)^2 . \tag{9}$$

Because the values of kp represent both $k_e p_e$ and $k_d p_d$, we may solve separately for values of p_e and p_d by dividing kp by k_e and k_d, respectively. At sin θ_d, $p_d = 1.0$; there are, of course, no values of p_e unless sin $\theta \leq$ sin θ_e. Corresponding values of α_e and α_d are found in the tables of Zessevitch and Merrill. Computed values of the light-loss are given by

$$1 - l_e = L_e \alpha_e , \tag{10}$$

$$1 - l_d = L_d \alpha_d . \tag{11}$$

The composite light-loss, i.e., the desired computed light-curve, is the sum of equations (10) and (11). Deviations from the smoothed curve through the normal points indicate the precision of the fit obtained. The sum of the squares of the deviations may be plotted against three values of $1 - \lambda_e$ on a parabolic curve to determine the best values of $1 - \lambda_e$ for a given set of values for k_e, k_d, and sin θ_e.

The next step was to make small variations in sin θ_e (to which the residuals are very sensitive), with the best value of $1 - \lambda_e$, to determine the value of sin θ_e that would yield the smallest deviations. Families of solutions in the case of V 444 Cygni were also made for $k_d = 0.70$, and new families for $k_e = 0.175$ and 0.225. The best elements obtained on the hypothesis of a sharp-edged luminous envelope about a bright core are given in Table 10. The residuals on the disk hypothesis for each normal point are given in Table 8.

TABLE 10

BEST ELEMENTS, DISK HYPOTHESIS

$k_e = 0.225$	$1 - \lambda_e = 0.0613$
$k_d = 0.75$	$1 - \lambda_d = 0.0622$
sin $\theta_e = 0.239$	$L_e = 0.0637$
sin $\theta_d = 0.403$	$L_d = 0.1030$
$i = 78°.4$	$L_w = 0.1667$
$r_0 = 0.2541$	$L_0 = 0.8333$

Representation with the best elements still gives small systematic deviations from the observed normal points, as shown in Figure 5. A perfect fit is not, of course, to be expected, in view of the crude theory upon which the computations are based. The sphere very likely does not have a perfectly sharp outer edge; the assumed spherical symmetry of the outer structure doubtless is not correct; and the distribution of light over the core probably is not uniform—to state only a few of the more obvious reasons why our theory is inadequate.

Because a diffused, rather than sharp-edged, spherical structure for the W component seemed logical, we were led to experiment with the computation of a few light-curves based on this theory. Since existing tables are useful only for sharp-edged disks, we found it necessary to perform mechanical integrations by graphical methods in order to treat

our problem. Two hypotheses were tested: (1) that the surface luminosity of the sphere decreased linearly with increasing distance from the core and (2) that the surface luminosity decreased exponentially with increasing distance from the core. The labor necessary for making complete solutions for the best fit was far too great to undertake; however, the results of our experiments, based on geometrical elements adopted from the disk solution, convince us that, improbable as it seems, the sphere must be nearly sharp-edged. The diffuse-edge hypothesis allows fair fits of the light-curve for small values of sin θ, but not for large ones. The reason is simply that only a sharp-edged sphere will begin and end the eclipse as abruptly as the observations indicate.

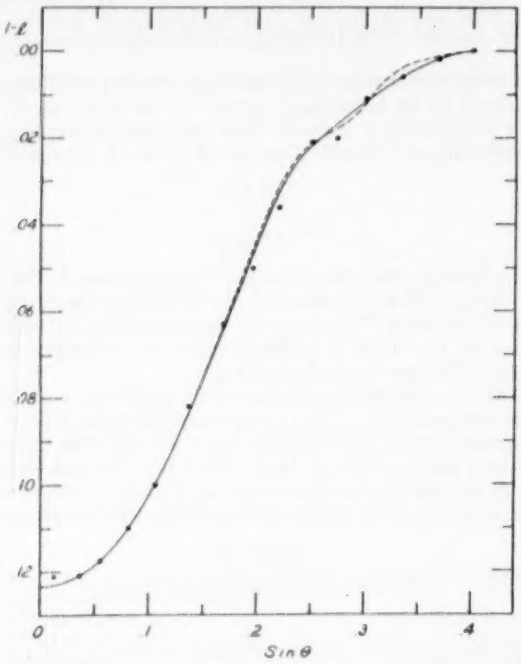

FIG. 5.—Normal points and computed curves for secondary minimum, λ 4500. The solid dots are reflected normals of ten observations each. The solid curve is the best fit obtained on the disk hypothesis. The broken curve is the best fit obtained on the ring hypothesis.

RING HYPOTHESIS

It appeared, from the above solution and extensive experimental computing, that the hypothesis of a "ring" of bright material disconnected from the core of the Wolf-Rayet component and superposed upon the disk, as shown in Figure 3, *b*, would reduce the systematic residuals found in the previous solutions. Again, there is no practical substitute for the trial-and-error procedure based upon physically consistent elements. Solutions on the ring hypothesis are far more laborious and not so straightforward; but, by this time, a computer is greatly aided by previous experience with the effects on the computed light-curve of changes in the various elements.

We adopt the following additional and alternative notation for a composite solution made up of a core, a disk pierced with a central hole whose diameter is equal to the

diameter of the core, and a ring. (A solution could also be made for a core, a simple disk, and a ring, although this method is more complicated because the total light of the core area remains unfixed until the solution is completed.) All primed symbols refer to a pierced disk. The symbols k_{r_1} and k_{r_2} refer, respectively, to the ratio of the inner and outer radius of the ring to the radius of the O component. Equation (8) will be used in the form

$$k'_d = (1 + k_e p_{0e}) \sqrt{1 + \tan^2 i \sin^2 \theta'_d} - 1 . \tag{12}$$

At any point in the eclipse, the equation for the fractional light-loss of the pierced disk is

$$\alpha'_d = \frac{\alpha_d - \alpha_e (k_e / k'_d)^2}{1 - (k_e / k'_d)^2} . \tag{13}$$

At conjunction we have

$$\alpha'_{0d} = \frac{\alpha_{0d} - \alpha_{0e} (k_e / k'_d)^2}{1 - (k_e / k'_d)^2} . \tag{14}$$

We adopt, on the basis of experience, $k_e = 0.225$, $\sin \theta_e = 0.239$, $\sin \theta'_d = 0.403$, and $\alpha_{0e} = 0.952$. Preliminary explorations revealed that $L_e = 0.0817$ is a reasonable value and therefore that $1 - \lambda_e = 0.778$. The value of $k_e p_{0e}$ is -0.1855. Values of i and r_o then follow. We solve for k'_d by equation (12) and find it equal to 0.745. From the relation $k_e p_{0e} = -0.1855 = k'_d p_{0d}$ we find p_{0d}. From the tables we find $\alpha_{0d} = 0.5718$. We now substitute α_{0d} and α_{0e} in equation (14) in order to find α'_{0d}:

$$\alpha'_{0d} = \frac{0.5718 - 0.952\,(0.225/0.745)^2}{1 - (0.225/0.745)^2} = 0.5337 . \tag{14}$$

Preliminary computations again were needed to find a good value of L_d, which proved, finally, to be 0.0450. From L'_d and α'_{0d} we find $1 - \lambda'_d = 0.0238$.

Computations for the ring include the following known and derived quantities: $k_e p_{0e}$, $L'_{r_2} = 0.0400$, $1 - \lambda'_{r_2} = 0.0219$, and $\alpha'_{0r_2} = 0.5475$. From previous experimental computing we estimate k_{r_1} to be equal to 0.50. The final step is to force the geometry into consistency with the light-elements by deriving k_{r_1} from equation (15), below, in a series of successive approximations:

$$\alpha'_{0r_2} = \frac{\alpha_{0r_2} - \alpha_{0r_1} (k_{r_1} / k_{r_2})^2}{1 - (k_{r_1} / k_{r_2})^2} . \tag{15}$$

Various values of k_{r_1} and corresponding α_{0r_1} are tried until α'_{0r_2} derived from equation (15) is equal to 0.5475, the value derived from $1 - \lambda'_{r_2}$ divided by L'_{r_2}. The best elements on the ring hypothesis are given in Table 11, the residuals are presented in the last column of Table 8, and the computed curve is indicated by the dashed line in Figure 5.

TABLE 11

BEST ELEMENTS, RING HYPOTHESIS

$k_e = 0.225$	$L_e = 0.0817$
$k_{r_1} = 0.455$	$L'_d = 0.0450$
$k_{r_2} = 0.500$	$L'_{r_2} = 0.0400$
$k'_d = 0.745$	$L_w = 0.1667$
$\sin \theta_e = 0.239$	$L_o = 0.8333$
$\sin \theta'_d = 0.403$	$1 - \lambda_e = 0.0778$
$i = 78°$	$1 - \lambda'_d = 0.0240$
$r_o = 0.2554$	$1 - \lambda'_{r_2} = 0.0217$

The residuals given in Table 8 indicate that the ring hypothesis has indeed reduced somewhat the tendency toward systematic deviations shown by the disk hypothesis. We do not believe, however, that the improvement is striking enough to merit adoption of the elements based on the ring hypothesis. Therefore, all the discussion that follows will be based upon the disk-hypothesis elements.

PRIMARY MINIMUM

The shape of the primary minimum is so seriously distorted by the physical effects of the extended atmosphere that very little quantitative data concerning the elements may be determined from the primary minimum alone. Derivation of the elements from the secondary minimum, however, should make possible the use of the primary minimum for a study of the physical effects themselves, because one now should be able to separate the physically caused light-variations from those caused by the simple geometry of the eclipse. Indeed, if the elements are really accurate, one would have the hope, at first, that separation of geometrical from physical effects could be accomplished with considerable success and that quantitative results bearing on the physics of the system would come from the primary minimum.

The most important geometrical constant required for investigation of the primary minimum is the ratio of the radii, k. Unfortunately, it is this very constant that is left in greatest doubt by the solution of the secondary minimum. We would expect that neither value of k derived on the disk hypothesis would represent the effective diameter of the W star as an opaque occulting object. In practice, we found that a new value, for an *effective* k, would, indeed, have to be derived from the observations of primary minimum. This circumstance complicates the analysis of the primary minimum and seriously limits the physical information that can be derived from the minimum.

The analysis of the primary minimum proceeded by trial of the easiest possible hypothesis, that of an opaque core for the W star, surrounded by a circular, semitransparent disk, eclipsing a circular luminous sharp-edged disk (the O component). We have arbitrarily set the darkening coefficient of the O component equal to 0.4. A solution for elements based upon this hypothesis can be made with existing tables. The inclination, the diameter of the O component, and the light-elements are adopted from the disk-hypothesis solution of the secondary minimum. From the primary minimum we derive the effective k of the opaque core, the effective k of the absorbing disk, and the mean transmission of the disk from the observed depth of the minimum, from the time of beginning of light-loss, and from the minimum's general shape.

The light-loss of the O component at any moment during primary minimum is given by

$$1 - l_o = (1 - l_c) + (1 - l'_d), \tag{16}$$

where the subscripts c and d refer to the light occulted by the core and by the absorbing disk of the W component, respectively. The solution for $1 - l'_d$ is complicated by the fact that it is not independent of k_c.

We shall first proceed with the solution for the light-loss caused by the disk, since its size is fixed for all models of the W component based on our chosen hypothesis. We estimate the beginning of eclipse to be at $\sin\theta = 0.65$. Substituting this value in equation (9), we find K'_d, the ratio of the disk radius to that of the O component, to be 1.632. We use existing tables and equation (9) for the solution, but, because primary eclipse is defined as the transit eclipse, we must use the *reciprocal* of 1.632, denoted by $1/K'_d$, which is equal to 0.6125. We must also use a *reduced* value of r_o. The reduced value, R_o, is related to r_o by

$$R_o^2 = \frac{(1 + K'_d)^2}{(1 + [1/K'_d])^2}\, r_o^2 = \frac{(1 + 1.632)^2}{(1 + 0.6125)^2}\, r_o^2 = 2.663\, . \tag{17}$$

From the tables we find values of a_d for a whole disk. In order to convert them to values of a_d' for a disk with a hole, we must subtract the corresponding values of a_c, corrected by a factor to reduce them to the system of the disk solution in which $1/K_d'$ and R_0 are used. This correction for the core is given by

$$a_d' = a_d - k_c^2 a_c . \tag{18}$$

Equation (18) for the transit of a pierced disk is analogous to equation (15) for the occultation of a pierced disk.

The computation for the light-loss caused by a semitransparent disk with a hole obviously cannot proceed without a value of k_c. Although, as stated above, neither of the k-values derived from the secondary-minimum solution would describe the effective diameter of the opaque core, we shall illustrate the solution technique by first trying our value $k_c = 0.225$. Values of a_c are computed by equation (9), in which the values of i and r_0 are those fixed by the solution of secondary minimum. We compute values of $k_c^2 a_c$ for each value of sin θ and then find the values of a_d' by equation (18). The light-loss at conjunction for a semitransparent disk with a hole is given by

$$1 - \lambda_d' = (1 - f) L_0 a_{0d}' , \tag{19}$$

where f is the mean effective transmission factor of the extended atmosphere. Since f is unknown, we must first solve for the light-loss caused by the opaque core, from equation (20):

$$1 - \lambda_c = L_0 k_c^2 a_{0c} . \tag{20}$$

We find $1 - \lambda_d'$ by subtracting $1 - \lambda_c$ from the total light-loss, $1 - \lambda_0$. A value for f will follow from equation (19). In the solution where $k_c = 0.225$, $1 - f = 0.243$. Values of the light-loss for each normal point are then computed. The model based on a core with $k_c = 0.225$ yields the residuals given in the fourth column of Table 8 and gives the computed curve indicated by the dashed line in Figure 6. It is now apparent that we can approach the final solution by finding an approximate value of $1 - f$ that will give very small residuals during the part of the eclipse due to the envelope alone. We find that $1 - f = 0.16$ will produce this result, and we impose this condition upon the solution. By trial and error we find a value of k_c which will give the observed depth of minimum. It appears that $k_c = 0.45$ will be satisfactory, and we now proceed to make a physically consistent solution, fixing the value of $k_c = 0.45$ and solving for $1 - f$. The residuals from this solution are small, though systematic. Two further refinements are to set the computed depth of minimum equal to 0.212, rather than 0.216, and the beginning of eclipse at sin $\theta = 0.675$. The final residuals for a model with $k_c = 0.45$ are given in the fifth column of Table 8; the computed curve is given by the solid line of Figure 6. The final elements are given in Table 12. Little further reduction in the size of the residuals on our chosen hypothesis is possible. The transmission factor, f, is found to be 0.858.

TABLE 12

BEST ELEMENTS, PRIMARY MINIMUM

k_c	= 0.45	L_0	= 0.8333
K_d'	= 1.722	$1 - \lambda_c$	= 0.114
sin θ_c	= 0.313	$1 - \lambda_d'$	= 0.098
sin θ_d	= 0.675	f*	= 0.858
i	= 78°.4	from secondary minimum	
r_0	= 0.2541	(disk hypothesis)	

* The quantity f is the mean effective transmission of light per unit area of the plane projection of the extended atmosphere of the W component.

The run of residuals for the case $k_c = 0.225$ indicated at once that a better fit can be obtained by an increase in the value of k_c. This is good observational evidence that the W component, when in the role of an occulting object, has an effective diameter considerably greater than that of the core itself. It means, therefore, that the structure surrounding the core has considerable opacity, as it must have if we are to have an acceptable hypothesis that this material can transmute the high effective temperature of the core into the relatively low color temperature observed for W stars. Indeed, as the final solution indicates, the effective occulting diameter of the W star is twice the core diameter, and the surface area is thus no less than four times that of the core. The residuals of the best fit, on the other hand, are small enough to suggest that the hypothesis of a uniform semitransparent disk surrounding the W component must be nearly correct. A schematic diagram of the system of V 444 Cygni according to the present analysis is given in Figure 7. The run of residuals in the region of $\sin\theta = 0.3$ is not disturbing. This is the region near which the transfer from absorption of the outer structure alone to a combination of absorption and occultation from the inner structure occurs. The computed curve shows a

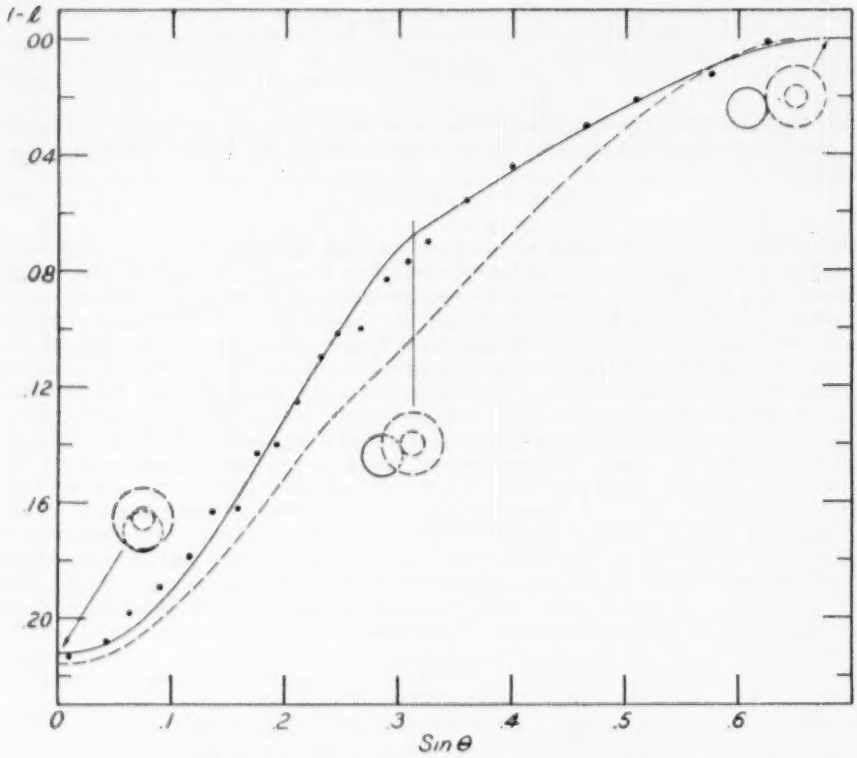

FIG. 6.—Normal points and computed curves for primary minimum, λ 4500. The solid dots are reflected normals of ten observations each. The broken curve is obtained by assuming a W-core diameter equal to that derived from the secondary minimum. The solid curve is the best fit obtained as described in the text. The small diagrams illustrate the apparent configuration of the system at three epochs during the minimum. The solid circle represents the *O*-component, the dashed circles represent the occulting parts of the W-star.

more sudden transition than the observed one; however, this can be easily explained as the result of our use of a model with sharp-edged components (particularly for the inner structure) in place of the edgeless condition that undoubtedly exists in reality. In order for the primary minimum to start as suddenly and decisively as it does, however (see Figs. 1 and 6), the absorbing envelope must, in effect, be nearly sharp-edged. The good fit of the portion of the curve due to the envelope alone is remarkable and good—evidence that our simplifying assumption of a uniform absorption for the envelope must be near the truth. Fortunately, a single, simple structure for the distribution of material in the absorbing envelope will explain at once both the evident sharp-edged effect and the apparently uniform distribution of effective absorption possessed by the envelope. *This structure is that of a thin, hollow shell.* A shell with a tenuous edge can act like a sharp-edged structure when it plays the role of an occulting object, owing to the extreme rapidity with which the absorbing power will vary as a function of radius; for both the den-

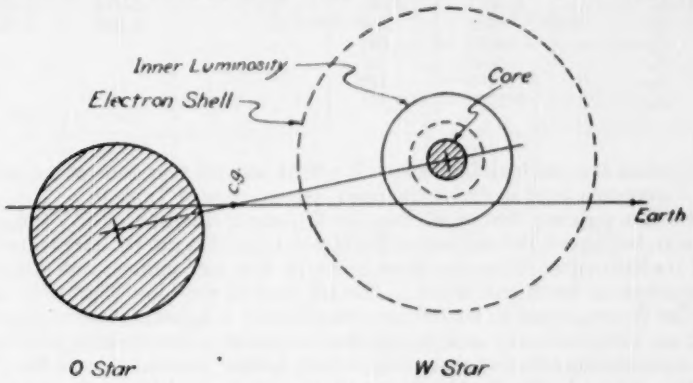

FIG. 7.—Schematic diagram of the system of V 444 Cygni. The hatched areas are at all times opaque. The regions of the W-star delineated by dashed lines are effective in primary minimum; those regions outlined by solid lines are effective in secondary minimum. Only the disk hypothesis is represented in this diagram. The outer solid line is the luminous disk. The inner dashed line represents the effective size of the W-star as an opaque occulting object.

sity of the material and the effective thickness (especially the latter) will be increasing at the same time, as the radius grows smaller. As the center is approached more closely, however, the hollow region is encountered, with a resultant tendency toward uniformity of absorption. We regard this description of the distribution of absorbing material in a thin, hollow sphere as one of the chief contributions made by our photometric study of V 444 Cygni. It is an unfortunate circumstance that the complexity of the structure results in so large a degree of indeterminacy to the solution as to prevent a careful analytical examination of the properties of the absorbing envelope from the light-curve.

ELEMENTS FROM THE LIGHT-CURVE AT λ 7200

Analysis of the light-curve in the red also started with the secondary minimum. We found that a satisfactory fit could be obtained by adopting from the λ 4500 solution the geometrical elements i, r_o, k_e, and k_d and by solving for the light-elements, L_o, L_e, and L_d. The solution for the light-elements was very simple and straightforward because we could represent the λ 7200 light-curve by changing only the values of $1 - \lambda_e$ and $1 - \lambda_d$. The rectified primary minima were almost identical in both colors, except that the λ 7200 primary was slightly shallower than the primary at λ 4500. The derived value of L_o (from the secondary minimum) was just enough smaller than Beals's value to repre-

sent exactly the λ 7200 primary minimum without change in any other element. There is, perhaps, some suggestion that the eclipse of the W component's disk begins later at λ 7200 than at λ 4500, an indication that the disk may appear slightly smaller in the longer wave length. The effect, however, is too small to be measured without use of observations of improved precision. The light-elements are given in Table 13, and the

TABLE 13

LIGHT-ELEMENTS AT λ 4500 AND λ 7200

Secondary Minimum			Primary Minimum		
	λ 4500	λ 7200		λ 4500	λ 7200
$1-\lambda_c$	0.0613	0.086	$1-\lambda_c$	0.114	0.111
$1-\lambda_d$	.0622	.060	$1-\lambda_d$	0.098	0.095
L_c	.0637	.089			
L_d	.1030	.100			
L_W	.1667	.189			
L_O	0.8333	0.811			

normal points and residuals in Table 9. It will be recalled that pairs of normal points in Table 7 were combined to derive the observational data of Table 9.

These data indicate, first of all, that the W component appears, by comparison with the O star, brighter in the red than in the blue—a fact that can be determined by inspection of the light-curve. They also show, however, that the luminous-disk structure of the W component is much less bright in the red than in the blue. That is to say, as one views the W component in longer-wave-length light, it appears more and more like the core alone. This result may indicate that the material of which the inner structure is composed shows strong selective absorption, which, in turn, accounts for the red color of the Wolf-Rayet star, despite the high temperature of the core. We may have here a general explanation for the surprisingly low apparent color temperature of Wolf-Rayet stars.

The almost total insensitivity of the primary minimum to change in wave length is the evidence that the outer atmosphere is composed of a preponderant number of free electrons, compared with the number of other kinds of particles. The particular constant involved is, of course, the factor f, which was found to be independent of wave length. The small change in the depth of the minimum is entirely accounted for by the change in relative luminosities of the two components with wave length.

IV. INTERPRETATION

ABSOLUTE DIMENSIONS

Our values for the orbital inclination, i, and r_o, can be combined with the spectrographic elements in the usual way to yield absolute dimensions for the system of V 444 Cygni. Two spectrographic orbits are available, O. C. Wilson's[3] and E. S. Keeping's;[1] Table 14 gives derived values of absolute elements based upon both of these orbits.

The chief difference between the two spectrographic orbits lies in the K-value (semi-amplitude) for the O star, for which Wilson gives 120.7 ± 5.8 km/sec, while Keeping finds 172.6 ± 5.5 km/sec. This difference results in the generally larger dimensions yielded by Keeping's data.

TEMPERATURES

Effective temperatures can be derived for the W star by comparison with the O star, provided that the temperature of the latter is known. The comparison between the two stars can be made by employing the absolute magnitudes in the usual way.

The spectrographic and photometric orbits have yielded absolute masses and diameters for both components of V 444 Cygni. The mass and the diameter of the O star can be used independently to provide two determinations of absolute bolometric magnitude by comparison with other systems of binary stars composed of early-type components.

The properties of three early-type systems have been exhaustively discussed by Kuiper[20] from the point of view of determining relations between the bolometric absolute magnitudes of such stars and their masses and radii. The stars are AO Cassiopeiae, 29 Canis Majoris, and Y Cygni. Figure 8 is a plot of significant data of these three stars and of three more, AH Cephei,[21] SX Aurigae,[22] and V Puppis.[22] The last three stars are included because they depend upon new determinations not available to Kuiper and because they evidently define mass-luminosity and radius-luminosity laws different from those defined by the AO Cassiopeiae sequence. The mass and radius data for V 444 Cygni A establish beyond reasonable doubt that this star belongs to the AO Cassiopeiae sequence, and we therefore derive absolute bolometric magnitudes for V 444 Cygni A by employing Figure 8. From Keeping's data we find $M_{bol} = -8.9$ (from mass) and $M_{bol} = -8.1$ (from radius). Wilson's data yield $M_{bol} = -8.1$ and -7.8. Owing to the closer agreement between the two values derived from Wilson's spectrographic elements, we adopt -8.0 for the absolute bolometric magnitude of V 444 Cygni A.

TABLE 14

ABSOLUTE DIMENSIONS OF SYSTEM OF V 444 CYGNI

	O. C. Wilson		E. S. Keeping	
	Solar Units	log	Solar Units	log
Radius of orbit:				
O star	10.5		14.7	
W star	26.2		26.0	
Separation	36.6		40.7	
Radius of components:				
O star	9.3	0.968	10.3	1.013
W core	2.1	0.32	2.3	0.36
W disk	7.0		7.8	
W envelope	16		18	
Mass:				
O star	26.4	1.422	32.8	1.516
W star	10.4	1.017	18.5	1.267
Density:				
O star	0.033		0.030	
W core*	1.12		1.52	

* Calculated on the assumption that the entire mass of the W star is concentrated in the core.

We now use the data in Kuiper's Table 3[23] and the equation

$$M_v = \frac{29{,}500}{T_e} - 5 \log R - 0.42 + 2.5 \log \left(1 - 10^{-11760/T}\right) \qquad (21)$$

[20] *Ap. J.*, **88**, 472, 1938.

[21] C. M. Huffer and Olin J. Eggen, *Ap. J.*, **106**, 313, 1947.

[22] D. M. Popper, *Ap. J.*, **97**, 394, 1943.

[23] *Ap. J.*, **88**, 446, 1938.

to derive, respectively, the absolute visual magnitude, M_v, and the effective temperature of the O component. The quantity M_v for the W star can now be derived by employing Beals's magnitude difference, 1.75. From equation (21) we then find the effective temperature of the W component, assuming, first, that all radiation is intercepted after coming from the core and, second, that all radiation is dissipated from a sphere the size of the luminous shell. These data are given in Table 15. The relation between luminos-

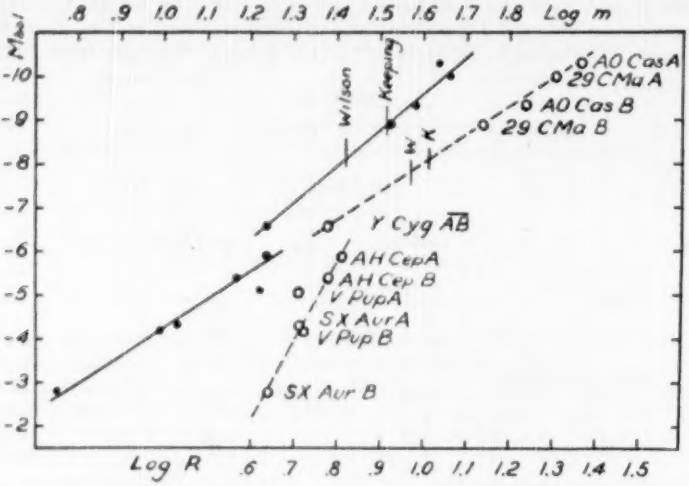

FIG. 8.—Determination of the luminosity of the O-star from its mass and radius. The solid lines represent mass luminosity, the broken lines represent radius luminosity for selected stars identified on the diagram.

TABLE 15

LUMINOSITY AND TEMPERATURE DATA FOR COMPONENTS OF V 444 CYGNI

	O-Star	W-Star		O-Star	W-Star
M_{bol}	−8.0		log T_e	4.48	
Bol corr.	−3.17		T_e	30,200° K	80,000° K (core) 16,500° K (shell)
M_v	−4.83	−3.08			

ity and spectral type given by Kuiper's Table 3 yields, for the derived spectral type of the O star, the value O9, which is bracketed by the observed values O6 (Beals) and B1 (O. C. Wilson).

The shell temperature is in reasonable agreement with the determination of 13,070° by Gaposchkin[24] and with various determinations of the apparent color temperatures of Wolf-Rayet stars, the most recent of which is that by W. Petrie.[25] The core temperature is in good agreement with many determinations of excitation temperature of W stars, well represented by the work of Aller.[26]

PARALLAX

The total absolute magnitude of V 444 Cygni, $M_v = -5.03$, and the apparent visual magnitude, 8.04, lead to a distance modulus of 13.1 mag., or a parallax of 0".00025; but

[24] *Ap. J.*, **93**, 202, 1941.

[25] *Pub. Dom. Ap. Obs., Victoria*, **7**, 392, 1947. [26] *Ap. J.*, **97**, 135, 1943.

these values are greatly in error, owing to the heavy absorption of light in this region of space. A special study has been made of the region by Stebbins, Huffer, and Whitford,[37] and we can use their color-excess data directly for a determination of the amount of space absorption. The eight early-type stars that lie nearest in the sky to V 444 Cygni are listed with their true distance moduli, $m_0 - M$, and observed color excesses, E_1, as given by these authors, in Table 16. The data make two points clear: first, that the

TABLE 16

COLOR EXCESSES OF STARS NEAR V 444 CYGNI

Star	m_0-M	E_1	Star	m_0-M	E_1
HD 192422	9.1	+0.27	HDE 228841	10.8	+0.32
192639	9.7	+ .26	193443	9.3	+ .24
E 228548	10.6	+ .39	193514	9.5	+ .33
193183	8.2	+0.28	E 229221	10.0	+0.50

reddening in the relatively large range in distance by a factor of 3.3, represented by eight stars, is only roughly correlated with distance and, second, that the most distant star (E 228841) seems, at first, not nearly distant enough to be a reliable indicator of reddening for V 444 Cygni. However, let us accept the value of E_1 for E 228841, and compute from it the visual absorption up to this point in space. According to Stebbins, Huffer, and Whitford, the visual absorption is $7E_1$, or no less than 2.2 mag. for E 228841. Subtracting this from 13.1, the apparent distance modulus for V 444 Cygni, we find a corrected distance modulus of 10.9 mag., which places V 444 Cygni at approximately the same distance as E 228841. Inasmuch as the latter is, by chance, also the closest star of Table 16 to V 444 Cygni, we feel that adoption of the above value of absorption is justified, and we adopt 10.9 mag. as the distance modulus of V 444 Cygni; the corresponding distance is 1500 parsecs ($\pi = 0''.00067$).

COLORS

We have measured, on an arbitrary color system having a scale nearly the same as International, a relative color difference of 0.02 mag. between V 444 Cygni and HD 193514; the difference is in the sense that V 444 is redder than HD 193514. Stebbins, Huffer, and Whitford give for HD 193514, on their C_1 scale, $E_1 = +0.33$ and $C_1 = +0.10$, which lead to a normal or unreddened color on the C_1 scale of -0.23 mag. for this star. The color becomes -0.35 mag. on the International System, and from this value and our color difference we find -0.33 mag. for the unreddened International color index of V 444 Cygni. The color determination is for the mixture 80 per cent light from the O9 star and 20 per cent light from the W star. If we assume that the color of the W component is -0.05 mag. (as estimated from its derived temperature), then the correction to free the mixture from the color of the W component is -0.04 mag., which makes the International color index of the O star alone, freed of the effects of space-reddening and of the presence of the W star, -0.37 mag. Stebbins, Huffer, and Whitford (in their Table 2) give a normal $C_1 = -0^m.23$ for type O, equivalent to International $C = -0^m.34$. The close agreement in color acts as a partial over-all check on the consistency of the absolute dimensions and of the correction for space-reddening.

THE "REFLECTION EFFECT"

A comparison of the light-curves in the two colors (Fig. 1) shows that the equivalent of a "reflection effect" exists and that it is larger at the longer wave length, which is a fact that is expressed quantitatively by a larger value for the coefficient of cos θ derived for

[37] *Ap. J.*, **91**, 44–45, 1940.

λ 7200 during the rectification process. A thick atmosphere will probably be distorted by the gravitational action of the O star, which will cause a thickening at the side of the W star pointed toward the O star, and a thinning on the opposite side. Kopal[28] has suggested that this tidal effect can cause a brightening of the system when the thin side is toward the observer, owing to the reduced veiling of the core. Inasmuch as the thin side faces the observer near primary minimum, the effect should be the opposite of that of a true re-radiation effect, though in other respects its influence on the light-curve should be much the same. Our observations show that the system appears bluer near primary minimum than near secondary, and our solution indicates that the inner structure, or "disk," reddens the light from the core. Thus, if the role of the thick atmosphere is played by our inner disk, one would expect that tidal distortion would cause the binary to appear abnormally blue and bright near primary minimum; we find that it does appear bluer, and the small amount of "reflection effect" observed at λ 4500 raises the suspicion that the star is abnormally bright at the same time. Further observational material could possibly turn this effect to use, as an aid in improving our understanding of the properties of the W atmosphere. An ultraviolet light-curve of the variation between minima would be of particular interest, because the "reflection effect" might be reversed entirely for the shorter wave lengths.

The nature of the light-variation between minima is further complicated by possible effects of the electron envelope, provided that this envelope is tidally distorted. A thickening of the "electron envelope" on the side facing the O component will increase absorption of light from the inner structure of the W component in the region of primary minimum, thus adding to the "reflection effect" and supplying a third source of light-variation between minima. It is evident that a physical interpretation of the causes for light-variation between minima is difficult.

SOURCE OF THE EMISSION BANDS

The spectrophotometry of the λ 4686 emission band by O. C. Wilson[29] indicated that there was little, if any, perceptible eclipse of the λ 4686 light. Our model offers the inner luminous structure as a likely source for the emission bands; but any demonstration indicating that the λ 4686 light does not take part in the eclipse is evidence, though not necessarily proof, that the emission bands must come from somewhere else. Wilson's photographic spectrophotometry was not of highest accuracy; nevertheless, he has shown that the effect to be expected is large enough to have been detected by his methods, had it existed, and his results therefore cannot be directly explained by our model. Wilson has suggested that the effect might be decreased or masked entirely by compensation by some other effect not otherwise suspected. It is difficult to understand what type of structure can be assigned to the W component that will cause emission bands without suffering eclipse. Until some means is found for reconciling the photometric and spectrographic results, it may be well to place the origin of the emission bands in the category of an unsolved problem.[30]

RANDOM VARIATIONS IN LIGHT AND PHASE

The phase-shifts of the minima of V 444 Cygni (Table 5) and its intrinsic random variations in light are by no means unique. Both these effects have been noted in many

[28] *Ap. J.*, **100**, 211, 1944. [29] *Ap. J.*, **95**, 419, 1942.

[30] At the December, 1949, meeting of the A.A.S., W. A. Hiltner presented a paper in which he gave the light-curve for the λ 4686 band of the Wolf-Rayet eclipsing binary CQ Cephei. The light-curve was determined by means of a remarkable process of direct photoelectric spectrophotometry, and it indicated that the intensity of λ 4686 showed a conspicuous *increase* in intensity during both eclipses. This observation appears in direct contradiction to our explanation for the site of the emission bands. However, results obtained for CQ Cephei do not necessarily apply to V 444 Cygni, for the ordinary light-curves for the two stars indicate that their geometry must differ considerably. A direct test will, of course, depend upon precise spectrophotometry of V 444 Cygni itself.

other eclipsing variables, and they are currently receiving attention. In his study of β Lyrae, Kuiper devoted considerable discussion to changes in period of this star. In particular, Kuiper has shown that a transfer of mass from the larger to the smaller component will result in a lengthening of the period. No appreciable lengthening of the period has been noted for V 444 Cygni since it has been under observation. In addition, however, Kuiper[31] has pointed out that a change in the diameter of a component of a binary star can cause a change in the period. This possibility suggests a relationship between the instabilities in period and light of V 444 Cygni, for one would expect a temporary change in luminosity to accompany a temporary change in the diameter of a star. The cause for a change in diameter is, of course, still unexplained.

Temporary changes in the phases of minima of eclipsing variables need not necessarily be explained on the basis of changes in period. The eclipse phenomenon is related directly to the relative positions of the effective center of opacity of the occulting star and of the effective center of illumination of the occulted star. Either or both of these effective centers could possibly shift temporarily with respect to the center of gravity of the body with which it is associated. Such a phenomenon could cause a phase shift of a minimum without requiring a change in angular momentum of the system.

In the long process of observing V 444 Cygni and in the many discussions that have taken place with others interested in this unusual star, we have become indebted to many persons for help and advice. The 1943 observations were made with the help of C. A. Wirtanen, O. C. Wilson, G. P. Nagtegaal, V. K. Rasmussen, and Miss E. Pisani. We are indebted to O. C. Wilson, C. S. Beals, Z. Kopal, W. A. Hiltner, and G. Münch for discussion and advice.

[31] *Ap. J.*, **93**, 172, 1941.

MEASUREMENTS IN THE COMBINATION SPECTRA OF RW HYDRAE, BF CYGNI, AND CI CYGNI

PAUL W. MERRILL
Mount Wilson and Palomar Observatories
Received February 4, 1950

ABSTRACT

This article describes a preliminary study of combination spectra with a dispersion of 10 A/mm. Two hundred and sixty measured emission lines are listed with their estimated intensities in four combination spectra.

RW Hydrae.—Displacements of bright lines indicate a probable cycle of about 376 days. During the observed interval the velocity-curve for the dark lines had a slope opposite to that of the bright lines, tending to support the binary-star hypothesis. The triplets of *He* I yielded velocities differing from those of the singlets.

BF Cygni.—The rich bright-line spectrum presents many points of interest. Several lines of *Fe* II exhibited changing relative intensities that are difficult to ascribe to differences in population of the atomic levels concerned. Lines at λ 4177.7 and λ 6318.1 remain unidentified.

CI Cygni.—Forbidden lines of the following ions were measured: *O* III, *Ne* III, *Ne* V, *Fe* II, *Fe* V, *Fe* VII. The permitted *O* III line λ 3444 is sharp, while the [*Ne* V] line λ 3425 is broad. This behavior differs from that regularly observed in planetary nebulae.

Conclusions.—Systematic observations with fairly high dispersion will be required to reveal the true nature of "symbiotic" stars. Suggestions for future programs are included.

A combination spectrum presents an incongruous superposition of bright lines requiring high excitation upon a low-temperature dark-line spectrum resembling that of a red star. A number of combination spectra have previously been studied at several observatories on spectrograms having dispersions of 30–80 A/mm. A brief summary of the results, with numerous references, will be found in *Mount Wilson Contribution*, No. 688.[1] The behavior of the rich, bright-line spectrum is very complex. Lines of various elements, and even lines of different types of the same element, exhibit differences in structure and displacement; and the pattern changes radically with time in a way not yet well determined.

I have obtained a number of coudé spectrograms of four symbiotic stars for a preliminary study of the observational difficulties and of the importance of the returns. Results on Z Andromedae have already been reported.[2] The present article summarizes similar measurements on a few spectrograms of RW Hydrae, BF Cygni, and CI Cygni (see Table 1). The magnitudes were kindly supplied by the Harvard Observatory.

The inclusive list (Table 2) of emission lines measured on the coudé spectrograms of these four stars may be useful in other investigations. Wave lengths of a few forbidden lines are from recent measurements by O. C. Wilson[3] in the spectra of planetary nebulae; nearly all the others are from the *Revised Multiplet Table*.[4] The relative intensities of certain lines in each star are subject to considerable variation from time to time. Moreover, estimates in Table 2 are strongly affected by observational circumstances. Hence they will not yield an accurate comparison of the four stars; but they should give some idea of the observational material and of the general behavior of various lines in the four stars.

[1] *Ap. J.*, **99**, 15, 1944.

[2] *Mt. W. Contr.*, Nos. 728, 744; *Ap. J.*, **105**, 120, 1947; **107**, 317, 1948.

[3] *Mt. W. and Palomar Obs. Reprint*, No. 15; *Ap. J.*, **111**, 279, 1950.

[4] Charlotte E. Moore, *A Multiplet Table of Astrophysical Interest*, rev. ed.; *Contr. Princeton U. Obs.*, No. 20, 1945.

RW HYDRAE

HD 117970: 1900 R.A. $13^h28^m.8$; Dec. $-24°53'$; Mag. 9.7–10.9; Period 370 days

The absorption-line spectrum from the blue to the red closely resembles that of α Ceti, class gM2. Emission lines (see Table 2) are not so numerous as in some other combination spectra. The singlet lines of neutral helium, especially those of the $^1P-{}^1D$ series, are remarkably strong relative to the triplet lines, indicating that the density of the emitting gas is unusually low.

TABLE 1

COUDÉ SPECTROGRAMS

Plate (Ce)	Date	J.D. 243	Emulsion	Exp. (Min.)	Phot. Mag.
	RW Hydrae 132824				
4137	1946 Jan. 17	1838	103*a*-E*	166	10.3
4184	Feb. 17	1869	103*a*-E	220	10.4
4198	Mar. 21	1901	103*a*-E	110	10.4
4204	Mar. 23	1903	IIa-O	300	10.4
4312	June 19	1991	103*a*-D	176	10.3
4682	1947 May 6	2312	IIa-O	248	10.6
5129	1948 Mar. 22	2633	IIa-O	200	10.5
5682	1949 June 12	3080	IIa-O	174	10.6
	BF Cygni 191929				
5228	1948 July 18	2751	103*a*-E	250	11.2
5230	July 19	2752	IIa-O	454	11.2
5321	Sept. 13	2808	103*a*-E	340	11.3
5688	1949 June 13	3081	103-O	220	11.8
	CI Cygni 194635				
5332	1948 July 20	2753	IIa-O	436	13.0
5275	Aug. 16	2780	103*a*-E	360	13.0
5754	1949 July 14	3112	IIa-O	450	12.8

* Plates on the 103a-E or the 103a-D emulsions are of the visual region, dispersion 20 A/mm; those on the IIa-O or 103-O emulsions are of the photographic region, dispersion 10 A/mm.

The hydrogen lines, wholly in emission, yield consistent velocities, with the exception of $H\zeta$ and $H\alpha$. The $H\zeta$ line, λ 3889.05, is displaced shortward about 8 km/sec by the effect of the blended *He* I line λ 3888.65. The very intense $H\alpha$ line yields an average measured displacement of +21 km/sec with respect to the other *H* lines, the cause possibly connected with the overexposure of the image. The velocities from the singlet lines of *He* I are reasonably consistent and agree quite well with those of *H*. The velocities from the triplet lines are rather scattering but are, on the average, 18 km/sec greater than those from the singlets. A similar average difference of about +9 km/sec was found upon re-examining measures of the older low-dispersion spectrograms.[1] A displacement of the same sign was found in the spectrum of Z Andromedae.[2] Measures of the *He* II line λ 4686 are of low weight; taken at face value, they indicate a considerable negative displacement with respect to lines of *He* I and *H*.

TABLE 2

Emission Lines Observed in Combination Spectra

I.A.	Ident.	Estimated Intensity			
		RW Hya	BF Cyg	CI Cyg	Z And
3132.86	*O* III	.....	.....	2	.....
3312.30	*O* III	.....	.....	.....	1
40.74	*O* III	.....	.....	2	2
45.82	[*Ne* V]	.....	.....	4	4
3403.32	*Cr* II	.....	.....	.....	tr*
05.74	*O* III	.....	.....	tr	.....
11.76	*O* IV	.....	.....	tr	.....
21.20	*Cr* II	.....	.....	.....	tr
22.74	*Cr* II	.....	.....	.....	tr
25.86	[*Ne* V]	.....	.....	12	8
28.67	*O* III	.....	.....	2	1
30.3	[*Fe* V]	.....	.....	.....	tr
44.10	*O* III	.....	.....	12	5
38.98	*Mn* II	.....	.....	.....	tr
41.98	*Mn* II	.....	.....	.....	tr
3586.57	[*Fe* VII]	.....	.....	5	1
3634.28	*He* I	.....	.....	tr	.....
57.27	*H* 36	.....	tr	.....	.....
57.93	*H* 35	.....	tr	.....	.....
58.64	*H* 34	.....	tr	.....	.....
59.42	*H* 33	.....	1	tr	.....
60.28	*H* 32	.....	1	tr	.....
61.22	*H* 31	.....	1	tr	tr
62.26	*H* 30	.....	1	tr	tr
63.41	*H* 29	.....	2	tr	1
64.68	*H* 28	.....	2	1	1
66.10	*H* 27	.....	2	1	2
67.68	*H* 26	.....	3	1	2
69.47	*H* 25	.....	3	1	3
71.48	*H* 24	.....	3	2	3
73.76	*H* 23	tr	3	2	4
76.36	*H* 22	tr	3	2	4
77.82	*Cr* II	.....	1	.....	1
79.36	*H* 21	tr	3	2	5
82.81	*H* 20	tr	4	3	5
84.25	*Cr* II	.....	tr	.....	tr
85.19	*Ti* II	.....	tr	.....	tr
86.83	*H* 19	tr	4	3	5
91.56	*H* 18	tr	4	3	5
97.15	*H* 17	1	5	3	6
3703.86	*H* 16	1	5	4	6
05.04	*He* I	.....	tr	tr	1
06.03	*Ca* II	.....	1	.....	tr
11.97	*H* 15†	1	5	4	7
12.99	*Cr* II	.....	1	tr	1
15.45	*Cr* II	.....	tr	tr	tr
19.49	*Fe* I	.....	tr	.....	tr
21.94	*H* 14	1	6	4	7
34.37	*H* 13	1	6	4	8
36.90	*Ca* II	.....	1	tr?	1?
41.63	*Ti* II	.....	tr	.....	1
48.49	*Fe* II	.....	1	.....	.....
50.15	*H* 12	2	7	5	8
54.6	bl‡	?	.....	tr	2

* Trace: a very weak image.

† 3706.03. Ca II. Probably blended with 3706.22 *Ti* II.

‡ 3754.6. Identification uncertain; λ 3754.69 *Cr* II, 54.67 *O* III, and 55.5 [*Fe* V] may all contribute.

TABLE 2—*Continued*

I.A.	Ident.	Estimated Intensity			
		RW Hya	BF Cyg	CI Cyg	Z And
3759.29	*Ti* II	?	.....	2	4
59.8	bl§	?	.....	6	2
61.32	*Ti* II	.....	?	tr	1
62.89	*Fe* II	.....	tr	.....	.....
64.09	*Fe* II	.....	tr	.....	tr
69.46	*Ni* II	.....	1	.....	tr
70.63	*H* 11	2	7	6	9
83.4	bl‖	.....	2	.....	1
97.90	*H* 10	3	8	7	10
3819.64	*He* I	.....	3	2	3
24.44	*Fe* I	.....	.....	.....	tr
24.91	*Fe* II	.....	2	.....	tr
29.35	*Mg* I	.....	1	.....	tr
32.30	*Mg* I	.....	1	.....	tr
35.39	*H* 9	4	8	7	10
38.29	*Mg* I	.....	1	.....	1
39.6	[*Fe* V]	.....	.....	.....	2
48.24	*Mg* II	.....	1	tr	1
49.58	*Ni* II	.....	tr	.....	.....
50.40	*Mg* II	.....	tr	.....	1
53.66	*Si* II	.....	tr	.....	tr
56.02	*Si* II	.....	2	tr	2
62.59	*Si* II	.....	2	tr	2
67.53	*He* I	.....	.....	.....	1
68.76	[*Ne* III]	2	.....	4	8
71.82	*He* I	.....	tr	.....	tr
78.02	*Fe* I	.....	tr	.....	.....
78.58	*Fe* I	.....	tr	.....	.....
86.28	*Fe* I	.....	tr	.....	.....
88.65	*He* I	bl	bl	bl	bl
89.05	*Hζ*	8	10	12	12
91.60	[*Fe* V]	.....	.....	1	2
95.72	[*Fe* V]	.....	.....	.....	1
3900.55	*Ti* II	.....	1	.....	tr
05.53	*Si* I	1	3	2	1
13.46	*Ti* II	.....	.....	.....	tr
14.48	*Fe* II	.....	2	tr	1
26.53	*He* I	tr	.....	tr	1
30.31	*Fe* II	.....	1	tr	tr
33.66	*Ca* II	tr	3	3	1
38.29	*Fe* II	.....	3	2	2
45.21	*Fe* II	.....	2	tr	tr
61.59	*O* III	.....	.....	tr	tr
64.73	*He* I	3	4	2	6
67.49	[*Ne* III]	tr	.....	1	8
68.47	*Ca* II	tr	2	2	tr
70.07	*He*	8	12	15	15
74.16	*Fe* II	.....	1	tr	.....
4009.27	*He* I	2	1	1	2
26.19	*He* I	1	5	3	4
67.05	*Ni* II	.....	2	.....	.....
68.62	[*S* II]	.....	1	.....	1
71.6	[*Fe* V]	.....	.....	.....	tr
76.36	[*S* II]	.....	.....	.....	tr
97.31	*N* III	2	tr	2	3
4100.04	*He* II	.....	.....	1	.....
01.74	*Hδ*	12	18	20	20

§ 3759.8. Blend of λ3759.83 [*Fe* VII] and 59.87 *O* III.

‖ 3783.4. Perhaps blend of λ 3783.35 *Fe* II and 83.44 [*Fe* V].

TABLE 2—*Continued*

I.A.	Ident.	Estimated Intensity			
		RW Hya	BF Cyg	Cl Cyg	Z And
4102.93	*Si* I*	1	2	1	1
20.84	*He* I	1	tr	tr	2
22.64	*Fe* II	.....	3	.....	1
24.79	*Fe* II	.....	tr	.....	.....
28.05	*Si* II	.....	1	.....	tr
28.74	*Fe* II	.....	1	.....	tr
43.76	*He* I	5	1	2	5
61.52	*Ti* II	tr	tr	.....	.....
63.64	*Ti* II	.....	1	.....	tr
68.97	*He* I	tr	.....	.....	tr
71.90	*Ti* II	.....	tr	.....	.....
73.45	*Fe* II	.....	6	1	2
77.7	?	.....	4	.....	tr
78.86	*Fe* II**	1	6	2	3
99.83	*He* II	.....	.....	2	tr
4216.19	*Fe* I	.....	tr	.....	.....
26.73	*Ca* I	.....	tr	.....	.....
33.17	*Fe* II	2	6	3	4
42.38	*Cr* II	.....	tr	.....	.....
43.98	[*Fe* II]	tr	1	1	2
44.81	[*Fe* II]	.....	tr	tr	tr
58.16	*Fe* II	.....	2	.....	tr
67.14	*C* II	.....	.....	.....	1
71.76	*Fe* I	.....	1	.....	.....
73.32	*Fe* II	.....	2	.....	tr
75.57	*Cr* II	.....	tr	.....	.....
76.83	[*Fe* II]	.....	1	.....	2
78.13	*Fe* II	.....	tr	.....	tr
87.40	[*Fe* II]	.....	2	tr	3
90.22	*Ti* II	tr	tr	.....	tr
94.10	*Ti* II	.....	tr	.....	tr
96.57	*Fe* II	tr	5	1	2
4300.05	*Ti* II	tr	1	.....	1
01.93	*Ti* II	.....	1	1	tr
03.17	*Fe* II	.....	3	1	1
07.90	*Ti* II	1	1	.....	tr
12.86	*Ti* II	.....	1	.....	tr
14.29	*Fe* II	.....	2	.....	tr
37.92	*Ti* II	.....	1	.....	.....
38.67	*He* II	.....	.....	1	.....
40.47	*Hγ*	20	30	30	30
51.76	*Fe* II	1	6	2	3
59.34	[*Fe* II]	tr	1	tr	2
63.21	[*O* III]	6	tr	6	9
69.40	*Fe* II	.....	1	.....	.....
74.82	*Ti* II	.....	tr	.....	.....
75.93	*Fe* I	.....	1	.....	.....
83.54	*Fe* I	.....	2	.....	tr
84.21	[*Fe* II]	.....	.....	tr	tr
85.38	*Fe* II	.....	2	tr	1
87.93	*He* I	12	2	3	5
94.06	*Ti* II	.....	1	.....	.....
95.03	*Ti* II	.....	tr	.....	.....
95.85	*Ti* II	.....	tr	.....	.....
99.77	*Ti* II	.....	1	.....	.....
4413.60	*Fe* II††	.....	2	.....	tr

* 4102.93. *Si* I blended with 4103.37 *N* III.

** 4178.86. *Fe* II possibly blended, especially in BF Cyg, with 4178.95 [*Fe* II].

†† 4413.60. *Fe* II possibly blended with 4413.78 [*Fe* II].

TABLE 2—*Continued*

I.A.	Ident.	Estimated Intensity			
		RW Hya	BF Cyg	CI Cyg	Z And
4416.27	[*Fe* II]	tr		tr	2
16.82	*Fe* II		3	?	1
27.31	*Fe* I		1		
37.55	*He* I	2			1
57.95	[*Fe* II]				1
61.65	*Fe* I		1		
64.46	*Ti* II		tr		
68.49	*Ti* II		tr		tr
71.48	*He* I	10	10	8	6
72.92	*Fe* II		1		
81.23	*Mg* II		1		tr
82.17	*Fe* I		1		
88.75	[*Fe* II]				1
89.18	*Fe* II		3	tr	1
91.40	*Fe* II		4	tr	1
4501.27	*Ti* II		tr		tr
08.28	*Fe* II		3	tr	2
15.34	*Fe* II	tr	4	1	3
20.22	*Fe* II		4	1	2
22.63	*Fe* II		3	1	2
34.17	*Fe* II		2		1
41.52	*Fe* II		2	?	?
41.59	*He* II			2	2
49.47	*Fe* II		7	2	6
55.02	*Cr* II		tr		
55.89	*Fe* II	1	6	2	3
58.66	*Cr* II		tr		1
63.76	*Ti* II				tr
71.10	*Mg* I		tr	2	
71.98	*Ti* II				tr
76.33	*Fe* II		3	tr	2
80.06	*Fe* II		tr		
82.84	*Fe* II		2	tr	
83.83	*Fe* II	2	6	5	7
88.22	*Cr* II				1
4620.51	*Fe* II		2	tr	1
29.34	*Fe* II	2	7	5	7
34.16	*N* III	1		3	3
40.64	*N* III	2		7	6
41.90	*N* III	?			tr
47.40	*C* III	1		tr	1
49.14	*O* II			tr	tr
50.16	*C* III				tr
58.05	[*Fe* III]		10		
66.75	*Fe* II	tr	3		1
85.68	*He* II	40		30	20
99.28	[*Fe* VII]			2	2
4701.54	[*Fe* III]		4		
13.14	*He* I	12	2	4	4
31.44	*Fe* II		2		1
33.91	[*Fe* III]		tr		
54.69	[*Fe* III]		1		
69.43	[*Fe* III]		1		
4859.32	*He* II			2	
61.33	*Hβ*	50	60	60	60
4921.93	*He* I	20	tr	2	6
23.92	*Fe* II	2	3	tr	3
58.91	[*O* III]	1			4
5006.84	[*O* III]	3			7
11.26	[*Fe* III]		tr		?

TABLE 2—*Continued*

I.A.	Ident.	Estimated Intensity			
		RW Hya	BF Cyg	CI Cyg	Z And
5015.68	*He* I	20	1	tr	4
18.43	*Fe* II	1	1	tr	3
47.74	*He* I	tr			
5316.61	*Fe* II		2	1	
5411.52	*He* II			1	tr
5720.9	[*Fe* VII]			4	
54.8	[*N* II]		2		
5875.63	*He* I	15	15	25	8
5991.38	*Fe* II		tr		
6086.85	[*Fe* VII]			7	3
6238.38	*Fe* II		tr		
47.56	*Fe* II		2		
48.92	*Fe* II		tr		
6300.30	[*O* I]		2	3	1
11.02	[*S* III]		1		
18.1	?		4		
47.09	*Si* II		3		
63.85	[*O* I]		tr		
69.45	*Fe* II		tr		
71.36	*Si* II		1		
83.75	*Fe* II		3		
85.47	*Fe* II		2		
6416.90	*Fe* II		2		
32.65	*Fe* II		5	1	
42.97	*Fe* II		2		
56.38	*Fe* II		10		
91.28	*Fe* II		1		
93.05	*Fe* II		2		
6516.05	*Fe* II		5	1	
48.06	[*N* II]		9		
62.80	*Hα*	200	300	300	300
83.43	[*N* II]		20		
6678.15	*He* I	30	3	10	8

The measured displacements of various lines (Table 3) present a curious pattern. The meager data tend to bear out a cycle of about 1 year, perhaps equal to that of the light-curve. The plots in Figure 1 have been made on the assumption that the period is 370 days. As in the earlier measurements,[1] the velocities from lines of *H*, *He* I (singlets), and *N* III are in reasonable agreement. In the spring of 1941 the velocities seemed to be increasing. Comparison with the more recent measurements, chiefly in 1946, shows that the period is probably a few days more than a year. The overlapping portions of the curve (not well determined at either epoch) are about 1878 days apart. If five cycles have intervened, the period would be 376 days. The fact that the velocity-curve for the dark lines has a slope opposite to that of the bright lines seems to support the binary hypothesis, but more data are needed before a definite conclusion can be drawn.

BF CYGNI

1900 R.A. 19^h20^m0; Dec. $+29°29'$; Mag. *9.3–13.4*

Previous observations with low dispersion[6] showed that changes in the spectrum of BF Cygni are great and surprisingly rapid. The coudé spectrograms bring out details

[6] *Mt. W. Contr.*, No. 687; *Ap. J.*, **98**, 334, 1943.

more clearly than the earlier plates and show certain interesting changes, but they do not happen to include the striking variations of the lines of [*O* III]. Radial velocities derived from emission lines are in Table 4.

On plates Ce 5230 and 5688 (Table 1) numerous hydrogen lines and the Balmer continuum are strong in emission. On Ce 5688 these emission lines, measured as far as *H* 36, are accompanied on their shortward edges by narrow, well-defined absorption components measured from *H* 10 to *H* 35. Velocities from the emission lines progress from +49 km/sec at *H* 5 to +33 km/sec at *H* 35; velocities from the absorption components progress from −1 km/sec at *H* 10 to +8 km/sec at *H* 35. The absorption lines have the slower Balmer decrement; hence the slight positive progression may be due to the decreasing effect of the emission border, but the explanation of the negative progression of the emission lines is not obvious. On the same plate, Ce 5688, a faint emission component measured at *Hβ*, *Hγ*, and *Hδ*, yields the displacement −61 km/sec.

The peculiar difference in the behavior of the triplet and singlet lines of *He* I noted in

TABLE 3

RW HYDRAE: RADIAL VELOCITIES FROM VARIOUS LINES
(Km/Sec)

PLATE (CE)	J.D. 243	*H*	*He* I		*He* II	[*O* III]		[*Ne* III]	*N* III	*M* II	ABSORPTION	
			Sing.	Trip.		λ 4363	λ 4959 λ 5007				Velocity	No.
4137 red	1838	− 5.3	− 5.7	(+ 7.)	(−48)	.....	.....	.....	.....	.....	+22.4	22
4184 red	1869	+ 4.4	+ 1.0	+19.5	(−38)	.....	.....	.....	.....	.....	+22.5	31
4198 red	1901	+ 9.5	+ 5.	+34.	(−24)	.....	.....	.....	.....	.....	+17.8	9
4204	1903	+ 3.6	+ 1.3	+12.8	−24	+19	.....	(+6)	− 3	+ 9.0	+14.5	17
4312 yellow	1991	+19.7	.....	+41.2	.....	.....	.....	.....	.....	.....	+ 8.7	8
4682	2312	+ 6.2	+ 9.1	+23.1	− 7	+17	.....	+15	+ 7	+11.6	+ 9.5	8
5129	2633	+ 0.2	+ 5.4	+13.1	−20	+16	.....	+19	− 3	+ 8.4	+15.5	24
5682	3080	+13.6	+11.9	+37.	(+23)	+ 2	+6	+19	+17	+ 6.7	+ 6.1	18

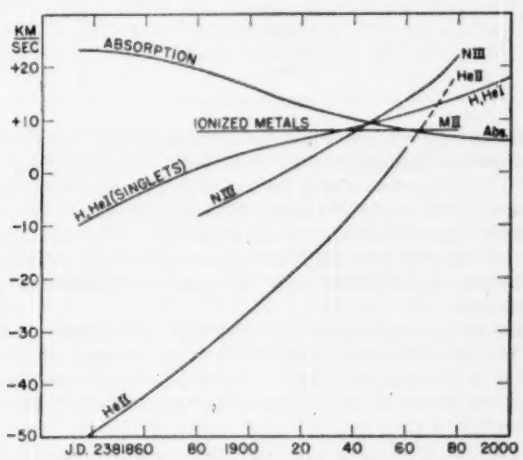

FIG. 1.—Radial velocities derived from various lines in the spectrum of RW Hydrae

RW Hydrae does not occur on the present plates of BF Cygni. On plate Ce 5688 the line λ 3888 seems to have an abnormal negative displacement, separating it from the strong $H\zeta$ line. The appearance may possibly be caused partly by an anomalous shortward component of $H\zeta$ comparable to that measured at $H\beta$, $H\gamma$, and $H\delta$.

A comparison of plates Ce 5230 and 5688 shows that on the second plate the lines of *He* I, *Mg* II, and [*Fe* II] are stronger, while those of *Fe* I, *Si* I, and *Ti* II are weaker. The interpretation of these complex changes may require extensive observations.

TABLE 4

BF CYGNI: RADIAL VELOCITIES FROM VARIOUS LINES
(Km/Sec)

Plate (Ce)	*H*	*He* I	*M* I*	*M* II†	[*Fe* II]	[*Fe* III]	[*N* II]
5228	+7.7 *Hα*	+ 1.4 2	.....	− 6.4 15	.....	.....	−12.0 2
5230	−7.2 32	− 7.8 8	−1.3 20	− 2.9 84	− 4.8 5	− 6.5 5	.....
5321	−9.9 *Hα*	+ 2.7 2	.....	+ 0.4 12	.....	.....	−14.4 2
5688	See text	+25.8 9	.....	+10.6 45	+ 6.5 6	+15.4 3	.....

* Neutral metals: *Mg* I, *Si* I, *Fe* I.

† Ionized metals: *Mg* II, *Si* II, *Ca* II, *Ti* II, *Cr* II, *Fe* II, and *Ni* II.

TABLE 5

RELATIVE INTENSITIES OF LINES OF *Fe* II
(Ce 5688:Ce 5230)

Mult.	Transition	No.	Rel. Int.
27	$b^4P-z^4D^\circ$	4	0.81
28	$b^4P-z^4F^\circ$		
	λ 4178	1	1.1
	λ 4296	1	1.4
37	$b^4F-z^4F^\circ$	8	0.94
38	$b^4F-z^4D^\circ$		
	λ 4549	1	0.41
	λ 4583	1	0.51
	Others	5	0.87

About 40 bright lines of *Fe* II were measured on plates Ce 5230 and 5688. Most of these lines have about the same intensity on the two plates, the multiplets[4] included being 3, 14, 22, 27, 29, 32, 37, 38; but two strong lines of multiplet 38, λ 4549 and λ 4583, are decidedly weaker on the second plate,[6] while λ 4296 of multiplet 28 is stronger. Microphotometer measures by Miss Louise Lowen are in Table 5. High accuracy is not possible on these narrow, low-density spectra. The explanation of the peculiar irregularities in intensity is not obvious; it is difficult to ascribe them to differences in population of the atomic levels concerned.

On both plates of the red region, Ce 5228 and 5321, the following bright lines are surprisingly strong: λλ 6383, 6385, 6442, 6491, 6493. They correspond to the second unclassified group of *Fe* II in the *Multiplet Table*.[4] The stellar intensities are in line with those listed. Mrs. Charlotte Moore Sitterly informs me that this multiplet has recently been classified as $z^4D^\circ-c^4D$.

[6] The weakening seems even greater on a low-dispersion spectrogram taken by Dr. E. R. Dyer, Jr., on August 15, 1949. I am indebted to Dr. Dyer for obtaining this plate.

Well-marked bright lines at λ 4177.7 and λ 6318.1 have not been identified. The first one may possibly be the same line as that measured at λ 4177.65 in the post-maximum spectrum of χ Cygni.[7] The probability seems against the identification of λ 6318.1 with [*K* v] λ 6316.6 or with *Fe* II $z^4D^\circ_{3(1/2)}-c^4D_{3(1/2)}$, λ 6317.98.

CI CYGNI

1900 R.A. $19^h40^m.5$; Dec. +35°26′; Mag. *10.8–13.0*

As in the other stars, the displacements of various groups of lines (Table 6) present

TABLE 6

CI CYGNI: RADIAL VELOCITIES FROM VARIOUS LINES
(Km/Sec)

Lines	Ce 5232	Ce 5275	Ce 5754
H	+11.0 29	+11.9* 3	+15.6 18
He I sing.	+11.6 9	+13 1	+18.2 5
He I trip.	+13.8 7	+24 1	+28.7 2
He II	+ 7.0 4	+ 5 1	+22.5 6
Fe II	+13.9 24	+ 9.6 3	+17.0 17
O III	+ 7.8 4	+12.4 3	+13.7 3
N III	+ 9.6 3	.....	+21 1 4
[*O* III] λ 4363	+20 6 1	.....	+17.5 1
[*Ne* III]	+24.8 2	.....	+17.4 2
Abs.	.....	+13.3 4	.....

* $H\gamma$, $H\delta$, $H\epsilon$, +11.9; $H\alpha$, +22.2.

a complicated pattern. The anomalous displacement of multiplet *Fe* II (37), previously measured,[1] does not occur on these coudé plates; but the unexplained weakening of *Fe* II (38), noted in BF Cygni, is shown by plate Ce 5754.

Forbidden lines of the following ions have been measured: *O* III, *Ne* III, *Ne* V, *Fe* II, *Fe* V, and *Fe* VII. On three plates showing the λ 3400 region, the permitted *O* III line λ 3444 is sharp, while [*Ne* V] λ 3425 is broad, with a wing or ill-defined component shortward. The behavior is the reverse of that in planetary nebulae,[3] where λ 3425 is regularly narrower than λ 3444. This fact is of interest in view of the possibility that objects like CI Cygni may exhibit in a rudimentary fashion some of the phenomena of planetary nebulae.

CONCLUSIONS

Not enough high-dispersion spectrograms of any star have been obtained to bring out in detail the complicated cyclical behavior or to allow great progress in solving the extraordinary physical problems involved. But as sample observations they have proved quite satisfactory. Their value lies (*a*) in revealing numerous faint lines in a continuous or complicated background, (*b*) in showing fairly small differences in line structure, and (*c*) in making possible measurements of displacements of individual lines accurate to a few kilometers per second. These items are of especial importance because differences in the behavior of lines of various ions and even of various multiplets from the same ion make very detailed investigations imperative. These stars abound in exceptions to normal behavior; almost nothing can be predicted or taken for granted. Hence, to solve the engaging physical and astronomical problems which they present, we will have to extend our knowledge the hard way by very detailed study of numerous high-dispersion spectrograms. The true physical nature of these "symbiotic" objects will probably remain obscure until such investigations can be made. Items that call for future study are:

[7] P. W. Merrill, *Mt. W. Contr.*, No. 735; *Ap. J.*, **106**, 274, 1947.

1. Cyclical changes in the structure, intensity, and displacement of bright lines of various elements.
2. Unusual differences in the behavior of multiplets from the same ion.
3. Resemblances to planetary nebulae. Lines of *O* III and [*Ne* V] in the region λλ 3100–3400 should be included in the investigation.
4. Displacements of absorption lines in the M-type spectra.

Future programs.—The eighth-magnitude star AG Pegasi, BD+11°4673, which has a combination spectrum differing somewhat from those discussed in the present article, is now under observation at Mount Wilson. The results will be reported soon.

The southern declination of RW Hydrae and the fact that its period differs so slightly from a year make difficult a satisfactory investigation from northern latitudes. This variable should be observed from a southern station.

Spectrograms of AX Persei, CI Cygni, and Z Andromedae should be obtained about every 3 weeks throughout the observing season for 3 or 4 years. The rapidly changing variable BF Cygni should be observed every night until its cyclical behavior is ascertained. The time is in sight when satisfactory spectrograms of these objects at 10 A/mm can be obtained with average seeing in 3 hours. At this rate the program just suggested would present relatively little difficulty.

STUDIES OF FAINT B-TYPE STARS

DANIEL M. POPPER
Department of Astronomy, University of California, Los Angeles
Received September 20, 1949

ABSTRACT

Magnitudes, colors on the C_1 scale, spectral types, and radial velocities for 253 O–B6 stars having magnitudes mostly between 8.5 and 11 are tabulated. The stars included are, in general, those described in two earlier papers; considerable additional data have been determined, including colors for all stars. A brief discussion of some of the results is given.

In two previous papers[1] observations of the radial velocities and spectral types of 268 B-type stars with magnitudes between 8 and 12 were presented. In Paper I (118 stars) photographic magnitudes and color indices were also published; in Paper II (150 stars) no colors were given, while magnitudes were available for a majority of the stars. The complete material for the colors and magnitudes of the stars of Paper II has now been reduced.

Photographic magnitudes of the stars of Paper II are derived from the same sources as those discussed in Paper I. The accompanying tabulation shows the sources of the

	Source	No. of Stars
A	UV camera	106
B	Ross camera	54
C	*Bergedorfer Spektral-Durchmusterung*	24
D	Stebbins, Huffer, and Whitford	4
E	No modern determination	10
	A and B combined	42
	B and C combined	6
	A and D combined	5
	B and D combined	2

magnitudes of the combined material. Fifteen stars of type later than B6 have been deleted from the earlier lists, leaving 253.

The magnitudes of 17 stars depend on a single UV exposure apiece, and those of 47 on a single Ross plate. The UV magnitudes, on the average, are based on 2.7 plates per star, the far southern stars having generally 3 or more plates each. According to Seyfert,[2] the probable error of a magnitude determined from a single Ross plate is ± 0.10. For a UV magnitude, which depends on measures of extra-focal images, the internal agreement between different plates is considerably better. The mean systematic difference, Ross *minus* UV is -0.06 mag. (± 0.17, taken without regard to sign); Ross *minus* Bergedorf is $+0.06$ mag. (± 0.26, taken without regard to sign).

The adopted magnitudes are given to 0.1 mag. in Table 1. Although the precision of the magnitudes varies considerably from star to star, for the most part the uncertainty is not greater than 0.1 mag. When the decimal is unreliable, a colon (:) follows the adopted magnitude.

[1] C. K. Seyfert and D. M. Popper, *Ap. J.*, **93**, 461, 1941; hereafter cited as "Paper I"; D. M. Popper, *Ap. J.*, **100**, 94, 1944; hereafter cited as "Paper II."

[2] *Ap. J.*, **91**, 117, 1940.

Some of the published values of Papers I and II have been revised on one or more of the following bases: (1) Inclusion of additional observational material. (2) Adoption of the magnitudes of the *Bergedorfer Spektral-Durchmusterung*, without the systematic correction applied in Paper I. (3) Adoption of the UV magnitudes as reduced, without the correction of −0.11 mag. used in Paper I. Rediscussion of the colors (see below) removes the basis for the correction. (4) Revision of the magnitudes of stars south of declination −30°. This revision is based on the removal of an apparent discrepancy between the colors of southern stars of Paper I determined photographically and those determined spectrophotometrically. The line of reasoning involved is fairly complex and need not be given here, except to state that, in order to compensate for an incorrect reduction from colors on Stebbins' C_1 scale (spectrophotometrically determined) to colors on the International System (photographically determined), an incorrect extinction factor had been employed. The colors of southern stars from the two methods are in good agreement if the proper factors are used. The fictitious correction, −0.11 mag., mentioned in (3) has a similar origin.

In addition to determining the colors of the stars of Paper II, it has been necessary to revise completely those published in Paper I. All colors are reduced to the C_1 system rather than to the International System. As described in Paper I, colors have been determined both photographically and spectrophotometrically. The sources for the adopted colors are as follows:

Source	No. of Stars
Spectrograms and photographs combined	161
Spectrograms alone	62
Stebbins, Huffer, and Whitford	30

The preponderance of the weight of the colors lies in the spectrophotometric determinations. The average number of spectrograms used for the 223 stars is 1.8. The mean difference, on the C_1 scale, between the two values of the color of a star from two spectrograms is ±0.06 mag., corresponding to a probable error of ±0.025 mag. The larger value, ±0.08, quoted in Paper I is on a scale 1.6 times the C_1 scale and, in addition, appears to have an error in it; for a recomputation for the stars of Paper I alone yields ±0.03 mag. on the C_1 scale. The spectrophotometric procedure employed to obtain colors from the spectrograms is described in Paper I. An example of a calibration-curve of the measured colors, C_{sp}, against C_1 (Stebbins' values) is shown in Figure 1. The calibrations for the stars of Paper II are more secure than those for the stars of Paper I. In the table of observations (Table 1) no attempt is made to indicate the reliability of each adopted color. For most stars the uncertainty should not exceed 0.04 mag. If the second decimal is completely uncertain, a colon follows the adopted value.

It is well known[3] that one obtains relationships between colors of space-reddened stars which are different from those for stars of varying temperature. This difference is clearly shown in the spectrophotometric measures. Figure 2 shows the color correlations between C_1 and C_{sp} for unreddened B stars, reddened B stars, and relatively near-by A5–F2 stars of the North Polar Sequence. The slopes, C_{sp}/C_1, are 1.5 for unreddened stars and 2.6 for space reddening. The C_1 values are taken from two of Stebbins' papers.[3, 4] The wave-length base line of the C_{sp} system is 2.3 times as long as that of the C_1 system.

The adopted radial velocities of some of the stars of Paper I have been altered slightly, in order to unify the system of weighting the individual measurements. The velocities of

[3] See, e.g., J. Stebbins and A. E. Whitford, *Ap. J.*, **102**, 318, 1945.

[4] J. Stebbins, C. M. Huffer, and A. E. Whitford, *Ap. J.*, **91**, 61, 1940.

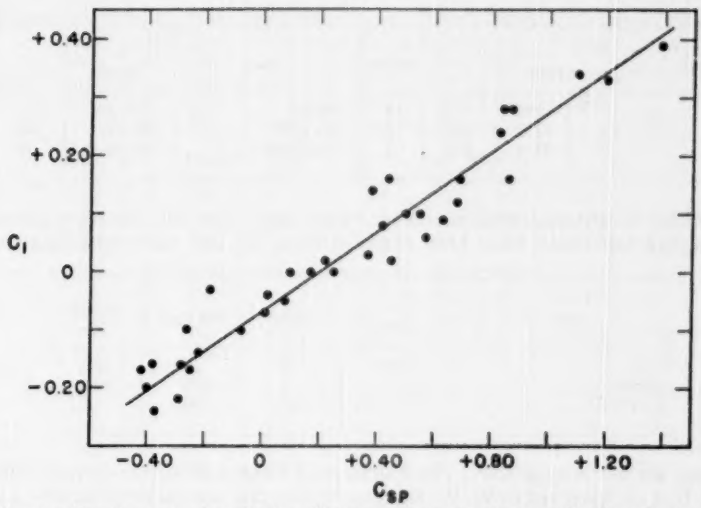

FIG. 1.—A calibration-curve for reducing differences in spectrophotometric color, C_{sp}, to differences in C_I.

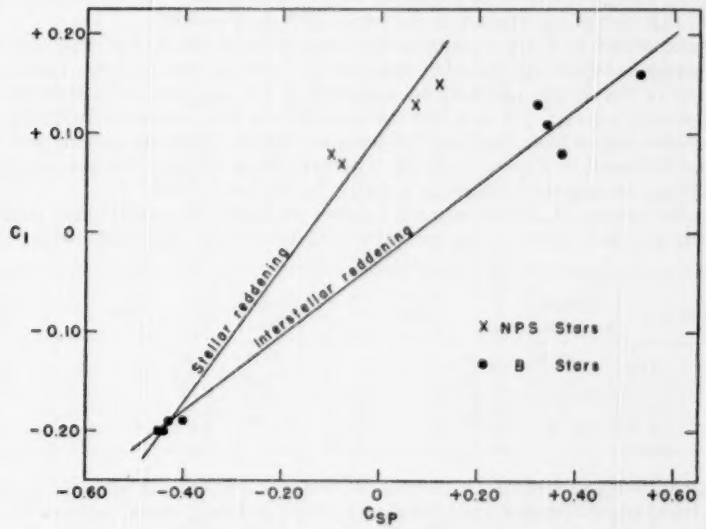

FIG. 2.—Spectrophotometric separation of stellar and interstellar reddening

the stars given in the accompanying tabulation have been altered by the inclusion of an additional spectrogram of each. The revised velocities are listed in Table 1.

Star	α (1900)	l	Paper	Star	α (1900)	l	Paper
236644	$1^h\ 5^m.3$	93°	II	233622	$9^h14^m.7$	135°	I
243827	5 21.7	142	II	134-1627	18 12.2	344	II
172-905	8 37.8	232	I	+22°3836	19 46.8	28	II

In addition to all main-sequence B-type stars later than B6, the stars given in the accompanying tabulation have been removed from the list, since additional material

Star	α (1900)	Paper	Old Type	Revised Type
9-53	$3^h0^m.2$	II	A2p	sdA
123884	14 5.1	I	cB9	sdA
+24°3632	19 1.8	II	cB8	F2

shows they are not B-type stars. The spectrum of Bergedorf 9-53 is correctly described in Paper II. I am indebted to W. W. Morgan for pointing out that HD 123884 also has a spectrum characteristic of A-type subdwarfs. The spectral type of HD 236963 ($2^h20^m.9$, Paper I) has been revised from cB2.5 to B2.

Data for the 253 faint B stars are given in Table 1. The stars of Papers I and II are combined in a single list in order of galactic longitude, starting from the region of Norma, $l = 300°$, and continuing around to the region of Vela, $l = 236°$.

The first column of Table 1 contains the designation of the star. Simple numbers are *Henry Draper* numbers. Hyphenated numbers are selected area and star number in the *Bergedorfer* or *Potsdamer Spektral-Durchmusterung*. For the remaining stars the BD or CD designation is given. The next two columns contain the galactic co-ordinates, l and b, to the nearest degree from the Lund Observatory tables. Right ascensions and declinations may be found in Papers I and II. The next three columns contain, in order, the spectral type, photographic magnitude, and color on the C_1 scale.

The color excesses, E_1, in the seventh column are based on normal colors provided by W. W. Morgan and shown in the accompanying tabulation. For types earlier than O9,

Type	Normal C_1 (Mag.)	Type	Normal C_1 (Mag.)	Type	Normal C_1 (Mag.)
O5	−0.29	O9	−0.27	B3	−0.23
O6	− .28	B0	− .26	B5	−0.20
O7	− .28	B1	− .25		
O8	−0.27	B2	−0.24		

Morgan's scale is extrapolated by means of Kuiper's temperature scale for B stars[5] and Petrie's for O stars.[6] These normal colors are about 0.04 mag. more negative[7] than those adopted by Stebbins, Huffer, and Whitford.[4]

[5] *Ap. J.*, **88**, 446, 1938. [6] *Pub. Dom. Ap. Obs. Victoria*, Vol. **7**, No. 21, 1947.

[7] Cf. discussions by J. H. Oort (*B.A.N.*, Vol. **8**, No. 308, 1938) and P. J. van Rhijn (*Groningen Pub.*, No. 51, 1946) in support of the more negative scale.

TABLE 1

OBSERVATIONS OF B STARS

Star	l	b	Spec.	m_{pg}	C_1	E_1	r_{ptm}	V_e	V_E	ρ_e	ρ_E
124448	286	+13	Bp	9.7	−0.20	+0.04	(2.75)	− 65A	−46A	−65	−46
144695	300	0	O9	9.6:	+ .04	+ .31	1.82	.....	.....	.....	.....
−46°10590	302	+ 2	O9	10.2	+ .02	+ .29	2.63	.....	.....	.....	.....
148989	303	− 2	cB1	9.1	+ .08	+ .33	3.63	− 40C	.....	−36	.....
150197	305	− 2	O8	9.6	+ .03	+ .30	1.91	.....	−33A	.....	−29
147756	305	+ 2	B(4)ne	8.5:	+ .01	+ .22	(0.40)	.....	.....	.....	.....
151300	306	− 3	O6	9.7	+ .05	+ .33	1.74	− 47A	.....	−42	.....
151018	307	− 2	B0	9.3	+ .13	+ .39	1.20	− 48C	.....	−44	.....
152386	309	− 2	O8f	8.3	+ .10	+ .37	(0.79)	− 17A	−13A	−12	− 8
180-1052	310	− 2	B0	9.5	+ .14	+ .40	1.26	− 27B	−27A	−21	−21
−40°10757	311	+ 1	(B3)n	9.8:	− .20:	+ .03:	(1.82:)	.....	.....	.....	.....
154313	312	− 2	O8	9.4	+ .17	+ .44	0.96	− 29A	.....	−22	.....
153295	321	− 1	Bne	9.4	+ .10:	+ .34:	(0.42:)	.....	.....	.....	.....
155134	313	− 3	B2	9.0	+ .02	+ .26	0.83	− 18A	−20A	−11	−13
150475	313	+ 4	O8.5	8.6	+ .01	+ .28	1.32	− 22B	− 8C	−15	− 1
155959	314	− 3	B0.5	9.1	+ .10	+ .35	0.96	− 13C	−24A	− 6	−17
156134	319	0	c−B0.5	8.5	+ .12	+ .37	1.32	.....	.....	.....	.....
155336	320	+ 2	B2	9.4	+ .07	+ .31	0.79	+ 1B	−16A	+10	− 7
−35°11760	321	− 3	cB5	10.5	+ .18	+ .38	5.75	+ 7B	.....	+16	.....
−35°11892	322	− 5	B3	10.2	− .03	+ .20	1.10	.....	−24C	.....	−15
−34°11820	322	− 3	B1	10.9	+ .20	+ .45	1.10	− 32B	0B	−23	+ 9
−33°12242	322	− 2	cB0.5	10.1	+ .32	+ .57	2.19	− 31A	−21B	−21	−12
−33°12155	323	− 1	O8	9.6	+ .27	+ .54	0.69	− 22C	.....	−12	.....
157-521	324	0	B4	11.3	+ .05	+ .26	1.26	− 2B	.....	+ 9	.....
163667	327	− 5	B1.5n	8.8	+ .02	+ .26	0.79	.....	.....	.....	.....
164019	330	− 4	O9	9.1	− .07	+ .20	2.29	− 32A	− 3B	−20	+ 8
−18°4365	330	+13	B1	9.2:	− .16	+ .09	2.29:	+ 24B	−34A	+37	−22
160730	331	+ 2	O8	10.5	+ .21	+ .48	1.38	− 72C	.....	−60	.....
166611	332	− 5	B1	9.7	+ .09	+ .34	1.00	− 23A	+17A	−11	+28
162718	332	− 1	Bne	9.1	+ .20	+ .43:	(0.25)	.....	.....	.....	.....
168941	333	− 8	O9.5	9.0	− .15	+ .11	3.31	+109C	−14A	+98	− 3
165517	333	− 4	B0	8.6	+ .12	+ .38	0.91	.....	+10B	.....	+22
−25°12786	333	− 4	B5n	10.8	+ .08	+ .28	0.91	.....	.....	.....	.....
−24°13687	333	− 2	B2	10.2	+ .12	+ .36	0.96	− 22B	− 9C	−10	+ 3
−25°12556	333	− 2	B1	10.7	+ .08	+ .33	1.66	.....	.....	.....	.....
166056	335	− 4	B3	9.3	+ .01	+ .24	0.60	.....	.....	.....	.....
−22°12627	336	− 3	B2	10.2	+ .10	+ .34	1.00	− 10B	.....	+ 2	.....
−20°5043	338	− 3	O7	10.0:	+ .21	+ .49	1.05:	+ 28A	.....	+41	.....
−20°5061	338	− 3	B5n	9.8	− .01	+ .19	0.76	.....	+15A	.....	+28
167722	339	− 3	B3n	9.1	− .08	+ .15	0.83	.....	.....	.....	.....
−20°5108	340	− 4	B0.5	9.4:	+ .10	+ .35	1.05:	+ 17A	+13A	+30	+27
−19°4955	340	− 3	cB1.5	10.0:	+ .39	+ .63	1.58:	+ 6A	.....	+20	.....
166188	340	− 1	B2ne	9.2	+ .09	+ .33	0.66	.....	−16B	.....	− 2
134-292	341	0	B1.5	9.3	− .06	+ .18	1.45	− 23A	− 8A	− 9	+ 6
166418	341	0	B0	8.4	+ .07	+ .33	1.00	.....	−24B	.....	− 9
168352	342	− 2	B2	8.7	+ .02	+ .26	0.72	− 16A	−29A	− 2	−15
165049	342	+ 2	c−B1.5	8.3	+ .09	+ .33	0.96	− 24B	−17A	− 9	− 2
168607	343	− 2	cB8e	9.6	+ .52	+ .65	1.26	.....	.....	.....	.....
168625	343	− 2	cB2	9.5	+ .48	+ .72	0.87	− 4A	−13A	+10	+ 2
134-464	343	0	B0.5	10.0	+0.27	+0.52	0.69	− 14B	.....	+ 1	.....

TABLE 1—*Continued*

Star	l	b	Spec.	m_{pg}	C_1	E_1	r_{phm}	V_o	V_E	p_o	p_E
165319	343	+ 2	B0	8.3	+0.11	+0.37	0.83	+ 30C	− 9C	+45	+ 6
134-2076	344	− 1	B0	9.8	+ .16	+ .42	1.32	+ 21A	.....	+36	.....
134-1269	344	0	B1	10.0	+ .04	+ .29	1.45	− 28A	.....	−14	.....
167451	344	0	cB1	8.8	+ .17	+ .42	2.19	.....	− 2A	.....	+13
134-1627	344	0	cB4	10.9	+ .24	+ .45	5.01	− 2B	.....	+13	.....
134-2608	345	− 2	B0.5	10.4	+ .26	+ .52	0.83	+ 23A	− 6A	+38	+ 8
−12°4982	346	0	B0	9.6	+ .28	+ .54	0.76	+ 23A	.....	+38	.....
169754	348	− 1	B0.5	9.7	+ .36	+ .61	0.42	.....	.....	.....	.....
177812	5	− 3	cB1.5	8.8	+ .14	+ .38	2.63	+ 40C	+14B	+57	+32
230211	14	+ 4	B4e	10.1	+ .05	+ .26	0.72	− 3A	+ 5A	+16	+24
231564	16	− 4	c-B1	10.7:	+ .33	+ .58	1.20:	.....	+28A	.....	+46
230780	16	+ 2	B5	10.7	+ .03	+ .23	0.96	.....	.....	.....	.....
231285	18	− 1	B0.5n	10.0	+ .22	+ .47	0.87	− 17C	+ 1A	+ 1	+17
230705	19	+ 4	B3	10.6:	− .01:	+ .22:	1.20:	+ 5A	−11A	+24	+ 8
231616	21	− 1	B3	10.5	+ .13	+ .36	0.66	+ 13C	−23A	+31	− 5
+22°3559	22	+ 6	B3	10.4	− .02:	+ .21:	1.15:	− 19A	+ 6B	+ 1	+26
+19°4266	27	− 7	Bn	10.0	− .09	+ .14:	(1.26)	.....	.....	.....	.....
+22°3781	27	− 1	O9	9.7	+ .06	+ .33	1.82	+ 4A	.....	+23	.....
+22°3782	27	− 1	O9	9.1	+ .08	+ .35	1.32	+ 20A	.....	+38	.....
+23°3730	27	0	cB8	10.0	+ .31	+ .44	3.47	+ 17A	− 3B	+36	+16
+21°4017	28	− 5	B0	10.5	+ .06	+ .32	2.75	+ 30A	−15B	+48	+ 3
+22°3836	28	− 3	cB1	9.4	+ .19	+ .44	2.63	+ 4A	+ 7A	+23	+25
+23°3759	28	− 1	B0	9.2	+ .16	+ .42	1.00	− 21B	+26B	− 3	+45
+25°3952	29	− 1	O8	10.5	+ .18	+ .45	1.51	+ 7C	.....	+25	.....
+23°3915	31	− 7	B5n	9.6	− .10	+ .10	1.00	.....	.....	.....	.....
+29°3732	33	+ 2	B2	9.7	− .09	+ .15	1.82	+ 5A	.....	+24	.....
+28°3598	34	− 2	B0	10.2	+ .28	+ .54	1.00	.....	+ 1C	.....	+19
+29°3842	35	− 1	B1	10.3	+ .20	+ .45	0.83	+ 14C	−12C	+32	+ 6
+29°3944	36	− 3	B5	9.7	− .03	+ .17	0.79	− 10A	.....	+ 7	.....
+31°3921	37	− 1	B0.5	8.8	+ .15	+ .40	0.66	+ 34C	− 7A	+52	+11
227424	38	0	B3n	10.2	− .05	+ .18	1.15	.....	+30B	.....	+48
+32°3749	39	− 2	O(8)ne	10.4	+ .24	+ .51	1.15	.....	.....	.....	.....
227704	39	+ 1	B0	8.7	− .03	+ .23	1.74	− 24B	−28A	− 6	−10
226868	39	+ 2	B0	9.4	+ .19	+ .45	1.00	− 13A	−24B	+ 5	− 6
226951	39	+ 2	B0.5	8.9	− .02	+ .23	1.38	− 9C	−10B	+ 9	+ 8
227018	39	+ 2	O6	9.0	+ .04	+ .32	1.32	+ 41B	−12C	+59	+ 6
227960	40	0	O8.5	9.3	− .10	+ .17	2.88	− 8B	−16A	+10	+ 1
228041	40	0	Bne	9.0	+ .03	+ .26:	(0.79)	.....	.....	.....	.....
227415	40	+ 1	B0	9.6	+ .08	+ .34	0.69	.....	−22A	.....	− 4
227611	40	+ 1	Be	8.8	+ .01	+ .24:	(0.48)	.....	.....	.....	.....
227173	40	+ 2	B4n	11.0	+ .11:	+ .32:	0.32:	.....	.....	.....	.....
227245	40	+ 2	O8	10.0	+ .13	+ .40	1.51	− 13A	− 4A	+ 5	+14
227836*	41	+ 1	Bve	10.5	+ .02	+ .25:	(1.0)	− 25A	−37C	− 7	−19
228053	41	+ 1	cB1	9.0	+ .07	+ .32	3.63	+ 7A	−11A	+25	+ 6
228199	41	+ 1	B0.5	9.0	.00	+ .25	1.38	+ 2A	−20A	+20	− 3
227607	41	+ 2	B3	10.1	+ .05	+ .28	0.76	+ 5C	− 8B	+23	+10
227728	42	+ 2	B2	9.8	− .10	+ .14	1.91	− 19A	−30A	− 2	−12
228461	43	+ 1	B1	9.6	+ .08	+ .33	1.00	+ 6B	−26B	+23	− 9
228279	43	+ 1	B4n	10.3	.00	+ .21	0.95	.....	.....	.....	.....
229049	44	0	B0	9.7	+0.08	+0.34	0.72	− 17A	− 3B	+ 1	+14

* Stebbins gives m_{pv} = 9.6. The *Henry Draper Extension* has m_{pg} = 10.9. Seven UV plates obtained between December, 1941, and October, 1946, give m_{pg} = 10.5 and show no variation. My C_1 determinations are in good agreement with Stebbins'.

TABLE 1—*Continued*

Star	l	b	Spec.	m_{pg}	C_1	E_2	r_{phot}	V_*	V_E	p_*	p_E
228256	45	+ 3	Bne	10.2:	+0.01:	+0.24:	(0.91:)	.....	.....	.....	.....
40-1659	53	+ 1	B4	11.1	.00	+ .21	1.38	− 13C	− 6A	+ 4	+10
235350	57	+ 5	B2.5	9.2	+ .06	+ .29	0.58	− 18A	− 6C	− 2	+10
41-2761	62	− 6	B3	10.6	− .11	+ .12	1.82	− 54C	−17B	−40	− 3
235673	66	− 2	O7.5	9.0	+ .01	+ .28	1.58	− 40B	−23A	−26	−10
235618	66	+ 1	B1	10.0	+ .15	+ .40	0.91	− 5A	.....	+ 9	.....
239626	67	+ 7	B0.5	9.5	+ .11	+ .36	1.10	− 19B	−22A	− 4	− 6
18-390	67	+ 7	B2	10.9	+ .06	+ .30	1.66	− 49C	.....	−35	.....
239758	68	+ 4	B5ne	9.3	− .14	+ .06	1.05	.....	.....	.....	.....
235874	70	− 6	B3.5	9.2	− .19:	+ .03:	1.26:	− 56A	−23B	−44	−12
235807	70	− 2	B1	9.5	− .05	+ .20	1.66	.....	−23B	.....	−11
239828	70	+ 3	cB4	10.0	+ .27	+ .48	3.02	− 39B	−40C	−26	−27
239923	72	+ 2	cB4	9.4	+ .35	+ .56	1.66	.....	−13C	.....	− 1
235989	73	− 6	B(4)n	9.2	− .18	+ .03	(1.20)	.....	−33B	.....	−22
239989	74	+ 2	B3.5	10.0	+ .13	+ .35	0.48	− 37A	−33A	−26	−21
236044	76	− 5	B0	9.3	− .05	+ .21	2.51	− 37B	.....	−26	.....
240165	76	− 3	B0n	10.3	+ .08:	+ .34:	2.29:	.....	.....	.....	.....
240171	76	− 3	B2.5	10.0	− .01	+ .22	1.00	− 19B	−12A	− 8	− 1
19-315	79	− 1	B1	10.9	+ .17	+ .42	1.26	− 68A	−39B	−57	−29
19-363	79	0	B1.5	11.2	+ .12	+ .36	1.74	− 76A	−18A	−66	− 8
240311	80	− 2	B6	10.8:	+ .06	+ .24	0.87:	− 12A	.....	− 2	.....
240319	80	− 2	B4	10.4	+ .19	+ .41	0.44	.....	+ 5B	.....	+15
19-1233	80	0	B3	11.0	+ .16	+ .39	0.69	− 24A	−26B	−15	−16
19-1778	80	+ 1	O7	11.0	+ .24	+ .52	1.45	− 67C	.....	−57	.....
240458	83	− 6	B4ne	9.4	− .03	+ .19	0.69	.....	−24B	.....	−16
8-1454	91	− 1	O7	11.1	+ .10	+ .38	2.75	.....	.....	.....	.....
8-1482	91	0	cB2	9.3	+ .18:	+ .42:	2.75:	− 29A	.....	−23	.....
236589	92	− 6	B0.5	8.9	− .10	+ .15	2.00	− 54B	−38A	−48	−32
236644	93	− 5	B3	9.6	− .08	+ .15	0.63	− 59B	−33B	−54	−28
8-640	93	− 3	B2.5	11.5	− .06:	+ .17:	3.80:	− 12A	−25C	− 6	−19
8-1105	93	− 2	c–B2	11.5	+ .12	+ .36	3.47	− 33B	−12B	−26	− 5
8-1128	93	− 2	B1.5	10.1	+ .05	+ .29	1.32	+ 6A	−31B	+12	−25
236633	93	− 2	B1n	9.2	+ .13	+ .38	0.69	.....	.....	.....	.....
8-1717	93	− 1	B5n	11.5	− .04	+ .16	1.91	.....	.....	.....	.....
8-1675	93	0	B1	11.8	.00	+ .25	3.98	− 52A	−41A	−46	−35
8-1680	93	0	B(5)ne	11.1	+ .16	+ .36	(0.69)	.....	.....	.....	.....
8-1720	93	0	B(4)ne	11.2	+ .14	+ .36	(0.79)	.....	.....	.....	.....
236664	94	− 3	B4n	9.5:	+ .02	+ .24	0.58	.....	.....	.....	.....
236683	94	− 3	B2	9.7	− .03	+ .21	1.38	− 31B	−45B	−26	−40
8-736	94	− 2	B3n	11.0	+ .14	+ .37	0.79	.....	.....	.....	.....
8-1779	94	− 1	B3	11.9	+ .16	+ .39	1.10	.....	− 8A	.....	− 2
236800	96	− 2	B3	9.6	− .03	+ .20	0.83	− 25C	−15B	−20	−10
236827	97	− 2	B3.5	9.5	− .01	+ .21	0.72	− 42A	−17A	−38	−12
236896	98	− 1	B5	9.9	.00	+ .20	0.76	− 48A	−26B	−43	−21
232534	100	−10	B(3)ne	9.5	− .09	+ .14	(1.00)	.....	− 3B	.....	− 2
236917	100	− 5	B4ne	9.8	− .09	+ .13	1.05	− 27B	−45B	−23	−42
236954	101	− 1	c–B2.5	9.6	+ .22	+ .45	0.87	− 49A	−29B	−46	−26
236960	102	− 1	B1	9.9	+ .19	+ .44	0.72	− 45A	0B	−41	+ 3
236961	103	− 3	B1	9.4	+ .20	+ .45	0.58	− 34A	.....	−31	.....
236963	104	− 3	B2	9.3	−0.04	+0.20	1.20	− 37A	−13B	−35	− 8

TABLE 1—*Continued*

Star	l	b	Spec.	m_{pg}	C_1	E_1	r_{phm}	V_e	V_E	ρ_e	ρ_E
236971	104	− 2	B1	9.7	+0.12	+0.37	0.91	− 51A	− 4B	−49	− 2
236995	105	− 1	cB6	8.9	+ .13:	+ .30:	3.80:	− 52A	−28A	−49	−26
237007	105	+ 2	B2:	9.4	+ .06:	+ .30:	0.83:	.....	.....	.....	.....
237011	105	+ 2	B1.5	10.4	+ .18	+ .42	0.87	− 43C	− 9A	−40	− 6
237015	105	+ 2	B4	9.0	− .02	+ .19	0.58	− 15A	+ 5B	−13	+ 7
237019	105	+ 2	O7	9.2	+ .10	+ .38	1.15	− 67B	−22C	−65	−20
9-274	106	+ 1	B4n	11.0	+ .09	+ .30	0.91	− 44C	+ 4A	−42	+ 6
9-911	106	+ 2	B1n	10.6	+ .20	+ .45	1.00	.....	−22B	....	−22
9-1612	106	+ 3	B(6)ne	10.7	+ .23	+ .42	(0.40)	.....	.....	.....	.....
237056	108	0	B1ne	9.2	+ .13	+ .38	0.69	.....	.....	.....	.....
9-106	108	+ 2	B1n	10.5	+ .13	+ .38	1.26	.....	−30C	....	−29
237153	110	+ 4	c–B3	10.1	+ .35	+ .58	0.55	− 39A	−47A	−38	−46
237174	112	+ 3	B3	9.2	− .09	+ .14	0.87	− 13A	− 7A	−13	− 7
232774	113	− 4	B(5)n	9.2	+ .10	+ .30	(0.36)	.....	.....	.....	.....
237213	115	+ 3	cB3	9.0	+ .13	+ .36	3.16	+ 14A	−14A	+13	−15
232947	119	+ 4	B0	9.7	+ .10	+ .36	1.66	− 48C	−21A	−50	−23
232932	120	+ 1	B5	9.3	− .02	+ .18	0.63	− 8B	.....	−10	....
232971	120	+ 5	B5ne	9.6	+ .04	+ .24	0.55	.....	.....	.....	.....
232999	123	+ 4	cB2	9.7	+ .16	+ .40	3.63	+ 1A	−15B	− 2	−18
24-1035	126	+ 1	B5	10.6	+ .02:	+ .21:	1.05:	.....	−14A	....	−18
24-1094	127	+ 2	B5ne	11.4	+ .26	+ .46	0.50	.....	.....	.....	.....
24-491	128	− 1	Bn	11.2	+ .11:	+ .34:	(0.96:)	.....	.....	.....	.....
24-554	128	0	B2e	10.5	+ .06	+ .30	1.38	− 12C	−10B	−18	−15
24-986	128	+ 3	B(4)ne	11.1	+ .03	+ .24	(1.20)	− 45B	−26B	−50	−31
24-211	129	0	B4	10.8	− .12	+ .09	2.00	.....	.....	.....	.....
24-738	129	+ 2	B4	10.7	+ .06	+ .27	0.91	+ 1A	+ 4A	− 4	− 1
233622	135	+45	B3n	9.2:	− .18	+ .04	1.26:	+ 26C	.....	+25	....
242926	141	0	O7.5	9.3	+ .01	+ .28	1.82	− 8C	− 9C	−17	−18
243035	141	0	B0	10.8	− .09	+ .17	6.03	.....	+41A	....	+32
243070	141	0	B1.5	10.9	− .07	+ .17	3.47	− 12B	+11A	−21	+ 2
243827	142	+ 1	c–B2	10.9	+ .11	+ .35	2.75	+ 71B	.....	+62	....
245967	143	+ 3	B3	10.5	+ .07	+ .30	0.83	+ 8C	.....	− 2	....
246901	144	+ 3	cB1+K	8.7	+ .29	.....	.....	− 1A	+ 2A	−11	− 7
247795	145	+ 3	B(4)ne	9.4	− .06	+ .16	(0.79)	.....	.....	.....	.....
248890	147	+ 4	B3.5	10.4:	− .15	+ .07	2.00:	− 13B	+11B	−24	+ 1
248903	147	+ 4	B3	9.4	− .08	+ .15	0.91	.....	−23A	....	−33
246579	149	− 3	B5n	10.0	− .04	+ .16	0.96	.....	.....	.....	.....
249179	149	− 3	B(5)ne	9.6	− .06	+ .14	(0.83)	.....	.....	.....	.....
245770	149	− 1	B1ne	9.7	+ .05	+ .30	1.20	.....	+ 1C	....	−11
247331	151	0	B3ne	8.7	− .11	+ .12	0.76	− 14B	.....	−25	....
243780	152	− 6	B3+F8	9.9:	+ .33	.....	.....	+ 21B	−12B	− 8	−25
250289	154	− 2	c–B4	8.4	+ .19	+ .40	0.44	+ 18C	+ 8A	+ 5	− 4
248434	155	− 1	B(5)ne	10.4	− .07	+ .13	1.26	.....	.....	.....	.....
248893	155	0	B0	9.6	+ .13	+ .39	1.38	+ 23B	+12A	+10	− 1
251204	155	+ 2	B0	10.5	+ .05	+ .31	2.88	.....	.....	.....	.....
251696	155	+ 3	B5n	10.2	− .07	+ .13	1.15	.....	.....	.....	.....
253339	155	+ 4	B3ne	10.6	+ .12	+ .35	0.69	.....	.....	.....	.....
255191	156	+ 6	cB1	10.9	+ .14	+ .39	6.61	.....	.....	.....	.....
253021	157	+ 3	B2	10.7	+ .15	+ .39	1.05	.....	.....	.....	.....
254577	157	+ 5	B0	9.8	+0.20	+0.46	1.15	+ 18C	− 6B	+ 6	−19

TABLE 1—*Continued*

Star	l	b	Spec.	m_{pg}	C_1	E_1	r_{phm}	V_o	V_E	ρ_o	ρ_E
254755	157	+ 5	O9	9.3	+0.19	+0.46	0.91	+ 9B	−10A	− 4	−23
250163	158	− 1	Bne	9.9	+ .07	+ .30:	(0.63)				
253214	158	+ 2	B4ne	9.4	+ .02	+ .23	0.58	− 6C	+ 1A	−20	−12
256725	160	+ 5	O5.5	9.3	− .02	+ .26	2.00	+ 38A	+36A	+24	+22
254428	165	0	B0.5	9.1	+ .02	+ .27	1.32	+ 18A	+15B	+ 3	0
250980	166	− 5	B2ne	9.2	− .04	+ .20	1.15	− 1A	+ 2B	−17	−14
265134	168	+ 8	O9n	8.8	− .15	+ .12	2.88		+10B		− 4
256577	170	− 1	B2e	9.7	− .02	+ .22	1.32		+26B		+10
259597	171	+ 1	B3ne	8.4	− .16	+ .07	0.83		+19A		+ 3
259828	172	+ 1	B5	10.8:	− .14	+ .06	2.09:	+ 11B		− 5	
258982	173	0	B2	9.1	+ .03	+ .27	0.83		+16C		0
263775	175	+ 3	B3	10.5	− .03	+ .20	1.26	+ 38B	+29A	+22	+12
264600	175	+ 4	Bn	10.9	− .01	+ .22:	(1.38)				
+0°1576	179	0	O9	9.4	+ .06	+ .33	1.58	+ 41C	+30B	+24	+13
+0°1627	180	+ 1	B2	9.5	− .03	+ .21	1.26				
+0°1638	180	+ 1	O8n	10.1	+ .01	+ .28	2.63		+49A		+32
+1°1560	180	+ 2	B2n	9.7	+ .07	+ .31	0.91		+27B		+10
+1°1699	181	+ 6	B4n	9.3:	− .07	+ .14	0.79:				
−1°1471	183	+ 2	B1	10.2	+ .04	+ .29	1.58	+ 75A		+57	
−3°1668	185	+ 1	B3	9.8	− .12	+ .11	1.32	+ 45A	+23B	+28	+ 5
−2°1892a†	185	+ 3	B3	10.4	− .07	+ .16	1.45	+ 42C		+24	
−4°1806a†	186	+ 3	B3	10.6	− .07	+ .16	2.51	+ 68C		+51	
−3°1746	186	+ 3	B5e	10.6	− .15	+ .05	2.00	+ 65A		+47	
−5°1971	187	+ 3	B(5)ne	10.3	− .04	+ .16	(1.10)				
123-96	196	− 1	Bne	10.3	− .02	+ .21:	(1.10)				
55885	197	− 1	B(5)ne	9.0	− .06	+ .14:	(0.63)	+ 57A	+58A	+38	+39
123-414	197	− 1	Bne	10.0	+ .08	+ .31:	(0.63)				
123-548	197	0	B5	10.0	− .15	+ .05	1.82	+ 65C		+46	
123-602	197	0	B5	10.5:	− .09	+ .11	1.45:	+ 33C		+14	
123-778	198	0	B4	10.8	+ .06	+ .27	0.96				
123-822	198	0	c–B3	8.7	− .13	+ .10	2.09	+ 65B	+46A	+47	+27
123-1778	198	+ 2	cB1.5	9.0	− .04	+ .20	6.03	+ 83A	+47A	+65	+29
123-1955	198	+ 2	O7	9.7	+ .12	+ .40	1.32	+ 54B	+32B	+35	+14
62413	210	− 1	B4e	10.0	− .08	+ .13	1.15	+ 40A	+25A	+20	+ 6
62780	210	− 1	Bne	8.9	− .04	+ .19:	(0.63)				
64639	210	+ 3	Bne	9.7	− .07	+ .16:	(1.05)				
65886	211	+ 3	B4	9.3	− .07	+ .14	0.79				
63290	212	0	cB1	9.5	+ .17	+ .42	2.29	+ 43A	+25B	+25	+ 6
148-1118	217	+ 1	B4	11.7	− .20	+ .01	4.17	+ 8C		−10	
63150	219	− 5	Bne	9.0:	− .09	+ .14:	(0.79:)				
−44°4543	231	− 2	B0	10.3	− .07:	+ .19:	4.36:				
172-905	232	− 1	cB1.5	8.7	+ .12	+ .36	2.75	+ 37B	− 2B	+20	−19
172-1753	232	0	B0	10.0	+ .15	+ .41	1.51	+ 27A		+11	
172-880	233	− 2	Bne	10.0	− .09:	+ .14:	(1.26:)				
172-1522	233	− 1	B1	9.9	− .04	+ .21	1.91				
172-1789	233	0	B1n	9.0	+ .06	+ .31	0.83		0A		−16
172-1822	233	0	B2	9.8	− .03:	+ .21:	1.45:	− 19A		−35	
172-1864	233	0	B0.5	9.2	+ .07	+ .32	1.10				
172-2000	234	0	B1	9.5	+ .21	+ .46	0.58	+ 16A		0	
78958‡	234	+ 3	B0.5	9.6	+ .20	+ .45	0.79	+ 44A		+28	
80834	234	+ 6	Bne	9.8	+ .02:	+ .25:	(0.76:)				
−46°4786	235	0	B1	9.6	+ .09	+ .34	0.96	+ 22B		+ 6	
−47°4551	236	0	O7	9.0	+0.18:	+0.46:	0.66:	− 13B		−29	

† The locations of these stars are described in Paper II.
‡ Erroneously listed as 78959 in Paper II.

The column of photometric distances, r_{ptm}, is evaluated from the relation

$$\log 1000\, r_{ptm} = 0.2\,(m_{pg} - M_{pg} - 9E_1 + 5)\,.$$

Whitford's extension of the wave-length dependence of space reddening[8] to λ 21,000 indicates that the ratio, 9, of total photographic absorption to E_1, previously employed by the photoelectric observers, is substantially correct.

The adopted absolute magnitudes, M_{pg}, are photovisual magnitudes, recommended by Dr. Morgan several years ago, corrected by color indices of −0.5 mag. for O stars, −0.4 for B0–B2 stars, and −0.3 for B3–B5 stars. They are shown in the accompanying tabulation. Reference is made to Table 1 of Paper II for an evaluation of my spectral

Type	M_{pg}			Type	M_{pg}		
	Normal	c⁻	c		Normal	c⁻	c
O5–O8	−4.5	.....	.....	B2	−2.9	−4.4	−6.7
O9–B0*	−4.6	.....	.....	B3	−1.8	−3.8	−6.7
B0.5	−3.9	−5.4	−6.7	B5	−1.3	.....	−6.7
B1	−3.4	−4.9	−6.7				

* $M_{pg} = -2.7$ is used for HD 227415 and HD 229049, stars with spectra similar to that of τ Sco.

types in terms of the luminosity classes of the Yerkes *Atlas*. The M_{pv} for the c stars is strengthened by Bidelman's work on the Perseus cluster.[9] Values of r_{ptm} in parentheses are unreliable because of uncertainty in the adopted values of M (principally Bne stars); values followed by colons are unreliable because of poorly determined values of m_{pg} or of C_1.

The V_* and V_K are the measured radial velocities obtained from stellar lines and from the interstellar K line, respectively. The accompanying designation A, B, or C shows that

Designation	Probable Error (Km/Sec)
A	0 to ±4.0
B	±4.1 to ±8.0
C	±8.1 to ±12.0

the probable error, evaluated from the agreement between velocities from the two (occasionally three and rarely four) spectrograms, lies between the values listed herewith. Velocities with probable errors greater than 12.0 km/sec have been omitted. The quantities ρ_* and ρ_K in the last two columns are the measured velocities corrected for a standard solar motion of 20 km/sec toward right ascension 18^h and declination +30° (1900). Diagrams showing the distribution of spectral types, of ρ_*, and of ρ_K, along the galactic circle are contained in Paper II. The velocities and color excesses are shown in Figures 3, 4, and 5 of the present paper.

DISCUSSION

The two most uncertain factors entering into the distances of Table 1 are the absorption corrections and the spectroscopic absolute magnitudes. Techniques have improved greatly for determining colors since 1939–42, when these observations were made. With regard to the spectroscopic absolute magnitudes, the spectrograms were not exposed with this problem in view and are not sufficiently wide. Moreover, a satisfactory

[8] *Ap. J.*, **107**, 102, 1948.

[9] *Ap. J.*, **98**, 61, 1943.

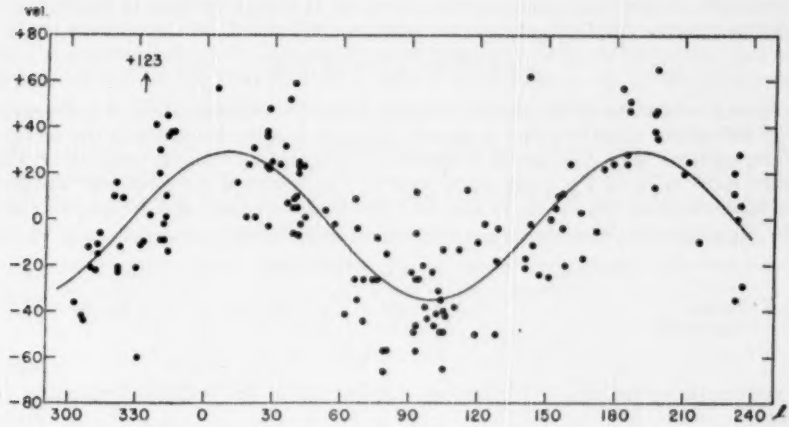

FIG. 3.—Stellar radial velocities. The curve has the constants $(A\bar{r}) = 32.0$ km/sec, $K = -2.8$ km/sec, $l_0 = 325°$.

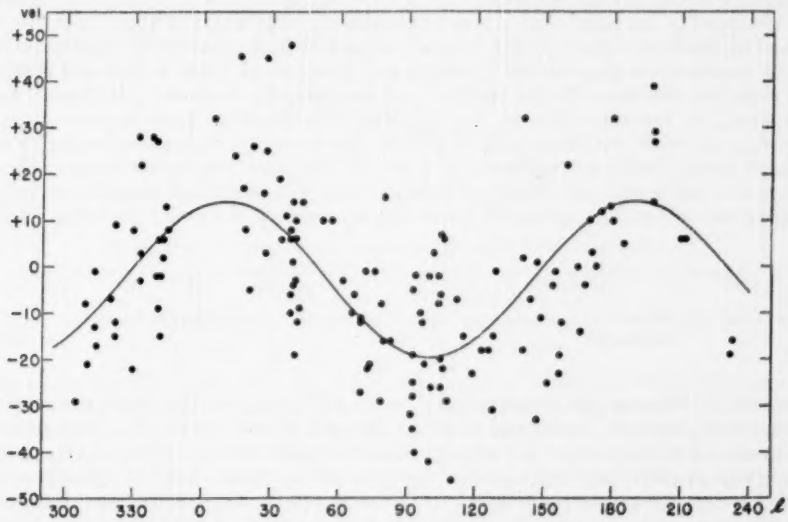

FIG. 4.—K-line radial velocities. The curve has the constants $(A\bar{r}) = 16.8$ km/sec, $K = -2.8$ km/sec, $l_0 = 325°$.

system of standard stars was not available. Consequently, a complete analysis of the data of this paper for some of the spatial and dynamical properties of the sample of B stars is not presented. A brief discussion is given, however. It supersedes that of Paper I.

Solutions for the constants of galactic rotation, $(A\bar{r})$ and K, in the relation

$$\rho = (A\bar{r}) \sin 2(l - l_0) + K$$

were carried out for the stellar velocities and K-line velocities separately. A is the amplitude of differential galactic rotation at unit distance, l_0 is the longitude of the center of rotation, assumed to be 325°, and K is assumed to be constant with varying l and r. Each velocity listed in Table 1 is given equal weight. The results of the solutions[10] are given in the accompanying tabulation. It may be noted that the values of K found are close to

Velocities	No.	$(A\bar{r})$	K
Stellar	151	33.1 km/sec	−2.7 km/sec
Interstellar	135	17.3	−2.4

the systematic correction, −2.1 km/sec, applied to all the measured velocities (see Paper I).

In previous discussions of differential galactic rotation from radial velocities[11] it has been customary to use the observational data to solve for one or more of the constants A, l_0, M (average for a group of stars of one spectral type), or an average coefficient of absorption, a. Our present knowledge of these quantities (except a, which is not needed) has advanced to the point that it is not immediately clear which of them might be improved by the B-star observations. Instead, a check of their consistency could be carried out by means of the photometric distances and velocities of Table 1, provided that one had sufficient confidence in the reliability of the data. To illustrate this point, I have computed, for the stars used in the radial-velocity solutions given above, values of $A \times \bar{r}_{\text{ptm}}$, in which A is taken to be 18 km/sec/kpc and $\bar{r}_{\text{ptm}}$ is formed by weighting each distance from Table 1 according to $\sin^2 2(l - l_0)$. For each interstellar distance the assumption is made that the effective r is half of r_{ptm}. The results are given in the accompanying tabulation. The agreement is not very satisfactory, the indication being that the

Velocities	$A \times \bar{r}_{\text{ptm}}$	$(A\bar{r})$
Stellar	28.6 km/sec	33.1 km/sec
Interstellar	13.3	17.3

photometric distances are systematically too small. In view of the uncertainties of the photometric distances, mentioned above, it does not appear worth while to investigate the cause of the discrepancy. My principal aim is to point out the desirability of checking any system of photometric distances of distant stars by means of radial velocities whenever possible, since so many quantities, both observed (m, C_1, spectral type, luminosity classification) and adopted (M, normal values of C_1, ratio of total absorption to color excess), enter into the determinations of r_{ptm}. It may be noted that Bidelman's discussion of the Perseus cluster[9] shows a discrepancy between $(A\bar{r})$ and $A \times r_{\text{ptm}}$ of 9.3 km/sec in the same direction as that found here.

[10] The constants for the curves in Figs. 3 and 4 differ slightly from those given here because they were obtained in an earlier analysis.

[11] J. S. Plaskett and J. A. Pearce, *Pub. Dom. Ap. Obs. Victoria*, Vol. 5, No. 4, 1936; A. H. Joy, *Ap. J.*, 89, 271, 1939; R. J. Trumpler, *Ap. J.*, 91, 186, 1940; and R. E. Wilson, *Ap. J.*, 92, 213, 1940.

The distribution of color excesses, E_1, around the galactic circle is shown in Figure 5 for the McDonald observations. The results are similar to those of Stebbins, Huffer, and Whitford.[12]

There is no correlation of E_1 with apparent magnitude. The correlation with spectral type (or, equivalently, with luminosity), however, is striking, as shown in the accompanying tabulation. All stars with E_1 greater than 0.46 mag. are c stars or are earlier

Type	cB	c⁻B	O5–O9	O9.5–B0.5	B1	B2	B3	B4–B6
E_1	0.44	0.42	0.35	0.33	0.33	0.26	0.22	0.19

than B1. This correlation results from the statistical increase of E_1 with distance, which

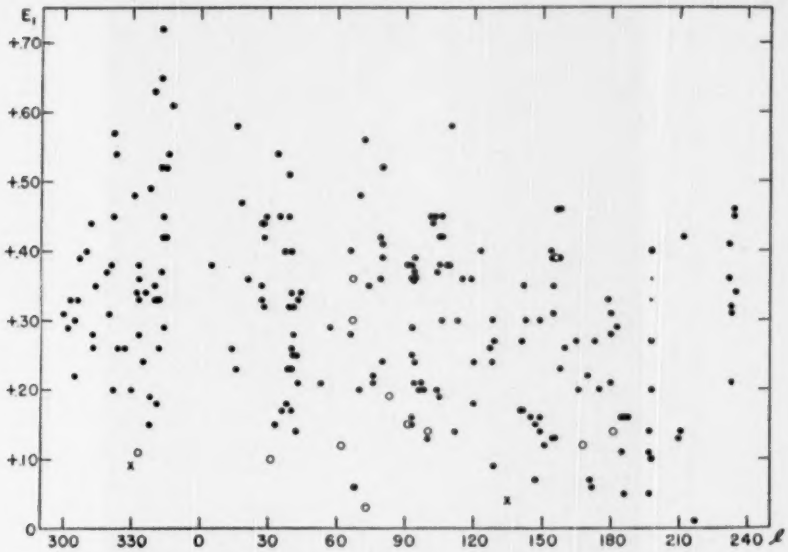

FIG. 5.—Observed color excesses. Filled circles, $b < 6°$; open circles, b between 6° and 10°; crosses, $b > 10°$.

tends to restrict stars of a given apparent magnitude to a distance range considerably less than is expected from consideration of their luminosity range alone.

The bluest stars of the McDonald list are all more than 5° from the galactic plane or have longitudes far from 325°. Of the 25 most highly reddened stars of the combined Mount Wilson and McDonald lists,[13] with E_1 greater than 0.50 mag., 10 lie in the region at longitudes 340°–348° and latitudes 0° to −4°. This group contains the 3 most highly reddened stars, HD 168607, HD 168625, and HD 169034.[14] Five stars lie in the Cygnus region and 2 east of the Perseus cluster. Almost all these 25 stars are located near the

[12] *Ap. J.*, **90**, 459, 1939.

[13] The Mount Wilson values of E_1 are reduced to the adopted system by applying the differences between the normal colors of the two investigations.

[14] To this group may be added RY Scuti, a ninth-magnitude B-type eclipsing binary with a similar color. Although part of its reddening may occur in the extended envelope around this star, the similarity of its color to that of neighboring reddened B stars is striking.

boundaries of *large-scale* dark areas. This effect is not particularly noticeable on the individual photographs of the Ross-Calvert *Atlas*, but it is seen clearly on a composite photographic map reproduced in a small size[15] on which large-scale brightness changes show with exaggerated contrast (see Fig. 6). The inference is that a photographic absorption of 4.5 mag. or more within a distance of less than 2 kiloparsecs from the sun is associated almost entirely with regions of large-scale heavy obscuration. The total absorption in the centers of such regions must be considerably greater than 5 mag. and the increase of absorption toward the center from the edge very rapid.

It is a pleasure to acknowledge the advice received from Dr. W. W. Morgan during the preparation of this paper, which was delayed by the war and by subsequent circumstances.

[15] E.g., as published in Bok and Bok, *The Milky Way* (Philadelphia: Blakiston Co., 1941).

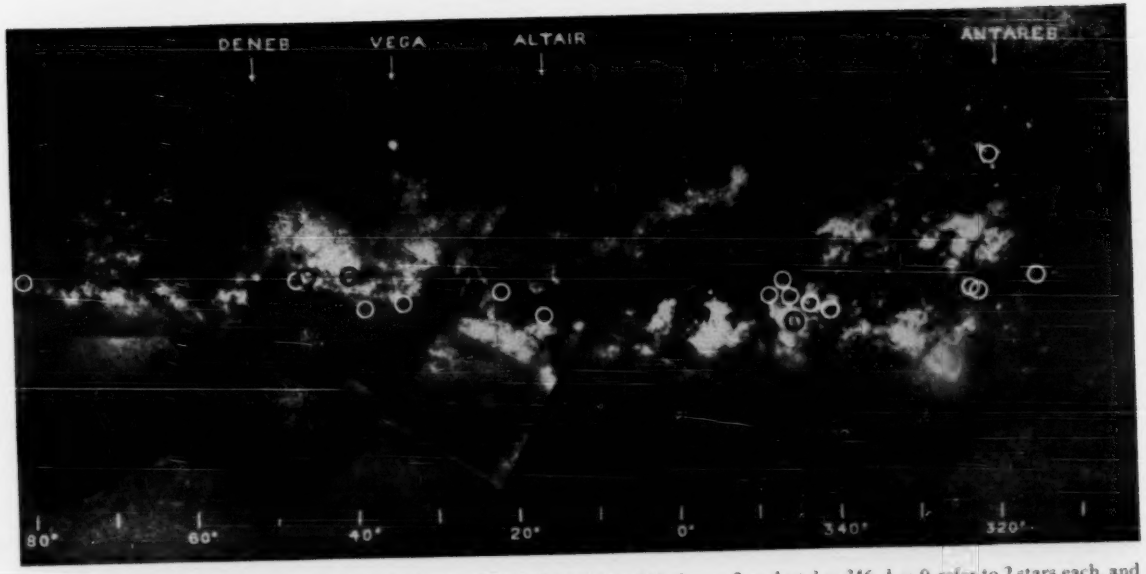

FIG. 6.—Location of B stars with $E_1 \geq 0.50$ mag. The points at $l = 343$, $b = -2$ and at $l = 346$, $b = 0$ refer to 2 stars each, and the point at $l = 345$, $b = -2$ to 3 stars. Stars marked on a copy of a mosaic by Struve and Miss Calvert of Ross-Calvert photographs.

THE SPECTROSCOPIC BINARY DELTA ORIONIS*

PARIS PIŞMIŞ, GUILLERMO HARO, AND OTTO STRUVE
Observatorio Astronómico Nacional, Tacubaya, D.F. Mexico, and
McDonald Observatory, University of Texas
Received March 2, 1950

ABSTRACT

A new velocity-curve has been derived from spectrograms obtained at the McDonald Observatory in 1947 and 1948. The new curve is distinctly unsymmetrical and confirms the suspicion that the longitude of the periastron is advancing approximately at the rate of 1° in twenty orbital revolutions. The other elements agree closely with those found previously at the Yerkes Observatory.

A forward movement of the line of apsides of the spectroscopic binary δ Orionis was suspected in an earlier investigation carried out on spectrograms taken at the Yerkes Observatory. A discussion of the orbits based on these and on earlier investigations of δ Orionis is given by Luyten, Struve, and Morgan.[1] Although an apsidal motion of δ Orionis seems to be present, the speed of this motion shows considerable scatter. In view of this, it was felt desirable to redetermine the orbital elements of this binary after a reasonable lapse of time.

The present study of δ Orionis was made on spectrograms taken with the Cassegrain quartz spectrograph attached to the 82-inch telescope of the McDonald Observatory during the months of November, December, and January, 1947–1948, nearly ten years after the Yerkes observations.[2]

The plates have a dispersion of 40 A/mm at λ 3933 and, as a rule, are of excellent quality. The lines used for the determination of the radial velocities are listed in Table 1.

TABLE 1

LIST OF LINES MEASURED ON SPECTROGRAMS OF δ ORIONIS

Wave Length (A)	Line	Wave Length (A)	Line	Wave Length (A)	Line
3271.940	*H* 14	3835.386	*H* 9	4101.737	*Hγ*
3734.370	*H* 13	3889.051	*H* 8	4116.104	*Si* IV
3750.154	*H* 12	3970.074	*He*	4120.812	*He* I
3754.67	*O* III	4026.362	*He* I	4340.468	*Hδ*
3759.87	*O* III	4069.897	*O* II	4387.928	*He* I
3770.632	*H* 11	4075.868	*O* II	4471.477	*He* I
3797.900	*H* 10	4088.863	*Si* IV		
3819.604	*He* I	4096.543	*O* II		

The number of lines measured on each spectrogram ranged from 12 to 20. The K line of *Ca* II was also measured whenever possible.

Table 2 gives the list of the plates measured. The first three columns are self-explana-

* *Contributions from the McDonald Observatory, University of Texas*, No. 190.

[1] *Pub. Yerkes Obs.*, Vol. 7, Part IV, 1939.

[2] The spectrograms were obtained on Mr. Struve's regular program of spectroscopic binaries. The measurements were made by Mrs. Pişmiş-Recillas and Mr. Haro; and the discussion was carried out by Mrs. Pişmiş-Recillas.

TABLE 2

RADIAL VELOCITIES OF δ ORIONIS

Plate (CQ)	Date	U.T.	Phase from Node (Period)	Rad. Vel. (Km/Sec)	Rad. Vel. Ca II (Km/Sec)	Measurer
6299	1947 Nov. 25	3h28m	0.872	+ 78.9		G. H.
6308	25	6.34	.875	+100.1		G. H.
6322	26	6.03	.065	+ 96.0		P. P.
				+ 87.9		G. H.
6333	26	11.34	.105	+ 75.4	+ 0.2	P. P.
6334	26	11.43	.106	+ 88.6		P. P.
6340	27	5.07	.233	− 8.4	+12.3	G. H.
6341	27	5.10	.233	− 7.3	+18.4	G. H.
6350	27	9.24	.264	− 28.5		P. P.
6351	27	9.30	.265	− 25.7	+ 6.2	G. H.
6363	28	4.35	.403	−101.7	+ 3.1	P. P.
6372	28	8.22	.431	− 94.7	+12.2	G.H.
6388	29	9.23	.613	− 47.3		P. P.
				− 49.2		G. H.
6389	29	9.28	.613	− 47.7	+15.2	G. H.
6399	30	5.09	.756	+ 23.0	+12.0	G. H.
6400	30	5.17	.757	+ 30.6	+ 7.0	P. P.
				+ 33.0	+ 5.9	G. H.
6408	30	9.25	.787	+ 34.5		P. P.
6409	30	9.32	.788	+ 33.6		G. H.
6417	Dec. 1	5.39	.934	+ 35.9		P. P.
6418	1	5.43	.935	+104.6	+ 2.7	G. H.
6441	4	7.44	.473	+ 93.0		P. P.
				− 91.5	+20.8	G. H.
6442	4	7.48	.473	− 91.4	+20.8	P. P.
6445	5	10.25	.667	− 88.7		G. H.
6466	6	8.55	.830	− 16.8	+ 4.8	P. P.
6467	6	8.58	.831	+ 71.8	+ 8.5	G. H.
				+ 59.1		P. P.
6479	7	11.32	.024	+ 64.1	− 0.7	G. H.
6480	7	11.40	.025	+103.1		G. H.
6489	8	8.40	.177	+117.8		P. P.
6490	8	8.45	.178	+ 38.8	+ 1.5	P. P.
6502	9	10.18	.368	+ 30.9		P. P.
				− 71.8	+18.8	P. P.
6512	24	10.05	.979	− 73.7		G. H.
6513	24	10.09	.979	+121.3		P. P.
6530	26	8.27	.316	+117.0	+28.4	P. P.
6531	26	8.35	.317	− 40.8	+ 3.8	P. P.
6540	27	6.03	.473	− 39.8	− 2.3	P. P.
6541	27	6.07	.473	− 74.8	+ 0.8	P. P.
6552	28	7.11	.656	− 74.4	+16.0	G. H.
				− 14.9	+19.0	G. H.
6564	29	7.22	.834	− 11.2	+22.0	P. P.
6565	29	7.47	.834	+ 62.3	+14.8	G. H.
6610	1948 Jan. 3	5.20	.689	+ 69.9	+ 3.7	G. H.
6611	3	5.24	.689	+ 16.4		G. H.
6630	4	6.46	.874	+ 11.8	+ 6.5	P. P.
6631	4	6.49	.874	+ 86.8	+15.5	P. P.
				+ 97.4		G. H.
6644	5	9.13	.057	+ 98.5		P. P.
6645	5	9.18	.066	+113.9		G. H.
6659	6	8.29	.235	+105.6		P. P.
6660	6	8.40	.236	+ 4.4		G. H.
				+ 0.7		P. P.
6677	7	10.12	.422	+ 6.9	+24.6	G. H.
6678	7	10.18	0.423	− 73.5		G. H.
				− 72.3		P. P.

tory. The phases in the fourth column are computed from the nodal passage and the period given by Luyten, Struve, and Morgan:[1]

$$\text{JD } 2428382.263 + 5^{d}.732476E .$$

They are given in fractions of the period. The fifth column lists the radial velocity determined from all lines except *Ca* II. The velocity determined from this last line is given in the sixth column. The last column gives the initials of the measurer. Ten plates were measured by both measurers. A comparison of these gives:

$$\text{Rad. vel. (G. H.) minus rad. vel. (P. P.)} = +0.4 \pm 1.3 .$$

Accordingly, the radial velocities of both observers were treated without applying any corrections.

The observations were then combined into normal places. In Table 3 are given the

TABLE 3

NORMAL POINTS

Phase from Node (Period)	Weight	Radial Velocity (Km/Sec)	Phase from Node (Period)	Weight	Radial Velocity (Km/Sec)	Phase from Node (Period)	Weight	Radial Velocity (Km/Sec)
0.024	2	+110.4	0.316	2	− 40.3	0.756	3	+ 28.8
.062	4	+100.8	.364	2	− 72.7	.787	3	+ 34.6
.105	2	+ 82.0	.419	4	− 85.5	.832	5	+ 65.2
.177	2	+ 34.8	.473	6	− 82.6	.877	5	+ 91.6
.234	5	− 0.8	.613	3	− 48.0	.934	2	+ 98.8
0.264	2	− 27.1	0.671	5	− 4.7	0.979	2	+119.1

phases corresponding to these normals, with the weights, and the corresponding velocities are listed in the second and third columns, respectively. Figure 1 is a graph of these normal points with the computed curve drawn through them. The different sizes of the points roughly indicate their weights.

The preliminary elements of the orbit were determined by the Russell-Wilsing method. They are given below. A comparison of the velocity maximum with that given by Luyten,

$\gamma = +11.4$ km/sec $\qquad e = 0.089$
$K = 100.4$ km/sec $\qquad T_0 =$ JD 2432509.453
$\omega = 68°.7$

Struve, and Morgan indicated a small correction to the period. The improved value is 5.732357 days.

To derive the corrections to the preliminary elements, a least-squares solution was carried out, following Sterne's method.[2] The definitive elements for δ Orionis, with their mean errors, are as follows:

$\gamma = +11.8$ km/sec $\qquad e = 0.085 \pm 0.004$
$K = 99.7 \pm 1.2$ km/sec $\qquad T_0 =$ JD 2432509.466 $\pm 0^{d}.004$
$\omega = 70°.8 \pm 2°.2$

For the sake of comparison, the definitive elements derived from the earlier Yerkes material are also given:

$\gamma = 12.4$ km/sec $\qquad e = 0.079 \pm 0.009$
$K = 101.0 \pm 0.9$ km/sec $\qquad T =$ JD 2428382.26
$\omega = 38° \pm 7°$

[2] *Proc. Nat. Acad. Sci.*, **27**, 175, 1941.

The elements K and e are reasonably accordant with the earlier determination, but ω differs widely. Considering the good quality of the present material and the small mean errors, we believe that the line of apsides has moved forward by an appreciable amount.

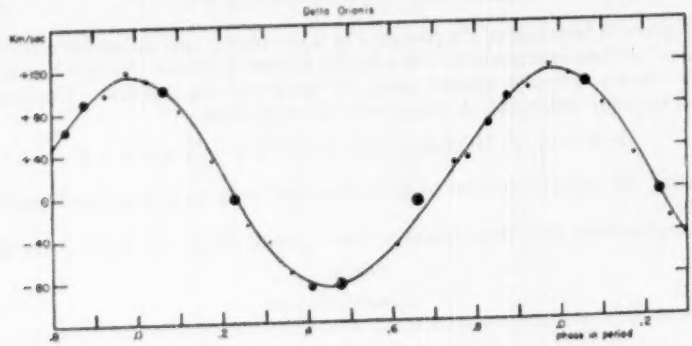

FIG. 1

The rate of this motion is of the order of 1 revolution in 7200 orbital revolutions, or 1° in 20 orbital revolutions. But it is not yet certain that spurious effects are absent in the velocity-curve of this star.

The radial velocities derived from the interstellar line K of *Ca* II show no periodicity. The mean value from the twenty-seven plates on which this line was measured is +10.2 km/sec.

THE SPECTRA OF THE WOLF-RAYET STARS IN THE REGION λλ 6500–8800*

P. SWINGS AND P. D. JOSE

McDonald Observatory and Institut d'Astrophysique, Liége, Belgium

Received February 10, 1950

ABSTRACT

The spectra of seven Wolf-Rayet stars have been observed in the region λλ 6500–8800. For the identifications, tables of predicted lines of *C* II–IV, *O* II–VI, and *Si* III and IV were prepared. All strong emission lines are satisfactorily explained in the WC sequence; in the WN sequence, a fairly strong complex emission near λ 8240 remains unidentified.

No spectroscopic information on Wolf-Rayet stars is available in the near-infrared region.[1] Spectrograms in this region were obtained in June, 1949, for seven Wolf-Rayet objects, using the fast plane-grating spectrograph at the prime focus of the McDonald reflector. The linear dispersion is 370 A/mm at λ 6600, 345 A/mm at λ 7500, and 312 A/mm at λ 8500. The I-N emulsion used was hypersensitized with ammonia; the exposures ranged from 20 minutes to 4 hours. Fourteen spectrograms of good quality were obtained, seven of WC objects and seven of WN objects. The list of the observed stars is given in Table 1.

TABLE 1

WOLF-RAYET STARS OBSERVED IN THE NEAR-INFRARED REGION

Carbon sequence	HD 184738 (WC8 + nebula) (2 exp.)
	HD 164270 (WC8) (2 exp.)
	HD 168206 (WC7) (2 exp.)
	HD 192103 (WC7) (1 exp.)
Nitrogen sequence	HD 151932 (WN6+) (2 exp.)
	HD 192163 (WN6) (3 exp.)
	HD 193077 (WN5) (2 exp.)

Of these objects, HD 168206 is a binary,[2] while HD 193077 is a suspected binary.[3] From Hiltner's period, the phase for our spectrograms of HD 168206 would be about 14.4 days, which would correspond to velocities of the order of +330 km/sec for *He* II emission, +125 km/sec for *C* III and *C* IV emission, and −10 km/sec for *H* absorption. However, no correction has been entered in our list of wave lengths, although we usually find the measured wave lengths of HD 168206 to be higher than those of the other WC objects. The list of stars observed does not represent the two sequences as well as we desired: adverse observing conditions prevented us from extending the investigation to a greater number of objects. It is hoped that the work may be pursued at some later time.

The spectrograms are reproduced in Figures 1 and 2. It is readily apparent that the WC stars are much richer in infrared lines than are the WN objects. The difficulties encountered in measuring Wolf-Rayet spectra in the usual spectral region have also been encountered in the infrared. In addition, great difficulty arose in relation to the identifica-

* *Contributions from the McDonald Observatory, University of Texas*, No. 188.

[1] C. S. Beals (*Pub. Dom. Ap. Obs., Victoria*, **4**, 271, 1930) observed five lines beyond *Hα*, to λ 7117 (Table 1, p. 277).

[2] W. A. Hiltner, *Ap. J.*, **102**, 492, 1945. [3] Hiltner, *ibid.*, **101**, 356, 1945.

Table 2

Carbon Sequence

Identification			HD 184738 (WC8)		HD 164270 (WC8)		HD 168206 (WC7)		HD 192103 (WL7)	
Element	λ	Designation	Int	λ	Int	λ	Int	λ	Int	λ
Hα	•6562.8	$2^2P^o-3^2D$	12	64.5					20	65.4
He II	6560.1	$4^2P^o-6^2G$			15	81.8	8	77.9	10	96.4
C II	•6578.0	$3s^2S_{\frac{1}{2}}-3p^2P^o_{1\frac{1}{2}}$								
C II	6582.8	$3s^2S_{\frac{1}{2}}-3p^2P^o_{\frac{1}{2}}$								
C IV	6591.9	$6s^2S_{\frac{1}{2}}-7p^2P^o_{\frac{1}{2}, 1\frac{1}{2}}$								
C III	6617.6	$5p^3D_3-6d^3D^o_3$	1?	7.7	1s?	13.8				
O IV	6632.1	$5d^2P^o_{2\frac{1}{2}}-3d'''^2F_{2\frac{1}{2}}$							1?	31.8
(O II	6627.7	$3d^2P_{1\frac{1}{2}}-4p^2P^o_{1\frac{1}{2}})$								
He I	6678.1	$2'P^o_1-3'D_2$	3	78.7	4	80.2			3	78.7
(O V	6685.3	$4d'P^o_1-7d'D_2)$								
C III	•6744.2	$3s^3P^o-3p^3D$	2	30.1	8	36.5	4	47.3	15	40.8
C III	6730.7									
C III	6727.1									
C III	6742.2									
(C II	6750.2	$3p^4D-3d^4D^o)$								
(C II	6738.4									
(O III	6737.1	$4d^3D^o_3-3s'^3D_3)$								
(O III	6743.0	$3d^3P_2-6d^3D^o_3)$								
(O IV	6745.8	$3s'^4P_{2\frac{1}{2}}-4d^4D^o_{3\frac{1}{2}})$								
C II	6783.7	$3s^4P^o_{2\frac{1}{2}}-3p^4D_{3\frac{1}{2}}$	3	80.7	8	85.0			2	82.1
C II	6779.7	$3s^4P^o_{1\frac{1}{2}}-3p^4D_{2\frac{1}{2}}$								
(C III	6779.4	$3d^3P^o-6s^3S)$								
(C III	6791.5									
(C III	6798.2									

Table 2 (continued)

Identification			HD 184738 (WC8)		HD 164270 (WC8)		HD 168206 (WC7)		HD 192103 (WC7)	
Element	λ	Designation	Int	λ	Int	λ	Int	λ	Int	λ
C III	6803.6	$9d\,^3D_3$-$4d\,^3P^o_2$					17	10.7		
O IV	6817.5	$3p^*\,^2D^o_{2\frac{1}{2}}$-$3d^*\,^2F_{3\frac{1}{2}}$								
(O III	*6847.8	$4p\,^3D_1$-$4d\,^3P^o_1$)			17	53.5				
C III	*6857.3	$3p\,^3D$-$3d\,^3D^o$							2s	61.4
C III	6862.9									
C III	6871.7									
C III	*6881.9	$3p\,^3P$-$5p\,^3P^o$			17	00.0			4	94.6
C III	6899.4									
(OV	6888.9	$3d\,^3P^o_2$-$4s\,^3S_1$)								
(O II	6895.3	$3d\,^4F$-$4p\,^4D^o$)								
(O II	6906.6									
(O III	6952.8	$4s\,^1P^o_1$-$4p\,^1S_o$)			0	46.2			0	38.3
(O IV	6931.4	$3s\,^2P^o_{\frac{1}{2}}$-$3p\,^2P_{\frac{1}{2}}$)								
(C II	6959.3	$4p\,^4P_{2\frac{1}{2}}$-$5d\,^4D^o_{3\frac{1}{2}}$)			1-07	69.4			1	72.1
C III	7036.9	$3s\,^1P^o_1$-$4d\,^1D_2$	5	35.6	6	33.1	3	53.5	5	25.6
He I	*7065.2	$2\,^3P^o_{2,1}$-$3\,^3S_1$	4	64.4	8	62.3			15	60.2
(C III	7047.8	$5p\,^3P_2$-$6d\,^3P^o_2$)								
(C II	7063.4	$3p\,^4S$-$3d\,^4P^o$)								
(C II	7052.9									

Table 2 (continued)

Identification			HD 184738 (WC8)		HD 164270 (WC8)		HD 168206 (WC7)		HD 192103 (WC7)	
Element	λ	Designation	Int	λ	Int	λ	Int	λ	Int	λ
(O III	*7109.1	$4s^3P^o_1$-$4p^1D_2$)	2	8.2	3	10.9			27	4.4
(O II	7110.9	$3d^2D_{2\frac{1}{2}}$-$4p^2P^o_{1\frac{1}{2}}$)								
(C II	7119.4									
(C II	7115.1	$3p^4D$-$3d^4F^o$)								
(C II	7112.4									
							2	26.9		
(C I	7118.5	$3p^3D$-$4s^3F^o$)								
C III	*7136.8	$5p^3P_2$-$6d^3D^o_3$	1-2	33.0	2	29.3			3	38.8
C III	7158.4	$3d^1D^o_2$-$5d^1D_2$			1	56.4				
(O IV	7154.6	$3d'^2F^o_{3\frac{1}{2}}$-$4p^2D_{2\frac{1}{2}}$)								
(O III	7189.7	$4p^3D_3$-$4s^3P^o_2$)			1	84.0			0	79.5
C II	*7231.1	$3^2P^o_{\frac{1}{2}}$-$3^2D_{1\frac{1}{2}}$	8	29.1						
C III	7210.4	$5p^3P^o_2$-$6d^3D_3$			20	31.5	10	33.9	12	34.2
C II	*7236.2	$3^2P^o_{1\frac{1}{2}}$-$3^2D_{2\frac{1}{2}}$	8	34.4						
(O III	7243.3	$3d^3F_2$-$6d^3D^o_3$)								
(O III	7249.8	$4s^3P^o_2$-$4p'^3D_2$)								
			0	71.7						
He I	*7281.3	$2'^1P^o_1$-$3'^1S_0$			2	83.2			17	88.8
(O II	7280.9	$3d^2D_{2\frac{1}{2}}$-$4p^2D^o_{2\frac{1}{2}}$)	0	94.8						
(O III	7294.3	$3d^3F_3$-$6d^3D^o_3$)								
O III	7317.6	$5s^3P^o_2$-$3d^3D_3$							0	23.0
C III	7352.7	$3p'^1D_2$-$3d'^1P^o_1$							0	45.6
(O III	7343.8	$5s^3P^o_2$-$3d^3D_2$)								
(O V	7359.6	$4s'^3P^o_1$-$4p'^3D_2$)								

Table 2 (continued)

Identification			HD 184738 (WC8)		HD 164270 (WC8)		HD 168206 (WC7)		HD 192103 (WC7)	
Element	λ	Designation	Int	λ	Int	λ	Int	λ	Int	λ
C IV	*7380.2	$6p^2P^o_{\frac{1}{2},1\frac{1}{2}}$-$7d^2D_{1\frac{1}{2},2\frac{1}{2}}$	1	81.1	1?	70.7	1	90.8	8	78.9
(O II	7369.3	$3d^4P_{2\frac{1}{2}}$-$4p^4D^o_{3\frac{1}{2}}$)								
(O III	7366.1	$3d^3F_4$-$6d^3D^o_3$)								
O IV	7418.0	$6d^2D_{2\frac{1}{2}}$-$7f^2F^o_{3\frac{1}{2}}$	1-0	20.0					3	25.8
O V	7437.3	$4s^3S_1$-$4p^3P^o_1$	0-1	32.9						
C III	7485.2	$5d^3D_3$-$6f^3F^o_4$	2	81.8	5	81.6			8n	91.9
(O V	7483.0	$4s^3S_1$-$4p^3P^o_2$)								
C II	*7506.8	$5p^2P^o$-$3p^2D$	2	18.4	4	15.9				
C II	7521.6									
C II	7525.7									
C II	7509.4	$4p^{3\frac{1}{2}}P^o$-$3p^2P$								
C II	7520.0									
C II	7520.5									
C II	7531.0									
O III	7514.1	$4s^3P^o_2$-$4p^3P_1$								
O IV	7510.5	$4p^2D_{1\frac{1}{2}}$-$4d^2P^o_{\frac{1}{2}}$								
O II	7504.0	$3d\ ^2G_{4\frac{1}{2}}$-$5f^2G^o_{4\frac{1}{2}}$								
O III	7550.4	$3s^3P_o$-$3p^3S^o_1$	1	51.4	1s?	49.7				
C III	*7576.6	$3s^3P^o$-$4d^3D$	3	83.9	7	85.9	5	...	10	?95?
C III	7585.8									
C III	7595.2									
C III	7611.8									
C III	7625.5									

Table 2 (continued)

Identification			HD 184738 (WC8)		HD 164270 (WC8)		HD 168206 (WC7)		HD 192103 (WC7)	
Element	λ	Designation	Int	λ	Int	λ	Int	λ	Int	λ
C III	7592.8	$3d^3F^o$-$5g^3G$								
C III	7614.0									
C III	7613.5									
O III	7606.0	$3s^3P_1$-$3p^3S^o_1$								
O IV	7588.6	$4p^2D_{1\frac{1}{2}}$-$4d^2P^o_{1\frac{1}{2}}$								
Si IV	7656.7	$6p^2P^o_{1\frac{1}{2}}$-$7s^2S_{1/2}$	1-0	62.5						
O IV	7651.9	$3p'^2D^o$-$5p^2F$								
O IV	7669.0									
Si IV	7678.3	$6f^2F^o_{3\frac{1}{2}}$-$7g^2G_{4\frac{1}{2}}$	0	82.3			1	81.9		
C IV	7704.5	$6d^2D$-$7f^2F^o_o$	3	8.8	5	5.3				
C III	7707.4	$3p'^1P_1$-$3d'^1D^o_2$								
O III	7711.2	$3s^3P_2$-$3p^3S^o_1$								
C IV	*7704.5	$6d^2D$-$7f^2F^o$	2	26.4	5	32.2	6	27.7	20	26.0
C IV	7723.7	$6f^2F^o$-$7g^2G$								
CIV	7726.1	$6g^2G$-$7h^2H^o$								
C IV	7726.6	$6h^2H^o$-$7g^2G$								
C IV	7728.0	$6g^2G$-$7f^2F^o$								
C IV	7746.2	$6f^2F^o$-$7d^2D$								
(O IV	7715.1	$4p^2D_{2\frac{1}{2}}$-$4d^2P^o_{1\frac{1}{2}}$)								
(Si IV	7716.8	$6g^2G_{4\frac{1}{2}}$-$7h^2H^o_{5\frac{1}{2}}$)								
(Si IV	7730.8	$6h^2H^o$-$7g^2G$)								

Table 2 (continued)

Identification			HD 184738 (WC8)		HD 164270 (WC8)		HD 168206 (WC7)		HD 192103 (WC7)	
Element	λ	Designation	Int	λ	Int	λ	Int	λ	Int	λ
C III	*7771.1	$3p^3S_1$-$3d^3P^o_o$	3	73.0					27	75.2
(Si III	7772.3	$3d^3D^o_2$-$5g^3G_3$)								
(O I	7772.0	$3^5S^o_2$-3^5P_3)								
C III	*7779.9	$3p^3S_1$-$3d^3P^o_1$	2	83.8	6	87.6				
C III	*7795.9	$3p^3S_1$-$3d^3P^o_2$	3	95.7					27	99.8
(Si III	7803.3	$3d^3D_3$-$5g^3G_{3,4}$)								
(C II	7853.2	$4f^2F^o_{2\frac{1}{2}}$-$3p^4D_{1\frac{1}{2}}$)	2	56.9			1?	59.0	4	61.8
O III	7872.5	$4p^3D_2$-$4d^3D^o_2$	2	81.4	2n	76.7				
O III	7910.5	$4p^3D_2$-$4d^3D^o_1$	0	13.3						
O IV	7938.1	$3d'^2P^o_{1\frac{1}{2}}$-$4f^2D_{1\frac{1}{2}}$	0	43.7			1?	37.1	2	46.2
O IV	7944.4	$4p^2D_{2\frac{1}{2}}$-$8f^2F^o_{2\frac{1}{2},3\frac{1}{2}}$								
C III	7969.3	$5g'G_4$-$6f'F^o_3$	1?	69.7	1	61.0	1?	63.6		
C IV	7957.7	$6d^2D$-$7p^2P^o$								
O III	7962.8	$4p^3D_3$-$4d^3D^o_3$								
C III	8019.5	$5d'D_2$-$6f'F^o_3$			2-3	19.0				
C II	8061.9	$3p^4P$-$3d^4P^o$			2	68.9				
C II	8062.5									
C II	8076.5									
(OV	8061.0	$4p^3D_1$-$4d^3P^o_o$)								
(OV	8068.8	$3d'P^o_1$-$4s'S_o$)								
C III	8144.5	$5g^3G$-$6f^3F^o$			1s?	42.0				
C III	8145.1									
C II	8161.4	$3d^2P^o_{1\frac{1}{2}}$-$4p^2P_{1\frac{1}{2}}$	1?	64.1						

Table 2 (continued)

Identification			HD 184738 (WC8)		HD 164270 (WC8)		HD 168206 (WC7)		HD 192103 (WC7)	
Element	λ	Designation	Int	λ	Int	λ	Int	λ	Int	λ
O III	*8172.2	$4s'^3P^o_1$-$4p'^3D_2$	5	96.1	8	95.3	4	3.8	8	...
O V	8205.2	$4p^3D_2$-$4d^3P^o_1$								
C II	8176.8	$3d^2P^o$-$4p^2P$								
C II	8177.5									
C II	8193.0									
C III	*8255.0	$3d^3F^o_2$-$5d^3D_3$	1?	42.1	5	47.4			6	42.1
							2	55.5		
C III	*8272.0	$3d^3F^o_3$-$5d^3D_3$	1	60.7	5	66.0			5	62.2
C III	8297.2	$3d^3F^o_4$-$5d^3D_3$			2?	97.6				
C III	*8322.4	$3d'^3P^o_1$-$6d'^3D_2$	2	8.8						
C III	8335.1	$3p'^3S_o$-$6p'^3P^o_1$			4	20.0				
C I	*8335.2	$3s'^3P^o_1$-$3p'^3S_o$	3	28.3			4	41.0	8	27.6
C III	8333.6	$4d^3D$-$3d^3F^o$								
C III	*8342.7		4	43.0	10	40.1				
C III	8348.7									
C III	8359.0									
C III	8360.1									
O V	8311.6	$7d'^3D_2$-$8p'^3P^o_1$								
O III	8339.5	$4p^5D^o_2$-$4d^5P_1$								
C II	8330.1 to 8357.1	$3p^4P$-$3d^2D^o$								
O III	8356.7	$4p'^3P_1$-$4d'^3D^o_2$	1	54.6						
He I	8361.77	3^3S-6^3P^o								

Table 2 (continued)

Identification			HD 184738 (WC8)		HD 164270 (WC8)		HD 168206 (WC7)		HD 192103 (WC7)	
Element	λ	Designation	Int	λ	Int	λ	Int	λ	Int	λ
C II	8379.1	$4d\,^4P^o_{3\frac{1}{2}}$-$5f\,^4D_{3\frac{1}{2}}$	1-0	95.6	2?	80.9			2?	87.7
C II	8398.7	$4d\,^4F^o_{4\frac{1}{2}}$-$5f\,^4D_{3\frac{1}{2}}$								
C III	8367.4	$4p\,^3P^o$-$3p\,^3P$								
C III	8370.9									
C III	8393.2									
C III	8396.7									
O II	8376.5	$4p\,^4D^o$-$5s\,^4P$								
O II	8382.8									
O III	8365.1	$4p\,^3D$-$3p\,^3P^o$								
O III	8377.1									
O III	8385.8									
P_{20}	8392.40	$3\,^2D$-$20\,^2F^o$								
C II	8413.9	$3p\,^4S_{1\frac{1}{2}}$-$3d\,^4D^o_{2\frac{1}{2}}$	0?	15.2	2?	5.5				
C II	8413.6	$4d\,^4F_{4\frac{1}{2}}$-$5f\,^4G_{5\frac{1}{2}}$								
C IV	8403.9	$6p\,^2P^o_{\frac{1}{2},1\frac{1}{2}}$-$7s\,^2S_{\frac{1}{2}}$								
O II	8404.5	$4p\,^4D^o$-$5s\,^4P$								
O II	8417.0									
P_{19}	8413.3	$3\,^2D$-$19\,^2F^o$								
O I	*8446.3	$3\,^3S^o_1$-$3\,^3P_2$	1	42.9						
O III	8442.3	$4p\,^5D^o_3$-$4d\,^5P_2$								
P_{18}	8437.96	$3\,^2D$-$18\,^2F^o$								
O III	8461.9	$4p\,^3D_2$-$3p\,^3P^o_2$	0	66.8						
C III	*8499.7	$3s'\,^3S_o$-$3p'\,^3P^o_1$	3	0.2	8	97.7	3	8.0	8	99.1

Table 2 (continued)

Identification			HD 184738 (WC8)		HD 164270 (WC8)		HD 168206 (WC7)		HD 192103 (WC7)	
Element	λ	Designation	Int	λ	Int	λ	Int	λ	Int	λ
C II	8568.7	$4d^4F^o$-$5f^2F$	0	72.0						
C II	8579.5	$4d^4F^o$-$5f^2F$								
C II	8590.5	$4d^4F^o_{3\frac{1}{2}}$-$5f^4F_{4\frac{1}{2}}$								
C II	8594.8	$4d^4F^o_{3\frac{1}{2}}$-$5f^2F_{2\frac{1}{2},3\frac{1}{2}}$								
P_{14}	8598.4	3^2D-14^2F^o								
O III	8581.7	$4p^5D^o_4$-$4d^5P_3$								
C II	8611.9	$4d^4F^o_{4\frac{1}{2}}$-$5f^4F_{4\frac{1}{2}}$			2?	11.1				
C II	8615.4	$4d^4F^o_{4\frac{1}{2}}$-$5f^2F_{3\frac{1}{2}}$								
O III	8612.8	$4p^3D_3$-$3p^3P^o_2$								
C III	*8665.4	$5f^3F^o$-$6g^3G$	3	63.4	6	61.2	3	60.6	8	65.9
C III	8666.7	$5f^3F^o$-$6g^3G$								
C III	8667.2	$5f^3F^o$-$6g^3G$								
(C III	8662.0	$5p'^3P^o_1$-$6s^3S_1$)								
O IV	8669.9	$4p^2D_{2\frac{1}{2}}$-$4d^2F^o_{2\frac{1}{2}}$								
C II	8681.3	$4s^2S$-$2p^3\ ^2P^o$								
C II	8695.4	$4s^2S$-$2p^3\ ^2P^o$								
O II	8680.0	$4d^4F$-$5f^4F^o$								
O II	8690.6	$4d^4F$-$5f^4F^o$								
P_{13}	8665.0	3^2D-13^2F^o								

NOTES TO TABLE 2

•λ 6562.8—In HD 164270 and HD 168206 the shortward wing is stronger than the longward. In HD 168206 the emission is definitely double.

•λ 6578.0—*C* IV contributes probably to the emission in the WC7 stars but not appreciably to that in the WC8 objects.

•λ 6744.2—In HD 164270 there may be some weak emission between λ 6736 and λ 6785.

•λ 6847.8—The *O* III identification is doubtful, since it is an intersystem combination.

•λ 6857.3, •λ 6881.9—In HD 192103 there may be some absorption between λ 6861 and λ 6895. The complex emission λλ 6861–6895 is also weakly present in HD 168206.

•λ 7065.2—This line has a complex profile in HD 164270, the longward half appearing weaker than the shortward; it may actually be a double line.

•λ 7109.1, •λ 7136.8—On one spectrogram of HD 164270 the emission near λ 7120 appears single at λ 7120.0, with $W = 880$; on the other plate the double character is suspected. In HD 168206 the emission appears single.

•λ 7231.1, •λ 7236.2—This is the strongest infrared line in the WC8 stars. The total half-width is $W = 433$ in HD 184738, $W = 950$ in HD 164270 (with probable weak reversal). In HD 168206 the line is double, with components centered at λ 7219.4 (int. 10, $W = 344$) and λ 7253.7 (int. 9, $W = 468$). In HD 192103 the line is double, with components at λ 7217.9 (int. 12, $W = 465$) and λ 7250.6 (int. 11, $W = 533$).

•λ 7281.3—The double structure in HD 184738 is uncertain; on one plate the emission is measured as single at λ 7281.9.

•λ 7380.2—In HD 164270, the emission is suspected to be double at λλ 7355.3–7379.5. The shortward component may be due to *O* III (λλ 7343.8–7366.1).

•λ 7506.8—In HD 164270 there is some emission between these two lines.

•λ 7576.6—This emission, which is present in all four stars, is sharply and deeply cut by atmospheric absorption; it is hard to estimate the position of the maximum, or even the line intensity or structure. In HD 168206 the emission begins at λ 7576.6. In HD 192103 it extends from λ 7569.4 to λ 7621.4. In HD 184738 a line is measured at λ 7618.2 on the longward side of the atmospheric absorption.

•λ 7704.5—This is a very intense, wide, and shallow emission in HD 192103, the large width being mainly due to the blending of several $7 \rightarrow 6$ transitions in *C* IV. In HD 184738 the λ 7726.4 emission is wider than λ 7708.8, and a triple structure is suspected at λλ 7725.1, 7733.2, and 7744.5.

•λ 7771.1, •λ 7779.9, •λ 7795.9—While the triple structure of this group appears fairly well on one spectrogram of HD 184738, the emission on another plate is found to be a wide line with minimum at λ 7790.1. In HD 164270 no definite structure appears. In HD 192103 there seem to appear at least two components.

•λ 8172.2—This emission is complex in HD 192103. Either it may be described as double, with first component at λ 8179.8 ($W = 431$) and second at λ 8209.7 ($W = 390$); or it may be triple with two fairly sharp components at λλ 8172.6–8187.2 and a broader one at λ 8209.7. By comparison with the *C* II line at λ 8161, the *C* II contribution to this emission should be minor.

•λ 8255.0, •λ 8272.0—In HD 168206 the double structure is not seen; in HD 192103 it is only suspected.

•λ 8322.4, •λ 8335.2, •λ 8342.7—This is a complex emission. It is resolved on one spectrogram of HD 184738. In HD 164270 and HD 192103 the structure is only suspected. On one spectrogram of HD 168206 there seems to be a reversal at λ 8341.0.

•λ 8446.3—This line may belong to the nebula.

•λ 8499.7—This emission has a complex structure in HD 192103. In HD 168206 there is a weak central reversal.

•λ 8665.4—In HD 192103, this emission appears to have three maxima at λλ 8647.0 (int. 8), 8664.1 (int. 7), and 8680.2 (int. 6).

Table 3

Nitrogen Sequence

	Identification		HD 151932 (WN6+)		HD 192163 (WN6)		HD 193077 (WN5)	
Element	λ	Designation	Int	λ	Int	λ	Int	λ
Hα	6562.8	$2^2P^o-3^2D$	10	62.9	20	62.2	20	62.3
He II	6560.1	$4^2F^o-6^2G$						
N II	*6610.6	$3p'^1D_2-3d'^1F^o_3$					1-2	11.5
N III	*6642.6	$4d^2D_{2\frac{1}{2}}-3d^4D^o_{2\frac{1}{2}}$					1	42.7
He I	6678.1	$2^1P^o_1-3^1D_2$	3	80.8	8	76.3	2-3	85.7
N V	*6719	$7^2S-8^2P^o$			2	21.6	1s	16.6
(N I	6645.0	$3p^4D^o_{3\frac{1}{2}}-5s^4P_{2\frac{1}{2}})$						
N III	*6767.4	$3d^2P^o_{2\frac{1}{2}}-6d^2D_{2\frac{1}{2}}$			1?	69.8		
			4A	74.5			5A	69.4
(N II	*6888.7	$3p^5S^o_2-3d^5P_3)$			3	93.3		
N III	6965.4	$3p'^2D_{2\frac{1}{2}}-4d^2F^o_{2\frac{1}{2}}$			2?	65.4		
He I	*7065.2	$2^3P^o_{2,1}-3^3S_1$	2	71.6	2	57.0	1	53.5
(Si IV	7046.1	$5d^2D_{2\frac{1}{2}}-6p^2P^o_{1\frac{1}{2}})$						
N IV	*7109.2	$3p^3P^o_1-3d^3D_2$	4	5.0	25	11.4	20	14.4
N IV	*7123.1	$3p^3P^o_2-3d^3D_3$	4	22.3				
N II	*7139.8	$3d^3P^o_2-4p^3D_3$	1?	47.8			2?	43.0
(He II	7177.5	$5^2G-11^2H^o)$			3?	69.9		
			0?	83.9			1?	72.0
N II	7217.0	$3d^3P^o_1-4p^3D_2$	2	16.4			2	20.6
N II	7459.3	$3d^3P^o_0-4p^3D_1$			2s?	53.0		
He I	7281.3	$2^1P^o_1-3^1S_0$			2s?	79.6		
N V	*7320.8	$7^2P^o-8^2D$	2	33.8				

Table 3 (continued)

Identification			HD 151932 (WN6+)		HD 192163 (WN6)		HD 193077 (WN5)	
Element	λ	Designation	Int	λ	Int	λ	Int	λ
N III	7355.5	$3p^2D_{1\frac{1}{2}}$-$3d^2D^o_{2\frac{1}{2}}$			0	50.2		
Si III	7355.0	$4d^3D_{3,2,1}$-$3d^3P^o_2$						
N III	*7410.8	$3s^4P^o_{1\frac{1}{2}}$-$4s^2S_{\frac{1}{2}}$			1	10.3		
N III	7403.7	$3p^2D$-$3d^2D^o$						
N III	7418.3							
N II	7444.0	$3d'F^o_3$-$4p^3D_2$	1s?	38.6				
N II	7510.1	$3d^3P^o_2$-$4p'P_1$	1s?	5.3				
N V	*7600.2	$7d^2D$-$8f^2F^o$	3	...	15	?90.9	10	?90.1
N V	7615.8	$7f^2F^o$-$8g^2G$						
N II	7609.1	$3d'P^o_1$-$4p^3P_2$						
He II	7592.7	5^2G-10^2H^o						
N III	7685.6	$5d^2D_{2\frac{1}{2}}$-$6f^2F^o_{3\frac{1}{2}}$			3?	86.9		
Si IV	7678.3	$6f^2F^o_{3\frac{1}{2}}$-$7g^2G_{4\frac{1}{2}}$						
N III	7859.9	$3d^4F^o_{4\frac{1}{2}}$-$5g^2G_{3\frac{1}{2},4\frac{1}{2}}$					2	68.3
N II	7897.9	$4p'P_1$-$5s'P^o_1$			1s?	7.8	0	91.5
N II	7906.3	$3d'P^o_1$-$4p^3D_2$						
N III	*8022.2	$5f^2F^o_{3\frac{1}{2}}$-$6g^2G_{3\frac{1}{2},4\frac{1}{2}}$			4	5.3		
N III	*7970.1	$4d^2D$-$3d^4F^o$			3	35.0		
N III	7983.3							
N III	8003.1							
N III	8005.7							
N III	8025.7							
N III	7967.1	$3s^2P^o$-$3p^4D$						
N III	7989.7							
N III	7999.5							
N III	8039.5							

Table 3 (continued)

Element	Identification λ	Designation	HD 151932 (WNo+) Int	λ	HD 192163 (WN6) Int	λ	HD 193077 (WN5) Int	λ
N III	8062.5	$3s^2P^o_{1\frac{1}{2}}$-$3p^4D_{1\frac{1}{2}}$	27	55.7				
N II	8089.1	3p'D-3d^{3}F^o	2n?	7.6				
N II	8128.2							
....	*.....	.....			6	13.2	4	12.1
....	*.....	.....	8	29.5	7	42.7	6	44.6
(N II	*8253.3	$4p^3D_1$-$5s'P^o_1$)			4-5	?59.4	1?	55.8
(N II	8288.1	$4p^3D_2$-$5s'P^o_1$)						
(N II	8297.4	$3d'P^o_1$-$4p'P_1$)						
N III	8306.4	$3s^2P^o_{\frac{1}{2}}$-$3p^2P_{1\frac{1}{2}}$			1s?	12.2	1?	27.8
He I	*8361.8	3^3S-6^3P^o					2	59.4
N II	8589.3	$4p^3P_1$-$5s'P^o_1$	2	88.9				
(N I	8594.0	$3s^2P_{\frac{1}{2}}$-$3p^2P^o_{\frac{1}{2}}$)						
N II	8660.7	4p^{3}D-5s^{3}P^o	2	99.9				
N II	8675.7							
N II	8695.2							
N II	8699.1							
N II	8698.4	4d^{3}F^o-5f^{3}G						
N II	8702.2							
N II	8710.8							
N II	8703.3	$4d^3F^o_4$-$5f'G_4$						
N II	8686.9	$2p^3P^o_1$-$3p'S_o$						
(N I	8680.2 to 8747.3	$3s^4P$-$3p^4D^o$)						
N III	8738.3	$4p^2P_{1\frac{1}{2}}$-$4d^4P^o_{2\frac{1}{2}}$	0	40.7				
P_{12}	8750.5	3^2D-12^2P^o)						

NOTES TO TABLE 3

*λ 6610.6, *λ 6642.6—These two lines are difficult to measure and somewhat uncertain. Other transitions of the $4d^3D-3d^4D^o$ multiplet may contribute to the emission at λ 6642.7; these other transitions are λλ 6644.5, 6638.6, 6628.9, 6652.3, and 6630.1.

*λ 6719, *λ 6767.4—Measurement difficult in HD 192163.

*λ 6874.5—This looks like an absorption feature; however, it may simply be a narrow spacing between two unidentified emissions.

*λ 6888.7—This emission is also weakly present in HD 151932 and HD 193077.

*λ 7065.2—Difficult to measure in shortward wing of the intense *N* IV emission.

*λ 7109.2, *λ 7123.1—Other weaker components of the *N* IV multiplet contribute to this emission. In HD 192163 the width is hard to determine, since weak additional emissions appear in the wings which extend farther than in HD 193077.

*λ 7139.8—Difficult to measure on longward side of the intense *N* IV emission.

*λ 7320.8, *λ 7410.8—Measurement difficult and uncertain.

*λ 7600.2—This is a strong emission which is sharply and deeply cut by atmospheric absorption. It is not possible to determine the line centers and widths with accuracy. Four $8 \rightarrow 7$ transitions of *N* V fall near λ 7600.

*λ 8022.2, *λ 7970.1—This may be a single emission with reversal at λ 8021.5.

*λ 8213.2, *λ 8242.7, *λ 8259.4—Complex pattern. The triple structure is well marked on two of the three spectrograms of HD 192163 (see Fig. 2). In HD 151932 a broad emission with sharp reversal at 8229.5 is observed; the line extends from λ 8198.6 to λ 8255.4. In HD 192163 there may be a reversal at λ 8228.6, between the components of intensities 6 and 7. In HD 193077 the minimum (reversal?) is measured at λ 8228.6.

*λ 8361.8—There may be a minor contribution by the $3p^3D-4d^4D^o$ multiplet of *N* III, extending from λ 8344.3 to λ 8387.0.

tions. As appears readily from an examination of the *Revised Multiplet Table*, little laboratory work has been done on the infrared spectra of the ions which are of interest for Wolf-Rayet stars (*C* II–IV, *N* II–V, *O* II–VI, *Si* III and IV). On the basis of the term table recently published by C. E. Moore,[4] all the permitted transitions between known terms were computed for the wave-length region λλ 6500–8800. For *C* II, the intersystem combinations are weak, yet have been considered; for *C* III no intercombination has been computed. In *N* II, the singlet and triplet terms are well connected by intersystem combinations; intercombinations have also been considered for *N* III, but not for *N* IV; for *N* V, the predicted wave lengths are rather poor, since they are based on extrapolations in term-series formulae. Since the oxygen ions should give only fairly weak lines, the intersystem combinations have been mostly omitted for *O* II–VI. The same applies to *Si* III.

It is obvious that such tables of predicted lines do not permit as safe and complete identifications as would tables of laboratory lines. Only little help may be found in the relative intensities; moreover, certain predicted transitions may actually be too weak to appear in the laboratory, while new lines may be found experimentally, leading, actually, to new terms. Unsatisfactory as the procedure is, there did not seem to be any alternative, pending a laboratory investigation of the infrared region of the spectra of the ions concerned. Indeed, it is hoped that the publication of the present results will serve as an incentive to laboratory spectroscopists.

Our results are collected in Tables 2 and 3. For each star, we give the estimated intensities and the mean wave lengths of the line centers. Doubtful identifications or minor contributions are in parentheses. Asterisks preceding entries in the first column of wave lengths refer to notes concerning the stellar lines. Most strong lines of the WC stars are satisfactorily identified. The line at λ 7862 is not well identified, while the patterns near λ 8330 and λ 8250 are not convincingly disentangled. The situation is worse in the case of the WN stars. The double emission at λ 8005 and λ 8035 is not too well explained. Worse still is the case of the complex emission near λ 8240. In this pattern the two strongest components near λ 8213 and λ 8244 are unexplained. An important contribution by the $3s^4P-3p^4P^o$ multiplet of *N* I, extending from λ 8188 to λ 8242, appears unlikely; *He* II can play only a minor role. From a comparison between the three stars it seems that the pattern is due to at least two ions. It is rather tempting to assume that λ 8213 and λ 8244 are due to *N* III. The half-widths of the lines in kilometers per second (ejection velocities) are listed separately in Tables 4 and 5.

Figures 1 and 2 show that a strong emission appears in both sequences around the intense telluric absorption near λ 7600. This emission starts on the shortward side of the atmospheric absorption. In the WC sequence, the emission is fairly well explained by the $3s^3P^o-4d^3D$ multiplet of *C* III, while in the WN sequence the identification with *N* V + *N* II does not seem so convincing. The profiles of the emissions appear so similar in the WC and WN sequences (although not quite identical) that one would feel tempted to attribute these emissions to the same atom. Pending more definitive identifications no attempt will be made here to discuss either the widths of the lines or the possibility of coexistence of carbon and nitrogen lines.

Our thanks are due to Mrs. D. Crespin Sengier for her help in preparing the tables of predicted lines.

[4] *Atomic Energy Levels* (Circ. Nat. Bur. Stand. No. 467), 1949.

FIG. 1.—Infrared spectra of WC stars

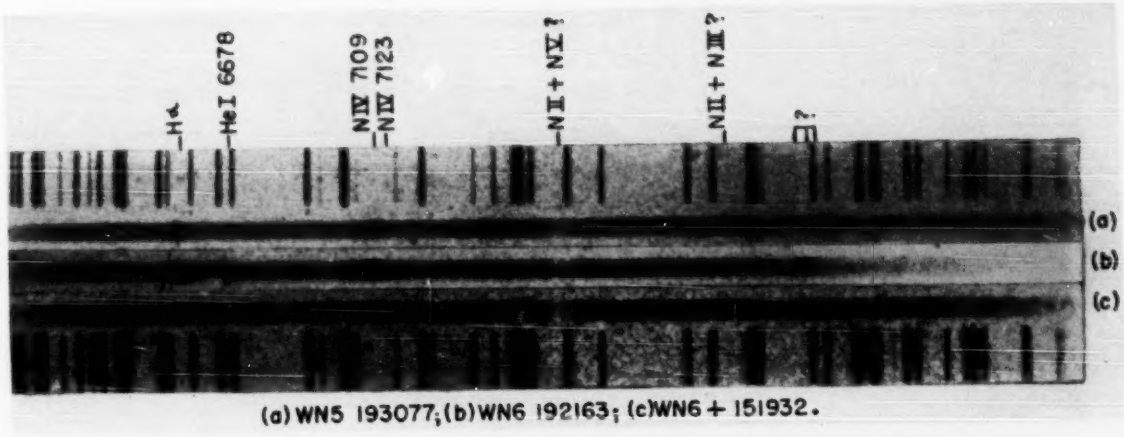

FIG. 2.—Infrared spectra of WN stars

TABLE 4

LINE WIDTHS (CARBON SEQUENCE)

HD 184738 (WC8)		HD 164270 (WC8)		HD 168206 (WC7)		HD 192103 (WC7)	
λ	W	λ	W	λ	W	λ	W
						6565.4	557
		6581.8	780	6577.9	1070		
		6680.2	730			6596.4	537
6730.1	738	6736.5	815	6747.3	1077	6740.8	600
6780.7	526	6785.0	555			6894.6	683
7035.6	309	7033.1	328	7053.5	1165	7025.6	897
7064.4	332	7062.3	785			7060.2	595
				7126.9	924		
		7231.5	950			7378.9	520
				7681.9	730		
		7705.3	385				
		7732.2	428	7727.7	842	7726.0	935
		7787.6	830				
						7861.8	744
		8068.9	586				
		8195.3	605	8203.8	740		
				8255.5	675		
		8320.0	791	8341.0	726	8327.6	995
		8497.7	330	8508.0	797	8499.1	875
						8665.9	750

TABLE 5

LINE WIDTHS (NITROGEN SEQUENCE)

HD 151932 (WN6+)		HD 192163 (WN6)		HD 193077 (WN5)	
λ	W	λ	W	λ	W
6562.9	500	6562.2	1283	6562.3	754
6680.8	840	6676.3	1215		
		6721.6	1005?		
		6895.3	886		
		6965.4	1017		
		7057.0	1020		
		7111.4	1323	7114.4	599
		7169.9	945		
		7590.9	1105	7590.1	993
		8213.2	347	8212.1	248
8229.5	1030	8242.7	371	8244.6	378
		8259.4	348		

THE SPECTRUM OF COMET BESTER (1947k)*

P. SWINGS AND THORNTON PAGE
University of Liége, McDonald and Yerkes Observatories
Received January 16, 1950

ABSTRACT

An extensive program of observations, planned in advance, was carried out during the predicted return of Comet Bester in March and April, 1948, as the comet receded from heliocentric distance 0.8 A.U. to 1.55 A.U. The eighteen spectra obtained extend over various parts of the observable region from λ 3070 to λ 8760, most of them from λ 3500 to λ 6800 on grating dispersion. These, together with seventeen direct photographs, provide virtually a continuous record of changes in the comet during the observing period. Since the slit of the spectrograph was oriented along the tail, extending about 4.5 minutes of arc from the nucleus, our spectrograms record the extent of the various molecular bands away from the nucleus.

Based on this material and on observations of other comets, the following topics are discussed:

a) Variations with heliocentric distance, r.—In Comet Bester the ratios CN/C_2, λ 4050/*CH*, λ 4050/*CN*, λ 4050/C_2 and probably *OH*/*NH* all increase regularly with increasing *r*. No flares or sudden changes in spectrum were observed.

b) Extent of bands from the nucleus.—CO^+, N_2^+, λλ 3378, 3509, and 3674 are found exclusively in the tail; *CN*, C_2, *NH*, *OH*, λ 4050, and NH_2 follow in order of decreasing extent from the nucleus.

c) The far ultraviolet region.—The ratio *OH*/*NH* varies from comet to comet, being somewhat less than unity for Comet Bester, greater than unity for Comet 1941d, and much less for 1947n and 1941c, which are in other respects comparable. In Comet Bester the *OH* bands have a peculiar rotational distribution, probably due to the fluorescence mechanism.

d) The photographic regions.—Twenty lines in the "λ 4050 group" behave in Comet Bester as if they originate from one molecular species.

e) The red and infrared regions.—The existence of bands (tentatively identified with the "red system" of *CN*) at λ 7906 is confirmed, and other bands of the "red system" at shorter wave lengths tentatively identified. A number of other faint maxima between λ 7000 and λ 8700 are noted.

f) The spectrum of the tail.—Nine bands of the CO^+ "comet-tail system" are recorded, the (3, 0) band being abnormally strong. Four bands of the "Baldet-Johnson system" of CO^+ are observed. Tentative identifications of the "β system" of *NO* and the "Schumann-Runge system" of O_2 are noted. The strong emissions at λλ 3378, 3509, and 3674 are identified with CO_2^+, the third ionized molecule to be identified in comet tails.

A summary of identifications and conclusions is given at the end of the paper.

I. INTRODUCTION

When the determination of the orbit of Comet Bester (1947k) indicated that this object would become fairly bright and easily observable after its perihelion passage on February 16, 1948, we decided to plan carefully a program of spectroscopic observations, with the following three aims in view:[1] (*a*) to obtain slit spectrograms of the tail, especially in the ultraviolet region; (*b*) to obtain spectrograms of the head throughout the region from λ 3000 to λ 9000, in sufficient numbers to permit a study of the variations with heliocentric distance; and (*c*) to compare these spectra with those of other comets, especially those observed before perihelion passage.

Very little information is available on the ultraviolet spectrum of comet tails. As far as we know, ultraviolet tail spectra have been obtained only with slitless instruments—e.g., for the following comets: 1907d (Daniel) by J. Evershed,[2] to λ 3580; 1908c (Morehouse) by De la Baume Pluvinel and Baldet,[3] to λ 3269; 1911c (Brooks) by the same

* *Contributions of the McDonald Observatory, University of Texas*, No. 186.

[1] As this paper goes to press we have received Fehrenbach and Cortès, *Ann. d'ap.*, **12**, 66, 1949, containing a discussion of the spectra of Comets 1947k and 1948g, which, however, duplicates nothing here.

[2] *M.N.*, **68**, 16, 1907.

[3] *C.R.*, **154**, 1286, 1912; Baldet, thesis, p. 36.

observers,[4] to λ 3790; and Halley by Slipher and Lampland,[5] to λ 3585. The only slit spectrograms of comet tails known to us have been taken at the Lick Observatory of 1908c (Morehouse)[6] and of 1911c (Brooks),[7] covering the region from λ 3850 to λ 4800. One fair slit spectrogram of the tail of Comet 1940c (Cunningham) was obtained at the McDonald Observatory but was rather weak. The results of its examination will appear shortly.[8]

Ultraviolet slit spectrograms of comet tails not only may reveal new molecules existing in the tail but may also yield profiles of the known molecular bands, and hence the rotational temperatures of the corresponding molecules. Our understanding of the physical mechanisms at play in comet tails is still so rudimentary that any addition in observational evidence is of importance. It is obvious that only molecules with a very long life can be found in the tails at large distances from the nucleus. There are few molecules known which would be able to live for days or weeks in the field of solar radiation before becoming photo-dissociated or photo-ionized. Actually, new bands found in comet tails may lead physicists to the discovery of "photo-resistant" molecules, in the same way that astronomical observations of CH^+ and CH_2 bands preceded and inspired considerable laboratory work.

While a great deal of qualitative observational information has already been gathered on the heliocentric-distance variations of the absolute and relative intensities of the different bands in comet spectra, there still remains a number of questionable points in the mere description of these phenomena. For example, K. Wurm, in his excellent review of cometary problems,[9] assumes that the ratio CN/C_2 increases as the heliocentric distance, r, decreases, which he bases on Baldet's observations[10] of Comet Brooks (1911c) from $r = 1.42$ to $r = 0.5$, and on van Schewick's[11] photometric investigation of Comet Finsler (1937f). Observations of comets at the McDonald Observatory do not confirm this statement, especially in the case of Comet 1948I.[12] Similarly, Wurm's statements on the behavior of the ratio CH/λ 4050, based mainly on old observations of Comet Brooks, are not confirmed by the recent investigation of Comet 1948I.[12] Such information is required for confirmation of Wurm's theory of "dissociation series."[9]

Within the temporary gaseous atmosphere surrounding the nucleus of a comet and extending into its tail, our usual thermodynamical concepts of temperature and pressure become meaningless. There can be practically no collisional effects, and the problem becomes one of pure photochemistry. If the emission of gas from the nucleus were suddenly interrupted, for instance, the intensity of the CN and C_2 bands would certainly decline and vanish in a few days, the CO^+ bands of the tail after a few weeks. Wurm's theoretical procedure for studying molecular abundances in comets is similar to that followed in discussing a series of radioactive disintegrations. For detailed confirmation of this theory, a longer series of spectra is required than is provided in this paper and more quantitative intensity data than are given here.

Spectroscopic comparisons between different comets, and especially between comets observed before and after perihelion passage, are of great value. As far as we know, no single comet has been described spectroscopically before and after perihelion passage, be-

[4] *C.R.*, **147**, 666, 1908, and **148**, 759, 1909; *Ap. J.*, **34**, 89, 1911; Baldet, thesis, p. 24.

[5] *Lowell Obs. Bull.*, **2**, 3, 1911.

[6] Campbell and Albrecht, *Lick Obs. Bull.*, **5**, 58, 1908; H. D. Curtis, *Lick Obs. Bull.*, **5**, 135, 1909.

[7] W. H. Wright, *Lick Obs. Bull.*, **7**, 8, 1912.

[8] P. Swings and H. Sauvenier, *Bull. Acad. R. Belgium*, **35**, 931, 1949.

[9] *Mitt. Hamburger Sternw.*, **8**, 51, 1943.

[10] Thesis, p. 44.

[11] *Zs. f. Ap.*, **21**, 142, 1942.

[12] P. D. Jose and P. Swings, *Ap. J.*, **111**, 41, 1950.

tween which epochs significant differences are expected in the relative intensities of different bands. M. G. J. Minnaert[13] has treated theoretically the superficial temperature of a sphere with a diameter of 1 km, following the orbit of Halley's comet. In the case of both a stone and an iron nucleus he found that the surface temperature after perihelion passage should for a long time remain higher than before passage. In a recent unpublished investigation, E. Lebon[14] has applied Minnaert's idea to the short-period Comet Encke, with results very similar to those of Minnaert for Comet Halley.

We therefore expect differences in the relative intensities of cometary bands at a given heliocentric distance, before and after perihelion, due to differences in the surface temperature of the nucleus. Other factors, such as the finite life of the molecules, exhaustion of gases, rotation and irregularities of the solids, etc., may further affect these relative band intensities.

Pending spectroscopic observations of the same comet before and after perihelion passage, the best we can do at present is to compare different comets at the same heliocentric distance, some before passage, others after, as in Section III, below. Comparisons between different comets may also help to clarify our ideas regarding the nature, sizes, and distributions of solid particles in the nuclei and the way gases are absorbed and liberated.

The remainder of this paper is divided into seven sections. Each of Sections III–VII presents a pertinent part of the observational results, together with discussion and conclusions. Section VIII is a summary of conclusions.

II. THE OBSERVATIONAL MATERIAL

Comet Bester (1947k) passed perihelion on February 16.433, 1948, the perihelion distance being $q = 0.748$. All our observations were made (by Page) after perihelion. During the observing period the radial velocity of the comet relative to the sun, dr/dt, varied from 17.4 km/sec on March 3 to 24.2 on April 13.[15] The absolute magnitude has been determined by J. Bouška and V. Vanýsek and by P. Ahnert.[16] The value after perihelion was $m_0 = 6.6$, practically the same as that of the two bright comets 1947n ($m_0 = 6.2$) and 1948l ($m_0 = 5.9$). However, these latter two objects had much smaller perihelion distances, which accounts for their temporarily higher brightness than 1947k. Comet Bester definitely has a higher absolute magnitude than Comet Encke ($m_0 = 10.3$ in 1947).

A total of 18 spectra and 17 photographs of Comet Bester was obtained with the 82-inch reflector of the McDonald Observatory, as listed in Table 1.[17] Fourteen of the spectra were obtained at the prime focus with the B spectrograph, a grating instrument with an $f/0.65$ solid Schmidt camera of UV glass,[18] and dispersion about 330 A/mm. The unique characteristics of this instrument made large parts of the present investigation possible. Its unocculted slit length corresponds to about 5 minutes of arc. The telescope was guided with the nucleus at one end of the slit, and the slit was oriented along the tail. The photographs, also taken at the prime focus of the 82-inch telescope, were made primarily to check the direction of the comet tail, which was thin and filamentary during most of the observing period (see Fig. 1). The only practical method of avoiding a

[13] *Proc. Amsterdam*, **50**, 826, 1947.

[14] Thesis, Liége, 1949.

[15] Kindly provided by Dr. L. E. Cunningham in a private communication.

[16] *Bull. Astr. Inst. Czechoslovakia*, **1**, 62, 1949; *A.N.*, **277**, 135, 1949.

[17] A preliminary report of these observations was made to the A.A.S. by Page, *Pub. A.S.P.*, **60**, 249, 1948.

[18] A more complete description of this instrument will soon be published; see also Page, *A.J.*, **54**, 47, 1948.

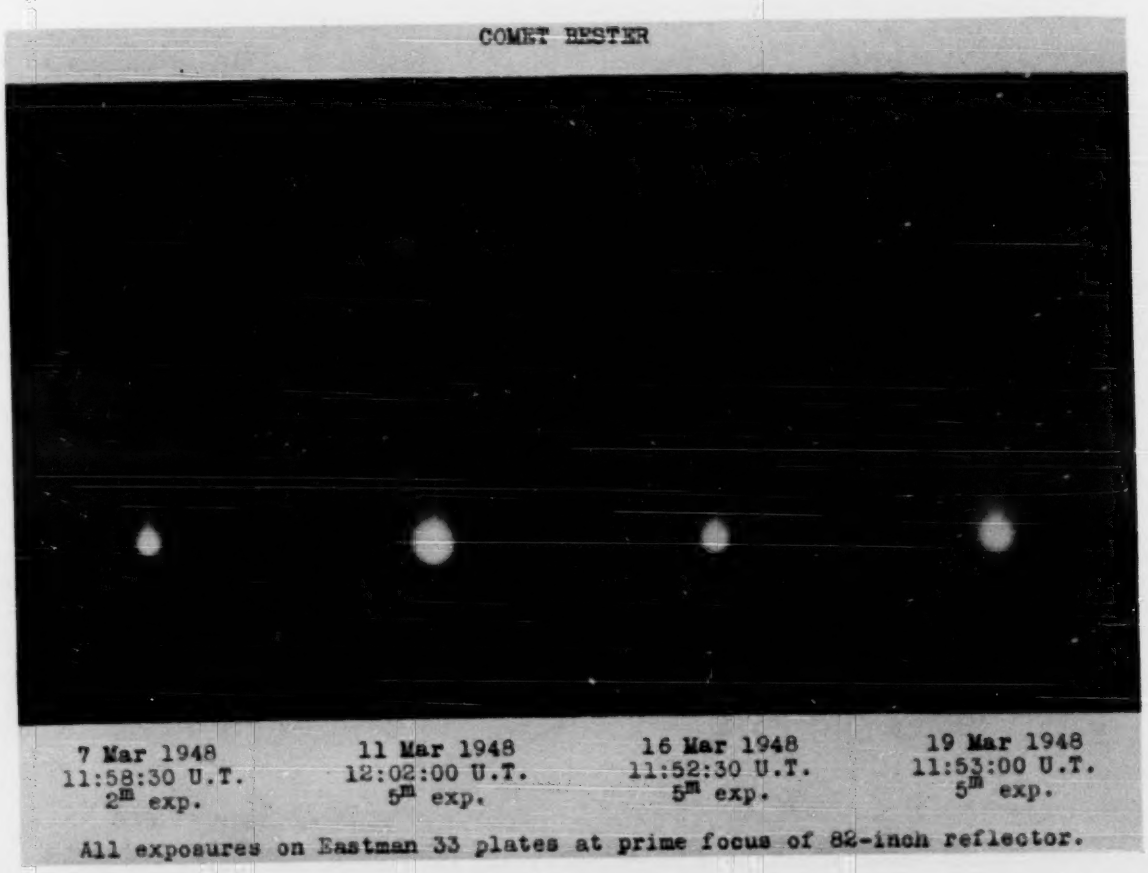

FIG. 1.—Four exposures on Eastman 33 plates at the prime focus of the 82-inch reflector, showing the faint, filamentary, and changing tail of Comet Bester (1947k). Scale of reproduction: 1 mm = 30″.

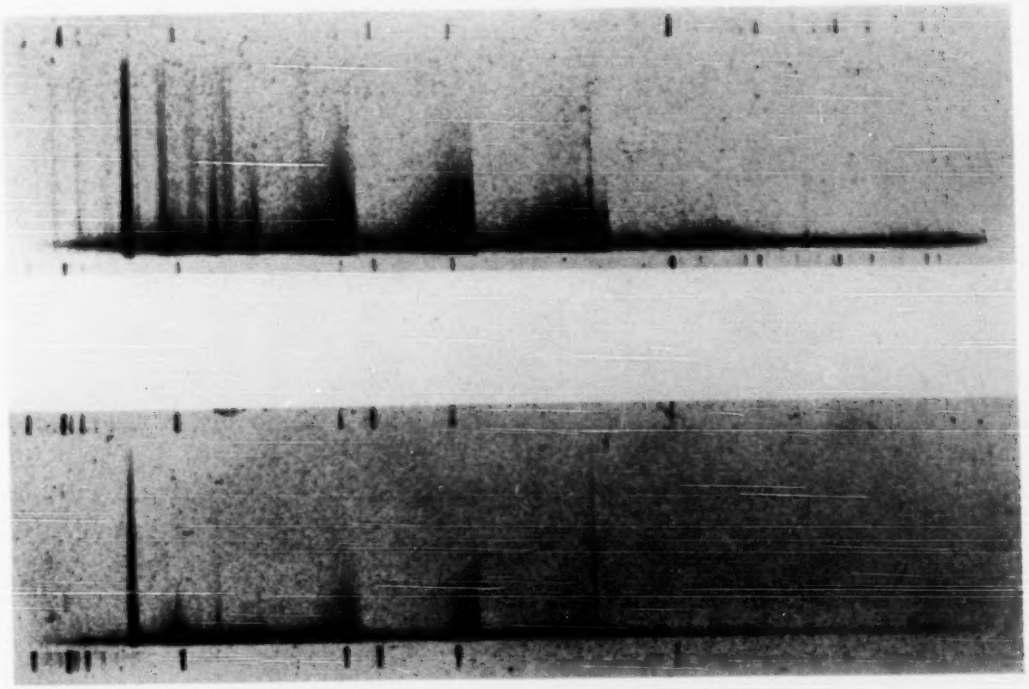

FIG. 2.—Two enlarged spectra of Comet Bester with approximately linear dispersion from λ 3650 to λ 6900 on Eastman 103*a*-F*. The nucleus is near the lower comparison spectrum; the slit is oriented along the tail, with a length corresponding to 280″ in the sky. Upper spectrum (B 133, exp. 50 min.) was taken at $r = 0.86$ A.U.; the lower (B 206, exp. 2 hr.) at $r = 1.30$ A.U. The comparison spectrum is from a cadmium-solder spark and a neon tube.

trailed image of the comet was to set the variable-rate telescope drive and the declination drive for proper guiding beforehand and then to make the exposures without guiding. This pre-setting was generally accomplished during exposures on the spectra, the direct photograph being made immediately thereafter.

For the infrared spectra,[19] a narrow strip of Wratten "a" gelatin filter covered a portion of the B spectrograph slit, to eliminate the blue and ultraviolet second-order spectrum. The nucleus of the comet was guided on the edge of this filter, so that the resulting spectrogram shows pure infrared spectrum in the filtered part and the second-order spectrum superimposed on the unfiltered part. The second order of *CN* λ 3883 served as

TABLE 1

COMET BESTER (1947k), ALL PLATES AND FILMS

Plate or Film No.	1948 Date U.T.	Exp. (Min.)	Emulsion	Mid-Alt.	Slit			Region λλ	r (A.U.)	Remarks
					w (Mm.)	l (″Arc)	p.a.			
	Mar.									
B 99	2.51	20	103*a*-F	15°	0.40	290	58°	3500–6500	0.80	Poor focus
B 103	3.49	50	103*a*-F*	10½	.20	103	60	3600–6700	0.81	Excellent def.
PFC 1874	4.50	1	103*a*-F	16½				(Tail 150″)	0.82	Fair def.
B 115	6.49	30	103*a*-F*	16	.10	290	247	3600–5500	0.83	Good line extension
PFC 1875	6.51	1	103*a*-F	21½					0.83	Trailed
PFC 1876	6.51	1	E 33	22				(Tail 125″)	0.83	Poor def.
B 121	7.48	30	103*a*-F*	14	.20	290	270	3500–6700	0.84	Fair def.
PFC 1877	7.50	2	E 33	20				(Tail 640″)	0.84	Fair
B 133	9.48	50	103*a*-F*	17½	.20	290	273	3500–6700	0.86	Excellent def.
PFC 1880	9.50	2	E 33	25					0.86	Trailed
B 136	11.47	45	103*a*-F*	20	.20	290	267	3450–6700	0.88	Good def.
PFC 1884	11.50	2	E 33	27				(Tail 640″)	0.88	Excellent def.
PFC 1885	11.50	5	E 33	28				(Tail 2000″)	0.88	Excellent def.
B 151	13.47	75	I-N*	22	.50	290	267	(Nothing)	0.90	a filter
B 161	14.48	(45–15)	103*a*-F*	25	.20	290	265	3650–5000	0.92	Weak (clouds)
B 163	15.46	120	I-N*	21	.50	100	270	5800–8800	0.93	a filter on ½ of
B 165	16.45	120	I-N*	21	.50	100	270	5800–8800	0.94	image
PFC 1887	16.49	5	E 33	33½				(Tail 1000″)	0.94	Trailed
PFC 1889	17.49	1.3	E 33	33½				(Tail 50″)	0.95	Fair def.
B 190	18.46	90	103*a*-O†	29½	.20	290	275	3400–5000	0.96	Excellent def.
PFC 1890	18.50	3	E 33	38½				(Tail 640″)	0.96	Fair def.
PFC 1891	18.50	1	E 33	39				(No tail)	0.96	
B 192	19.45	90	103*a*-O†	27	.16	290	270	3400–4400	0.97	Good def.
PFC 1892	19.49	6	E 33	39				(Tail 460″)	0.97	Good def.
Qf/1 10477	25.42	195	103*a*-O†	31	.013	44	270	3000–3700	1.04	Far UV good
Gf/1 10486	26.45	125	103*a*-O†	41	.013	44	270	3800–5000	1.06	Fair def.
	Apr.									
Gf/1 10559	3.47	45	103*a*-F*	63	.013	44	270	3800–5700	1.16	Excellent def.
B 199	11.46	60	103*a*-F*	59	.20	290	180	3600–6700	1.27	Good def.
PFC 1893	11.49	6	E 33	60					1.27	Poor
B 206	13.41	(120)	103*a*-F*	53	.20	290	296	3460–5600	1.30	(Clouds)
PFC 1894	13.47	5	E 40	56					1.30	Trailed
PFC 1895	13.47	1.1	E 40	56					1.30	Trailed
PFC 1896	14.48	2	E 40	53					1.31	Trailed
PFC 1897	14.48	5	E 40	53					1.31	Trailed
Qf/1 10838	May 1	106	103*a*-F		0.013	25	270	3800–6700	1.55	Good def.

* Ammonia hypersensitized.

† Films baked to increase sensitivity.

[19] Obtained as for Comet 1947n. See Swings and Page, *Ap. J.*, **108**, 526, 1948.

a useful wave-length check. The two 2-hour infrared exposures on Eastman I-N* (hypersensitized) film with wide (33 A) slit represent about the limit of detection in the near infrared. The apparition of a brighter comet seems to be the only hope at present for improving these observational results.

Although the films were hypersensitized and pressed against the oiled surface of the solid Schmidt camera, they were all handled as for accurate photographic photometry; calibrating spots were impressed on another part of the same hypersensitized sheet of film, and characteristic curves were derived therefrom. No standardization was attempted. In the ultraviolet and visual regions, band intensities were largely estimated by eye in the eyepiece of the measuring engine. However, microphotometer tracings were made of twelve spectra, and rough intensities were reduced without regard for variation in emulsion sensitivity with wave length. Such "intensity-curves," reduced from tracings of the two infrared spectra, B 163 and B 165, are shown in Figure 3, compared with curves obtained in the same manner for the spectrum of a *CN* discharge tube and the night sky.[20]

Two spectra were obtained with the Cassegrain spectrograph,[21] using the $f/1$ (80-mm) Schmidt camera with dispersion 105 A/mm at λ 4000. Another was made with all-quartz optics, dispersion about 125 A/mm at λ 3300, transmitting to λ 3070. Because of the larger scale at the Cassegrain focus, only a 40″ extent from the nucleus along the comet's tail could be focused on the slit for these three spectrograms.

Thirteen of the spectra were measured carefully for as accurate wave lengths as the small dispersions would allow. Each spectrum was measured twice (by Page), and corrections were made for curvature of the slit image. In some cases independent measures were made by Swings.

In most parts of the observed wave-length region, lines or band heads were measured on two or more spectra. Intercomparison of these independent measures resulted in the elimination of spurious lines, a final "adopted" wave length for each accepted line, and an estimate of the error in wave length, which is about ±2 A. A third characteristic of each line, in addition to wave length and intensity, is its extent from the nucleus, which could be readily measured on these spectra, and was of value in this procedure.

III. VARIATION OF THE MOLECULAR EMISSIONS WITH HELIOCENTRIC DISTANCE

Our series of spectrograms from $r = 0.80$ to $r = 1.55$ reveals a number of conspicuous intensity variations. It is well known that local transitory features in comet heads may have spectra which differ from those of other regions, such differences presumably being due to differences in the size or constitution of solids in the head, and to their motions. However, in the present series there is virtual continuity in the variations of the relative intensities, and it is reasonable to assume that local spectral irregularities and bursts do not play a significant role in the general evolution observed.

There follow short, general descriptions of the best spectrograms:

$r = 0.80$ and 0.81.—*CN* is much longer than C_2; in the central part of the head, (0, 0) of *CN* has about the same intensity as (0, 0) of C_2; λ 4050 has about the same intensity as (0, 1) of *CN* and (2, 0) of C_2 but is much shorter; λ 4050 is a little stronger than the strongest *CH* line; the strongest NH_2 is conspicuous but very short.

$r = 0.83$.—*CN* is very much longer than C_2: for example, (0, 1) of *CN*, which is weaker than (1, 0) of C_2 in the nucleus, extends farther out into the head; λ 4050 is definitely more intense than the strongest *CH* but extends similarly in the head; NH_2 is extremely short.

[20] By the courtesy of Dr. J. G. Phillips, who had constructed the *CN* discharge tube at the Yerkes Observatory, and Dr. A. B. Meinel, who made available a tracing of the night-sky spectrum before publication.

[21] Fully described by G. W. Moffitt, *Contr. McDonald Obs.*, No. 1, p. 74, 1936.

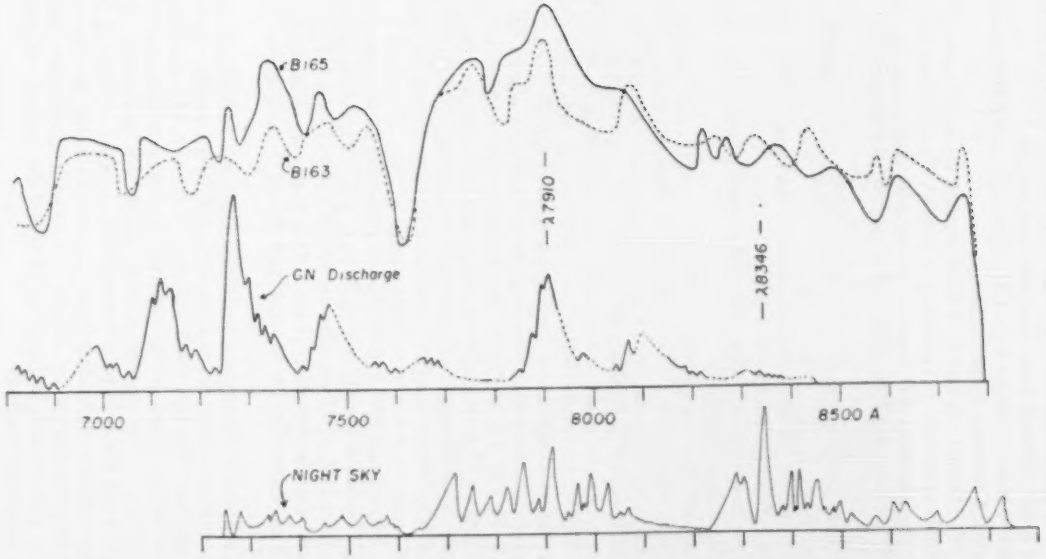

FIG. 3.—Unstandardized "intensity-curves" in the infrared spectrum. Comet Bester (films B 163 and B 165) compared with a *CN* discharge and with the spectrum of the night sky.

$r = 0.84$ *and* 0.86.—Same as for $r = 0.83$ in the head; NH_2 is conspicuously strong and short (see Fig. 2).

$r = 0.88$.—λ 4050 is appreciably stronger than CH; the tail spectrum in the ultraviolet has an appearance quite different from the blue-violet region.

$r = 0.92$.—λ 4050 is much stronger than CH; NH_2, CH, and λ 4050 have the same extension in the head; CN is much longer than C_2.

$r = 0.96$ and 0.97.—Strong tail bands; λ 4050 is much stronger than CH (see Fig. 5).

$r = 1.04$.—The only spectrogram extending to λ 3070. The OH lines extend to shorter distances from the nucleus than NH lines of the same intensity (see Fig. 4).

$r = 1.06$.—λ 4050 is very much stronger than CH; CN is stronger relative to C_2 than at $r = 0.80$.

$r = 1.16$.—λ 4050 is much stronger relative to CN, C_2, and especially CH, than at $r = 0.83$.

$r = 1.27$.—The ratio CN/C_2 has increased with r; the ratios λ 4050/CN, λ 4050/C_2, and λ 4050/CH are still larger than at $r = 1.16$.

$r = 1.30$.—The same evolution continues; NH_2 is still conspicuous but very short; CN is of tremendous length (see Fig. 2).

$r = 1.55$.—C_2 has almost disappeared; CH is very weak; CN is long and strong; λ 4050 has the same intensity as (0, 0) of CN in the nucleus, but is extremely short.

Summarizing these observations, as far as they concern the head, we may state:[17] (*a*) The intensity ratios CN/C_2, λ 4050/CH, λ 4050/CN, and λ 4050/C_2 increase regularly with increasing r. (*b*) The bands of CN always extend farther from the nucleus than do those of C_2. (*c*) The lines of NH_2 and of the λ 4050 group are always very short.

Certain of these observed molecules may result from the same parent (e.g., C_2 and CN); others may give rise to another observed radical by photo-dissociation or photo-ionization (e.g., NH_2 to NH, CH to CH^+). The behavior of the intensity ratios of such molecules with heliocentric distance will eventually find interpretation in Wurm's series of photo-dissociations. The theory of such dissociation series is still very limited,[22] owing to lack of knowledge both of the "parent"-molecules and also of the "descendants." For example, we do not know what the immediate parent of the CH radical is, nor are we sure of the relative importance of the photo-dissociation and photo-ionization processes on CH—whether CH gives rise mostly to $C + H$ or to CH^+. Part of our ignorance of the descendants results from lack of information on the intensity of solar radiation in the far ultraviolet. Moreover, the identification of the λ 4050 group is still in doubt; recent laboratory work in Liége, especially by Monfils and Rosen,[23] casts grave doubts on its identification with CH_2.

The variation of absolute intensity of a molecular band as a function of r is connected with the rate of liberation of the parent-molecule at different surface temperatures of solid bodies in the nucleus. This rate itself will depend upon r; will be different for different molecules; and will be influenced by the sizes, shapes, rotations, and relative locations of the solids making up the nucleus. A small pebble will be warmed up more than a big rock; a metallic body will behave differently from a stone; a rotating body will be affected by the solar radiation differently from one always facing the sun; some of the bodies may be shielded from the sun by others. Sudden or irregular spectroscopic variations are presumably due to such interactions between the bodies—for example, to a change in shielding caused by motions.

The qualitative interpretation of the molecular extensions into the head can be under-

[22] R. Collet (thesis, Liége, 1949, unpublished) has tried the following dissociation series: $CH_4 \rightarrow CH_2 + H + H \rightarrow CH + H + (H + H) \rightarrow C + H + H + (H + H)$; $CH_4 \rightarrow CH_2 + H_2 \rightarrow CH + H + H_2$; and $H_2O \rightarrow OH + H \rightarrow O + H + H$. Although most of the physical constants involved are unreliable, the results seem encouraging. In the case of CH and OH, ionization should be included, since CH^+ is observed, and probably also OH^+.

[23] *Nature*, **164**, 713, 1949.

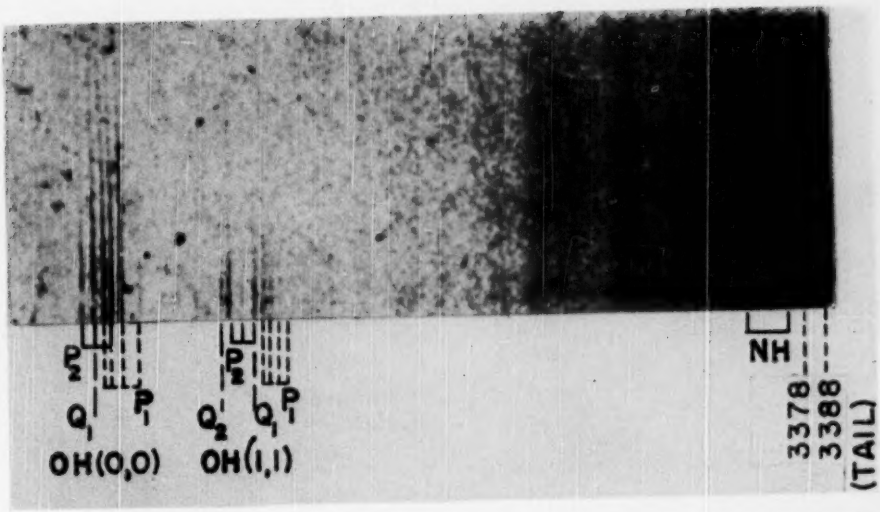

FIG. 4.—Enlargement of the far ultraviolet spectrum of Comet Bester at $r = 1.04$ A.U. ($Qf/1$ 10477, quartz-prism dispersion on Eastman 103*a*-O), showing bands of *OH* and *NH*. The nucleus appears near the bottom. The length of the slit corresponds to 40″ in the sky.

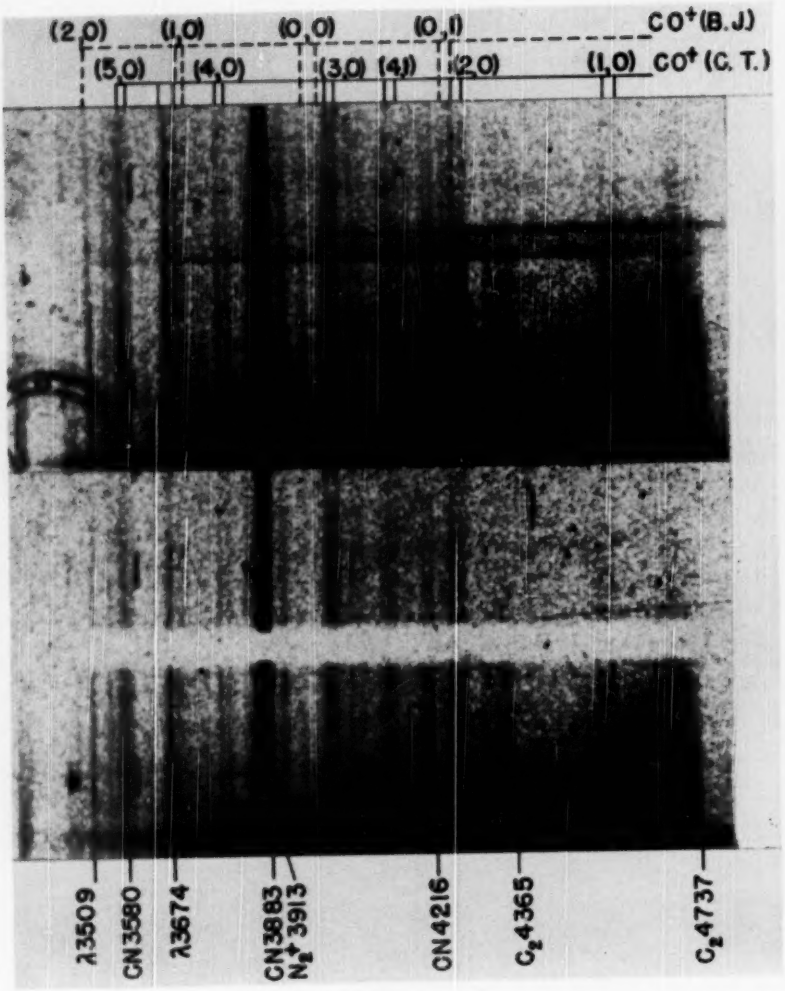

FIG. 5.—The ultraviolet tail spectrum of Comet Bester enlarged from films B 190 and B 193 (linear dispersion, λλ 3650–3800), taken at $r = 0.96$ A.U. (*upper*) and $r = 0.97$ A.U. (*lower*).

stood in terms of the average duration of a molecule and in terms of the velocity it acquires in the photo-dissociation of its parent-molecule. No detailed, numerical discussion will be possible until we know these parent-molecules and the velocities acquired by the observed radicals. We can only say from our observations that the product of average life by mean photo-dissociation velocity must be larger for CN than for C_2 and very much larger for CN than for CH, NH_2, and the molecule responsible for the λ 4050 group. Even this statement may require modification, owing to the distribution of solids in the comet head, a factor which has been considered in an attempt to explain apparently discordant results on the extensions of OH and NH in different comets.[24]

IV. THE SPECTRUM OF THE HEAD IN THE ULTRAVIOLET

The bands usually observed in the ultraviolet region are the following: (0, 0) and (1, 1) of OH at λ 3090 and λ 3135; (0, 0) of NH at λ 3350; (1, 0) of CN at λ 3590; and possibly (0, 0) of OH^+ at λ 3565. As shown in Figure 4, the OH emission appears strongly on the spectrogram obtained at $r = 1.04$, and the structure of the two OH bands deserves careful scrutiny.

The (0, 0) band of the $^2\Sigma^+ \rightarrow {}^2\Pi_{iniv}$ *system of OH.*—This band reveals a rotational intensity distribution which differs appreciably from previous observations. Table 2 sum-

TABLE 2

(0, 0) BAND OF *OH* IN COMET 1947k AND IN PREVIOUSLY OBSERVED COMETS*

Comet..	1947k		1940c		1941d		1942a		LABORATORY WAVE LENGTHS AND INTENSITIES†			
r.....	1.04		1.0		1.25–1.51		1.75 A.U.					
dr/dt....	+22.2		−34.6		−21.8		−14 KM/SEC					
	Int.	λ	Int.	λ	Int.	λ	Int.	λ	λ	G. H.	R	Notation‡
	.....	.....	2	78.5	1.0	79.0	1–0	78.7	78.43	3	10	$Q_2(1\frac{1}{2})$
	1	3081.5	1	81.6	3	81.7	4	81.9	81.64	2	10	$P_2(1\frac{1}{2})$
	3	3086.3	2	86.3	.....	.....	1	86.3	86.38	2	8	$P_2(2\frac{1}{2})$
	5n	3090.3	4	90.3	1	90.2	0	89.7	90.46	2	10	$Q_1(\frac{1}{2})$
	.....	.....	.....	.....	.....	.....	.....	.....	89.85	3	12	$Q_1(1\frac{1}{2}, 2\frac{1}{2})$
	.....	.....	.....	.....	.....	.....	.....	.....	90.36	2	10	$Q_1(3\frac{1}{2})$
	.....	.....	.....	.....	.....	.....	.....	.....	91.18	2	10	$P_2(3\frac{1}{2})$
	5	3093.7	1	93.7	2	93.6	2	93.9	93.72	2	4	$P_1(1\frac{1}{2})$
	5	3096.2	3	96.4	.....	.....	.....	.....	96.34	2	5	$P_1(2\frac{1}{2})$
	.....	.....	.....	.....	.....	.....	.....	.....	97.00	2	8	$P_2(4\frac{1}{2})$
	5	3099.6	2	99.4	.....	.....	0	99.4	99.57	2	.....	$P_1(3\frac{1}{2})$
	0	3103	.....	.....	.....	.....	.....	.....	03.34	2	10	$P_1(4\frac{1}{2})$
	1	3107	.....	.....	.....	.....	.....	.....	07.54	2	8	$P_1(5\frac{1}{2})$

* Sources: 1940c: Swings, Elvey, and Babcock, *Ap. J.*, **94**, 320, 1941; 1941d: Elvey, Swings, and Babcock, *Ap. J.*, **95**, 218, 1942; 1942a: Popper and Swings, *Ap. J.*, **96**, 156, 1942.

† "G. H.": according to Grebe and Holst; "R": observed at the Ryerson Physical Laboratory (Beutler, unpublished).

‡ The J'-values are given in parentheses.

marizes the wave lengths observed in Comets 1947k (Bester), 1940c (Cunningham), 1941d (Van Gent), and 1942a (Whipple-Bernasconi-Kulin). For Comet Bester the maximum of the P_2 branch is roughly at $J' = 2\frac{1}{2}$ or $K' = 2$; and P_2 $(5\frac{1}{2})$ at λ 3102.10 is probably not present. The maximum of the P_1 branch is at $J' = 1\frac{1}{2}$ or $K' = 2$, and the faintness of P_1 $(4\frac{1}{2})$ relative to P_1 $(5\frac{1}{2})$ can be explained only by assuming that the level $J' = 3\frac{1}{2}$ is underpopulated because of strong solar absorptions at the exciting wave lengths leading to $J' = 3\frac{1}{2}$, account being taken of the radial velocity, dr/dt. The Q_1 branch is blended with P_2 $(3\frac{1}{2})$ but definitely contributes to the emission at λ 3090.3,

[24] P. Swings, *Ann. d'ap.*, **11**, 124, 1948.

which is broader than P_2 ($2\frac{1}{2}$) or P_1 ($1\frac{1}{2}$). Because of the low population of the level $J' = 3\frac{1}{2}$, as indicated by the faintness of P_1 ($4\frac{1}{2}$), the line Q_1 ($3\frac{1}{2}$) at λ 3090.36 can play only a minor role in the blend. A maximum in the Q_1 branch at $J' = 1\frac{1}{2}$ or $K' = 2$ is not excluded.

The lines observed in Comet Bester are schematized in the level diagram of Figure 6, which omits P_1 ($4\frac{1}{2}$) and P_1 ($5\frac{1}{2}$). Although the R_2 branch near λ 3072 is absent, as in previously observed comets, the laboratory intensities of the R_2 lines are not much weaker than those of P_2. The absence of R_2 in Comet Bester may be due to the absorption of the UV-glass correcting plate of the Schmidt camera in the Cassegrain spectrograph, and possibly also to ozone absorption in this region. Absorption features in the ultraviolet solar spectrum cannot be the reason for the absence of R_2 when P_2 is strong. The same applies to the Q_2 branch at λ 3078, which is not observed in the (0, 0) band. The R_1 branch near λ 3080 is also absent.

The effect of the distribution in population on the different rotational levels is espe-

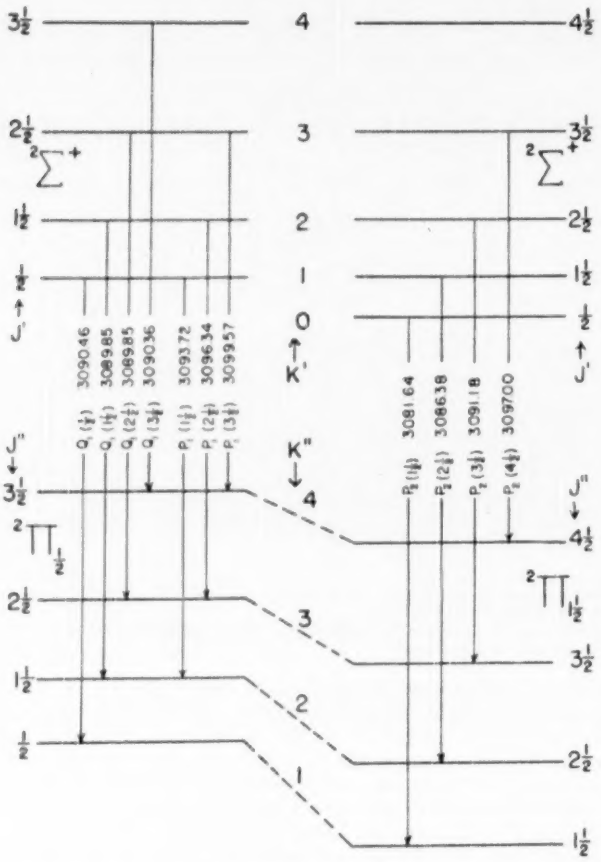

FIG. 6.—Energy levels contributing to the (0, 0) band of *OH*. The levels $P_1(4\frac{1}{2})$ and $P_1(5\frac{1}{2})$ are omitted

cially apparent in λ 3090. In Comets 1942a and 1941d the observed emission is mainly Q_1 ($\frac{1}{2}$), while in Comets 1947k and 1940c it is a blend of Q_1 ($\frac{1}{2}$, $1\frac{1}{2}$, $2\frac{1}{2}$, $3\frac{1}{2}$) and P_2 ($3\frac{1}{2}$).

Generally speaking, the (0, 0) band corresponds to higher J-values in Comet 1947k than in the spectra of Comet 1940c, which were taken at the same heliocentric distance. Since it is reasonable that the populations in the rotational levels should be determined mainly by the absorption of solar radiation, we assume that the difference in rotational distribution between 1947k and 1940c is due to the different radial velocities, dr/dt being, respectively, +22.2 and −34.6 km/sec. The difference corresponds to a Doppler shift from one comet to the other of 0.6 A at λ 3000, which may, indeed, affect the distributions noticeably. On the other hand, the differences in intensity distribution between 1940c and 1941d or 1942a, which were observed at different heliocentric distances, are

TABLE 3

REGION λλ 3130–3160 IN COMET 1947k

Observed		(1, 1) Band of *OH*		(0, 0) Band of *CH*	
Int.	λ	λ	Notation	λ	Notation
0.1	3131.6	31.45	$R_1(3\frac{1}{2})$		
2	3135.0	34.56	$Q_2(1\frac{1}{2})$	35.6	$R_2(2)$
		36.17	$Q_2(2\frac{1}{2})$	36.2	$R_1(2)$
		33.98	$R_1(2\frac{1}{2})$		
3	3137.9	37.74	$P_2(1\frac{1}{2})$	37.4	$R_2(1)$
		37.03	$R_1(1\frac{1}{2})$	39.1	$R_1(1)$
		37.88	$Q_1(3\frac{1}{2})$		
0	3140.6	40.75	$R_1(\frac{1}{2})$		
1	3142.9	42.49	$P_2(2\frac{1}{2})$	42.9	$Q_2(1)$
3	3147.5	47.44	$P_2(3\frac{1}{2})$	47.5	$P_1(1)$
		47.3	$Q_1(\frac{1}{2})$	46.5	$P_2(1)$
		46.58	$Q_1(1\frac{1}{2})$		
		47.26	$Q_1(2\frac{1}{2})$		
		48.41	$Q_1(3\frac{1}{2})$		
2	3150.5	50.00	$P_1(1\frac{1}{2})$	50.4	$P_1(2)$
				49.8	$P_2(2)$
2-1	3153.7	52.95	$P_1(2\frac{1}{2})$	52.9	$P_1(3)$
		52.44	$P_2(4\frac{1}{2})$		
1	3156.8	56.22	$P_1(3\frac{1}{2})$	55.7	$P_1(4)$
0	3159	60.05	$P_1(4\frac{1}{2})$	58.4	$P_1(5)$

primarily due to the different values of r, combined with the smaller differences in radial velocity.

The (1, 1) band of the $^2\Sigma^+ \rightarrow {}^2\Pi_{ine}$ *system of OH.*—Because the lines around λ 3150 are so strong in the spectrum of Comet Bester at $r = 1.04$ and since the intensity distribution among them differs so much from that within the (0, 0) transition of *OH*, it might be assumed that they are blended with the (0, 0) band of the Fortrat system of *CH* ($c^2\Sigma^+ \rightarrow x^2\Pi$). Table 3 gives identifications of the lines observed near λ 3150. There are good reasons for thinking that the contribution by *CH* is minor: First, the $c^2\Sigma^+ \rightarrow x^2\Pi$ ultraviolet system should be weak compared with the violet $A^2\Delta \rightarrow x^2\Pi$ system, near λ 4313, as exhibited in the solar and interstellar absorption bands of *CH*. At $r = 1.04$ this violet system (λ 4313) has already become rather weak. Second, the fluorescence excitation of the ultraviolet system of *CH* requires solar radiation around λ 3150, where the amount of energy available is much smaller than at λ 4313. Finally, if the contribution of *CH* were important, the Q branch (which should be stronger than the P and R branches) would be stronger than is observed.

On the other hand, if we assume the λ 3150 emission to be due to pure *OH*, we find that the R_2 branch, to the violet of Q_2, is absent or extremely weak. This cannot be explained by atmospheric or instrumental absorption. The R_1 branch is also weak. Moreover, in view of the weakness of (1, 1) relative to (0, 0) of *CN* and the absence of (1, 1) of the violet system of *CH*, the intensity of the λ 3150 emission appears to be too high for identification with the (1, 1) transition of *OH*, which is a heteronuclear molecule and should therefore have a low vibrational temperature. The (1, 1) band of *OH* would be excited mainly by absorption of solar radiation in the (1, 0) band of *OH*, near λ 2811,[25] since most *OH* molecules must be in their lowest vibrational level, $v'' = 0$. The fact that the (0, 0) and (1, 1) bands of *OH* are excited by different regions of solar radiation may suffice to explain the very different rotational intensity distributions within the two

TABLE 4

NH BANDS IN COMET 1947k NEAR λ 3350

1947k		1940c*		1947n†		LABORATORY λ	NOTATION
Int.	λ	Int.	λ	Int.	λ		
		2	50.8	1	49.6	50.85	$R_2(1)$
						49.55	$R_1(2)$
						49.29	$R_2(1)$
10n	From 3351.4 to 3358.6	4	54.1	2	53.7	53.64	$R_1(1)$
						53.96	$R_2(0)$
						54.2	$Q_2(1)$
		8	57.9	10	58.1	57.83	$R_1(0)$
						57.6	$Q_2(1)$
						57.82	$Q_2(2)$
						58.42	$Q_2(3)$
1	3361.5	2	61.5			61.73	$Q_1(1)$
						61.01	$Q_1(2)$
						62.7	$P_2(2)$
2s	3365.2	2	64.7	1	65.0	64.94	$P_2(2)$
5	3369.4	3	69.1	1	69.3	69.12	$P_1(2)$
						69.3	$P_2(3)$
1?	3372	1	72.0			72.07	$P_1(3)$

* Swings, Elvey, and Babcock, *Ap. J.*, **94**, 320, 1941.

† Swings and Page, *Ap. J.*, **108**, 526, 1948.

bands. A theoretical calculation of the two synthetic profiles seems to be the only means for deciding on the amount of blending by *CH*. Although, as shown in Figure 4, the λ 3150 emission is confined to the nucleus and the (0, 0) band of *OH* is also much stronger in the central part of the head, *CH* is also a "nuclear" emission; so the identification of the λ 3150 emission cannot be based on extension into the head.

The (0, 0) band of the $^3\Pi \rightarrow {}^3\Sigma$ *transition of NH.*—This very intense emission is not so well resolved in our present material as it was for Comet 1940c. The measured wave lengths and their identifications are given in Table 4, together with the measurements

[25] This region of the solar spectrum has now been observed from V2 rockets. For a table of solar wave lengths see Durand, Oberly, and Tousey, *Ap. J.*, **109**, 1, 1949. Also H. E. Clearman, chap. iv, Sec. B, p. 125, of *The Atmospheres of the Earth and Planets*, ed. G. P. Kuiper (Chicago: University of Chicago Press, 1949). The (1, 0) band of *OH* in comets should be mainly between λ 2819 and λ 2852. The fluorescence would be affected by the resonance line of *Mg* I at λ 2852, by the longward wing of the enormously strong resonance doublet of *Mg* II, and by several other absorption lines, mainly of *Fe* I, *Fe* II, and *Co* I.

for Comets 1940c and 1947n. It is apparent that the main contributors are the P_1, Q_1, and R_1 branches corresponding to the sublevel of highest statistical weight, $^3\Pi_2$; but even in these branches only low values of K'' are observed. The R branches especially are limited to $K'' \leq 1$, plus a possible contribution of R_1 (2). This indicates that the K' levels above 2 have no appreciable population. In the P_2, Q_2, and R_2 branches corresponding to $^3\Pi_1$, R_2 is observed only for $K = 1$; P_2 (2), Q_2 (1, 2), and possibly Q_2 (3) are also present. In the P_3-Q_3-R_3 group corresponding to $^3\Pi_0$, R_3 is absent or very weak, Q_3 appears doubtfully in a blend, and P_3 is probably absent.

It is difficult to ascertain whether the NH (1, 1) transition is weakly present or not. By comparison with NH (0, 0) and neglecting a possible effect of solar absorption lines in the fluorescence excitation, the (1, 1) transition of NH should be detected by R_1 (0) at λ 3368; R_1 (1) at λ 3364, and P_1 (2) at λ 3376. The R_1 (0) and R_1 (1) would not be easily detected, as they would appear in the shortward wings of two strong NH (0, 0) lines; there is no evidence for P_1 (2).

Since most NH molecules must lie in their lowest vibrational level, $v'' = 0$, the excitation of the (1, 1) band would require absorption in the (1, 0) transition. Since this transition is very weak compared with NH (0, 0), while in OH the (1, 0) band, although weaker than (0, 0), has an appreciable intensity, we can understand why (1, 1) of NH does not appear, while (1, 1) of OH is present.

Relative intensities of the OH and NH bands.—Bands of OH, and especially of NH, are strong in Comet Bester. The intensity of NH may be related to the high intensity of the emissions at λ 6299, λ 6363, and others in the visual region usually attributed to NH_2. In the case of Comet 1941d (Van Gent), in which NH is very weak compared with OH and CN, the NH_2 emissions in the visual region are also very weak. It seems reasonably safe to assume that NH and NH_2 result from the photo-dissociation of the same parent-molecule, ammonia.[26] Whether NH results from direct photo-dissociation of NH_3 or from that of NH_2 is at present not known.

The parent-molecule of OH has usually been considered to be H_2O, although the very low vapor pressure of H_2O at low temperatures would be expected to limit the OH band to small heliocentric distances, as emphasized by Wurm.[9] Such a fact is not confirmed by the observations. In Comet Bester, the OH band is strong at $r = 1.04$. It has been observed at still larger heliocentric distances, for example, in Comets 1940c ($r \leq 1.05$), 1941d ($1.25 \leq r \leq 1.53$), 1942a ($1.6 \leq r \leq 1.8$), and 1947i ($r \simeq 1.1$). At $r = 1.5$ one would expect virtually all H_2O to be in the form of ice.[24]

The relative intensities of the OH and NH bands vary in an extreme and unpredictable way from comet to comet. Table 5 summarizes the data available to us on this effect. In the intensity ratios listed we have corrected roughly for observing conditions and instruments used.

It is to be noted that the observed ratios of OH/NH do not seem to depend on the time or distance of perihelion passage or on whether the comet is young (newly found) or old. It varies considerably with heliocentric distance. From $r = 1.53$ to $r = 1.25$ in Comet 1941d the ratio OH/NH decreases considerably; this continues from $r = 1.20$ to $r = 0.63$ in Comet 1940c. In other words, from $r = 1.53$ to $r = 0.63$ the increase in intensity is much more pronounced for NH than for OH.

The region around the (1, 0) band of CN at λ 3590, and the identification of OH^+.—This region contains the (0, 0) band of OH^+, the presence of which has been suspected.[27] Its confirmation is difficult because of (*a*) the presence of numerous laboratory bands of

[26] While one should not necessarily identify the cometary solids with the meteorites, it seems rather strange that no NH_2 has been found among the occluded gases of meteorites (Merrill, *Proc. Amer. Phil. Soc.*, **65**, 119, 1926). Nor has NH_2 been found in terrestrial rocks (Nikogosjan, *Mem. 3d Conf. Mineralogy*, p. 55, 1940; in Russian, cited by B. A. Vorontsov-Velyaminov, *A.J. Soviet Union*, **22**, 317, 1945).

[27] P. Swings, *Pub. Lick Obs.*, Ser. II, No. 3; *Ap. J.*, **95**, 270, 1942; J. Hunaerts, *Bull. Astr. Obs. R. Belgium*, **3**, 320, 1945; and R. Herman, *C.R.*, **227**, 962, 1948.

this region, due to CN, OH^+, CO^+, N_2^+, O_2, NO, N_2, and C_2, all of which can be present in comets, and (*b*) the extreme complexity of the exciting solar spectrum in this region, which should lead to peculiar rotational intensity distributions.

The (1, 0) band of the violet system of CN is fairly strong in Comet Bester. The (2, 1) transition at λ 3586 probably does not play any significant role, since the (2, 2) band at λ 3862, which arises from the same upper vibrational level $v' = 2$ and which is slightly stronger than (2, 1) in the laboratory, is not observed. In Comet 1940c the (2, 2) band of CN was found to play only a minor role when the (0, 0) band was overexposed and the comet close to the sun.[28]

The main transitions in the $^2\Pi_i \rightarrow {}^2\Sigma^-$ system of OH^+ are (0, 0) with R head at λ 3565 and (0, 1) at λ 3983. Other laboratory bands such as the (1, 1) transition at λ 3695 and (1, 0) at λ 3332, arising from $v' = 1$, are unlikely to reach any intensity in comets. Hunaerts' suggestion[27] that the (0, 1) band of OH^+ may contribute appreciably to the

TABLE 5

VARIATIONS IN THE RATIO OH/NH

Comet	Observational Conditions	OH/NH	Remarks
Encke	After $q=0.34$ at $r=0.95$	$\frac{1}{2}$	Old comet
1940c	Before $q=0.38$ at $r=1.03$	$\frac{1}{2}$	New comet
1941c	After $q=0.79$ at $r\approx1$	$(\frac{1}{10})$	New comet
1941d	Before $q=0.89$ at $r=1.53$–1.25	(2)	New comet
1942a	After $q=1.06$ at $r=1.6$–1.8	$\frac{1}{2}$	New comet
1947k	After $q=0.75$ at $r=1.04$	$\frac{1}{2}$	New comet
1947n	After $q=0.11$ at $r=1.02$	$(\frac{1}{10})$	New comet

emission near λ 4000 is not confirmed by observation. First, all the cometary lines near λ 4000 are very short and behave like the characteristic nuclear λ 4050 group with respect to variation with r. Second, (0, 0) of OH^+ is at best very weak; (0, 1) should be still weaker and hence could not play a significant role in the λ 4050 group. A similar conclusion results from the laboratory work of R. Herman.[27]

Although the presence of OH^+ is not excluded, as shown by the measures and suggested identifications in Table 6, it is not confirmed. For these identifications great help was obtained from the synthetic, low-temperature, rotational profiles of the OH^+ bands, computed by Hunaerts.[27] Line λ 3563 seems to require the presence of OH^+; λ 3569 appears too strong to be due to the R branch of CN (1, 0) alone; there may be a contribution of OH^+ in λ 3594; and the emission observed at λ 3616 may be partly due to OH^+ (the P_1, P_2, and P_3 branches around $K' = 6$). A convincing identification will require spectrograms of higher resolution in this region.

V. THE REGION λλ 3800–5000 IN THE SPECTRUM OF THE HEAD

The $\Delta v = 0$ and -1 sequences of the violet system of CN are of the usual complex type; however, since the structures of the CN bands on our spectrograms of 1947k are not so well resolved as in prevously observed comets, they will not be described here. The (1, 1) band is present, as expected from the observation of the (1, 0) transition.

Nothing unusual appears in the $A^2\Delta \rightarrow x^2\Pi$ system of CH, which is the main characteristic of this molecule. On our strongly exposed spectrogram for $r = 1.06$, the $\beta^2\Sigma^- \rightarrow x^2\Pi$ system of CH (on the longward side of CN [0, 0] λ 3883) also appears. The structures of these two bands of CH do not differ markedly from those in Comet 1940c, which have been described in detail.[29]

Twenty "nuclear" lines observed between λ 3960 and λ 4108, the strongest at

[28] P. Swings, *Lick Obs. Bull.*, **19**, 131, 1941.

[29] Swings, Elvey, and Babcock, *Ap. J.*, **94**, 320, 1941.

λ 4051.1, belong to the "λ 4050 group." No striking intensity change occurs within the group from $r = 0.81$ to $r = 1.55$, as shown by Table 7, which gives intensities measured from tracings without standardization, as described in Section II above.

C. Fehrenbach[10] has suggested that λ 4013 and λ 4067 are stronger in Comet 1948g than in laboratory spectra and that another emission overlaps that usually attributed to CH_2. Our results on Comet 1947k, and those by Jose and Swings[12] on Comet 1948l, do

TABLE 6

REGION λλ 3550–3620, COMET 1947k COMPARED WITH COMET 1940c

1940c ($r = 0.63$)				1947k							
Int.	λ	Identification*		r					Description†	Adopted Mean λ	Ident.
				0.86	0.88	0.96	0.97	1.04			
1–0	3565	OH^+	$R_3(1, 2, 3, 4)$	.....	.....	.....	.....	63.3(2)	.....	3563.3	OH^+ (0, 0)
2	3572.2	$CN(1, 0)$	$R(14)$‡	.....	.....	71.0	68.0	74.4(2n)	1, >250″	3569.5	$CN(1, 0)$
		OH^+	5 lines	.....	.....	.....	.....	.....	.....	.....	$OH^+(0, 0)$
1–2	3577.3	$CN(1, 0)$	$R(5)$‡	78.9	76.2	81.	79.8	.....	2, >250″		
		(OH^+	6 lines)	.....	.....	.....	.....	.....	.....	3580.4	$CN(1, 0)$ $CO^+(5, 0)$
2–3n	3584.3	$CN(1, 0)$	$P(2)$–$P(14)$	.....	.....	.....	.....	83.7(1s)	.....		$N_2^+(1, 0)$
		(OH^+	4 lines)	.....	.....	.....	.....	.....	.....	.....	.....
1–0	3589.4	$CO^+(5, 0)$	.....	.....	.....	.....	.....	.....	.....	.....	.....
		OH^+	4 lines	.....	.....	.....	.....	.....	.....	.....	.....
1–2	3597.4	$CO^+(5, 0)$	.....	98	.....	95.4	93.4	97.7(4n)	1, >250″	3594.4	$CO^+(5, 0)$
		OH^+	3 lines	.....	.....	.....	.....	.....	.....	.....	$OH^+(0, 0)$
.....	3617.					17.	15.7	14.9(2n)	2n, 15″§	3616.3	?OH^+ (0, 0)?

* According to P. Swings, *Ap. J.*, **95**, 270, 1942; with additions from J. Hunaerts, *Bull. Astr. Obs. R. Belgium*, **3**, 320, 1945. All the OH^+ lines correspond to values of $k' \leq 3$.

† For spectra at $r = 0.96$ and 0.97; the first figure is the intensity; the second is the extension of the line from the nucleus in seconds of arc.

‡ Blend of lines around this transition.

§ This line is long but is strongly enhanced in nucleus.

TABLE 7

INTENSITIES OF LINES OF THE λ 4050 GROUP AT VARIOUS HELIOCENTRIC DISTANCES, COMET 1947k

λ	r			
	0.81	0.86	1.30	1.55
3992	.....	4.0	6.0	9.8
4033	8.5	.....	.....	6.0
4043	8.5	8.7	10.6	13.0
4051	.....	.....	.....	15.0
4068	8.8	6.1	7.8	10.0

[10] *C.R.*, **227**, 519, 1948.

not substantiate Fehrenbach's suggestion. Table 7 shows that there may be a variation by a factor of ½ in the ratio λ 4033/λ 4043 between $r = 0.81$ and $r = 1.55$. It is possible that this change might be explained by the change in dr/dt from +17 to +25 km/sec if we knew the analysis of the bands. Experimental work on the λ 4050 emission is highly desirable.

The bands of CH^+ are not easily detected on the small scale of our spectrograms, since most of them are overlapped by the tail emissions of CO^+. In the (0, 0) transition of CH^+ two of the characteristic lines, λ 4230 and λ 4254, are too near CO^+ bands, but λ 4238 does not appear with certainty. In the (1, 0) band, two lines are definitely observed at λ 3962 and λ 3972, and the line λ 3954 is blended in a CO^+ emission. We conclude that CH^+ is actually observed, the evidence being mainly the (1, 0) transition.[31]

Recent papers have emphasized the structure appearing within the Swan bands of C_2.[32] Such structure has been described in detail for 1947n[33] and 1948l.[34] Discrete emissions appear between the heads within the $\Delta v = +1$ sequence, and also within the other Swan sequences. It is not clear whether the fairly sharp features observed, especially within the $\Delta v = +1$ sequence, are due to some emission by an as yet unidentified molecule or to an effect of the solar absorption lines on the fluorescence excitation. It would

TABLE 8

DOUBLET APPEARING BETWEEN THE (3, 2) AND (2, 1) HEADS OF C_2

Comet 1940c	Comet 1947n	Comet 1948l
λ 4703.5	λ 4704.0	λ 4705.0
λ 4707.1	λ 4708.8	λ 4708.4

be possible to separate these two by drawing synthetic profiles of the Swan bands, taking into account the profile of the solar spectrum.

Certain of these emissions are observed in several comets, e.g., the doublet between the (3, 2) and (2, 1) heads of C_2, as shown in Table 8. Others are not found in all comets. Our material on 1947k does not reveal such a structure, probably because of the low dispersion and strong exposures intended to bring out the tail spectrum.

Theoretical profiles of the C_2 bands have now been determined by J. Hunaerts.[35] They reveal, for example, a secondary maximum near λ 4706 between the (3, 2) and (2, 1) heads, the wave length of the maximum depending on the radial velocity. This wave length agrees with the emission observed in Comet 1911c (λ 4706) and in Comet Halley (λ 4705.9). The doublet observed in Comets 1940c, 1947n, and 1948l must be at least partly due to these C_2 bands.

VI. THE VISUAL AND INFRARED REGION OF THE SPECTRUM OF THE HEAD

Recent work on the infrared spectrum of the bright Comet 1947n[19] revealed the presence of two strong nuclear emissions at λ 7906 and λ 8106, the first of which is also observed in Comet 1947k. A probable identification is with the red system $^2\Pi \rightarrow {}^2\Sigma$ of CN, λ 7906 and λ 8106 being, respectively, the (2, 0) and (3, 1) transitions. In contrast with

[31] A search for SiO_2, such as was conducted by A. McKellar (*Ap. J.*, **99**, 162, 1944), did not reveal any convincing coincidence in Comet Bester.

[32] N. T. Bobrovnikoff, *Ap. J.*, **99**, 173, 1944; A. McKellar, *Ap. J.*, **99**, 162, 1944; Swings and Page, *op. cit.*, p. 526; Jose and Swings, *Ap. J.*, **111**, 41, 1950.

[33] Swings and Page, *op. cit.*

[34] Jose and Swings, *op. cit.*

[35] *Ann. Obs. R. Belgium*, Vol. 5, Fasc. 1, 1949.

the violet system $^2\Sigma \rightarrow {}^2\Sigma$ of *CN*, the infrared bands are confined to the nucleus; thus they are probably not excited by a fluorescence mechanism, as the violet system is. It is desirable to look for other emissions of the red system in the visual region, the most promising being (4, 0), (5, 1), and possibly (6, 1). Before reliable identifications may be made, synthetic low-temperature profiles are required for these *CN* bands, and in this case, since the excitation is not by fluorescence, no effect of solar absorption lines would have to be considered. The rotational temperature in the comets is low, as revealed by the small width of the infrared emissions. Since the bands of the red system have three heads roughly equally spaced with $\Delta\lambda \simeq 20$ A, each vibrational transition may actually give rise to several "lines."

Pending calculation of synthetic profiles, the identifications listed in Table 9 are merely suggestions. While λ 6332 is certainly due mainly to NH_2, the emission at λ 6200.6, and possibly those at λ 5730.1 and 5747.5, may well be due to *CN*.

TABLE 9

SUGGESTED IDENTIFICATIONS OF BANDS IN THE RED SYSTEM OF *CN*

MEASURED WAVE LENGTH (COMET BESTER)		DESCRIPTION*	COINCIDENCE WITH RED *CN* BAND	PREVIOUS IDENTIFICATION
$r = 0.81$	$r = 0.86$			
5730.1	32	2d, 15″	(6, 1)	.....
5747.5	.....	3d, 10″		.....
6200.6	.....	1, 20″	(4, 0)	.....
6332.2	33	2, 5″	(5, 1)	NH_2
6345	.....	1, 5″		NH_2

* Intensity and extension from the nucleus.

Table 10 lists the lines observed in Comet 1947k in the region longward of the (1, 0) band of C_2, omitting the Swan bands. A discussion of this and similar, previously published tables does not appear fruitful until a laboratory analysis of the NH_2 emission bands is completed. Coincidences with bands of various types of molecules may be found, some of them rather striking, e.g., *FeO*, noted by Rosen and Swings[36] independently in 1943, and, less striking, *NiO*, *CaO*, and *CrO*.[37] Many bands of *FeO*, such as λλ 4448, 4544, 4604, 5789.8, 5807.4, 5903.0, 6097.3, 6109.9, 6218.9, etc., are close to cometary wave lengths.

Two spectrograms on hypersensitized I-N emulsion (B 163 and B 165 in Table 1) cover the region to λ 8800, with a dispersion of 330 A/mm and slit-width 33 A. They were taken in the same manner as for Comet 1947n,[19] in which strong infrared emissions were found by us for the first time. The most important of these, λ 7906, appears also in Comet 1947k, the mean measured wave length being λ 7907. In 1947n a weaker band had been found at λ 8106; in 1947k a weaker emission, which is difficult to measure, has been estimated at λ 8084 and many other possible maxima appear, as shown in Figure 3. This figure shows, for comparison with the "intensity-curves" of films B 163 and B 165 of Comet 1947k, similar curves reduced from spectra of a *CN* discharge tube and of the night sky.[20] The spectrum of the *CN* discharge was taken with the same spectrograph, using the same emulsion, but with slit-width 7 A instead of 33 A, as used for the comet. The night-sky spectrum was obtained by Dr. A. B. Meinel with a similar grating spec-

[36] Private communications, unpublished.

[37] McKellar (*op. cit.*) has mentioned striking coincidences between cometary and SiO_2 emissions in the violet region.

trograph on the same type of emulsion (Eastman I-N) in an exposure of 8 hours. His slit-width corresponds to ½ A. We are indebted to Dr. Meinel for making available to us a tracing of this spectrogram before publication.

It is to be noted that λ 7916 appears rather strongly in the night-sky exposure of 8 hours. With the wider slit used for B 163 and B 165, this band might be expected to show in the 2-hour exposures where the spectrum of 1947k had raised the intensity above the threshold of the I-N emulsion. However, the lack of the even stronger λ 8346 indicates that the night-sky λ 7916 cannot contribute in a major way to λ 7910 observed in the comet.

In Comet 1947k, just as in 1947n, λ 7906 is confined to the nucleus, in contrast with the second-order (0, 0) band of *CN* (λ 3883), which extends farther into the head. The

TABLE 10

EMISSIONS IN THE VISUAL REGION
(The Swan Bands of C_2 Are Omitted)

Wave Length in 1947k				Description*	Adopted λ	Wave Length in 1947n	Suggested Identification
r							
0.81	0.86	0.88	1.30				
4780.9	.....	.....	.....	1, 15″	4781	91	NH_2?
4811	.....	.....	.....	1, 15″	4811	.....	.....
4839.1	.....	.....	.....	2, 15″	4839	.....	NH_2+C_2
.....	4930.0	.....	.....	3, 15″	4930	24.3	NH_2
5700.0	02	.....	.....	2n, 15″	5701	02.2	NH_2
5730.1	32	.....	.....	2n, 15″	5731	32.5	CN
5747.5	.....	.....	.....	3n, 10″	5748	.....	CN
5767.4	.....	.....	.....	½s, 10″	5767	.....	.....
5778.5	.....	.....	.....	1s, 10″	5779	.....	NH_2
5975.0	77.8	78	.....	2n, 15″	5977	74.9	NH_2
.....	5997.1	97	.....	2n, 15″	5997	98.0	$NH_2(+CN?)$
6018.5	.....	.....	.....	1, 10″	6019	17.2	$NH_2(+CN?)$
6094.1	96.8	.....	.....	2n, 10″	6096	94.8	NH_2
.....	6109.8	.....	.....	1, 5″	6110	06.6	NH_2
6152†	.....	.....	.....	1nn, 10″	6152	57.1	NH_2?
6200.6	.....	.....	.....	½, 20″	6201	.....	CN
6289	.....	.....	.....	½, 30″	6289	.....	NH_2
6299.3	00.0	98.2	98	2, 30″	6299	97.3	NH_2
6332.2	33	.....	.....	2, 15″	6333	29.5	$NH_2(+CN?)$
6345	.....	.....	.....	1, 5″	6345	45.2	$NH_2(+CN?)$
6363.5	64	.....	.....	2, 5″	6364	60.6	$NH_2(+CN?)$
6430	.....	.....	.....	1, 5″	6430	.....	NH_2
6452	.....	.....	.....	1, 5″	6452	.....	NH_2
6549.1	.....	.....	45	1, 5″	6547	38.6	NH_2
.....	.....	.....	6553	½s, 10″	6553	57.0	NH_2?
6564	.....	.....	64	½s, 5″	6564	71.9	NH_2
.....	6579	.....	81	2n, 5″	6580	80.3	NH_2?
.....	6590.6	.....	93	1, 5″	6592	96.5	NH_2?
.....	.....	.....	6599	1, 10″	6599	.....	NH_2
6620.5	19	15.1	17	2n, 10″	6618	15.6	NH_2
6641.8	40.2	.....	.....	1n, 10″	6641	36.9	$NH_2?(+CN?)$
6726	.....	.....	.....	.....	6726	22.1	NH_2?
.....	6748.8	.....	.....	2, 5″	6749	48.7	NH_2
6790	.....	.....	.....	.....	6790	.....	NH_2?

* Intensity and extension.

† From λ 6141.8 to λ 6162.3.

structure of λ 7906 is not so well defined in 1947k as in 1947n, and the maximum in the shortward wing does not appear so clearly.

The identification of three emissions—(2, 0), (3, 1), and (4, 2)—of the red system of *CN* remains probable, although not certain. The broad maximum appearing in Figure 3 from λ 6928 to λ 7037 may contain the (3, 0) band of *CN*; another shallow maximum around λ 7150 (extending from λ 7044 to λ 7186) may contain the (4, 1) transition of *CN*.

We have no resolution of the theoretical difficulties involved in this identification of *CN*.[19] Even if, as we suggested in our investigation of Comet 1947n, the red system is actually excited in a process of dissociation of a parent-molecule *CNX*, rather than by fluorescence, the problem of explaining the intensity of the emission would be difficult. A *CN* radical is able to emit by fluorescence several hundred quanta (at least) in the course of its life, while a *CNX* molecule would emit only once, at the moment of its photo-dissociation. For every *CN* radical formed, there would thus be emitted, at the most, one quantum in the red system by dissociation and at least several hundred quanta in the violet and red systems by fluorescence.

VII. THE SPECTRUM OF THE TAIL

Several excellent slit spectrograms of the tail have been obtained, extending into the ultraviolet to λ 3370; two of these are reproduced in Figure 2, and parts of two others in Figure 5. The main characteristics of the tail spectrum are, as is well known, the CO^+ "comet-tail system" ($A^2\Pi \rightarrow {}^2\Sigma$), and the N_2^+ "first negative system" (${}^2\Sigma \rightarrow {}^2\Sigma$), the lower electronic levels of these systems being the ground states of CO^+ and N_2^+. In addition to these bands, there are a number of emissions observed in Comet Bester which have not been observed or identified previously; most of these are rather weak, although two at λ 3509 and λ 3674 reach a considerable intensity. The CO^+ bands were very strong at heliocentric distance 0.8–1.0 but had virtually disappeared at $r = 1.1$. Table 11 gives the measured wave lengths and the identifications; for comparison we add the wave lengths measured by Baldet[3] in Comet Morehouse (1908c) and by Wright[7] in Comet Brooks (1911c).

Emissions due to CO^+.—All the bands of the (v', 0) series,[18] from $v' = 6$ to $v' = 1$ are observed; in the (v', 1) series, bands are found for $v' = 6$, 4, and 1. The absence of the other members of the (v', 1) series in Table 11 is due to blends or to the proximity of intense emissions. The C.T. bands are degraded to the red in the laboratory, which explains the fact that CO^+ wave lengths measured in the tail of Comet Bester have an average longward displacement of 3.7 A relative to the laboratory wave lengths of the *R* heads.

The C.T. system of CO^+ has the well-known typical aspect of doublets formed by the $Q_1 + R_1$ and $Q_2 + R_2$ heads, which are separated by 15–30 A. In the laboratory the Q_1 and Q_2 heads appear 2 or 3 A longward of R_1 and R_2, but they were not separated from R_1 and R_2 on our present spectrograms, these having a resolution of about 7 A. This instrumental width prevents our determining accurately the rotational temperature of the CO^+ molecules, which is estimated to be of the order of 300° K. This is low, as it is for all heteronuclear molecules of the head (*OH*, *NH*, *CH*, *CN*), in contrast with the high rotational temperature of the homonuclear molecule C_2. Hence, even if the instrumental resolution were sufficient to separate the *Q* and *R* heads of CO^+, it is by no means certain that these two heads would appear separately in the comet spectra. This prediction, based on the low rotational temperature, has been mentioned by K. Wurm.[9] The shift of our observed lines about 3.7 A to the red of the laboratory wave lengths of the *R* heads possibly results from the blending with *Q* and *P* branches and from the low temperature. It is consistent with a rotational temperature of the order of 300° K.

[18] The vibrational numbering of CO^+ is that of K. N. Rao, *Ap. J.*, **111**, 306, 1950. The v''s are three units lower than those used by previous investigators.

TABLE 11

SPECTRUM* OF THE TAIL OF COMET BESTER

COMET BESTER		MOREHOUSE		BROOKS		IDENTIFICATION			
Int.	λ	Int.	λ	Int.	λ	Mol.	Electronic Transition†	Vibrational Transition	Laboratory λ (Head)‡ and Intensity
2	3378.0					CO_2^+	M	1,0	70.6 (5)
									78.0 (5)
						NO	β	0,9	76.4 (10)§
		1	85			O_2	S.R.	0,14	70.1 (5)§
						CO_2^+	M	2,1	89.5 (3)§
1	3388.2								94.7 (3)
						NO	β	0,9	86.4 (10)§
1–0	3416	1	20			CO^+	C.T.	6,0	13.3 (4)
1–0	3431	1	36			CO^+	C.T.	6,0	27.9 (4)
1	3478								
						CO_2^+	M	0,0	03.7 (4)
4	3509.1	2	19						11.6 (4)
						CO^+	B.J.	2,0	11.7 (7)§
1–0	3525	2	30			O_2	S.R.	0,15	16.6 (5)§
						CO_2^+	M	2,2	34.4 (4)
2	3545.4	1n	30.86						46.0 (4)
						N_2^+	I Neg.	3,2	48.9 (3)
						CN	V	1,0	90.4 (8)
4	3580.4	2	86			CO^+	C.T.	5,0	84.2 (6)
						N_2^+	I Neg.	1,0	82.1 (4)
2	3594					CO^+	C.T.	5,0	00.8 (6)
						OH^+	$^3\Pi \rightarrow {}^3\Sigma$	0,0	‖
2n	3616.3	2	11			OH^+?	$^3\Pi \rightarrow {}^3\Sigma$	0,0	‖
						CO_2^+	M	0,1	63.2 (4)
4	3674.0								69.3 (3)
									74.1 (5)
						O_2	S.R.	0,16	73.2 (5)§
						CO^+	C.T.	6,1	88.1 (4)
2	3695	2	87			CO_2^+	M	1,2	80.5 (3)
									92.9 (4)
						CO^+	C.T.	6,1	05.3 (4)
1	3709	2	01			CO^+	B.J.	1,0	07.4 (9)
						CO^+	B.J.	1,0	11.9 (9)
						CO^+	B.J.	1,0	24.9 (8)
1	3726					CO^+	B.J.	1,0	29.7 (3)
1	3741					O_2	S.R.	1,17	42.2 (5)§
3	3781.3	6	83			CO^+	C.T.	4,0	77.8 (8)
2	3802.5	5	03			CO^+	C.T.	4,0	95.8 (8)
						CO_2^+	M	0,2	39.8 (5)
1–0	3839								53.1 (5)
						O_2	S.R.	0,17	41.1 (6)§

* Not including bands due to NH, CN, or C_2.

† Abbreviations:
C.T. = Comet-tail system ($A^2\Pi \rightarrow {}^2\Sigma$).
B.J. = Baldet-Johnson system ($B^2\Sigma \rightarrow A^2\Pi$).
V = Violet system ($^2\Sigma \rightarrow {}^2\Sigma$).
S.R. = Schumann-Runge system ($B^3\Sigma \rightarrow x^3\Sigma$).
β = Beta system ($^3\Pi \rightarrow {}^3\Pi$).
I Neg. = First negative system ($^2\Sigma \rightarrow {}^2\Sigma$).
M = $^2\Pi \rightarrow {}^2\Pi$ system of CO_2^+ analyzed by Mrozowski, *Rev. Mod. Phys.*, **14**, 216, 1942.

‡ For O_2 and CO_2^+, the wave lengths correspond to the origins.

§ Identification uncertain or incomplete; see text.

‖ Blend of lines; see section on OH^+.

TABLE 11—*Continued*

Comet Bester		Morehouse		Brooks		Identification			
Int.	λ	Int.	λ	Int.	λ	Mol.	Electronic Transition†	Vibrational Transition	Laboratory λ (Head)‡ and Intensity
4	3913.7	7	15	.....	.....	N_2^+	I Neg.	0,0	14.3 (6)
2	3951.3	1	49	.....	.....	CO^+	B.J.	0,0	53.6 (10)
						CO^+	B.J.	0,0	57.0 (7)
						CO^+	B.J.	0,0	73.5 (9)
1	3983	2	91	.....	.....	CO^+	B.J.	0,0	77.7 (4)
						O_2	S.R.	2,19	87.3 (4)§
7	4001.5	9	03	1	02	CO^+	C.T.	3,0	98.4 (9)
6	4024	9	23	1	22	CO^+	C.T.	3,0	18.7 (9)
0–1	4096	.....	.....	.....	.....	O_2	S.R.	1,19	95.9 (6)§
2n	4124	2	14	.....	.....	CO^+	C.T.	4,1	17.3 (2)
1	4140	3	41	.....	.....	CO^+	C.T.	4,1	38.9 (2)
1	4171	.....	.....	.....	.....	O_2	S.R.	2,20	73.2 (6)§
						CO^+	B.J.	0,1	31.6 (8)
1	4231	3	36	0	30	CO^+	B.J.	0,1	36.2 (3)
				0	38.5	N_2^+	I Neg.	1,2	36.6 (7)
5	4250.9	2	50	0–1	54.5	CO^+	C.T.	2,0	50.7 (10)
						CO^+	C.T.	2,0	73.1 (10)
4	4273.8	10	79	1	78	N_2^+	I Neg.	0,1	78.1 (8)
2	4543.8	9	49	0–1	47	CO^+	C.T.	1,0	39.4 (8)
1	4568.5	9	76	0–1	72	CO^+	C.T.	1,0	65.8 (8)
0–1	5048	3	21	.....	.....	CO^+	C.T.	1,1	39.7 (5)

It appears clearly from Figure 5 that the strongest C.T. band of CO^+ is the (3, 0) transition. The other intensities in the (v', 0) series, as estimated by eye from two spectrograms, are given in Table 12 in comparison with estimates for two other comets.

Although instrumental effects may account for some of the differences in these intensity estimates, we feel that the differences between various comets and laboratory estimates are real. Such differences would be entirely plausible, the populations on the v' levels depending on the excitation mechanism. Between comets of greatly different dr/dt there may be real differences in the populations of v' levels.

TABLE 12

Intensities in the (v', 0) Bands of CO^+, "Comet-Tail System"

λ	Transition*	Laboratory†	Comet Bester (1947k) Plates B 190+B 192	Comet Morehouse (1908c)	Comet Brooks (1911c)
4251–4273	(2, 0)	10	5+4	10	4
3998–4019	(3, 0)	9	7+6	9	4
3778–3796	(4, 0)	8	3+2	5	1
3584–3601	(5, 0)	7	...+2	.....	.....

* Vibrational numbering follows that of K. N. Rao, *Ap. J.*, **111**, 306, 1950.

† According to Baldet, *C.R.*, **180**, 271 and 820, 1925.

The CO^+ molecule possesses another electronic transition in the spectral region cov-

ered by our tail spectrograms. This system, called the "Baldet-Johnson system," connects the upper level $B^2\Sigma$ of the first negative system of CO^+ with the upper level $A^2\Pi$ of the C.T. system. This $B^2\Sigma \rightarrow A^2\Pi$ transition has double double-headed bands, which are degraded to shorter wave lengths.[38] Wurm[9] has suggested that this system should be found in comet tails.

The (0, 0), (0, 1), (1, 0), and (2, 0) transitions of the Baldet-Johnson system are identified with wave lengths in comet-tail spectra listed in Table 11. The cometary wave lengths are shifted by approximately 2.5 A toward shorter wave lengths. The cometary line λ 3509.1 appears too strong to be due exclusively to (2, 0) of the B.J. system of CO^+. Two bands at λ 4230 and λ 3951 practically coincide with CH^+ lines, but the absence of other CH^+ lines at large distances from the nucleus favors the identification of these bands in the tail with the B.J. system of CO^+.

The levels $v' = 0, 1, 2$ of the B.J. system are reached from the ground state $^2\Sigma(v'' = 0)$ by means of the $(v', 0)$ bands of the first negative system $B^2\Sigma \rightarrow {}^2\Sigma$ at λ 2189.8 for $v' = 0$; λ 2112.4 for $v' = 1$; and λ 2042.3 for $v' = 2$.

The solar radiation in this region is much weaker than in the violet region and is rich in strong absorption lines. This and the lower f-values usually assumed for the B.J. relative to the C.T. system account for the observed weakness of the B.J. system compared with the C.T. transition.

Emissions due to N_2^+.—Although most of the N_2^+ transitions are blended, the (0, 0) band at λ 3914 is very strong and wider than the CO^+ bands. The rotational temperature of N_2^+ is therefore probably higher than that of CO^+. If, as is likely, the N_2^+ bands of comets are excited by the fluorescence mechanism, the profiles of the cometary bands should be of the same type as those observed in the twilight sky. In both comets and twilight the solar absorption lines should distort the profiles in a similar way, but, since the rotational temperature of cometary N_2^+ probably differs from that of atmospheric N_2^+, the widths of the bands in comets and twilight spectra are expected to differ.

Emissions due to CO_2^+.—As shown in Figure 4, two emissions appear at λ 3378 and λ 3388 on the longward side of the *NH* band; these emissions are not strongly enhanced in the nucleus and appear definitely like tail lines. Figure 5 shows two strong tail emissions at λ 3509 and λ 3674 which cannot be attributed to CO^+ or N_2^+. The three measured wave lengths, λλ 3378, 3509, and 3674, agree closely with those of the origins of the (1, 0), (0, 0), and (0, 1) transitions in the $^2\Pi_u \rightarrow {}^2\Pi_g$ spectrum of CO_2^+. This molecule has not previously been identified in comet tails; hence its spectrum will be discussed here in some detail.

The bands of the $^2\Pi_u \rightarrow {}^2\Pi_g$ transition of CO_2^+ have recently been analyzed by S. Mrozowski;[39] they appear in the spectral range λλ 3000–5000 covered by our spectrograms. $^2\Pi_g$ is the ground electronic state of the CO_2^+ molecule, this being a favorable factor for possible emission of the CO_2^+ bands by fluorescence excitation due to solar radiation. The CO_2^+ bands have a fairly simple structure. The CO_2^+ molecule is linear in both $^2\Pi$ states. All the strong bands observed in the laboratory may be attributed to symmetrical vibrations, ν_1, the CO_2^+ molecules remaining in their lowest states of ν_2 (bending) and ν_3 (antisymmetrical) vibrations. In the laboratory a typical band consists of two narrow subbands $^2\Pi_{3/2} \rightarrow {}^2\Pi_{3/2}$ and $^2\Pi_{1/2} \rightarrow {}^2\Pi_{1/2}$, which are degraded toward longer wave lengths. In the $^2\Pi_{3/2} \rightarrow {}^2\Pi_{3/2}$ subband the origin coincides practically with an accumulation of lines due to the Q branch; the head of the R branch is displaced 0.4–0.7 A shortward of the origin; the P branch extends toward the red. The structure is similar in the $^2\Pi_{1/2} \rightarrow {}^2\Pi_{1/2}$ subband, except that the Q branch is not observed. The $^2\Pi_{3/2}$, $v'' = 1$, level is split by perturbations into two sublevels, 1^a and 1^b, so that the (0, 1) transition has ac-

[38] *Phys. Rev.*, **60**, 730, 1941; **62**, 270, 1942; **72**, 682 and 691, 1947; *Rev. Mod. Phys.*, **14**, 216, 1942. For the numerous previous attempts at classifying the CO_2^+ or CO_3 bands see references in Mrozowski's first paper. The strong double band λλ 2883–2896 of CO_2^+ is a $^2\Sigma_u^+ \rightarrow {}^2\Pi_g$ transition which has been analyzed by F. Bueso-Sanllehí, *Phys. Rev.*, **60**, 556, 1941.

tually three components: (0, 1[a]) and (0, 1[b]) of $^2\Pi_{3/2} \rightarrow {}^2\Pi_{3/2}$, and (0, 1) of $^2\Pi_{1/2} \rightarrow {}^2\Pi_{1/2}$.

For the identification of CO_2^+ in comet-tail spectra, it appears safe to adopt the mean laboratory wave lengths of the origins as the wave lengths of the subbands. Moreover, we would not expect the two (or three) subbands corresponding to each vibrational transition to be resolved on our spectrograms. Confining ourselves to the CO_2^+ bands corresponding to the symmetrical vibrations $v_1 \leq 2$, we find the coincidences with otherwise unidentified tail emissions shown in Table 13.

The identification of CO_2^+ appears convincing, although the (0, 2) transition seems too weak compared with the laboratory intensity. The absence of (2, 0) in the comet tails may be due either to instrumental reasons or to a low population of the CO_2^+ molecules on the excited level $v_1' = 2$.

It appears reasonably certain that we may now add to the two characteristic molecules of the comet-tail spectra, CO^+ and N_2^+, a third one, the ionized triatomic molecule CO_2^+.

TABLE 13

CO_2^+ BANDS IN THE SPECTRUM OF THE TAIL OF COMET BESTER

DESIGNATION	$^2\Pi_{3/2} \rightarrow {}^2\Pi_{3/2}$ SUBBAND		$^2\Pi_{1/2} \rightarrow {}^2\Pi_{1/2}$ SUBBAND		COMET TAIL		NOTES
	λ (Origin)	I (Lab.)	λ (Origin)	I (Lab.)	λ	I	
0, 0	3503.7	4	3511.6	4	3509.1	4	1
0, 1[a]	3663.2	4	3675.1	5	3674.0	4	
0, 1[b]	3669.3	3					
1, 0	3370.6	5	3378.0	5	3378.0	2	
0, 2	3839.8	5	3853.1	5	3839	1–0	
1, 2	3680.5	3	3692.9	4	3695	2	2
2, 0	3247.7	5	3254.8	5	.....	.....	
2, 1	3389.5(1[b])	3	3394.7	3	3388.2	1	3
2, 2	3534.4	4	3546.0	4	3545.4	2	4

NOTES TO TABLE 13

1. Slightly blended with a B.J. band of CO^+.
2. Blended with a C.T. band of CO^+.
3. Uncertain identification.
4. Blended with the (3, 2) band of N_2^+.

This ion extends into the tail to shorter distances from the head than CO^+ or N_2^+. It is well known that CO_2 dissociates into $CO + O$ by absorption of radiation near λ 1700.[40] Yet it is likely that CO_2^+ results from the photo-ionization of CO_2 rather than from the photo-dissociation of a more complex compound CO_2X. The present identification of CO_2^+ would thus indicate that by absorption of ultraviolet radiation an appreciable portion of CO_2 becomes ionized.

The CO_2^+ emissions also appear strongly in Comet Cunningham, 1940c.[8] In the spectrograms of Comet Morehouse[3] λ 3674 could probably not have been separated from the CO^+ band.

Molecules other than CO_2^+ produce striking coincidences with certain tail emissions not due to CO^+ or N_2^+. Although these molecules do not give rise to convincing identifications, they will be discussed here because of their bearing upon the CO_2^+ identification.

NO molecule.—The wave lengths measured at λ 3378 and λ 3388 agree well with those of the *R* heads (λ 3376.4 and λ 3386.4) of the two subbands in the (0, 9) transition of the β system ($^2\Pi \rightarrow {}^2\Pi$) of *NO*. The other (0, v'') transitions of *NO* would be blended, except (0, 8) at λλ 3207–3198, the absence of which is, to some extent, an argument against this

[40] K. F. Bonhoeffer and P. Harteck, *Grundlagen der Photochemie* (Dresden and Leipzig, 1933), p. 133.

identification. The *R* heads correspond to low rotational quantum numbers; hence their laboratory wave lengths should be close to those of the intensity maxima in a low-temperature source, such as a heteronuclear gas in a comet.[41] The laboratory ratio of intensities of these two *R* heads of *NO* has been determined by Cavallonni[42] as 112/96, whereas, in Comet Bester, λ 3378 is at least twice as strong as λ 3388 (see Fig. 4). However, such a difference could be due to the different excitation mechanisms and does not necessarily exclude in itself the identification of *NO*.

The (0, 8) transition of the γ system ($^2\Sigma \rightarrow {}^2\Pi$) of *NO* has its P_1 head at λ 3375.5. The intensity maximum would lie to the violet of λ 3375, probably too far to be identified with the observed wave length at λ 3378.

Identification of λ 3378 and λ 3388 with the (0, 9) transition seems doubtful because it is hard to understand how *NO* molecules could live for hours or days in the field of solar radiation without becoming photo-dissociated or photo-ionized. We do not know the dissociation or ionization continua of *NO*. However, most *NO* molecules would certainly be on their lowest vibrational level and probably in the lowest rotational states, which would slow down the dissociation.

Many other laboratory bands are known in this spectral region, and their wave lengths were examined for possible identification. The head of the second positive system of N_2 is at λ 3371; its intensity maximum should lie on the shortward side of λ 3371, too far to be identified with the observed λ 3378. The (0, 1) and (0, 2) transitions of this system are blended or close to strong emissions and cannot provide confirmation. The second positive system of N_2 requires too high excitation. The Vegard-Kaplan bands of N_2 give coincidences but are excluded by a discussion of the other transitions, as is also the case for CH_2O, CHO, HNO_3, SiF, S_2, CaF, SO, BO, N_2^+, and O_2^+.

O_2 molecule.—A number of coincidences between unidentified tail emissions and bands of the Schumann-Runge ($B^3\Sigma \rightarrow x^3\Sigma$) system of O_2 have been entered in Table 11. This system consists of bands degraded to longer wave lengths; the origins coincide practically with the heads. The main part of the system lies in the vacuum ultraviolet; only bands corresponding to large values of v'' are found in the region above λ 3000. In Table 11 there is no systematic difference between the cometary and the laboratory wave lengths for O_2. The coincidences are good;[43] yet the identification of the O_2 bands remains doubtful for the following reasons:

1. The relative position of the potential energy-curves of O_2 is such that the excitation of O_2 from the ground state $X^3\Sigma$ to the excited level $B^3\Sigma$ will frequently lead to dissociation. It is therefore unlikely that O_2 could live for a long time in the field of solar radiation before becoming photo-dissociated or photo-ionized, as is the case in the upper atmosphere of the earth.

2. The rotational temperature of O_2—a homonuclear molecule—would be expected to be higher than that of CO^+; yet these comet-tail bands (especially λ 3674) are as sharp as those of CO^+.

3. Although we cannot calculate the radiation pressure exerted on O_2 by solar radiation around λ 2200, it seems unlikely that O_2 molecules would be found at very large distances from the nucleus.

4. The line λ 3674, which nearly coincides with the (0, 16) transition of $B^3\Sigma \rightarrow x^3\Sigma$, is definitely too strong compared with lines near the (0, 15) and (0, 17) transitions. We would expect these three transitions to have the same intensity ratios in comets as they have in the laboratory, since they all arise from the same excited level $v' = 0$. It is true

[41] The analogous problem of the identification of *NO* in the spectrum of polar aurorae has been treated by M. Nicolet, *Phys. Soc. Gassiot Comm. Rep., London*, p. 111, 1948.

[42] *Zs. f. Phys.*, **76**, 527, 1932.

[43] No other system of O_2 gives promising coincidences; this applies to the forbidden (Herzberg) system as well as to the permitted transitions.

that recent investigations[44] have indicated that certain bands of the Schumann-Runge system may be enhanced under certain conditions of excitation. However, such enhancement cannot affect transitions arising from the same v' under the conditions of low density in the comet tail. The O_2 band certainly does not contribute appreciably to the intense tail emission at λ 3674.

Other molecules.—Among the ionized molecules, O_2^+ would seem to have the best chance of existing in comet tails. The first negative system of O_2^+, $^4\Sigma \rightarrow {}^4\Pi$, corresponds to excited states; but this need not prevent its appearing, since the Baldet-Johnson system of CO^+ is present. The strongest transitions of this negative system of O_2^+ are in the visual region, where observations of tail spectra are still scanty. The second negative system, $^2\Pi \rightarrow {}^2\Pi$, has as its lower level the lowest known state of O_2^+. Its bands are double-headed and degraded to the red. The series $(0, v')$, from $v' = 5$ to $v' = 10$, lies in the observed region, as do the transitions (1, 6) and (1, 7). However, reference to wave lengths of all these bands does not reveal any convincing coincidence with tail emissions.

Among neutral molecules we might expect N_2 and CO, since N_2^+ and CO^+ are the main characteristics of comet tails and presumably result directly from the photo-ionization of N_2 and CO. Moreover, it appears probable that N_2 may have a fairly long life in the solar-radiation field.

The different systems of N_2 have therefore been examined successively by comparison with the spectra of the night sky and aurorae. The forbidden Lyman-Birge-Hopfield system, connecting $a^1\Pi_g$ with the ground state $x^1\Sigma_g^+$ reveals a few coincidences for $19 \leq v' \leq 22$, $v'' = 0$ and 1. These coincidences are not promising, since a forbidden transition is unlikely to appear with an appreciable intensity in comets (at least in the case of fluorescence). The other forbidden system, the Vegard-Kaplan transition $A^3\Sigma \rightarrow x^1\Sigma$, and the first and second positive systems also show no promising coincidences with present cometary observations.

CO has no strong band system connected with the ground state,[45] but, in view of the identification of the Baldet-Johnson system of CO^+ in comets, transitions between excited states of *CO* should also be investigated. None of the various *CO* systems (Angstrom, Herzberg, Third Positive, etc.) reveals a striking coincidence, except the (0, 0) band of the Herzberg system, $C^1\Sigma \rightarrow A^1\Pi$, at λ 3680.9. This band is degraded to the violet, so that an intensity maximum may fall near the strong unidentified line at λ 3674 (see above). None of the other $(0, v'')$ transitions is able to confirm this coincidence because of blends or the proximity of strong emissions. The excitation required (about 10.5 volts) seems too high to warrant a high intensity of λ 3680.9.

Coincidences of tail emissions with the following bands reported by Fox and Herzberg[46] are also found: λλ 3384.4, 3434.0, 3506.6, 3599.2, 3618.0, 3670.8, and 3688.7.The three bands λλ 3618.0, 3670.8, and 3688.7 are now definitely attributed to the $^1\Pi \rightarrow {}^1\Pi$ system of C_2.[47] The three tail emissions which are found near these wave lengths extend into the tail in a way which is quite different from the Swan bands of C_2. The coincidences appear purely accidental.

Many other molecules, such as *BH*, *BO*, *SO*, *CaO*, etc., showing wave-length coincidences can be rejected.

VIII. SUMMARY OF CONCLUSIONS

In this paper it has been necessary to discuss the observational data in a number of small parts, from each of which conclusions have been drawn, some tentative, some

[44] M. W. Feast, *Nature*, **162**, 214, 1948; *Proc. Phys. Soc.*, *A*, **62**, 114, 1949; G. A. Hombeck, *J. Chem. Phys.*, **16**, 845 and 1005, 1948; H. G. Wolfhard and A. G. Gaydon, *Nature*, **164**, 23, 1949.

[45] The forbidden Cameron system, which is an intercombination to the ground state, is not found; the bands in the observed region are $(0, v'')$ with $9 \leq v'' \leq 13$.

[46] *Phys. Rev.*, **52**, 638, 1937.

[47] Herzberg and Sutton, *Canadian J. Res.*, *A*, **18**, 74, 1940, and J. G. Phillips, unpublished.

definite, some negative, and some positive. At the risk of misrepresenting the tentative nature of some of these, we list them here briefly for the benefit of the reader.

In Section IV, concerned with the far ultraviolet spectrum, the following observations are noted:

a) The (0, 0) band of $OH\ ^2\Sigma^+ \rightarrow {}^2\Pi_{inv}$ shows the rotational level $J' = 3$ underpopulated, probably due to absorption lines in the exciting (solar) spectrum.

b) The (0, 0) band of $CH\ c^2\Sigma \rightarrow x^2\Pi$ is probably present, though weak, and blended with *OH* (1, 1).

c) The (0, 0) band of $NH\ ^3\Pi \rightarrow {}^3\Sigma$ shows low population in rotational levels with $K' > 2$, and the (1, 1) band is probably absent.

d) The *OH* bands are strong in several comets at heliocentric distances greater than 1 A.U., where H_2O, the presumed parent-molecule, would be entirely in the form of ice, with almost zero vapor pressure.

e) The intensity ratio *OH*/*NH* decreases in several comets as heliocentric distance decreases.

f) The (0, 0) band of $OH^+\ ^3\Pi_i \rightarrow {}^3\Sigma^-$ at λ 3563 is possibly present in Comet Bester.

In Section V, concerned with the blue region of the spectrum, the following are noted:

a) Twenty lines of the "λ 4050 group" are all limited to the nucleus, and all show the same intensity variations in Comet Bester; they probably all arise from the same molecule or ion.

b) The (1, 0) lines of CH^+ at λ 3962 and λ 3972 are present.

In Section VI, concerned with the visual and infrared regions of the spectrum, the following are noted:

a) The presence of λ 7906 is confirmed in Comet Bester, and, although the explanation of its intensity is difficult, it is identified for the present with the (2, 0) band of $CN\ ^2\Pi \rightarrow {}^2\Sigma$.

b) Partly confirming the above identification, the (6, 1), (4, 0), and (5, 1) bands of $CN\ ^2\Pi \rightarrow {}^2\Sigma$ are tentatively identified in the red region.

c) The (4, 2), (4, 1), (3, 1), and (3, 0) bands of $CN\ ^2\Pi \rightarrow {}^2\Sigma$ are possibly present in the infrared.

In Section VII, concerned with the tail spectrum of Comet Bester, the following are noted:

a) The CO^+ bands disappeared at heliocentric distance about 1 A.U.

b) Nine bands of the $A^2\Pi \rightarrow {}^2\Sigma$ system of CO^+ are observed, with widths and maxima consistent with a rotational temperature of 300° K. The (3, 0) band is the strongest, and the relative intensities observed differ markedly from laboratory intensities.

c) Four bands of $CO^+\ B^2\Sigma \rightarrow A^2\Pi$ are present, though weak.

d) The (0, 0) band of $N_2^+\ ^2\Sigma \rightarrow {}^2\Sigma$ is strong, and its width indicates a rotational temperature higher than that for CO^+.

e) The three strong ultraviolet tail emissions λλ 3378, 3509, and 3674 are due to CO_2^+. This ionized molecule, which is identified for the first time in comet tails, extends into the tail to shorter distances from the head than CO^+ or N_2^+.

f) Other weak tail emissions are possibly due to the $B^3\Sigma \rightarrow x^3\Sigma$ system of O_2, but this identification is doubtful.

OH EMISSION BANDS IN THE SPECTRUM OF THE NIGHT SKY. I

A. B. MEINEL
Lick Observatory and Yerkes Observatory
Received February 24, 1950

ABSTRACT

High-resolution spectra of the infrared night sky obtained at Yerkes Observatory have shown conclusively that the previously unidentified infrared emissions are due to the rotation-vibration spectrum of *OH*. The agreement between the vibrational spacing, the rotational constants, and the doublet structure of the emissions and the predicted *OH* structure is excellent. The observation of vibrational levels up to $v = 9$ shows that small inaccuracies exist in the currently accepted vibrational constants. A more accurate determination of these constants could be made, despite the low dispersion of the spectrograph. Other bands of this system of *OH* occur in the region of 1 μ and may account for the radiation detected by Stebbins, Whitford, and Swings, which has been attributed to N_2.

INTRODUCTION

Spectra obtained by the author[1] during 1948 at Lick Observatory with a grating spectrograph showed the presence of a large number of intense infrared radiations that exhibited a complex structure. From these earlier spectra, it was possible to identify only the *P* and *R* branches of the (0, 1) transition of the atmospheric system of O_2 at 8629 A and 8659 A, respectively.[2] The remaining radiations could not be attributed to any known band system of O_2, N_2, *NO*, *CO*, *CN*, CO_2, or H_2O. The present paper constitutes a continuation of these investigations.

INSTRUMENTATION

The spectrograph used in the current investigation, while similar to the spectrograph used for the observations at Lick Observatory, differed in several respects. The glass aspherical corrector plate was replaced by a fused-quartz corrector that had been optically figured to a high degree of accuracy. The low dispersion of the quartz, combined with the excellent figure, enabled a wider spectral range to be observed without deterioration of the images by the residual chromatic aberration of the corrector. The image size, determined visually, is less than 10 μ. Photographic star images as small as 12 μ have been obtained on Eastman III-C emulsions.

A collimator, loaned to the author by the California Academy of Sciences, was added to the spectrograph, in order to reduce the over-all length of the system. The achromatic collimator has an aperture of 6.5 inches and a focal length of 96 inches. The secondary spectrum produced by this lens, which was corrected for the visual region, was not found serious in the infrared. The large ratio of 18 between the collimator and the camera reduced the secondary spectrum by a factor of 324. The residual spectrum was then eliminated by a very slight tip of the plateholder.

The spectrograph was mounted on the base and yoke of a United States Navy searchlight. This mounting was made to enable the spectrograph to be pointed at any region of the sky for auroral studies. The image of the sky was projected on the slit of the spectrograph by means of a short-focal-length lens. This objective lens enabled a spectrum of the sky to be obtained along a vertical arc of 30°. A second lens of the same focal length as the objective lens was placed directly in front of the slit to serve as a field lens. All the transmission optical elements were low-reflection coated with magnesium fluoride. The

[1] *Pub. A.S.P.*, **60**, 357, 1948.

[2] A. B. Meinel, *Trans. Amer. Geophys. Union*, **31**, 21, 1950.

spherical mirror of the camera was coated with a hard layer of vacuum-deposited silver.

The spectrograph, as described above, has enabled high-resolution spectra of the night sky to be obtained with a relatively short exposure. The maximum exposure time employed was 12 hours. This exposure time differs greatly from the exposure times required for the studies at Lick Observatory. The 32-hour exposure at Lick Observatory compares to a 4-hour exposure at Yerkes Observatory. It is felt that the difference is not due to a greater sky brightness at Yerkes Observatory but to the observing techniques. The present spectrograph, although it has more optical elements, is more efficient. The largest factor in the increased efficiency, however, is attributed to the hypersensitization of the Eastman I-N emulsion.

The method of hypersensitization currently employed by the author is as follows:

Bathe 3 minutes in { water ..... 100 cc; ammonia (28%) ..... 8 cc; alcohol ..... 100 cc }
Rinse 2 minutes in pure alcohol
Dry in a cool air blast

This procedure yields plates of uniformly high sensitivity and negligible fog when precautions are taken to avoid contamination with chemical dusts present in all dark rooms.

Prior to exposure, each plate was pre-exposed to infrared light up to a density of 0.3. While this lowers the contrast, it provides a more accurate representation of the spectrum by removing the threshold inertia of the plate and by placing all features on the linear portion of the characteristic curve of the emulsion. This procedure has enabled an exposure of 12 hours to show the band structure out to 8960 A.

The spectrum plates were calibrated with a tungsten-lamp spectrum beside the comparison spectrum. In addition, an adjacent piece of the original I-N plate was calibrated in a spot and a spectral sensitometer to enable reduction of the emission intensities. It was found that the sensitivity of the hypersensitized emulsion was very constant from plate to plate when the preceding method of hypersensitization was used.

A comparison spectrum of krypton was first employed. This spectrum, however, is handicapped by having only a few intense lines in the infrared. A comparison spectrum of xenon was substituted, since it gives a large number of lines of varying intensity from 7000 to beyond 10,000 A.

OBSERVATIONS

The first plate taken with this spectrograph on December 29, 1949, showed immediately that the structure of several of the emission groups was similar. Since the camera was not in perfect focus, further details could not be noted with certainty. The plate of highest resolution, taken on January 10, 1950, showed clearly the detailed structure of each of the emission groups. An enlargement of this spectrum is shown in Figure 1. The hardness of the individual emissions on the longward side of each band group presented strong evidence that these emissions were, in fact, resolved spectral lines and not molecular bands. This fact demonstrated that the actual rotational structure of a band was being observed.

The measured wave lengths of the emissions from 7251.4 A to 8962.2 A are given in Table 1. There are no observed emissions as strong as intensity 2 between 6364 A and 7251 A. The faint bands in this region, reported by numerous authors, are diluted by the high dispersion of the grating spectrograph to such an extent that they are not detectable on short exposures. The intensities, as shown in Table 1, are corrected for the characteristic curve and the wave-length sensitivity of the emulsion. It is very interesting to note that the [*O* I] line at 6300 A is rather weak, compared to these *OH* bands.

IDENTIFICATION

The *P*, *Q*, and *R* branches could readily be identified for each group of emissions upon the assumption that the spectrum showed rotational structure. A preliminary analysis of

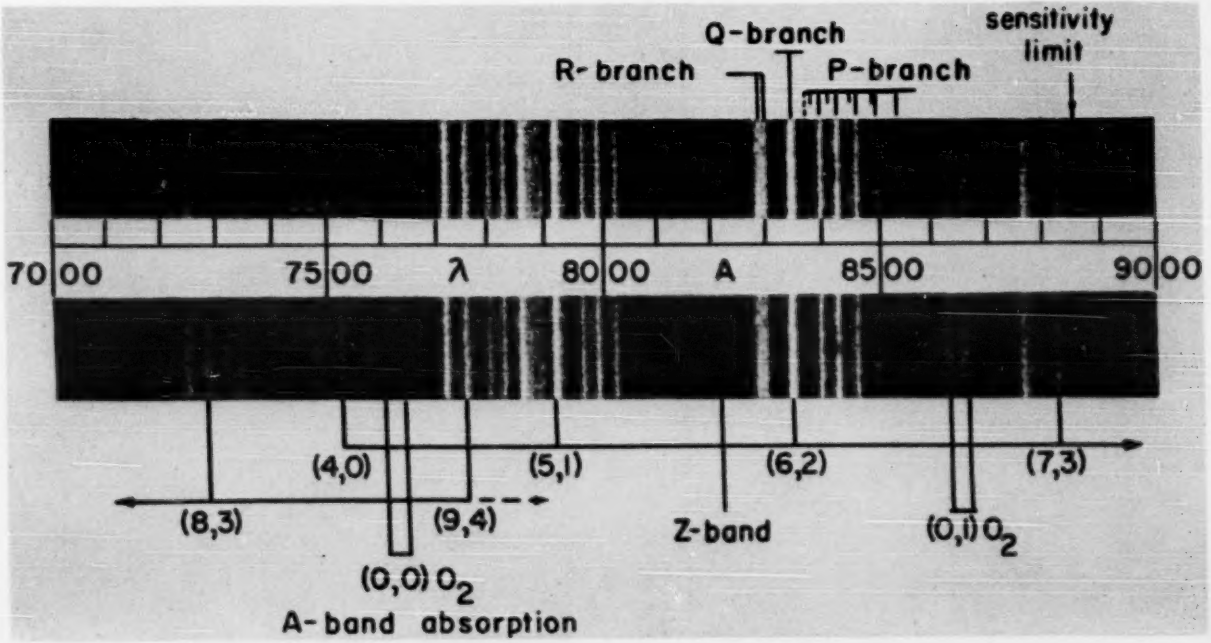

FIG. 1.—Infrared spectrum of the night sky, 7000–9000 A

TABLE 1

WAVE LENGTHS AND WAVE NUMBERS FOR EMISSION IN THE INFRARED SPECTRUM OF THE NIGHT SKY

λ (Air) A	ν (Vac) (Cm^{-1})	I	(v′, v″) R, Q, P
6300.3	15868.3	8	O 1
7251.4	13786.6	12	(8, 3)R
7284.2	724.5	12	(8, 3)Q
7323.6	650.7	5	(8, 3)P_1
7348.2	605.1	7	(8, 3)P_2
7375.8	554.2	5	(8, 3)P_3
7408.5	13494.3	4	(8, 3)P_4
7444.5	429.0	2	(8, 3)P_5
7481.8	365.8	7	(4, 0)R
7529.1	278.1	8	(4, 0)Q
7577.2	193.9	4	(4, 0)P_1
A-band	Absorption	.....	Region
7720.3	12949.2	28	(9, 4)R
7755.8	890.0	23	(9, 4)Q
7783.4	844.3	4	(9, 4)p_1
7799.0	818.6	17	(9, 4)P_1
7813.8	12794.4	5	(9, 4)p_2
7826.0	774.4	19	(9, 4)P_2
7857.8	722.6	57	(9, 4)P_3
7873.9	696.6		(5, 1)R
7892.6	666.7	7	(9, 4)P_4
7918.5	12625.2	42	(5, 1)Q
7952.6	571.0	5	(5, 1)p_1
7968.8	545.9	20	(5, 1)P_1
7983.8	521.9	8	(5, 1)p_2
7997.1	501.1	24	(5, 1)P_2
8018.7	12467.4	5	(5, 1)p_3
8029.7	450.3	19	(5, 1)P_3
8055.5	410.4	4	(5, 1)p_4
8066.1	394.2	12	(5, 1)P_4
8105.8	333.4	5	(5, 1)P_5
8289.8	12059.6	36	(6, 2)R
8300.0	044.8	31	(6, 2)R
8347.3	11976.6	74	(6, 2)Q
8384.8	923.6	8	(6, 2)p_1
8401.6	899.3	37	(6, 2)P_1
8418.0	11876.0	11	(6, 2)p_2
8432.3	855.9	44	(6, 2)P_2
8455.2	823.8	11	(6, 2)p_3
8467.4	806.8	35	(6, 2)P_3
8497.3	765.2	7	(6, 2)p_4
8506.7	11752.2	22	(6, 2)P_4
8544.9	699.7	4	(6, 2)p_5
8550.7	691.8	11	(6, 2)P_5
8594.4	632.2	5	(6, 2)P_6
8645.5	Minimum	(0, 1)	O_2 band
8778.4	11388.5	~210	(7, 3)R
8829.4	322.8	~200	(7, 3)Q
8889.3	246.4	~100	(7, 3)P_1
8923.7	203.1	~100	(7, 3)P_2
8962.2	154.9	~100	(7, 3)P_3

the strong lines of the *P* branch showed conclusively that the band was due to a hydride. The large values of $B_{v''} = 16$ cm^{-1} and $B_{v'} = 13$ cm^{-1}, combined with the doublet structure, limited consideration to the *OH* molecule.[3]

The grouping of the bands, as shown in Figure 1, indicated that the two emissions near 8800 A are the *R* and *Q* branches of another band. Subsequent exposures of longer duration have recorded the first three strong lines of the *P* branch, even though the sensitivity near 8900 is extremely low. The addition of this band and a very weak band at 7529 A made a total of six bands, of which four belong to one sequence and two to a second sequence.

VIBRATIONAL STRUCTURE

When the author communicated to Dr. Herzberg the foregoing results, together with a reproduction of the spectrum, Herzberg immediately noted that the two *OH* band sequences showed excellent coincidences with the extrapolated positions of the rotation-vibration bands of *OH*.[4] These coincidences were so striking that identification was almost certain, as surprising as this interpretation may seem in view of the large Δv-values. A subsequent analysis of the rotational structure by the author has confirmed this identification beyond any doubt. The values obtained by Herzberg, using the best-known values for the vibrational constants of *OH*, are shown in Table 2.

TABLE 2

COMPUTED AND OBSERVED BAND POSITIONS FOR *OH*

Sequence (v', v'')	λ (Comp) (A)	λ (Obs) (A)	Sequence (v', v'')	λ (Comp) (A)	λ (Obs) (A)
(4, 0)	7526	7529	(7, 3)	8850	8829
(5, 1)	7920	7918	(8, 3)	7293	7284
(6, 2)	8360	8347	(9, 4)	7762	7756

It is interesting that an extrapolation of the vibrational constants for *OH* derived from the ultraviolet electronic bands, which are only observed between low v-values, is satisfactory up to large v-values. The differences, however, are systematic and may indicate small errors in the accepted vibrational constants.

VIBRATIONAL CONSTANTS

Inasmuch as the predicted positions of the bands do not agree satisfactorily with the observed positions, a solution was made for new vibrational constants, with the observed data. The positions of the origin of the mean rotational band were extrapolated from the maximum of the strong observed *Q* branches.

The wave-number separation of the vibrational levels of a band system is given by the equation

$$\nu_v - \nu_{v+1} = \omega_e - 2\omega_e x_e (v+1) + 3\omega_e y_e (v+1)^2 + \ldots, \tag{1}$$

neglecting a small constant term in $\omega_e y_e$. The wave number of the origin of a band corresponding to a transition between the levels v' and v'', then, is

$$(v' - v'')\omega_e - 2\omega_e x_e \sum_{v''}^{v'} (v+1) + 3\omega_e y_e \sum_{v''}^{v'} (v+1)^2 = \nu_{v',v''}. \tag{2}$$

[3] A. B. Meinel, *Ap. J.*, **111**, 207, 1950.

[4] Private communication.

When this expression was evaluated with the observed band origins, the following values were obtained by a least-squares solution:

$$\omega_e = 3721.9 \pm 0.5\,, \qquad \omega_e x_e = 78.99\,, \qquad \omega_e y_e = -0.235\,.$$

The vibrational constants given above, however, do not fit two of the bands as shown in Table 3. This is apparently due to the blending of the (5, 1) Q branch with the P_3-line of the (9, 4) band in the one case. The Q branch of the (7, 3) band, on the other hand, is situated where the plate sensitivity is rapidly changing, thereby increasing the effective wave number of this branch.

TABLE 3

COMPARISON OF COMPUTED BAND POSITIONS USING NEW VIBRATIONAL CONSTANTS FOR *OH*

Sequence (v', v'')	ν (Comp) (Cm^{-1})	ν (Obs) (Cm^{-1})	$\delta\nu$ (O−C) (Cm^{-1})	Sequence (v', v'')	ν (Comp) (Cm^{-1})	ν (Obs) (Cm^{-1})	$\delta\nu$ (O−C) (Cm^{-1})
(4, 0)	13288.8	13287.9	−0.9	(7, 3)	11325.3	11332.6	+7.3
(5, 1)	12639.9	12635.0	−4.9	(8, 3)	13738.3	13735.7	−2.6
(6, 2)	11985.5	11986.4	+0.9	(9, 4)	12902.6	12901.2	−1.4

ROTATIONAL STRUCTURE

An analysis of the rotational structure of the *OH* bands confirms the interpretation indicated by the vibrational spacing. Figure 2 shows the observed line positions in the (5, 1) 7918 A band and the (6, 2) 8347 A band. The strong P branch and the weak P branch lines were combined in the manner indicated in Figure 2, in order to determine more accurately the rotational constants and the band origin according to the following equation:

$$P(K) = B_{v'} - B_{v''})\,K^2 - (B_{v'} + B_{v''})\,K + \ldots\,. \tag{3}$$

The rotational constants are related to the observed first (Δ') and second (Δ'') differences by the equations

$$B_{v'} + B_{v''} = \Delta' - \bar{\Delta}''\,(K + \tfrac{1}{2})\,, \tag{4}$$

$$B_{v'} - B_{v''} = \bar{\Delta}''\,. \tag{5}$$

Table 4 shows the values obtained for the (5, 1) and (6, 2) bands.

DOUBLET SPLITTING

The doublet structure of the bands is very noticeable in Figure 1, although the reproduction of the spectrum loses considerable faint detail. Hill and Van Vleck[5] have given a theoretical expression for the doublet splitting for cases intermediate between Hund's case *a* and case *b* states. The parameter in this expression is the ratio between the separation, A, of the $^2\Lambda_{\Lambda+1/2}$ and $^2\Lambda_{\Lambda-1/2}$ states and the rotational constants, B_v. In terms of the J-values, we have

$$F_{\underset{2}{1}}(J) = B_v\{(J+\tfrac{1}{2})^2 - \Lambda^2 \mp \tfrac{1}{2}[4(J+\tfrac{1}{2})^2 + Y(Y-4)\Lambda^2]^{1/2}\} + \ldots\,, \tag{6}$$

[5] *Phys. Rev.*, **32**, 250, 1928.

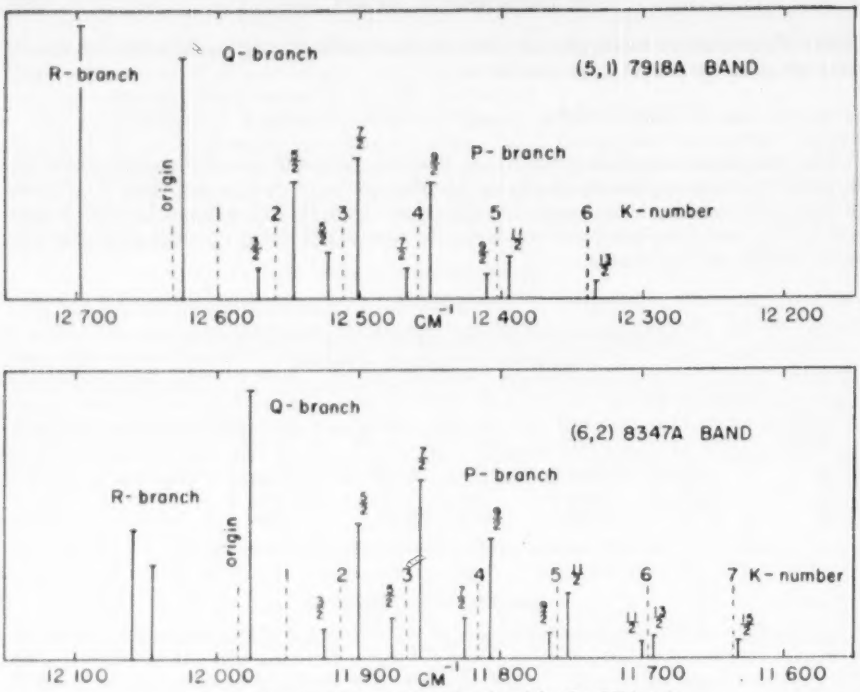

FIG. 2.—Observed line positions for the night-sky *OH* bands

TABLE 4

DETERMINATION OF ROTATIONAL CONSTANTS FOR THE *OH* BANDS

	(5, 1) 7918 A BAND			(6, 2) 8347 A BAND		
K	Δ' (Cm^{-1})	Δ'' (Cm^{-1})	$(B_{v'}+B_{v''})$ (Cm^{-1})	Δ' (Cm^{-1})	Δ'' (Cm^{-1})	$(B_{v'}+B_{v''})$ (Cm^{-1})
2	−47.0	−5.6	33.3	−45.2	−5.4	31.5
3	−52.6	−4.0	33.4	−50.6	−6.0	31.4
4	−56.6		31.9	−56.6	−6.4	31.9
5				−63.0		32.8
Average $(B_{v'}+B_{v''})$			32.9			31.9

	$B_{v'}$	$B_{v''}$	$B_{v'}$	$B_{v''}$
Observed	15.1	17.8	14.6	17.3
Computed	15.0	17.8	14.4	17.1

where $Y = \Delta/B_v$. The equation for a P branch of the $^2\Pi$ transition ($\Lambda = 1$), then, is

$$P_{\frac{1}{2}}(J) = {}^1\Pi(J) \mp \frac{B_{v'}}{2}\,[4(J-\tfrac{1}{2})^2 + Y'(Y'-4)]^{1/2} \pm \frac{B_{v''}}{2}\,[4(J+\tfrac{1}{2})^2 + Y''(Y''-4)]^{1/2} + \ldots \qquad (7)$$
$$= {}^1\Pi(J) \mp \delta(J),$$

where $^1\Pi(J)$ refers to the positions of a singlet P branch for half-integer J-values. The last term represents the doublet splitting of the F_1 and F_2 components for lines of equal J. The doublet splitting about the position of the lines defined by $F(K) = B_v K(K+1) + \ldots$ is related to the J-splitting by

$$P_1(K) = {}^1\Pi(K) + \{(B_{v'} - B_{v''})K + \tfrac{1}{4}(B_{v'} + 3B_{v''}) - \delta(J = K + \tfrac{1}{2})\}$$
$$P_2(K) = {}^1\Pi(K) - \{(B_{v'} - B_{v''})K - \tfrac{1}{4}(3B_{v'} + B_{v''}) - \delta(J = K - \tfrac{1}{2})\}. \qquad (8)$$

The computed and observed values of the doublet splitting are compared in Table 5 and

TABLE 5

COMPARISON OF THE OBSERVED AND COMPUTED DOUBLET SPLITTING FOR *OH*

J	$\delta(J)_{comp}$ (Cm^{-1})	$\delta(J)_{obs}$ (Cm^{-1})	K	$\overline{\delta(K)}_{comp}$ (Cm^{-1})	$\overline{\delta(K)}_{obs}$ (Cm^{-1})
$\frac{3}{2}$	$\pm$ [7.9]	$\pm$ [7.1]	2	$\pm$11.6	$\pm$12.3
$\frac{5}{2}$	12.1	11.6	3	10.0	10.2
$\frac{7}{2}$	16.3	16.0	4	8.8	8.5
$\frac{9}{2}$	20.4	20.8	5	7.6	6.8
$\frac{11}{2}$	$\pm$24.2	$\pm$26.2	6	$\pm$6.6	$\pm$ 5.4

Figure 3 for the (5, 1) 7918 A and (6, 2) 8347 A bands, using the value $A = -138.3\ cm^{-1}$. For *OH*, the splitting F_1 refers to the $^2\Pi_{3/2}$ component, and the splitting F_2 refers to the $^2\Pi_{1/2}$ component. The parentheses about the $\delta J(\frac{3}{2})$ term indicates that $J = \frac{3}{2}$ is missing in the $^2\Pi_{3/2}$ state. This quantity refers to the position of the missing component as obtained from the series for the intense P branch (F_1).

FAR INFRARED *OH* BAND POSITIONS

With the conclusive identification that the strong night-sky emissions are due to the rotation-vibration bands of *OH*, it is possible to utilize the vibrational constants to predict the positions of the sequences of this band system. The most striking fact about the observed bands is that they have large Δv-values, the two sequences being for $\Delta v = 4$ and 5. If the vibrational motion of a molecule is strictly harmonic, the selection rule for transitions is $\Delta v = \pm 1$. It is only for anharmonic oscillators that this selection rule can be violated. For such an oscillator, transitions with $\Delta v = 1, 2, 3, \ldots$, may occur; however, the transition probability rapidly decreases with an increase in Δv. Since the wave functions have not been computed for the *OH* state at the present time, it is not possible to evaluate the transition probabilities. It is certain, however, that the bands in the unobservable infrared must be much more intense than those currently observed in the photographic region.

The author has held the opinion for some time that an extension of this band system in the infrared could account for the 10440 A radiation of Stebbins, Whitford, and Swings. This suggestion has now been made independently by Herzberg. The identification of the 10440 A radiation by Swings as due to the (0, 0) band of the first positive sys-

tem of N_2 has been widely accepted, although it has not been possible to explain the absence of Vegard-Kaplan bands from $v' = 0$.

An observation by Meinel and Smith at Lick Observatory in November, 1949, gave evidence that the emission near 10400 A was not even approximately monochromatic. The observation was made by placing a red-sensitive photocell behind a slit in the focal plane of the spectrograph. The night-sky spectrum was scanned from approximately 11000 A to 7000 A with an equivalent slit-width of 300 A. The level of intensity was observed to be high at the long-wave-length limit of the photocell at 11000 A. The intensity level decreased uniformly with decreasing wave length, with a minor maximum

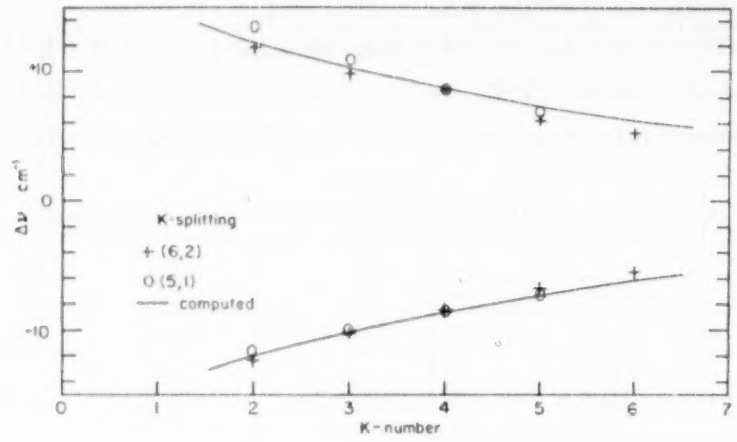

a

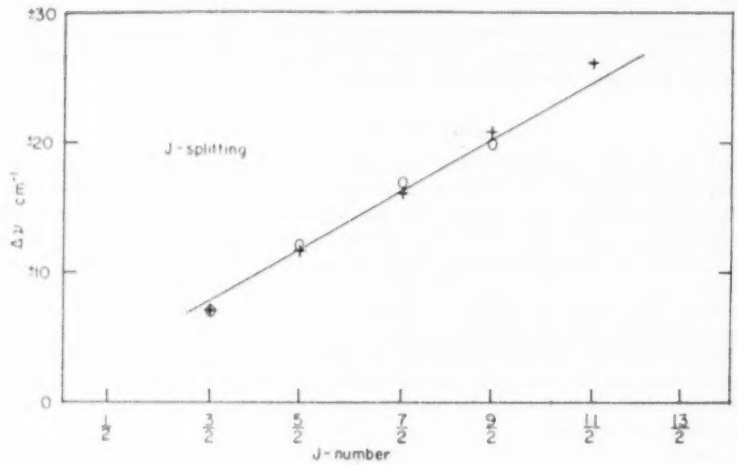

b

FIG. 3.—Observed doublet splitting of the night-sky *OH* bands

near 8000 A. This observation strongly indicated that numerous radiations were present beyond 9000 A. A more accurate photoelectric scanning of the spectrum is planned for the near future.

The origins for a large number of *OH* bands are given in Table 6 and Figure 4. The lengths of the lines in Figure 4 are arbitrary. Lines originating from levels 8 and 9 appear to be the strongest and are indicated by longer lines. It is interesting to note that the strongest member of the $\Delta v = 4$ sequence occurs at 10014 A. Overlapping this radiation are the bands of the $\Delta v = 3$ sequence. The sensitivity-curve of the filter and photocell used by Stebbins, Whitford, and Swings is plotted in Figure 4. This diagram shows that the 10440 A radiation may be attributed to a large number of very strong *OH* bands.

TABLE 6

OH BAND POSITIONS

$\Delta v = 1$	$\Delta v = 2$	$\Delta v = 3$
(9, 8) 2243.0 cm^{-1} 4.458 μ	(9, 7) 4656.0 cm^{-1} 2.148 μ	(9, 6) 7237.5 cm^{-1} 13817 A
(8, 7) 2413.0 4.144	(8, 6) 4994.5 2.002	(8, 5) 7743.2 12915
(7, 6) 2581.5 3.874	(7, 5) 5330.2 1.876	(7, 4) 8244.6 12129
(6, 5) 2748.7 3.638	(6, 4) 5663.1 1.777	(6, 3) 8741.8 11439
(5, 4) 2914.4 3.431	(5, 3) 5993.1 1.668	(5, 2) 9234.7 10829
(4, 3) 3078.7 3.248	(4, 2) 6320.3 1.582	(4, 1) 9723.5 10284
(3, 2) 3241.6 3.085	(3, 1) 6644.8 1.505	(3, 0) 10208.0 9796
(2, 1) 3403.2 2.938	(2, 0) 6966.4 1.436	
(1, 0) 3563.2 2.806		

$\Delta v = 4$	$\Delta v = 5$	$\Delta v = 6$
(9, 5) 9986.2 cm^{-1} 10014 A	(9, 4) 12900.6 cm^{-1} 7752 A	(9, 3) 15979.3 cm^{-1} 6258 A
(8, 4) 10657.6 9383	(8, 3) 13736.3 7280	(8, 2) 16977.9 5890
(7, 3) 11323.3 8831	(7, 2) 14564.9 6867	(7, 1) 17968.1 5565
(6, 2) 11983.4 8345	(6, 1) 15386.6 6500	(6, 0) 18949.8 5277
(5, 1) 12637.9 7913	(5, 0) 16201.1 6172	
(4, 0) 13286.7 7526		

These conjectures do not mean that the (0, 0) band of the first positive system of N_2 is completely absent. Stebbins, Whitford, and Swings observed fluctuations in the photoelectric deflection, while the near-infrared *OH* bands appear to be quite constant from night to night. Since infrared N_2 first positive bands appear with great intensity during auroral disturbances,[2] the fluctuations observed by the above authors may have been due to the abnormal excitation of the (0, 0) band.

VISIBLE REGION *OH* BAND POSITIONS

An examination of spectra obtained by H. W. Babcock,[6] Slipher,[7] and Sommer[7] shows the presence of the *OH* bands in the visible region of the night-sky spectrum. The very conspicuous emission on the shortward side of 6300 A on the spectrum published by Babcock, at 6258 A, corresponds to the strongest band of the $\Delta v = 6$ sequence at 6258.1 A (9, 3). This and the other coincidences are shown in Table 7. The

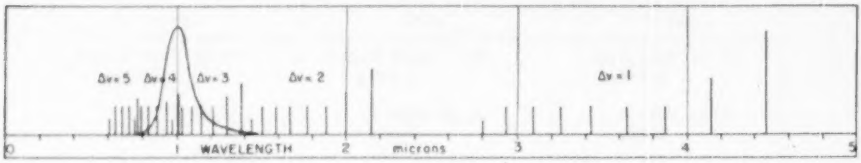

FIG. 4.—*OH* band positions in the infrared

TABLE 7

OBSERVED *OH* BANDS IN THE VISIBLE REGION

Babcock	Slipher	Sommer	*OH* Bands	Babcock	Slipher	Sommer	*OH* Bands
.....	7270	7290	(8, 3) 7280	6502	.....	.....	(6, 1) 6500
.....	6870	6863	(7, 2) 6867	6258	.....	.....	(9, 3) 6258

weak emission at 6502 A was not observed by Slipher or Sommer, while the 6258 A emission was too near to the intense 6300 A line to be observable except with the higher dispersion employed by Babcock. The emissions (8, 2) and (7, 1) would be much fainter and difficult to detect, inasmuch as they very nearly coincide with *Na* I at 5893 A and [*O* I] at 5577 A. The presence of the *OH* band system in the red region of the night-sky spectrum consequently eliminates a number of identifications ascribed to the first positive system of N_2. A detailed discussion of the intensity characteristics of the rotational and vibrational structure, as related to an excitation mechanism, will be presented in a following paper.

In conclusion, the author wishes to express his special indebtedness to Dr. Gerhard Herzberg for his instant recognition that the *OH* bands were due to the rotation-vibration spectrum of *OH*. This investigation has been sponsored by the Office of Naval Research in co-operation with the Lick Observatory and the Yerkes Observatory.

Note added in proof.—The author has received a private communication from J. Dufay, announcing independently the observation of the *OH*-band system in the visible region. An additional discussion of the *OH* bands in the visible region, with respect to previous identifications with the first positive bands of N_2 and $H\alpha$, is given in the March issue of the *Astrophysical Journal*.

[6] *Pub. A.S.P.*, **51**, 47, 1939.

[7] C. Fabry, J. Dufay, J. Cojan, *Étude de la lumière du fond du ciel nocturne* ("Éditions rev. d'opt." [Paris, 1934]).

NEW SOLAR LINES IN THE SPECTRAL REGION 1.97–2.49 μ*

LEO GOLDBERG, ORREN C. MOHLER, A. KEITH PIERCE, AND ROBERT R. MCMATH
McMath-Hulbert Observatory, University of Michigan, Pontiac, Michigan
Received February 20, 1950

ABSTRACT

Measurements of wave length and of percentage central absorption are given for 109 solar lines in the region 1.97–2.49 μ of the infrared solar spectrum. The lines were found on tracings obtained with the high-dispersion spectrometers and Cashman *PbS* cells of the McMath-Hulbert Observatory at Lake Angelus and at the Mount Wilson Observatory.

Forty-seven lines have been identified as arising from neutral atoms of *H*, *Na*, *Si*, *Mg*, *Al*, *Ca*, and *Fe*. The relative scarcity of solar lines in the 2.2 μ region is discussed, and a qualitative explanation is given in terms of the variation with wave length of the continuous absorption coefficient of H^- combined with the solar temperature gradient.

This paper is a further report[1] of progress in the survey of the near infrared solar spectrum on tracings obtained with high-dispersion spectrometers employing Cashman *PbS* cells as energy receivers. One phase of the survey involves the systematic tabulation of wave lengths, intensities, and, whenever possible, the identifications of all solar and telluric lines between 1.42 and 3.6 μ. Pending completion of this rather extensive work, which is intended to accompany an atlas of the infrared solar spectrum that is already in press, we believe that it is useful to publish preliminary lists of new solar lines as an aid to laboratory investigations of infrared atomic spectra. The preliminary lists are not intended to be complete, nor is the accuracy of the wave lengths greater than about 0.2 A. We have, for example, deliberately avoided, for the present, those portions of the solar spectrum that lie close to the edges of the water-absorption bands at 1.4 and at 1.8 μ. In these regions the selection of solar lines by high-low sun comparisons is inconclusive, and recourse must be had to comparisons of E-W limb spectra on the dryest possible days.

The first preliminary list[2] was made up of about 300 solar lines in the spectral region 1.52–1.75 μ. At the time of publication of the first list, records were available to an infrared limit of 2.5 μ, but, in view of then imminent instrumental modifications[3] that have since led to improvement in spectral resolution by a factor of 2 or 3, publication of the 2 μ lines was held up until the present time. Still further improvement in the quality of the infrared tracings has been obtained with a duplicate of the McGregor spectrometer, financed by a contract with the Office of Naval Research and attached to the Snow telescope under a co-operative arrangement with the Mount Wilson and Palomar observatories.

SOLAR LINES IN THE 2.2 μ REGION

The greater part of the 2.2 μ region is relatively free of telluric absorption. Beginning at about 1.95 μ, the spectrum emerges from the totally absorbing Ω band of H_2O and encounters the semitransparent region of the strong ω_0, ω_1, and ω_2 bands of CO_2,[4] which

* Supported in part by contract N6onr-232-V with the Office of Naval Research.

[1] Cf. summary article by Robert R. McMath and Leo Goldberg, *Proc. Amer. Phil. Soc.*, **93**, 362, 1949.

[2] Leo Goldberg, Orren C. Mohler, and Robert R. McMath, *Ap. J.*, **109**, 28, 1949.

[3] For a description of the infrared instrumentation in its present state of development, see Robert R. McMath and Orren C. Mohler, *J. Opt. Soc. Amer.*, **39**, 903, 1949.

[4] Leo Goldberg, Orren C. Mohler, Robert R. McMath, and A. Keith Pierce, *Phys. Rev.*, **76**, 1848, 1949.

extend to about 2.08 μ. Weak bands of CO_2 and its isotopes occur between 2.07 and 2.15 μ, but the isotope bands, together with a weak band of N_2O, appear only at low solar altitudes. The earth's atmosphere is remarkably transparent between 2.1 and 2.4 μ, the chief absorbing constituents being CH_4 and H_2O. Over 100 lines of methane appear in this region of the spectrum of the noonday sun, but the number is approximately tripled at low sun.[5]

Table 1 lists 109 solar lines in the spectral region from 1.97 to 2.49 μ. The detailed description of both Tables 1 and 2 is omitted here, since it would follow closely that already given for similar tables in an earlier paper dealing with solar lines in the 1.6 μ region. The first column gives the measured wave length, in I.A.; the second column the percentage central absorption; the third column the identification, on the basis of wave lengths predicted from term differences; the fourth column the predicted wave length; and the fifth column the laboratory wave length from the compilation by Kayser and Ritschl.[6]

IDENTIFICATIONS OF SOLAR LINES

As in the 1.6 μ region,[2] identifications of solar lines between 1.97 and 2.49 μ have been accomplished by comparisons with wave lengths predicted from C. E. Moore's[7] tables of atomic-energy levels. Forty-seven lines, or nearly half the total found, have been so identified with neutral atoms of *H*, *Na*, *Si*, *Mg*, *Al*, *Ca*, and *Fe*. The agreement between solar and predicted wave lengths is excellent, the differences rarely exceeding 0.2 cm^{-1}. Table 2 gives the predicted multiplets that form the basis for the identifications. The intensities in the second column are the solar percentage central absorptions. A dash in the intensity column signifies that a strong telluric line occurs at the predicted wave length, whereas a blank space means that the line is absent.

Among the lines identified, the most numerous are due to *Si* I. This element is a prolific source of infrared lines; it is interesting to note that, of four solar lines identified in the 3.3 μ region,[8] three are attributed to *Si* I. It is perhaps surprising to find but a single predicted multiplet of *Fe* I, namely, $x^5F^\circ - e^5D$. The scarcity of *Fe* I lines is more apparent than real, however, being due probably to incomplete information on high-lying terms. *Ca* I contributes a number of strong lines, but the majority of them are overlapped by strong CO_2 absorption. It should be mentioned that the *Ca* I multiplet $5p^3P^\circ - 5d^3D$ accounts for five strong solar lines near λ 16,200. The atomic-energy level tables for *Ca* were not available to us at the time of publication of the paper[2] dealing with the 1.6 μ region. The data for this multiplet are therefore included in Table 2.

FREQUENCY OF SOLAR LINES IN THE 2 μ REGION

The most important factors governing the appearance of the spectral lines of a given atom in the solar spectrum are (*a*) its abundance, (*b*) the excitation potential, and (*c*) the continuous opacity of the solar atmosphere for the wave length considered. Babcock and Moore[9] have pointed out that, even in the photographic infrared, most atomic lines are of high excitation potential. Approximately 90 per cent of all lines identified in the infrared solar spectrum between 1.5 and 3.6 μ have excitation potentials in excess of 5 volts. If the coefficient of continuous absorption were independent of wave length, one might therefore expect a gradual fading-out of solar lines with increasing wave length by virtue of the correlation between excitation potential and wave length.

[5] Robert R. McMath, Orren C. Mohler, A. Keith Pierce, and Leo Goldberg, *Phys. Rev.*, **76**, 1533, 1949.

[6] *Tabelle der Hauptlinien der Linienspektren aller Elemente* (Berlin: Julius Springer, 1939).

[7] *Atomic Energy Levels*, Vol. I, 1948 (*Circ. Nat. Bur. Stand.* No. 467).

[8] Orren C. Mohler and A. Keith Pierce, *Pub. A.S.P.*, **61**, 22, 1949.

[9] *The Solar Spectrum, λ 6600 to λ 13495* (Pub. Carnegie Inst. Washington, No. 579, 1947).

TABLE 1

SOLAR LINES IN THE SPECTRAL REGION 1.97–2.49 μ

λ (Sun)	Int.	Ident.	λ (Calc.)	λ (K and R)
19722.7	23	*Si*	23.2	
19776.9	35	*Ca*	76.9	77.4
19815.4	20	*Ca*	15.3	17.3
19853.4	21	*Ca*	53.1	56.9
19917.3	11	*Ca*	17.3	17.5
19930.0	22	*Si*	28.8	
19934.3	23	*Ca*	33.9	35.8
20303.6	13	*Si*	03.1	
20344.1	10	*Si*	43.5	
20717.6	5	⊙		
20724.0	4	⊙		
20765.9	10?	Atm CO_2 ⊙		
20813.1	8?	Atm CO_2 ⊙		
20823.3	6?	Atm CO_2 *Si*	21.1	
20857.0	10	Atm CO_2 ⊙		
20890.7	3	⊙		
20894.1	20	⊙		
20917.1	22	⊙		
20919.7	12	Atm CO_2 ⊙		
20967.5	6	⊙		
21023.2	5	⊙		
21061.3	20	⊙ Atm		
21093.4	38?	*Al* Atm	93.7	93.6
21164.4	24	*Al*	64.3	64.3
21226.0	2	*Mg*	26.1	
21260.0	9	⊙		
21354.4	22	Atm H_2O *Si*	54.6	
21370.0	3	⊙		
21389.7	3	⊙		
21429.0	3	⊙		
21441.0	9	*Si*	39.8–41.8	
21452.5	5	⊙		
21459.2	5	⊙		
21655.	12	*H*	55.4	
21721.2	6	*Si*	21.7	
21735.8	5	⊙		
21783.6	7	⊙		
21820.1	23	*Si*	19.2–20.2	
21858.3	5	⊙		
21874.7	5	*Si*	74.3	
21880.2	24	*Si*	80.2	
21895.8	7	⊙		
22056.5	29	*Na*	56.0	56.9
22062.9	28?	Atm *Si*	61.3	
22072.5	7	*Si*	72.0	
22083.7	23	*Na*	83.3	84.2
22257.6	15	*Fe*	56.9	
22381.0	13	*Fe*	81.0	
22393.2	7	*Fe*	93.0	
22420.5	5	⊙		
22473.2	13	⊙		
22608.0	12	Atm *Ca*	08.1	10.0
22620.3	20	*Fe*	20.1	
22625.1	14	*Ca*	25.2	24.6

TABLE 1—*Continued*

λ (Sun)	Int.	Ident.	λ (Calc.)	λ (K and R)
22627.0	6	*Ca*	27.0	
22651.8	18	*Ca*	51.4	
22653.8	9	*Ca*	53.8	55.9
22666.0	12	*Si*	66.2	
22708.1	10	⊙		
22740.7	10	⊙ Atm		
22795.5	4	⊙		
22808.7	23	*Mg*	07.2	
22930.9	5	⊙ Atm CH_4		
22935.0	8	*Si* Atm CH_4	34.8	
23007.5	5	⊙		
23024.0	7	*Mg*	26.2	
23072.0	3	⊙		
23106.6	5	*Si*	06.4	
23118.8	3	⊙		
23130.8	2	⊙		
23142.0	7	*Si*	42.6	
23145.1	12	Atm *Si*	45.0	
23230.2	3	⊙		
23262.2	8	⊙		
23269.5	3	⊙		
23274.7	6	⊙		
23281.5	8	Atm CH_4 ⊙		
23297.0	5	Atm CH_4 *Si*	98.0	
23349	15?	*Na* Atm CH_4	48.0	
23352.0	4	⊙		
23379.7	28?	*Na* Atm CH_4	78.7–78.9	
23410.7	5	Atm CH_4 ⊙		
23434.1	3	⊙		
23536.5	2	⊙		
23547.7	5	⊙		
23570.9	5	⊙		
23592.9	5	⊙		
23601.0	6	⊙		
23648.1	5	⊙		
23844.7	10	⊙		
23859.7	25?	*Mg* Atm CH_4	59.8	
23931.5	3	⊙		
23953.6	5	⊙		
23985.0	3	⊙		
24278.0	5	⊙		
24333.4	3	⊙		
24375.1	11	⊙		
24381.1	6	⊙		
24403.5	2	⊙		
24436.2	2	⊙		
24440.8	2	⊙		
24484.5	2	⊙		
24488.2	2	⊙		
24523.6	2	⊙		
24548.2	10	⊙		
24552.0	3	⊙		
24566.2	13	*Mg*	66.2	
24574.9	7	*Si*	75.6	
24895.5	25	*Si* Atm H_2O	95.5	

TABLE 2

MULTIPLETS IN THE 2 μ REGION

λ Pred.	Int.	E.P. Low	E.P. High	J	Multiplet	Remarks
			H			
21,655.4	12	12.69	13.26	—	$4^2F^\circ - 7^2G$, etc.	
			Na I			
22,083.3	23	3.18	3.74	1/2–3/2	$4s^2S - 4p^2P^\circ$	
22,056.0	29	3.18	3.74	1/2–1/2		
23,378.9	28?	3.74	4.26	3/2–5/2	$4p^2P^\circ - 4d^2D$	1
23,348.0	15?	3.74	4.26	1/2–3/2		1
23,378.7	28?	3.74	4.26	3/2–3/2		1
			Si I			
23,811.2		6.07	6.59	2–1	$4p^3P - 3d^1P^\circ$	
23,106.4	5	6.06	6.59	1–1		
22,934.8	8	6.05	6.59	0–1		
19,723.2	23	6.07	6.70	2–3	$4p^3P - 4d^3D^\circ$	
19,432.7	—	6.06	6.69	1–2		
19,386.6	—	6.05	6.69	0–1		
19,928.8	22	6.07	6.69	2–2		
19,509.1	—	6.06	6.69	1–1		
20,009.2	—	6.07	6.69	2–1		
19,494.6	—	6.10	6.73	1–2	$4p^3S - 5s^3P^\circ$	
20,343.5	10	6.10	6.70	1–1		
20,634.6		6.10	6.70	1–0		
24,575.6	7	6.20	6.70	2–3	$4p^1D - 4d^3D^\circ$	
24,895.5	25	6.20	6.69	2–2		2
25,021.1	—	6.20	6.69	2–1		
21,354.6	22	6.20	6.77	2–1	$4p^1D - 5s^1P^\circ$	2
22,666.2	12	6.59	7.14	1–2	$3d^1P^\circ - 5p^1D$	
20,303.1	13	6.59	7.14	1–0	$3d^1P^\circ - 5p^1S$	
22,133.7		6.70	7.26	3–3	$4d^3D^\circ - 4f^1F$	
21,880.3	24	6.69	7.26	2–3		
22,061.3	28?	6.70	7.26	3–4	$4d^3D^\circ - 4f^3F$	4
21,820.2	23	6.69	7.26	2–3		
21,778.4	—	6.69	7.26	1–2		
22,072.0	7	6.70	7.26	3–3		
21,874.3	5	6.69	7.26	2–2		
22,127.5		6.70	7.26	3–2		
21,819.2	23	6.73	7.30	2–3	$5s^3P^\circ - 4f^3D$	
20,499.1	—	6.70	7.31	1–2		
20,313.6	—	6.70	7.31	0–1		
21,439.8	9	6.73	7.31	2–2		
21,500.9	—	6.70	7.31	1–1		
21,441.8	9	6.73	7.31	2–1		
23,142.6	7	6.77	7.31	1–2	$5s^1P^\circ - 4f^3D$	
23,145.0	12	6.77	7.31	1–1		4
20,819.6	—	6.97	7.57	2–3	$4d^1D^\circ - 5f^3F$	
20,821.1	6?	6.97	7.57	2–2		3
21,675.1		7.00	7.57	2–2	$4d^3P^\circ - 5f^3D$	
21,721.7	6	7.00	7.57	1–2		
23,298.0	5	7.04	7.57	2–1	$5p^3D - 5d^3P^\circ$	1
23,086.7		7.03	7.57	1–1		

TABLE 2—*Continued*

λ Pred.	Int.	E.P. Low	E.P. High	J	Multiplet	Remarks
			Mg I			
24,566.2	13	6.56	7.06	2–3	$4d^1D - 5f^1F^\circ$	
22,807.2	23	6.69	7.23	3,2,1–4,3,2	$4d^3D - 6f^3F^\circ$	
23,859.8	25?	6.70	7.21	2,1,0–3,2,1	$5p^3P^\circ - 6d^3D$	1
21,226.1	2	6.70	7.28	2–1	$5p^3P^\circ - 8s^3S$	
23,024.2	7	6.75	7.29	1–2	$5p^1P^\circ - 7d^1D$	
			Al I			
21,164.3	24	4.07	4.65	3/2–1/2	$4p^2P^\circ - 5s^2S$	
21,093.7	38?	4.07	4.65	1/2–1/2		2
			Ca I			
16,197.0	14	4.51	5.27	2–3	$5p^3P^\circ - 5d^3D$	
16,150.6	9	4.51	5.27	1–2		
16,136.6	8?	4.51	5.27	0–1		3
16,204.0	12	4.51	5.27	2–2		
16,155.0	5	4.51	5.27	1–1		
16,208.5	15?	4.51	5.27	2–1		4
19,776.9	35	1.89	2.51	2–3	$4p^3P^\circ - 3d^3D$	
19,453.1	—	1.88	2.51	1–2		
19,309.3	—	1.87	2.51	0–1		
19,862.3	—	1.89	2.51	2–2		
19,505.8	—	1.88	2.51	1–1		
19,917.3	11	1.89	2.51	2–1		
19,853.1	21	3.89	4.51	1–2	$5s^3S - 5p^3P^\circ$	
19,933.9	20	3.89	4.51	1–1		
19,962.0	—	3.89	4.51	1–0		
19,815.3	20	4.60	5.22	2–3	$4d^1D - 4f^1F^\circ$	
22,651.4	18	4.66	5.20	3–4	$4d^3D - 4f^3F^\circ$	
22,625.2	14	4.66	5.20	2–3		
22,608.1	12	4.66	5.20	1–2		4
22,653.8	9	4.66	5.20	3–3		
22,627.0	9	4.66	5.20	2–2		
22,655.6		4.66	5.20	3–2		
			Fe I			
22,620.1	20	4.97	5.52	5–4	$x^5F^\circ - e^5D$	
22,381.0	13	5.01	5.56	4–3		
22,256.9	15	5.04	5.60	3–2		
22,620.2	20	5.06	5.62	2–1		
22,393.0	7	5.08	5.63	1–0		
24,487.9	2	5.01	5.52	4–4		
23,694.7	—	5.04	5.56	3–3		
23,164.3	—	5.06	5.60	2–2		
22,832.5	—	5.08	5.62	1–1		
26,069.3	—	5.04	5.52	3–4		
24,725.7	—	5.06	5.56	2–3		
23,784.6		5.08	5.60	1–2		

NOTES TO TABLE 2

1. Blend atm CH_4. 2. Blend atm H_2O. 3. Blend atm CO_2. 4. Blend atm.

It is now well established, however, from the work of Chandrasekhar and his collaborators[10] and of Chalonge and Kourganoff[11] that the absorption coefficient, which is due to bound-free and free-free transitions in H^-, does depend strongly on the wave length, with interesting consequences for the infrared line spectrum. As is now well known, the absorption-curve of H^- rises from λ 4000 to a maximum at about λ 8600 and thereafter decreases to a minimum at λ 16,600. At this point the free-free transitions become important, and the absorption increases steadily toward the longer wave lengths. Since the production of high-excitation infrared lines is favored by high temperature, it is clear that the opacity minimum at λ 16,600 is favorable for the appearance of infrared atomic lines. At longer wave lengths the increased opacity screens off the high-temperature layers of the atmosphere, and, on the average, the infrared lines will decrease both in numbers and in intensity.

These theoretical considerations are borne out qualitatively by the observed frequency of occurrence of infrared solar lines. Between 1.52 and 1.75 μ, about 300 solar lines with central absorptions greater than 4 per cent have been found, or an average of about 0.32 lines per cm^{-1}. On the other hand, the frequency of occurrence of lines of the same minimum intensity between 2.1 and 2.4 μ is about 0.11 per cm^{-1}. The relative infrequency of strong solar lines in the 2.2 μ region is not due to increased telluric absorption as compared with the 1.6 μ region, since the latter region includes two strong bands of CO_2 at 1.57 μ and 1.65 μ.

In conclusion we wish to thank Dr. I. S. Bowen for his kindness in making available the Snow telescope under a guest investigator arrangement between the Mount Wilson and Palomar and McMath-Hulbert observatories. Mr. Dale Vrabec secured the tracings at Mount Wilson, and Mr. Russell E. Donovan carried out the measurement and reduction. We gratefully acknowledge also continued grants-in-aid by McGregor Fund of Detroit.

[10] Cf. Chandrasekhar and Breen, *Ap. J.*, **104**, 430, 1946; Chandrasekhar and Münch, *Ap. J.*, **104**, 446, 1946.

[11] *Ann. d'ap.*, **9**, 69, 1946.

THE SPECTRA OF TWO ACTIVE REGIONS OBSERVED AT THE SUN'S LIMB

ROBERT S. RICHARDSON
Mount Wilson and Palomar Observatories
Received January 6, 1950

ABSTRACT

Emission was observed in 109 lines between 3968 and 5903 A in the spectrum of a prominence of the active sunspot type (Pettit's class III*c*). Emission was observed in 126 lines from 3670 to 5900 A in a flare of intensity < 1.

Atoms observed in the prominence and flare were *H*, *He* I, *Na* I, *Mg* I, *Al* I, *Si* I, *Ca* I, *Fe* I, *Ca* II, *Sc* II, *Ti* II, *Cr* II, *Fe* II, *Sr* II, *Y* II, and *Ba* II. The Balmer series appeared in emission in the flare to *H* 21, which is near the limit of transmission for the 75-foot spectrograph.

The intensity of emission in lines of hydrogen and helium was about the same in the prominence and the small flare, but most of the metallic lines appeared stronger in the prominence.

On February 27, 1946, about 1600 G.C.T., while sweeping the disk of the sun for flares at the 150-foot tower, I discovered a bright region on the east limb at 29° N., near Mount Wilson group No. 7978. This spot group was the first return of No. 7943, one of the largest ever recorded.[1] Examination of the spectrum revealed an unusual number of lines in emission, indicating a degree of excitation seldom found in the solar atmosphere. In particular, 5876 of *He* I (D_3) was not only very strong in the chromosphere but showed distinctly in emission on the disk.

The first plates taken of the spectrum of the D_3 region turned out too dense to be of use because the estimated exposure times were too long. An attempt was next made to photograph the entire spectrum from the D lines to H and K, of a point just outside the limb which then appeared most active. Four overlapping exposures of 530 A each were made from 1656 to 1708 G.C.T. in the first order of the 75-foot spectrograph with the Michelson No. 66 grating, where the dispersion is 0.71 A/mm, using a tangential slit set 2 mm outside the limb of the solar image, 420 mm in diameter. These plates proved of good quality and uniform density from 5903 to 3968 A.

When first seen at the 150-foot tower, the active region was thought to be a flare near the limb. The spectroheliograms taken at the 60-foot tower from 1623 to 1702 G.C.T., however, showed only a small marking near No. 7978 that looks more like a rather bright flocculus than a flare. Much more suspicious was the bright prominence over No. 7978, which E. Pettit[2] classified as an example of the active sunspot type (III*c*), probably originating in the region of the corona. This prominence is believed to be the object observed at the 150-foot tower.

The prominence was examined again about 1730 G.C.T. after the plates were developed, but it appeared so much fainter that no more exposures were made; and no unusual activity was observed on February 28, about 1600 G.C.T. This prominence first shows strongly defined on spectroheliograms taken on February 26 from 1827 to 2027 G.C.T. and cannot be identified on a spectroheliogram taken on February 28 at 1704 G.C.T.

The magnetometer record at Mount Wilson for February 27 shows a distinct crochet at 1606 G.C.T., consisting of a simultaneous decrease in horizontal intensity of 3 γ and a change in declination toward the east of 1′. This small disturbance appears distinctly marked, owing to the fact that the day was exceptionally calm. The record for March 1 shows a sudden commencement at 0139 G.C.T., followed by a minor disturbance that lasted for about 36 hours.

[1] Nicholson and Hickox, *Pub. A.S.P.*, **58**, 86, 1946.

[2] *Mt. W. Contr.*, No. 679; *Ap. J.*, **93**, 6, 1941.

TABLE 1

EMISSION LINES IN THE SPECTRA OF TWO ACTIVE REGIONS OBSERVED AT THE SUN'S LIMB

Wave Length	Ident.	Prominence Feb. 27 1946	Flare April 11 1947	Wave Length	Ident.	Prominence Feb. 27 1946	Flare April 11 1947
3679.36	*H* 21	...*	2	4063.60	*Fe* I	2	2
3682.81	*H* 20	...	3	4071.74	*Fe* I	2	2
3685.19	*Ti* II	...	4	4077.71	*Sr* II	4	4
3686.83	*H* 19	...	3	4101.74	*Hδ*	40	70
3691.56	*H* 18	...	5	4143.87	*Fe* I	1	1
3697.15	H 17	...	9	4173.45	*Fe* II	1	2
3703.86	*H* 16	...	8	4178.86	*Fe* II	2	6
3705.57	*Fe* I	...	1	4202.03	*Fe* I	1	1
3710.30	*Y* II	...	1	4215.52	*Sr* II	6	6
3711.97	*H* 15	...	20	4226.73	*Ca* I	5	4
3719.94	*Fe* I	...	3	4233.17	*Fe* II	5	6
3721.94	*H* 14	...	25	4246.83	*Sc* II	4	4
3734.37	*H* 13	...	25	4254.35	*Cr* I	2	3
3736.90	*Ca* II	...	3	4260.48	*Fe* I	1	–
3737.13	*Fe* I	...	2	4271.76	*Fe* I	3	2
3745.56	*Fe* I	...	2	4274.80	*Cr*	2	2
3748.26	*Fe* I	...	1	4289.72	*Cr* I	1	1
3750.15	*H* 12	...	32	4290.22	*Ti* II	2	1
3759.29	*Ti* II	...	5	4294.10	*Ti* II	3	2
3761.32	*Ti* II	...	5	4300.05	*Ti* II	4	...
3770.63	*H* 11	...	30	4303.17	*Fe* II	1	3
3797.90	*H* 10	...	35	4307.91	*Fe* I	4	2
3819.61	*He* I	...	2	4314.08	*Sc* II	1	–
3820.43	*Fe* I	...	1	4320.74	*Sc* II	...	1
3824.44	*Fe* I	...	1	4325.76	*Fe* I	4	3
3829.35	*Mg* I	...	2	4337.92	*Ti* II	3	2
3832.30	*Mg* I	...	3	4340.47	*Hγ*	50	75
3835.39	*H* 9	...	40	4351.76	*Fe* II	6	8
3838.29	*Mg* I	...	3	4374.94	*V* II	2	1
3856.37	*Fe* I	...	1	4375.93	*Fe* I	1	2
3859.91	*Fe* I	...	3	4383.55	*Fe* I	6	4
3878.58	*Fe* I	...	2	4385.38	*Fe* II	1	3
3886.28	*Fe* I	...	3	4395.03	*Ti* II	8	4
3889.05	*H* 8	...	45	4399.77	*Ti* II	1	–
3895.66	*Fe* I	...	1	4404.75	*Fe* I	3	3
3899.71	*Fe* I	...	1	4415.12	*Fe* I	1	–
3900.55	*Ti* II	...	2	4416.82	*Fe* II	1	1
3905.53	*Si* I	...	3	4417.72	*Ti* II	1	1
3913.46	*Ti* II	...	1	4427.31	*Fe* I	1	–
3922.91	*Fe* I	...	2	4443.80	*Ti* II	4	1
3927.92	*Fe* I	...	2	4468.49	*Ti* II	4	1
3930.30	*Fe* I	...	3	4471.48	*He* I	8	10
3933.66	*Ca* II	...	100	4491.40	*Fe* II	1	–
3938.29	*Fe* II	...	3	4501.27	*Ti* II	5	1
3944.01	*Al* I	...	1	4508.28	*Fe* II	2	2
3961.52	*Al* I	1	2	4515.34	*Fe* II	2	3
3968.47	*Ca* II	90	90	4520.22	*Fe* II	2	3
3970.07	*Hε*	35	50	4522.63	*Fe* II	3	2
4026.19	*He* I	–†	5	4533.97	*Ti* II	5	1
4045.82	*Fe* I	3	3	4534.17	*Fe* II	2	1

* No observations.

† Not visible.

TABLE 1—*Continued*

Wave Length	Ident.	Prominence Feb. 27 1946	Flare April 11 1947	Wave Length	Ident.	Prominence Feb. 27 1946	Flare April 11 1947
4549.62	*Ti* II	5	2	5206.04	*Cr* I	3	1
4554.03	Ba II	4	1	5208.44	*Cr* I	3	–
4555.89	*Fe* II	2	2	5226.53	*Ti* II	2	1
4563.76	*Ti* II	3	1	5227.19	*Fe* I	2	–
4571.97	*Ti* II	3	1	5234.62	*Fe* II	4	3
4583.83	*Fe* II	6	6	5269.54	*Fe* I	3	1
4588.22	*Cr* II	1	1	5270.36	*Fe* I	1	–
4589.96	*Ti* II	1	–	5275.99	*Fe* II	5	3
4620.51	*Fe* II	1	1	5284.09	*Fe* II	2	2
4629.34	*Fe* II	4	6	5316.61	*Fe* II	8	6
4805.10	*Ti* II	1	–	5328.04	*Fe* I	3	–
4824.13	*Cr* II	1	–	5336.81	*Ti* II	1	–
4861.33	*Hβ*	100	100	5362.86	*Fe* II	2	–
4920.51	*Fe* I	1	–	5371.49	*Fe* I	2	...
4921.93	*He* I	4	4	5397.13	*Fe* I	2	...
4923.92	*Fe* II	15	7	5405.78	*Fe* I	2	...
4934.09	Ba II	4	1	5425.27	*Fe* II	1	2
4957.60	*Fe* I	1	...	5429.70	*Fe* I	1	–
5015.68	*He* I	5	5	5434.53	*Fe* I	1	–
5018.43	*Fe* II	12	8	5446.92	*Fe* I	1	–
5167.32	*Mg* I	8	2	5455.61	*Fe* I	1	–
5167.49	*Fe* I	3	1	5526.81	*Sc* II	2	1
5169.03	*Fe* II	20	12	5534.86	*Fe* II	2	4
5172.68	*Mg* I	10	8	5875.62	*He* I	100	100
5183.60	*Mg* I	15	9	5889.95	*Na* I	10	8
5185.90	*Ti* II	1	...	5895.92	*Na* I	10	8
5188.70	*Ti* II	2	...				
5188.85	*Ca* I	1	...				
5197.57	*Fe* II	3	2				
5204.52	*Cr* I	2	–				

The spectrum of another active region on the limb was photographed by Nicholson in the first order of the 75-foot spectrograph from 3670 to 5900 A on April 11, 1947, at about 1530 G.C.T. Spectroheliograms taken from 1459 to 1554 G.C.T. show a small flare (< 1) on the west limb at about 5° S. that can be definitely identified as the object observed at the 150-foot tower. In this case there is no question that the object was a flare and not a bright flocculus or prominence. On our 6-inch spectroheliograms the flare appears to be at a slightly higher level than the chromosphere as photographed in the center of *Hα*.

Emission in the lines of hydrogen and helium was nearly equal for the prominence and flare, but most of the metallic lines appeared stronger in the prominence. Both had approximately the same sky background. Detailed comparison of individual lines indicates that this difference is real. It should be remembered, however, that the flare was only of intensity < 1.

The scale of intensities in Table 1 has been made to correspond roughly with that adopted by C. W. Allen[3] in his list of lines observed in emission in solar flares.

[3] *M.N.*, **100**, 635, 1940.

SOLAR EXCITATION TEMPERATURE OF *V* I

ALLAN R. SANDAGE
Mount Wilson and Palomar Observatories
Received February 7, 1950

ABSTRACT

The effect of temperature stratification in the solar atmosphere upon observed excitation temperatures has been investigated by constructing a theoretical curve of growth from line contours computed with Münch's model atmosphere. It is shown that for weak *V* I lines the predicted temperature is a function of excitation potential. A temperature of 5080° K is obtained from weak 0- to 3-volt *V* I lines. King and Wright's *V* I curve of growth is rediscussed, with corrections applied for the variation of the continuous absorption coefficient with wave length. The redetermined curve gives a temperature of 5110° ± 190° K, which is in good agreement with the theoretical result.

INTRODUCTION

The excitation temperature of a star, determined from a curve of growth, represents a weighted mean taken through the atmospheric layers producing the absorption lines. If the lines are formed in different atmospheric layers, the observed excitation temperature will be a function of the excitation potential. The occurrence of this situation does not necessarily mean deviations from local thermodynamic equilibrium but merely a shift in the effective depth of line formation, this shift being a function of the excitation potential. One way to investigate this effect would be to construct a theoretical curve of growth from lines whose profiles had been computed by taking into account the stratification of the atmosphere. The temperature derived from this theoretical curve could then be compared with that obtained from an observational curve. If the two values agreed, the model atmosphere adopted could be said to be valid in the sense of giving the observed mean temperature.

PREDICTED TEMPERATURE

The lines of *V* I appeared to be ideal for such an analysis. The relative *f*-values have been experimentally determined by R. B. King.[1] Further, most of the *V* I lines in the sun are weak and therefore lie near or on the Doppler portion of the curve of growth; hence an accurate determination of the observational excitation temperature is possible. In addition, the computation of the line profiles is simplified, since for weak lines the contours are nearly independent of the damping constant. It should be emphasized that the profiles are computed only to obtain the near linear portion of a theoretical curve of growth and not to compare with observed profiles. For this reason we are permitted to choose arbitrary *f*-values for the computed lines.

The line contours were computed for *V* I by B. Strömgren's method,[2] which takes into account the stratification of the atmosphere. The equations used were Strömgren's equations (25)–(29), with the exception that the coefficients of equation (25) were changed to conform with different boundary conditions for the equation of transfer. The modified equation (25) used in these calculations is

$$r_\nu = \frac{2}{\frac{4}{3}\sqrt{3} + \frac{1}{2}(x_0/n)} \cdot \frac{\frac{4}{3}\sqrt{3}\,\sqrt{\lambda_\nu} + \frac{1}{2}(x_0/n)\lambda_\nu}{1 + \sqrt{\lambda_\nu}}, \qquad (1)$$

where the notation is the same as Strömgren's.

[1] *Mt. W. Contr.*, No. 731; *Ap. J.*, **105**, 376, 1947.

[2] *Festschrift fur Elis Strömgren* (Copenhagen: Einar Munksgaard, 1940), p. 218.

To apply Strömgren's method, one must know the ratio, η_ν, of the line-absorption coefficient to that of the continuous spectrum at various optical depths. At the center of the line this ratio is given by

$$\eta_0(\tau) = \frac{\sqrt{\pi}\, e^2 g f \lambda N_0(\tau)\, 10^{-(5040/T)\chi}}{m c V(\tau)\, b(\tau)\, \kappa_\nu(\tau)}, \tag{2}$$

where $N_0(\tau)$ is the number of atoms in the ground state of the neutral atom, $V(\tau)$ is the velocity term, $\kappa_\nu(\tau)$ is the continuous absorption coefficient, and $b(\tau)$ is the partition function. The other symbols have their usual meanings. The value of $N_0(\tau)$ was computed in terms of an arbitrary abundance, N_0, by assuming Münch's model solar atmosphere, which is based upon the theoretical value of the H and H^- continuous absorption coefficient and the theoretical temperature distribution with depth.[3] At each point the Boltzmann and Saha equations were assumed to be valid for the local temperature and pressure given by the model. The continuous absorption coefficient, $\kappa_\nu(\tau)$, was computed at λ 5063 from Table 7 of Chandrasekhar and Breen's paper.[4] The thermal component of the velocity $V(\tau)$ is proportional to the square root of the temperature and hence is a slowly varying function of depth. The variation with depth of the turbulent component is unknown. It is therefore assumed that the variation of $V(\tau)$ is small and may be neglected. It was also assumed that the variation of the partition function $b(\tau)$ could be neglected.

All line profiles were computed at λ 5063. No error is involved in the temperature determination by constructing the theoretical curve of growth at one wave length. Indeed, the observational curve is effectively constructed at a single wave length by removing all wave-length dependence from the data.

The ratio of the line to continuous absorption coefficient for frequencies away from the center of the line is given with sufficient accuracy for weak lines by

$$\eta_\nu = \eta_0 e^{-v^2}. \tag{3}$$

The value of η_ν was computed for $v = 0.5$, 1, 1.5, and 2.

With η_ν known at various depths, Strömgren's equations (27)–(29) were used to compute the weighted means $\sqrt{\overline{\lambda_\nu}}$ and $\bar{\lambda}_\nu$. Six-point Gaussian integration was used to evaluate the integrals. The parameter λ_0 was chosen to be λ_ν ($\tau = 0.2$). Only for the 0- and 1-volt lines does η_0 vary rapidly enough with τ to cause a significant difference in the profile because of an incorrect choice of λ_0. This small difference was found to have no effect on the temperature determination. Substitution of $\sqrt{\overline{\lambda_\nu}}$ and $\bar{\lambda}_\nu$ in equation (1) gave the profile.

Eighteen lines, distributed in the excitation groups E.P. = 0, 1, 3, 5, and 7 volts, were computed. Lines at 7 volts do not occur, since the ionization potential of V I is 6.71 volts, but the computations were made to see whether the variation of temperature with excitation potential followed the same course as for the lower-excitation lines. The f-values were chosen small enough to make η_0 ($\tau = 0.2$) < 0.3 for the strongest line. This insures that the lines will lie near the linear portion of the curve. Actually, the strongest lines computed differed slightly in shape from the weaker lines and were therefore not exactly on the linear portion of the curve.

The equivalent widths of the lines were found, and segments of a theoretical curve of growth were constructed by plotting $\log W/\lambda$ against $\log gf\lambda$. Five segments were obtained corresponding to the five excitation potentials. The abscissa shift necessary to bring each segment into coincidence with the 0-volt curve is $(5040/T)\chi$. The second column of Table 1 gives the temperatures derived by this method.

[3] *Ap. J.*, **106**, 217, 1947. [4] *Ap. J.*, **104**, 430, 1946.

M. Minnaert has considered a similar problem.[5] The third column of Table 1 gives the results of a computation at λ 5000 for *V* I, using Minnaert's theory. The temperatures obtained are considerably higher than those indicated in the second column. The differences can be attributed to the model atmosphere used in each case. The model used by Minnaert is based upon Chalonge and Kourganoff's analysis of the solar-limb darkening.[6] This model gives higher temperatures than does Münch's theoretical model at the same depth. From all data now available, the excitation temperatures determined observationally by using *V* I, *Ti* I, and *Fe* I lines[7] favor the lower values predicted from Münch's model. The entries of Table 1 show that the higher-excitation lines indicate higher temperatures. This means that the effective depth of line formation increases with increasing excitation potential. This effect may also be seen from Table 2, where

TABLE 1

PREDICTED EXCITATION TEMPERATURES FOR *V* I

E.P.	*T* (° K)		E.P.	*T* (° K)	
	Münch Model	Minnaert's Analysis		Münch Model	Minnaert's Analysis
1	5070	5310	5	5130	5500
3	5090	5450	7	5190	5690

TABLE 2

VARIATION OF η_0 WITH τ FOR VARIOUS EXCITATION POTENTIALS

τ	E.P.				τ	E.P.			
	0	3	5	7		0	3	5	7
0.01	1.290	0.697	0.461	0.307	0.70	0.058	0.130	0.222	0.382
0.10	0.555	.421	.349	.291	1.00	.033	.099	.206	.433
0.20	0.300	.300	.300	.300	1.20	.024	.083	.193	.449
0.40	0.130	0.193	0.254	0.330	1.40	0.018	0.074	0.188	0.483

the variation of η_0 with τ is given. The values have been normalized to $\eta_0 = 0.3$ at $\tau = 0.2$. The differences between the values of η_0 at any τ are due entirely to the Boltzmann distribution.

An observational curve of growth which uses King's relative *f*-values is restricted to lines of excitation potential less than 3 volts. Hence, on the basis of Table 1, one should expect to obtain a temperature of either 5080° or 5400° K (depending upon the model) from the *V* I curve of growth.

The results of Table 1 should also be valid for *Fe* I and *Ti* I, since the ionization potentials of these elements are nearly identical with that of *V* I. Preliminary calculations showed that the variation of η_0 with depth for *Fe* I and *Ti* I was so nearly like that indicated in Table 2 that the excitation temperatures of these two elements should also be

[5] *B.A.N.*, **10**, 389, 1948; 394, 1949.

[6] *Ann. d'ap.*, **9**, 69, 1946.

[7] K. O. Wright, *Ap. J.*, **99**, 249, 1944; Goldberg and Pierce, *Quarterly Progress Report, ONR Project M 720-5* (Ann Arbor, October, 1947).

about 5100° K if Münch's model is assumed. The observational data, however, indicate somewhat lower temperatures.[7] The observed temperature discrepancy apparently cannot be explained by the slight differences of the ionization potentials of these elements.

OBSERVATIONAL RESULTS

To compare the predicted temperatures with those observed, the V I solar curve of growth was redetermined. Dr. R. B. King generously made available the equivalent widths of the 169 lines used in the initial determination.[8] Two corrections must be applied to a curve of growth whose lines cover a large wave-length range. These are (1) the variation with wave length of the continuous absorption coefficient and (2) the variation of the parameter x_0/n (Strömgren's eq. [26]). The observational curve of growth is obtained by plotting log W/λ as ordinate and

$$\log gf\lambda - \log \frac{\kappa_\nu}{\bar{\kappa}} + \Delta \log \eta_0 \qquad (4)$$

as abscissa. The term $\Delta \log \eta_0$ corrects for the variation of x_0/n and is taken from tables

TABLE 3

ABSCISSA SHIFTS OF CURVES-OF-GROWTH SEGMENTS FOR LINES OF DIFFERENT EXCITATION POTENTIALS

E.P.	V			E.P.	V		
	Corrected Curve	Uncorrected Curve	Wt.		Corrected Curve	Uncorrected Curve	Wt.
0.040	0.018	0.096	20	1.350	1.007	0.907	2
0.280	0.215	0.220	69	1.900	1.843	1.758	32
1.060	1.026	1.036	60	2.100	1.977	1.955	15
1.200	0.894	0.826	21	2.350	2.400	2.354	7

computed by M. H. Wrubel.[9] It is convenient to refer all lines to $x_0/n = 4$ (in Wrubel's notation $B^{(0)}/B^{(1)} = \frac{3}{4}$). The observational value of $\kappa_\nu/\bar{\kappa}$ is given by Münch.[10] To see the effect of these corrections, two curves of growth were constructed; one was plotted with the quantity defined by (4) as abscissa, while the abscissa for the second curve was log $gf\lambda$. It was at once evident that the points showed less scatter for the corrected curve (4).

There were eight groups of lines of different excitation potential, and thus eight shifted segments of the curve of growth. The equation of each segment was found by least squares from those points which were on or near the linear portion of the curve. The abscissa shift, V, necessary to bring each segment into coincidence with the 0-volt segment was computed from the equations of the segment and is given in Table 3. The weight of each group is the sum of the weights of the lines in that group.

The displacements, V, were plotted against excitation potential. The slope of the weighted least-squares line through the points gave the excitation temperature. This temperature represents the mean taken over the atmospheric layers producing the lines. No evidence was found for a change of slope with excitation potential. The accuracy of this method of analysis is, however, too low to show a variation as small as that indicated in the second column of Table 1.

[7] King and Wright, *Mt. W. Contr.*, No. 736; *Ap. J.*, **106**, 224, 1947.

[8] *Ap. J.*, **109**, 66, Table 3, 1949.

[9] *Ap. J.*, **102**, 385, 1945.

A temperature of 5110° ± 190° K was found from the curve which corrected for variable κ_ν and x_0/n. A value of 5400° ± 200° was obtained from the uncorrected curve. This latter value is identical with that found by King and Wright. It is evident that the corrections for variable κ_ν and x_0/n make a difference in the temperature determination. The first result, 5110°, is to be preferred. It is in good agreement with the expected value of 5080° K, obtained with Münch's model atmosphere. Minnaert's predicted temperatures are about 300° higher than these observational results indicate.

In conclusion, I should like to thank Dr. R. B. King for making his list of equivalent widths of V I lines available. It is also a pleasure to thank Dr. J. L. Greenstein for his helpful suggestions during the course of this investigation.

MULTIPLET INTENSITIES FOR THE LINES $^4S - {}^2D$ OF N I

C. W. UFFORD AND R. M. GILMOUR
University of Pennsylvania
Received January 21, 1950

ABSTRACT

The relative strengths of the transitions $1s^22s^22p^3\ {}^4S_{3/2}-{}^2D_{5/2}$ and $1s^22s^22p^3\ {}^4S_{3/2}-{}^2D_{3/2}$ in N I are computed, including spin-spin interaction. The radial integral which determines the influence of spin-spin coupling on the transition probability was calculated by numerical integration with wave functions found by interpolation from those of B, C, O, F, and Ne derived from the self-consistent field. The theoretical value of the ratio of the intensities in N I for $^4S_{3/2}-{}^2D_{5/2}$ and $^4S_{3/2}-{}^2D_{3/2}$ is 0.83.

It has been suggested[1] that the forbidden lines of N I might appear in the spectrum of the night sky. These lines, which have been observed by Bowen and Wyse[2] in the planetary nebulae, are the lines λ 5198.5 and λ 5200.7 of N I corresponding to the $^4S_{3/2} - {}^2D_{3/2}$ and $^4S_{3/2} - {}^2D_{5/2}$ transitions in the ground p^3 configuration.

The relative intensity of these lines has been calculated for O II.[3] The calculations for N I may be carried out in the same way. The lowest configuration of N I is $1s^22s^22p^3$ with terms $^4S_{3/2}$, $^2D_{5/2,\,3/2}$, and $^2P_{3/2,\,1/2}$ in this order from the ground state up. The spread of the configuration from ^4S to ^2P is roughly 29,000 cm^{-1}; the multiplet separations of the ^2D levels is -8 cm^{-1}; and that of ^2P is estimated as 0. Therefore, the configuration p^3 of N I is close to pure Russell-Saunders coupling, as was the case for O II.

The self-consistent field with exchange for N I has been worked out,[4] but it was not thought that the small difference introduced by exchange would be significant for our purposes. Therefore, an approximation to the self-consistent field without exchange was found by the interpolation method used by Brown, Bartlett, and Dunn.[5] Their results were recalculated with the help of Torrance's wave functions[6] for carbon. As there was only a small range for interpolation and the results were what might be expected from the Hartree functions with exchange, these wave functions should be accurate enough for our calculations in N I.

The values obtained for the three integrals s_q, ζ, and η of AUV, equations (4), (5), and (6), by numerical integration, are

$$s_q = 1.3\ e a_H^2\ , \tag{1}$$

$$\zeta = 82\ \text{cm}^{-1}\ , \tag{2}$$

$$\eta = 0.63\ \text{cm}^{-1}\ . \tag{3}$$

The integral ζ is best evaluated by extrapolation from the multiplet intervals in adjacent configurations, such as $2p^2$ and $2p^4$, where the first-order effect of spin-orbit interaction does not disappear because of half-completion of the shell. This extrapolation[7]

[1] By Professor Joseph Kaplan in conversation.

[2] I. S. Bowen and A. B. Wyse, *Lick Obs. Bull.*, **19**, 1, 1939; A. B. Wyse, *Ap. J.*, **95**, 358, 1942.

[3] L. H. Aller, C. W. Ufford, and J. H. Van Vleck, *Ap. J.*, **109**, 42, 1949. Hereafter abbreviated "AUV."

[4] D. R. Hartree and W. Hartree, *Proc. R. Soc., London, A*, **193**, 299, 1948.

[5] *Phys. Rev.*, **44**, 296, 1933.

[6] *Phys. Rev.*, **46**, 388, 1934.

[7] Cf., e.g., H. A. Robinson and G. H. Shortley, *Phys. Rev.*, **52**, 713, 1937.

gives $\zeta = 69$ cm^{-1}, a value which is less than the calculated value of equation (2) but which gives sufficient confidence in the value of η in equation (3).

Once the integrals ζ and η are known, the multiplet intervals in the ^{2}D and ^{2}P states can be calculated and compared with experiment. If we take $\eta = 0.63$ cm^{-1} and $\zeta = 69$ cm^{-1}, the values of the splittings obtained from AUV, equation (16), are

$$\Delta^2\mathrm{D} = -11.0 \text{ cm}^{-1}, \tag{4}$$

$$\Delta^2\mathrm{P} = -3.9 \text{ cm}^{-1}, \tag{5}$$

whereas the experimental values are[8]

$$\Delta^2\mathrm{D} = -8, \qquad \Delta^2\mathrm{P} = 0 \text{ cm}^{-1},$$

where the value of Δ^2P is estimated. The calculated values depend largely on η, which should be smaller to give the experimental separations. If the wave functions were made smaller near the origin, to reduce η, it would also reduce ζ and bring it more in accord with the value of 69 cm^{-1} interpolated from p^2 and p^4. This is opposite to the direction that taking exchange into account would change the wave functions, since, with exchange, the wave functions for the three terms ^{4}S, ^{2}D, and ^{2}P are all larger near the origin than are the wave functions without exchange. The disagreement with the observed splittings is probably caused by the neglect of polarization or, in other words, configuration interaction.

With the values of s_q, η, and ζ available, it is now possible to find numerical values for the strengths, AUV equations (19) and (20), and hence for the transition probabilities, A. With $\zeta = 69$ cm^{-1}, $\eta = 0.63$ cm^{-1}, and the frequency denominators[8] $(PD) = 9614$ cm^{-1}, $(DS) = 19{,}226$ cm^{-1}, and $(PS) = 28{,}840$ cm^{-1}, we find that

$$A\,(^2\mathrm{D}_{5/2}-{}^4\mathrm{S}_{3/2}) = (9.42+0.01+0.13+0.60)\,10^{-6} \text{ sec}^{-1} = 10.16\times10^{-6} \text{ sec}^{-1}, \tag{6}$$

$$A\,(^2\mathrm{D}_{3/2}-{}^4\mathrm{S}_{3/2}) = (6.07+0.42+3.78+8.05)\,10^{-6} \text{ sec}^{-1} = 18.32\times10^{-6} \text{ sec}^{-1}. \tag{7}$$

Because of the statistical weight factor, the intensity ratio, AUV equation (1), is one and a half times the quotient of equation (6) by equation (7). The first, or quadrupole, term constitutes the bulk of equation (6), while in equation (7) significant contributions are made by the spin-spin interaction, both by itself in the 8.05 term of the form η^2 and by combination with the conventional spin-orbit interaction in the 3.78 term of the type $\eta\,\zeta^2$.

With our choice of constants, the theoretical value of the ratio, AUV equation (1), of the intensities of the two components of the ^{4}S $-$ ^{2}D multiplet is

$$r = \frac{I\,(^4\mathrm{S}_{3/2} - {}^2\mathrm{D}_{5/2})}{I\,(^4\mathrm{S}_{3/2} - {}^2\mathrm{D}_{3/2})} = 0.83. \tag{8}$$

We are grateful to Professors L. H. Aller, D. H. Menzel, and J. H. Van Vleck for their stimulating interest in these calculations, and to the Research Corporation for a grant.

[8] Charlotte E. Moore, *Circ. Nat. Bur. Stand. 467*, 1, 32, 1949.

THE OSCILLATOR STRENGTH FOR THE 4s–4p TRANSITION IN *Ca* II*

LOUIS C. GREEN AND NANCY E. WEBER
Strawbridge Observatory, Haverford College
Received December 19, 1949

ABSTRACT

A number of computations have been made of the oscillator strength or *f*-value for the 4s–4p transition in *Ca* II. Three fields were used to obtain the necessary wave functions: a self-consistent field both with and without exchange and a field of the Kramers type. With each field the radial integrals for the dipole moment, for two forms of the dipole momentum, and for the dipole acceleration were evaluated. Each of these radial integrals was then used to calculate two values of the oscillator strength. One value was obtained by using the observed energy difference, and a second by using the difference of the eigenvalues of the particular wave functions employed in computing the radial integrals. Values from the same field and values from different fields were found to be in closer agreement when the calculated, rather than the observed, energies were employed. Comparison of the various results suggests that the true value of the oscillator strength for this transition probably lies within ±0.10 of the value 1.07.

A number of determinations have been made of the *f*-value or oscillator strength associated with the transition 4s–4p in *Ca* II. The calculations are based on wave functions derived by numerical integration of the Schrödinger equation, with suitable fields introduced. This work was undertaken with the hope that a comparison of a number of values for the oscillator strength for a particular transition, calculated by varying procedures, would give an indication of the confidence to be placed in the physical reality of the *f*-values so found. Chandrasekhar has given three expressions for the *f*-value,[1] using the dipole moment, momentum, and acceleration. He has pointed out that, if exact solutions of the Schrödinger equation are introduced into these expressions, the resulting *f*-values should be identical. On the other hand, if one uses approximate eigenfunctions, one of the expressions may give superior results. He further pointed out that, since intermediate distances count more heavily in minimizing the energy, wave functions derived by applications of the Ritz principle, would probably give superior results when used with the dipole momentum integral, since in this the values of the wave functions at intermediate distances contribute the major part. It seemed plausible, therefore, to suppose that some insight could be had into the level of approximation represented by the various types of solution and into the physical reality of quantities computed therefrom by comparing a number of determinations of a given *f*-value. It seemed probable that the closer the agreement between the results given by the different expressions for an *f*-value obtained from a particular field and the associated wave functions, the closer those wave functions would be to the exact solutions of the Schrödinger equation.

ATOMIC FIELDS AND WAVE FUNCTIONS

Three fields for *Ca* II were used: Hartree's self-consistent field, both with exchange[2] and without,[3] and a field of the Kramers type.[4] Hartree gives the 4s and 4p wave func-

* The major part of this work was supported by the Office of Naval Research, Contract No. N8 onr-570 Project No. NR 010-016.

[1] *Ap. J.*, **102**, 223, 1945.

[2] D. R. Hartree and W. Hartree, *Proc. R. Soc. London*, *A*, **164**, 167, 1938.

[3] *Ibid.*, **149**, 210, 1935.

[4] A. Zwaan, *Intensitäten im Ca-Funkenspektrum* (diss.; Utrecht, 1929).

tions with exchange,[2] but not those without. The latter, together with the wave functions from the Kramers field, were obtained by numerical integration of the radial part of the Schrödinger equation. The actual integrations were carried out on the relay calculators of the Watson Laboratory of the International Business Machines Corporation by a rapid method described elsewhere.[5] Zwaan gives 4s and 4p wave functions for his field, derived by a method partly numerical and partly analytic. It seemed wisest, however, to redetermine these functions in the same manner as the others and to obtain their eigenvalues.

EQUATIONS

The three expressions given by Chandrasekhar for the oscillator strength[1] were rewritten in a form slightly more convenient when both states are discrete. Since, in the expression involving the dipole momentum, the two radial functions enter in an asymmetrical way—one as the function itself and the other through its derivative—it seemed best to use the two forms for this expression with the role of the derivative interchanged. The resulting formulae for the oscillator strength are given below for the case of one electron outside closed shells and transitions which involve only this electron. Further, the wave function of the atom is taken as the product of a wave function of the core electrons only and a wave function of the outer electron, where the latter is of the usual type,

$$\psi = \frac{1}{r} R(r)\, Y(\theta, \phi).$$

It is assumed also that the wave function for the core electrons is the same before and after the transition. We then have, using the dipole moment,

$$f = \frac{1}{3} \frac{\nu}{R_y} \frac{\max(l, l')}{2l+1} \left[\int_0^\infty R \rho R' \, d\rho \right]^2; \tag{1}$$

using the dipole momentum with the derivative of the upper-state wave function,

$$f = \frac{4}{3} \frac{R_y}{\nu} \frac{\max(l, l')}{2l+1} \left[\int_0^\infty \left(R \frac{dR'}{d\rho} + \begin{Bmatrix} l' \\ -l \end{Bmatrix} \frac{RR'}{\rho} \right) d\rho \right]^2, \tag{2a}$$

and, with the derivative of the lower-state wave function,

$$f = \frac{4}{3} \frac{R_y}{\nu} \frac{\max(l, l')}{2l+1} \left[\int_0^\infty \left(-R' \frac{dR}{d\rho} + \begin{Bmatrix} l' \\ -l \end{Bmatrix} \frac{RR'}{\rho} \right) d\rho \right]^2; \tag{2b}$$

using the dipole acceleration,

$$f = \frac{4}{3} \left(\frac{R_y}{\nu} \right)^3 \frac{\max(l, l')}{2l+1} \left[\int_0^\infty R \frac{dV}{d\rho} R' \, d\rho \right]^2. \tag{3}$$

Here $\rho = r/a_0$, where a_0 is the radius of the first Bohr orbit in H; ν is the wave-number difference of the two states; R_y is the Rydberg constant expressed in wave numbers, $\max(l, l')$ is the larger of l and l', $\begin{Bmatrix} l' \\ -l \end{Bmatrix}$ is l' if l' is greater than l and is $-l$ if l' is less than l, $V = 2Z_p/\rho$, and primes go with the upper of the two states. These expressions were checked by computing a few f-values for hydrogen.

RESULTS AND DISCUSSION

The results of the calculations are presented in Table 1. The columns contain the following information: the first column gives the field; the second indicates whether the ob-

[5] L. C. Green, *A.J.*, **54**, 186, 1949 (to be described more fully elsewhere).

served value of the energy difference was used or the value calculated from the particular field; the third, fifth, seventh, and ninth columns contain the f-value calculated from formulae (1), (2a), (2b), and (3), respectively; the remaining columns give values of $1-D$ for the various radial integrals used in computing the f-values. The quantity $1-D$ has been used by Bates[6] to characterize the sensitivity of the integrals to small changes in the wave functions. It is defined as the ratio of the value of the radial integral to whichever is the larger, its positive or negative part. For large values of $1-D$ the radial integrals should not be sensitive to small changes in the wave functions; and, correspondingly, the f-values, for which $(1-D)^2$ is the quantity of interest, should be relatively stable.

TABLE 1

OSCILLATOR STRENGTH FOR THE TRANSITION 4s–4p OF Ca II

Field	Energy Difference	Formula (1)		Formula (2a)		Formula (2b)		Formula (3)	
		f	$1-D$	f	$1-D$	f	$1-D$	f	$1-D$
Self-consistent field with exchange	Obs.	1.19	0.995	0.93	0.751	0.93	0.748	2.79	0.059
	Calc.	1.10		1.02		1.02		3.66	
Self-consistent field without exchange	Obs.	1.36	1.00	0.96	0.781	0.96	0.784	0.67	0.007
	Calc.	1.14		1.14		1.14		1.14	
Zwaan's field	Obs.	1.06	0.916	1.03	0.952	1.04	0.940	0.57	0.017
	Calc.	1.05		1.04		1.05		0.58	

The value $f_1 = 1.19$, arising from the self-consistent field with exchange, is identical with the value given by Hartree and Hartree,[2] as it should be, since exactly the same wave functions were used. The value $f_{(2a)} = f_{(2b)} = 0.93$, also for the self-consistent field with exchange, is consistent with the value given by Bates and Damgaard[7] for their quantity σ^2. The value $f_1 = 1.36$ for the self-consistent field without exchange is 0.05 smaller than one obtains from Hartree's value of the radial integral.[2] Checks have not uncovered any error in the present work. However, as indicated above, Hartree does not give his 4s and 4p wave functions for the field without exchange, and these were redetermined for the present problem. The eigen-values so found agreed exactly to three figures with those of Hartree. The value $f_1 = 1.06$ for Zwaan's field is 0.02 smaller than the value that Zwaan gives; but this is not surprising in view of the very different methods of obtaining the wave functions in the two cases. The σ^2 given by Bates and Damgaard for the Coulomb approximation corresponds to an f-value of 0.99.

The striking feature of Table 1 is the improvement in the agreement of the f-values when the calculated energy differences are used instead of the observed. Much of the agreement, however, is the result of general theorems regarding the radial integrals for

[6] *Proc. R. Soc. London, A*, **188**, 350, 1947.

[7] *Phil. Trans. R. Soc. London, A*, **242**, 101, 1949.

eigenfunctions of the present type. The equality of the integrals arising in the two forms of the dipole momentum expression is immediately clear,

$$\int_0^\infty \left(R \frac{dR'}{d\rho} + \begin{Bmatrix} l' \\ -l \end{Bmatrix} \frac{RR'}{\rho} \right) d\rho = \int_0^\infty \left(-R' \frac{dR}{d\rho} + \begin{Bmatrix} l' \\ -l \end{Bmatrix} \frac{RR'}{\rho} \right) d\rho ,$$

for the product RR' equal to zero at $\rho = 0$ and $\rho = \infty$. The equality of the three different expressions follows by elementary, but somewhat laborious, means when the differential equation for R and R' is

$$\frac{d^2R}{d\rho^2} + \left\{ \epsilon + V - \frac{l(l+1)}{\rho^2} \right\} R = 0 . \tag{4}$$

We then have

$$\int_0^\infty R \rho R' \, d\rho = \frac{2}{\Delta\epsilon} \int_0^\infty \left(R \frac{dR'}{d\rho} + \begin{Bmatrix} l' \\ -l \end{Bmatrix} \frac{RR'}{\rho} \right) d\rho = -\frac{2}{(\Delta\epsilon)^2} \int_0^\infty R \frac{dV}{d\rho} R' \, d\rho .$$

This last result is in agreement with Chandrasekhar's point that the various expressions for the f-value must give the same result when exact solutions of a Schrödinger equation are introduced. The wave functions for the self-consistent field without exchange and for Zwaan's field are solutions of a Schrödinger equation (eq. [4]). Agreement of the f-values is, therefore, to be expected. However, since equation (4) is an approximation to the true Schrödinger equation of the problem, the agreement of the f-values, contrary to the initial expectation, does not indicate closeness of the eigenfunctions to exact solutions of the true equation but rather the closeness to the solution of the approximate equation.

It seems wise in the present case to regard all f-values determined from equation (3) with caution. In each case $1-D$ is very small, so that the radial integrals are sensitive to small changes in the integrands. Various procedures were used to find $dV/d\rho$, but the disagreement of the results, although small, was still large enough to lead to considerable uncertainty in the f-value in view of the small $1-D$.

In the case of the self-consistent field with exchange, the wave functions are not solutions of equation (4), and complete agreement of the f-values is not to be expected. The extent of the agreement may be taken as a measure of the closeness of the wave functions to exact solutions of some Schrödinger equation. Just as in the case of the self-consistent field without exchange, this equation may not be the true Schrödinger equation of the problem.

It is clear from the above cases that, on the basis of the agreement of the f-values alone, it is not possible to decide between two sets of eigenfunctions arising from different approximations.

When due allowance is made for the number of exact agreements in the f-values of Table 1 which result from the particular differential equations satisfied by the wave functions, there still remains better agreement with calculated energies than with observed. It is also true in Table 1 that f-values found from equation (1) or equation (2) with the calculated energies lie between the values found with the observed energy. To test the significance of the use of the calculated energies somewhat further, the Einstein coefficients for spontaneous emission were computed.[8] In this case there is no choice between the calculated and the observed energy. It could be argued against the use of the calculated energy that a transition might sometime be found for which the calculated energy difference was zero. However, on the basis of our present limited experience, it seems best to use the calculated energies.

There is some indication in the results for the self-consistent field with exchange that $1-D$ decreases more rapidly than should one's confidence in the derived f-values, and

[8] This computation was suggested to us by Professor D. R. Bates.

this is more true of $(1-D)^2$. Thus, $1-D$ varies by a factor of 17, and $(1-D)^2$ by almost 300; but the resulting f-values vary by less than a factor of 4. This behavior results from the fact that the wave functions are approximations to exact solutions of the wave equation. If the wave functions were, in fact, exact solutions, then, regardless of the size of $1-D$, the f-value would be the same if all other quantities in the integrands are known exactly. For approximate solutions the f-values will in general not differ greatly.

In view of the above results, it appears probable that the value 1.07 for the f-value for the 4s−4p transition is within ± 0.10 of the true value of this quantity. Further, since all the present work uses the same radial part in the 4p wave function for both levels of ^2P, the ratio of the f-value for $^2S_{1/2}-{}^2P_{1/2}$ to the f-value for $^2S_{1/2}-{}^2P_{3/2}$ will be $\frac{1}{2}$, that is, $f_H = 0.36$ and $f_K = 0.71$.

We wish to thank Dr. W. J. Eckert, of the Watson Laboratory of the I.B.M. Corporation, for having made available the facilities of the laboratory to one of us (L. C. G.). We must also thank Miss Eleanor Krawitz, of the laboratory staff, for her continued help and interest.

OSCILLATOR STRENGTHS FOR THE 4s−p AND THE 3d−f CONTINUA OF *Ca* II*

LOUIS C. GREEN AND NANCY E. WEBER
Strawbridge Observatory, Haverford College
Received January 23, 1950

ABSTRACT

Values of $df/d\epsilon$ for the 4s−p and the 3d−f continua of *Ca* II have been redetermined, using wave functions derived by numerical integration from a self-consistent field without exchange. For both continua the values found from the dipole moment, momentum, and acceleration expressions for $df/d\epsilon$ agree closely when calculated values of ϵ are used. The meaning of this agreement is examined. Evidence suggests that the oscillator strengths for the 4s−p continuum are somewhat more accurately known than has recently been supposed. The 3d−f continuum retains the large size found in previous work and is therefore distinctly not like hydrogen.

Values of the rate of change of the oscillator strength with energy have been determined for the 4s−p and 3d−f continua of *Ca* II. The calculations are based on wave functions derived by numerical integration from a Hartree self-consistent field without exchange. These continua, together with the others arising from the three lowest terms of *Ca* II, were treated in an earlier paper.[1] In this earlier work two sets of wave functions were employed. In both sets the wave functions for the continua were derived from a Hartree self-consistent field with exchange, but exchange was not included in deriving the wave functions themselves. In the first set the discrete-state wave functions included exchange, but in the second they were derived in the same manner as the wave functions of the continua. The wave functions of the first set clearly did not form a strictly homogeneous group. Those of the second set gave results in fair agreement with the work of Bates and Massey[2] on the 4s−p continuum when they included exchange in the wave functions of both the discrete state and the continuum. The second set of wave functions also gave a total f for the 3d−f continuum of only 40 per cent of that given by the first set, but still three times the value for hydrogen. Unfortunately, it was not clear just what level of approximation was represented by the second set. The present work was undertaken with the hope that it would yield some information as to the probable physical reliability of the existing values of $df/d\epsilon$ for these two astronomically important continua. This information can be found in part, by using Chandrasekhar's three expressions for the f-value,[3] using the dipole moment, momentum, and acceleration. He has pointed out that, if exact solutions of the Schrödinger equation are introduced into these expressions, the resulting f-values should be identical. On the other hand, if one uses approximate wave functions, one of the expressions may give superior results. He also pointed out that, for wave functions derived by applications of the Ritz principle, the expression involving the dipole momentum would be expected to give the better results. Initially, it also seemed probable that the closer the agreement between the results given by the different expressions for an f-value, the closer those wave functions would be to the exact solutions of the Schrödinger equation. It also seemed wise to determine just how large the effect of exchange is in the 4s−p continuum. This can be done by using wave functions without exchange and comparing the result with the work of Bates and

* The major part of this work was supported by the Office of Naval Research, Contract No. N8 onr-570, Project No. NR 010-016.

[1] L. C. Green, *Ap. J.*, **109**, 289, 1949.

[2] *Proc. R. Soc. London, A*, **177**, 329, 1941.

[3] *Ap. J.*, **102**, 223, 1945.

Massey, including exchange. Bates and Massey's own comparison[2] is not entirely satisfactory, since for the case without exchange they use a nonhomogeneous set of wave functions exactly similar to the first set described above. Finally, it also seemed desirable to find out whether the 3d−f continuum was really as dissimilar from hydrogen as the earlier work indicated.

WAVE FUNCTIONS AND EQUATIONS

The wave functions were derived by numerical integration of the radial part of the Schrödinger equation, by using a self-consistent field without exchange given by Hartree.[4] The actual integrations were carried out on the relay calculators of the Watson Laboratory of the International Business Machines Corporation by a rapid method described elsewhere.[5]

If we let ϵ be the energy of the free electron expressed in units of the ionization energy of hydrogen, then the expressions for $df/d\epsilon$, involving the dipole moment, momentum, and acceleration, are formally exactly the same as those for f between two discrete states. These expressions have been given in a convenient form[6] for the case of one electron outside closed shells and transitions which involve only this electron. The wave function of the atom is taken as the product of a wave function of the core electrons and a wave function of the outer electron, where the latter is of the usual type,

$$\psi = \frac{1}{r} R(r)\, Y(\theta, \varphi).$$

If it is assumed that the wave function for the core electrons is the same before and after the transition, we have, using the dipole moment,

$$\frac{df}{d\epsilon} = \frac{1}{3}\frac{\nu}{R_y}\frac{\max(l, l')}{2l+1}\left[\int_0^\infty R\rho R(\epsilon)\, d\rho\right]^2; \tag{1}$$

using the dipole momentum with the derivative of the upper-state wave function, we have

$$\frac{df}{d\epsilon} = \frac{4}{3}\frac{R_y}{\nu}\frac{\max(l, l')}{2l+1}\left[\int_0^\infty \left(R\frac{dR(\epsilon)}{d\rho} + \begin{Bmatrix} l' \\ -l \end{Bmatrix}\frac{R\cdot R(\epsilon)}{\rho}\right) d\rho\right]^2, \tag{2a}$$

and, with the derivative of the lower-state wave function,

$$\frac{df}{d\epsilon} = \frac{4}{3}\frac{R_y}{\nu}\frac{\max(l, l')}{2l+1}\left[\int_0^\infty \left(-R(\epsilon)\frac{dR}{d\rho} + \begin{Bmatrix} l' \\ -l \end{Bmatrix}\frac{R\cdot R(\epsilon)}{\rho}\right) d\rho\right]^2; \tag{2b}$$

using the dipole acceleration, we have

$$\frac{df}{d\epsilon} = \frac{4}{3}\left(\frac{R_y}{\nu}\right)^3\frac{\max(l, l')}{2l+1}\left[\int_0^\infty R\frac{dV}{d\rho}R(\epsilon)\, d\rho\right]^2. \tag{3}$$

Here $\rho = r/a_0$, where a_0 is the radius of the first Bohr orbit in H; ν is the wave-number difference of the two states; R_y is the Rydberg constant expressed in wave numbers; l is the orbital angular momentum quantum number of the bound electron, l' that of the free electron; $\max(l, l')$ is the larger of l and l'; $\begin{Bmatrix} l' \\ -l \end{Bmatrix}$ is l' if l' is greater than l and is $-l$ if l' is less than l; $R(\epsilon)/(a_0\rho)$ is the radial part of the wave function for the free electron normalized per interval in ϵ; $R/(a_0\rho)$ is the radial part of the wave function for the bound electron, and $V = 2Z_p/\rho$.

[4] D. R. Hartree and W. Hartree, *Proc. R. Soc. London*, *A*, **149**, 210, 1935.

[5] L. C. Green, *A.J.*, **54**, 186, 1949 (to be described more fully elsewhere).

[6] L. C. Green and N. E. Weber, *Ap. J.*, **111**, 582, 1950.

RESULTS AND DISCUSSION

The results of the calculations are presented in Table 1. The columns contain the following information: the first column gives the continuum; the second gives the energy of the free electron in units of the ionization energy of H; the third indicates whether the observed value of the energy difference was used in finding $df/d\epsilon$ or the value calculated from the self-consistent field; the fourth, sixth, eighth, and tenth contain $df/d\epsilon$ calculated from formulae (1), (2*a*), (2*b*), and (3), respectively; the remaining columns give values of $1 - D$ for the various radial integrals used in computing the values of $df/d\epsilon$. The quantity $1 - D$ has been used by Bates[7] to characterize the sensitivity of the integrals to small changes in the wave functions. It is defined as the ratio of the value of the

TABLE 1

VALUES OF $df/d\epsilon$ FOR THE 4s−p AND THE 3d−f CONTINUA OF *Ca* II

Continuum	ϵ	Energy Difference	Formula (1)		Formula (2a)		Formula (2b)		Formula (3)	
			$df/d\epsilon$	$1-D$	$df/d\epsilon$	$1-D$	$df/d\epsilon$	$1-D$	$df/d\epsilon$	$1-D$
4s−p	0.00	Obs.	0.0156	0.094	0.0122	0.566	0.0117	0.574	0.0092	0.125
		Calc.	0.0136		0.0139		0.0134		0.0138	
	0.20	Obs.	0.0191	.....	0.0157	.....	0.0157	.....	0.0123	.....
		Calc.	0.0171		0.0175		0.0175		0.0170	
	0.50	Obs.	0.0181	.....	0.0155	.....	0.0151	.....	0.0125	.....
		Calc.	0.0167		0.0169		0.0164		0.0161	
	1.00	Obs.	0.0139	.081	0.0125	.....	0.0122	.....	0.0108	.....
		Calc.	0.0130		0.0133		0.0129		0.0130	
3d−f	0.00	Obs.	1.499	.637	0.684	0.689	0.684	0.816	0.317	.982
		Calc.	1.017		1.008		1.008		1.014	
	0.20	Obs.	.....	.....	.....	.....	.....	.....	0.188	.....
		Calc.	.....		.....		.....		0.452	
	0.50	Obs.	.....	.....	.....	.....	.....	.....	0.103	.....
		Calc.	.....		.....		.....		0.196	
	1.00	Obs.	.....	.....	.....	.....	.....	.....	0.051	.943
		Calc.	.....		.....		.....		0.080	
	2.00	Obs.	0.032	0.115	.....	.....	.....	.....	0.022	0.930
		Calc.	0.029		.....		.....		0.028	

[7] *Proc. R. Soc. London, A*, **188**, 350, 1947.

radial integral to whichever is the larger, its positive or its negative part. The smaller the value of $1 - D$, the more sensitive the radial integral should be.

An examination of Table 1 reveals a striking agreement obtained for the values found from the various expressions for $df/d\epsilon$ when the calculated, rather than the observed, energy is used. Such an agreement has already been found for the 4s−4p transition of *Ca* II,[5] and an explanation of the agreement has been given in terms of several equalities involving the radial integrals for eigenfunctions of the differential equation

$$\frac{d^2R}{d\rho^2} + \left\{\epsilon + V - \frac{l(l+1)}{\rho^2}\right\} R = 0 . \tag{4}$$

These equalities can easily be shown to hold when one of the R's belongs to the continuum. Since in the present case our wave functions are solutions of equation (4), one cannot conclude that the good agreement of the f-values indicates that the wave functions used are necessarily very close to exact solutions of the true Schrödinger equation of the problem. The agreement indicates only the numerical accuracy of the work. In the 4s−p continuum, the percentage difference is larger than for the 4s−4p transition with the same central field,[6] but the absolute value of the difference is considerably smaller.

It is also interesting to note the variation of $1 - D$ both from one expression for $df/d\epsilon$ to another and also for changing values of ϵ. In earlier work,[6] formula (1), involving the dipole moment, gave the larger values of $1 - D$. In the 4s−p continuum, formulae (2*a*) and (2*b*) give the larger $1 - D$, and in the 3d−f continuum it is formula (3) which gives the largest value. This latter is surprising at first, since for both 4s−4p and 4s−p the values of $1 - D$ for formula (3) were in the neighborhood of 0.1 or less. However, for the 3d−f continuum, the product of the two wave functions in the integrand passes through its largest extremum before reaching its first node at relatively large ρ. Beyond this ρ, $dV/d\rho$ is very small, and, since $dV/d\rho$ is always negative, almost the whole contribution to the integral is of one sign. Even with increasing ϵ and the consequent inward movement of the nodes, this remains the case, so that at $\epsilon = 2.00$, $1 - D$ is still 0.930. On the other hand, using formula (1), $1 - D$ decreases from 0.637 at $\epsilon = 0$ to 0.115 at $\epsilon = 2.00$, owing to the fact that the weighting function, ρ, for the product of the wave functions, in contrast to $dV/d\rho$, increases to the right. With ρ as a weighting function, the first loop for $\epsilon = 0$ makes a smaller part of the total contribution to the radial integral than with $dV/d\rho$ as a weighting function, and cancellation becomes more important more quickly with increasing ϵ, when using the former.

Bates and Massey[2] have given values for $df/d\epsilon$ for the 4s−p continuum, using formula (1) with exchange in the wave functions of both the continuum and the discrete state. When their values are corrected for an error in normalization[1] by multiplying by the square of the ratio of the true normalization factor to the one used, they become, with the calculated energies, 0.0139, 0.0135, and 0.0133 for $\epsilon = 0.00$, 0.10, and 0.20, respectively. Strictly, this simple correction is justifiable only if the orthogonalization constants for the wave functions of the continuum make a negligible contribution in the differential equation. Bates and Massey indicate that they are small but do not give their values. A comparison of the $df/d\epsilon$ values in Table 1 with the above results, which include exchange, show approximately equal values for $\epsilon = 0$, but in Table 1 this is followed by a rise to a low maximum instead of a slow decline. However, the reality of this difference in behavior of the exchange and the nonexchange case is not certain, in view of the simple procedure for correction applied above and in view of the fact that Bates and Massey used the exchange terms for $\epsilon = 0.00$ in obtaining the continuous wave functions for $\epsilon = 0.10$ and 0.20. It is important to note that the sign of the radial integral for the dipole moment is unchanged by the inclusion of exchange. The change of sign reported by Bates and Massey seems, therefore, to have arisen from their use of a non-

homogeneous set of wave functions for their case "without exchange." There was already an indication of this in earlier work with wave functions without exchange from a field including exchange and with wave functions from a Kramers field.[1] The fact that the more refined treatment with exchange makes a much smaller difference than was formerly supposed suggests more confidence in the physical reality of the present results.

In view of the close agreement found for the f-values for the 4s−4p transition in *Ca* II when the results from Hartree's field without exchange were compared with those from Zwaan's field,[6] it was of interest to determine $df/d\epsilon$, using the latter field[8] for the 4s−p continuum for $\epsilon = 0$. The result obtained with the calculated energy was 0.0266 with $1 - D = 0.152$ from formula (1) and 0.0263 with $1 - D = 0.776$ from formula (*2b*). This result is only about half as large as that obtained earlier, using formula (1).[1] However, the discrete wave function in the earlier work was found by a partly numerical and partly analytic procedure, and the wave function for the continuum entirely numerically, whereas in the present case the two wave functions were found from identically the same field by the same procedure and therefore represent a more homogeneous set. Since, in addition, $1 - D$ for formula (1) is small for this transition, the difference from the earlier result is accounted for. On the other hand, the present result from Zwaan's field is still roughly twice the value found from Hartree's field.

For the 3d−f continuum, the most interesting result is that the present calculations substantiate the deviation from hydrogen indicated by earlier work.[1] It was to be expected that the magnitude and behavior with increasing ϵ would not be greatly changed, since the large value of $1 - D$ found for this continuum suggested that $df/d\epsilon$ would not be sensitive to small changes in the wave functions. Table 1 does not allow an immediate comparison with earlier results, except for $\epsilon = 0$, since the previous work made use of formula (1) and the observed values of the energies. However, in view of the agreement of the $df/d\epsilon$ values as found from the various formulae when the calculated energies are used for $\epsilon = 0$ and $\epsilon = 2.00$, it is reasonable to compute values for the fourth column from those in the tenth column. We obtain 0.605, 0.243, and 0.093 for $\epsilon = 0.20$, 0.50, and 1.00, respectively. From these values and those in Table 1 the total f is found to be 0.45, as compared with 0.30 found earlier. On the other hand, it would seem that the best value for the total f would be found by using the calculated energies and formula (3), the formula with the largest $1 - D$. This result is 0.36. It is to be compared with the value 0.098 for hydrogen.[9] A difference as large as this between the calculated value and the value of hydrogen should be considered in computations of the total recombination coefficient, for one should not treat only the ground state as deviating from hydrogen. This point is of interest in connection with Strömgren's correction to the Saha formula for the ionic equilibrium of interstellar material.[10]

CONCLUSIONS

Values of $df/d\epsilon$ for the 4s−p and the 3d−f continua are given in Table 1. The close agreement of the results from the dipole moment, momentum, and acceleration expressions when calculated, rather than observed, values of the energy are used is shown to have resulted from the fact that the wave functions employed were solutions of equation (4), and therefore indicates the numerical accuracy of the work rather than closeness to exact solutions of the true Schrödinger equation of the problem. It is pointed out that the choice of expression for determining $df/d\epsilon$ should be based, in part, on a consideration of the size of $1 - D$. The effect of exchange on the 4s−p continuum proves to be much smaller than was formerly supposed. This gives some confidence in the physical reality of the results obtained. The present work suggests that for the 4s−p con-

[8] A. Zwaan, *Intensitäten im Ca-Funkenspektrum* (diss.; Utrecht, 1929).

[9] H. Bethe, *Handbuch der Physik*, 2 Aufl., Vol. **24**, Part I (Berlin: Julius Springer, 1933), p. 443.

[10] *Ap. J.*, **108**, 255, 1948.

tinuum at $\epsilon = 0$, $df/d\epsilon$ is approximately 0.014, with the probability that, if anything, it is larger, rather than smaller, than this value. However, it is not yet clear in what way $df/d\epsilon$ for this continuum varies with increasing ϵ, although either a steep rise or a sharp fall seems unlikely. The 3d−f continuum retains the large size found in previous work and is therefore distinctly not like hydrogen. It seems probable that the magnitude of $df/d\epsilon$ at $\epsilon = 0$ for this continuum is approximately as given in Table 1.

We wish to thank Dr. W. J. Eckert, of the Watson Laboratory of the International Business Machines Corporation, for having made available the facilities of the laboratory to one of us (L. C. G.). We must also thank Miss Eleanor Krawitz, of the laboratory staff, for her continued help and interest.

THE TEMPERATURE OF INTERSTELLAR MATTER. III*

LYMAN SPITZER, JR., AND MALCOLM P. SAVEDOFF
Princeton University Observatory
Received January 27, 1950

ABSTRACT

Detailed computations reveal a large difference of kinetic temperature T between H I and H II regions. In observed H II regions T probably exceeds 7500° K, a lower limit established by observations of [O II] λ 3727, and is probably not greater than 13,000° K. The theoretical computations give actual temperatures ranging between 5000° and 10,000° near B stars and between 7000° and 13,000° near O stars; the exact value depends on the ratio of C, N, and O ions to protons and on the cross-section for electron excitation of these ions.

In H I regions the sources of energy gain are relatively weak; the temperatures of clouds are reduced to about 60° K by three processes: electron excitation of the low-lying levels in C II and Si II, inelastic collisions between H atoms and grains, and inelastic collisions between H atoms and H_2 molecules. Even under somewhat extreme assumptions, the temperature in an H I cloud does not exceed 200° K.

Values of the time t_E required to approach the equilibrium temperature are very short if the density is high. If the density of H atoms or ions is 10^3 per cubic centimeter, t_E is only about 10^8 years in both H I and H II regions. However, if the density of H atoms or ions is taken to be 10^{-3}, a value which may represent rarefied regions between clouds, the values of t_E are about 10^8 years in H II regions and 10^9 years in H I regions.

As a result of the low temperatures found in H I clouds, the average charge on a dielectric interstellar grain is very small but may rise to several volts in H II regions.

The physical processes which influence the random kinetic energy of the interstellar particles have been analyzed in two earlier papers.[1] Since equipartition of kinetic energy is established, it is convenient to describe the mean kinetic energy per particle by means of the "kinetic temperature." In the present paper the previous results are used to compute kinetic temperatures to be expected under differing conditions. The computations determine essentially the kinetic temperatures at which the gain of kinetic energy in ergs per second per cubic centimeter in all types of encounters equals the corresponding rate of loss of energy. The gain of kinetic energy per free electron per second, in encounters with particles of type j, has been denoted by G_{ej}, and the corresponding loss by L_{ej}. Similarly, G_{Hj} and L_{Hj} denote the corresponding rates of gain and loss for H atoms. Since gains and losses experienced by other particles are negligible, the condition of equilibrium gives

$$n_e \sum_j G_{ej} + n_H G_{Hc} = n_e \sum_j L_{ej} + n_H \sum_j L_{Hj} \tag{1}$$

Formulae for the different G_{ej}'s and for G_{Hc} are given in Paper I, while L_{ej} and L_{Hj} may be found from Paper II. As before, subscripts e, p, H, i, m, g, and c denote electrons, protons, H atoms, ions other than protons, H_2 molecules, grains, and cosmic rays, respectively.

One important modification has been made in the values of L_{ea} and L_{ei} given in Paper II. Equations (21) and (22) of that paper are based on an assumed de-excitation cross-section per unit weight of 2×10^{-17} cm² for a neutral atom. Dr. David R. Bates has

* This work was supported in part by a contract with the Office of Naval Research.

[1] L. Spitzer, Jr., *Ap. J.*, **107**, 6, 1948; **109**, 337, 1949 (subsequently referred to as "Paper I" and "Paper II," respectively).

kindly pointed out the existence of a "conservation theorem"[2] which may be used[3] to give upper limits on the cross-sections for excitation of atoms and ions by electrons. Since the theorem gives separate upper limits for electrons of each orbital quantum number l, this upper limit is useful primarily for excitations involving a change of multiplicity, since in this case electrons of only one particular angular momentum are important.

Most of the processes important in interstellar space are of this type, and the conservation theorem gives limiting cross-sections which are considerably smaller than most of the theoretical values. For example, the Hebb-Menzel[4] cross-sections for electron excitation of *O* III exceed the allowed upper limit by a factor of 2.8. Since the value of $\sigma_{BA}(a)$ adopted in Paper II gave the Hebb-Menzel cross-sections for *O* III, it is evident that in this case the adopted value is too great by at least a factor of about 3. Similar discrepancies are found for other atoms and ions, and in the extreme case of *Fe* II the upper limit is about one-tenth of the values adopted in Paper II. It appears improbable that σ_{BA} will have the full value permitted by the conservation theorem; thus[3] in the 1^1S-2^3S transition of *He* the experimentally determined cross-section is a factor of 8 or more below this upper limit. Accordingly, we have reduced the de-excitation cross-section by a factor of 10 from the previously adopted value, taking 2×10^{-18} cm^2 for $\sigma_{BA}(a)/g_A$. Evidently this estimate could be in error by a factor of 3, and in some cases perhaps even more. It may be noted that, if the previous value of the cross-section were retained, the computed temperatures of *H* II regions would be inadmissibly low unless n_i, the number of ions other than *H* and *He*, were reduced to $2 \times 10^{-4} n_H$ or less.

It should be emphasized that the kinetic temperatures computed in this paper, by the use of equation (1), are those that would exist in an ideal equilibrium state, with no transfer of heat by conduction or convection. Transfer of energy from mass motion into random thermal motion, which will heat up the medium when two clouds collide, is also neglected in equation (1).

The first of the following four sections lists the various astronomical assumptions made concerning the interstellar radiation field and the characteristics of the interstellar gas and grains. Section II gives results obtained for regions of ionized hydrogen (*H* II regions), including temperatures, the times required to approach equilibrium conditions, and the electric charge on the grains. Section III gives comparable results for regions where the hydrogen is predominantly neutral (*H* I regions). In Section IV is presented a summary of the conclusions which may be drawn on the basis of these results. The appendix discusses equipartition of energy among the interstellar particles and shows that, while electrons and *H* atoms may in extreme cases have different kinetic temperatures, almost complete equipartition of kinetic energy is probably the more usual situation.

I. Astronomical Assumptions

a) Radiation Field

The energy density of interstellar radiation at different frequencies determines both the rate at which photoelectrons are emitted from atoms and the mean kinetic energy of these electrons. These effects have already been analyzed in Paper I, where an effective color temperature T_{cj} was introduced as a parameter in the equation for each G_{ej}. Values of these parameters have already been listed both for general galactic starlight and for radiation from a single luminous star. In the latter case the values of T_{cp}, in particular,

[2] N. F. Mott, *Proc. R. Soc. London*, *A*, **133**, 228, 1931, and N. Bohr, R. E. Peierls, and G. Placzek (unpublished); cf. N. F. Mott and H. S. W. Massey, *Theory of Atomic Collisions* (2d ed.; Oxford: Clarendon Press, 1949).

[3] D. R. Bates, A. Fundaminsky, G. W. Leich, and H. S. W. Massey, *Proc. R. Soc. London*, *A* (in press 1950).

[4] *Ap. J.*, **92**, 408, 1940.

were listed not for stars of a particular spectral type but rather in terms of the temperature of the equivalent black bodies. We shall here assume that the radiation emitted by stars of types O, B, and A has an actual color temperature of 40,000°, 20,000°, and 9000° K, respectively. These values are consistent with those given in Kuiper's analysis of stellar temperatures.[5]

The intensity of stellar radiation also affects the ionization level of the interstellar gas. Here one must take into account the relatively sharp division of this gas between *H* I and *H* II regions, a phenomenon first pointed out by Strömgren.[6] It is clearly legitimate to assume that in *H* I regions there is virtually no radiation of wave length shorter than 912 A. Thus elements with an ionization potential higher than 13.5 volts will be considered neutral in these regions.

b) DENSITY AND COMPOSITION OF INTERSTELLAR GAS

The average density of the interstellar gas in the galactic plane is usually assumed to be in the neighborhood of 1 hydrogen atom per cubic centimeter. The best evidence supporting this value is provided by the observations obtained by Struve and Elvey[7] on the galactic emission of the Balmer lines, as analyzed by B. Strömgren.[8] The occurrence of gas clouds, so beautifully demonstrated by W. S. Adams' high-dispersion spectra of the interstellar K and H lines,[8] casts some uncertainty on this earlier estimate, which was based on the assumption of a homogeneous medium. A more recent analysis by Strömgren[9] indicates that 1 hydrogen atom per cubic centimeter can still be considered consistent with the observational evidence.

It seems very likely, however, that higher densities are encountered inside the obscuring clouds, with lower densities outside. Strömgren's analysis[9] of interstellar absorption lines indicates that the electron density n_e within a cloud is about 4×10^{-3} cm^{-3} and that, if the ratio n_e/n_H is set equal to 5×10^{-4}, corresponding to the standard stellar composition, n_H is about 8. Between the clouds, values of n_H less than 0.1 are found. This value for the density within a cloud is roughly consistent with the evidence that obscuring clouds occupy about 5 per cent of the space in the galactic plane, as found by Strömgren[9] and Spitzer[10] from studies of interstellar extinction. If the average value of n_H were 1 and if n_H between the clouds were very small, this estimate would yield 20 cm^{-3} for n_H within the clouds. It is likely that somewhat higher values may be found in denser clouds. In the Orion nebula, for example, Greenstein[11] finds that the density of protons is between 10^2 and 10^3 cm^{-3}.

In the present work, densities were assumed to cover as large a range as seemed of any interest, and the values of n_H considered were 10^{-2}, 1, and 10^2. The first of these values is probably moderately representative of the more rarefied regions of the intercloud medium, while the last represents that of the denser clouds. In *H* II regions these same values were taken for n_p, the number of protons per cubic centimeter.

While the composition of the interstellar gas may, as a first approximation, be assumed to be the same throughout interstellar space, the level of ionization will be very different in *H* I and *H* II regions. In *H* II regions all the atoms may be assumed to be ionized. The value of the ratio n_i/n_p may be taken as 2×10^{-3}, in agreement with recent summaries by Unsöld[12] and Kuiper;[13] n_i is the particle density of ions other than hydrogen and helium. This value is somewhat higher than for planetary nebulae, where Aller and Menzel[14] found values of n_i/n_p ranging from 3×10^{-4} up to 2.5×10^{-3}. Since the

[5] *Ap. J.*, **88**, 429, 1938.
[6] *Ap. J.*, **89**, 526, 1939.
[7] *Ap. J.*, **88**, 364, 1938.
[8] *Ap. J.*, **109**, 354, 1949.
[9] *Ap. J.*, **108**, 242, 1948.
[10] *Ap. J.*, **108**, 276, 1948.
[11] *Ap. J.*, **104**, 414, 1946.
[12] *Zs. f. Ap.*, **24**, 306, 1948.
[13] *The Atmospheres of the Earth and Planets* (Chicago: University of Chicago Press, 1948), chap. xii.
[14] *Ap. J.*, **102**, 239, 1945.

temperatures actually computed for *H* II regions with the assumed abundance of ions were actually somewhat less, in general, than the lower limit established by observations of [*O* II] λ 3727, computations were also made with n_i/n_p reduced by a factor of 10 to 2×10^{-4}. It is possible that the relative abundance of most atoms other than hydrogen may actually be considerably less in interstellar space than in the stars, since an appreciable fraction of these atoms may be locked up in interstellar grains. Alternatively, the collision cross-section occurring in L_{ei} may perhaps be less than the value assumed. The temperatures computed for *H* II regions with the low ion abundance are identical with what would be obtained with a high ion abundance but a lower cross-section. This alternative interpretation is not possible in *H* I regions, however, where n_e is reduced when n_i is lowered.

In *H* I regions, roughly three-fourths of the atoms (*N* and *O*) will be neutral, while the remaining fourth (*C*, *Mg*, etc.) will be almost completely ionized at all the densities considered; thus the "standard" values of n_a/n_H and n_i/n_H may be taken as 1.5×10^{-3} and 5×10^{-4}, respectively. As for *H* II regions, computations were also made for *H* I regions of low ion density, where these ratios have one-tenth their standard values. These relative abundances are summarized in Table 1.

TABLE 1

RELATIVE ABUNDANCE OF INTERSTELLAR PARTICLES

Region *H* I	n_e/n_H	n_g/n_H	n_i/n_H	n_a/n_H	n_m/n_H
Standard	5×10^{-4}	10^{-12}	5×10^{-4}	1.5×10^{-3}	*
Low ion density	5×10^{-5}	10^{-12}	5×10^{-5}	1.5×10^{-4}	*
Concentrated cloud	5×10^{-4}	10^{-10}	5×10^{-4}	1.5×10^{-3}	*

* Depends on n_g only, equaling 0.1 for $n_g = 10^{-10}$ cm^{-3} or more, and 0 for $n_g = 10^{-12}$.

Region *H* II	n_e/n_p	n_g/n_p	n_i/n_p	n_a/n_p	n_m/n_p
Standard	1	10^{-12}	2×10^{-3}	0	0
Low ion density	1	10^{-12}	2×10^{-4}	0	0

In accordance with the discussion in Paper II, a substantial abundance of H_2 molecules must also be considered when n_g exceeds 10^{-12}. It has been assumed that, whenever n_g is 10^{-10} cm^{-3}, or greater, the ratio of n_m, the number of hydrogen molecules per cubic centimeter, to n_H is 0.1. Thus, when n_H is unity, only a concentrated cloud is assumed to contain H_2, while with n_H equal to 10^2, n_m/n_H is set equal to 0.1 for all compositions.

It will be noticed that no mention is made here of *He* and *Ne* atoms. Close to some very hot stars the *He* atoms will be ionized, and the electron temperatures may be somewhat higher than the values found here. More usually, however, *He* will be neutral and will have little effect on temperatures. *Ne* atoms can be expected to have even less effect.

It should be noted that the formulae adopted for L_{ei} in Paper II are somewhat approximate in *H* I regions. The low-lying electronic levels, which are important in these regions, were represented by a level at 0.015 electron volts (e.v.); half the ionized atoms were assumed to possess this level. Since *N* and *O* will be neutral in *H* I regions, the only abundant ions with levels within 0.04 e.v. of the ground state will be *C* II and *Si* II. (The excited $^2P_{3/2}$ levels in *C* II and *N* III, with excitation potentials of 0.0079 and 0.022 volts, respectively, and with values of 2 and 4 for g_A and g_B, were inadvertently omitted from Table 2 of Paper II.) These excited levels have excitation potentials about

half and twice, respectively, the adopted value of 0.015 e.v. It was not thought worth while to compute more precisely the contribution of *C* II and *Si* II to L_{es}, since the error in T introduced by this approximate representation is less than other uncertainties in the temperature.

c) PROPERTIES OF INTERSTELLAR GRAINS

The total cross-sectional area of interstellar grains plays an important part in the temperature of *H* I regions. If the extinction efficiency factor Q were unity (if all grains were very much larger than the wave length of visible light), an average photographic extinction of 1.6 mag. per kiloparsec in the galactic plane would yield a total absorption cross-section of 4.8×10^{-22} cm^2/cm^3. Since the radius of the grains has been arbitrarily taken as 10^{-5} cm, the corresponding value of n_g, the number of grains per cubic centimeter, would equal 1.5×10^{-12}. According to current ideas, most of the obscuring particles have dimensions comparable with the wave length and have an extinction efficiency factor of the order of magnitude of 1. Hence 10^{-12} seems a reasonable average value for the ratio of n_g to n_H, and this value has been adopted here as standard. The various particle distributions considered by van de Hulst[15] lead to values of the total geometric cross-section about the same as those used here.

According to certain theories on the formation of stars,[16, 17] the interstellar clouds are produced by the radiation pressure of galactic light on the grains; this pressure pushes the grains toward one another and results in an increase in the concentration of grains relative to the gas. Hence temperatures have also been computed for concentrated clouds, with a value of 10^{-10} for n_g/n_H, an increase of 100 over the standard value of this ratio. This increased relative abundance of grains, which definitely represents an extreme case, has not been assumed for the intercloud regions, where n_H is taken to be 10^{-2}.

The internal temperature of the grains, denoted by T_g in Paper II, is an important parameter in the equation for L_{Hg}. The factors determining T_g have been analyzed in some detail by van de Hulst.[18] The results are somewhat uncertain, with temperatures ranging from 10° to 20° K for dielectric spheres and from 30° to 100° K for metal spheres. A recent theoretical explanation[19] of the polarization of light in interstellar space suggests that the percentage of the metallic particles is somewhat higher than was envisaged by van de Hulst. However, it is still likely that a larger proportion of the interstellar grains are dielectric; accordingly, T_g has been set equal to 20° K in these computations.

Finally, the photoelectric properties of the grains must be specified. Computations have been made for the three types of surfaces described in Table 8 of Paper I. Surface A is equivalent in photoelectric sensitivity to the best photocells, while surface B is ordinary metal with lower efficiency. Surface C is nonmetallic and gives no photoemission. It seems likely that the actual grains are much closer to surface C than to surface B. Grains of surface A seem highly implausible but cannot be entirely excluded.

II. REGIONS OF IONIZED HYDROGEN

a) TEMPERATURES

A graphical method was used to determine, under each set of assumptions, the temperature at which the sum of all the G's is equal to the sum of the L's. This process was much simplified by the fact that, in *H* II regions, only G_{ep} and L_{es} were appreciable. The

[15] *Rech. Astr. Obs. Utrecht*, Vol. **11**, Part 2, 1949.

[16] F. L. Whipple, *Ap. J.*, **104**, 1, 1946.

[17] L. Spitzer, Jr., *Centennial Symposia, Harvard Observatory Mono.* No. 7 (Cambridge, Mass.: Harvard College Observatory, 1948), p. 87.

[18] *Op. cit.*, Vol. **11**, Part 1, 1946.

[19] L. Spitzer, Jr., and J. W. Tukey, *Science*, **109**, 461, 1949.

results for the different cases are shown in Table 2. Temperatures are given for a rarefied *H* II region produced by general galactic starlight and for *H* II regions around stars of types O, A, and B. Values for general galactic starlight are given for only the lowest density, since at higher densities the *H* II region will not usually extend far enough from any one star to make the contributions from other stars of much importance.

The low temperatures found in this table are the result of the thermostatic action of the various low-lying ionic levels, an effect first analyzed in detail by Menzel and his collaborators.[4, 20] For any particular ionizing radiation, the temperature depends primarily on n_i/n_p; obviously, the temperature will fall if the number of ions which cool off the gas is increased relative to the number of protons which heat up the gas.

At low densities the temperatures depend very little on the density. At the higher densities, collisional de-excitation becomes important, the population of the lower levels approaches the Boltzmann distribution, and the rate of dissipation of energy per gram of matter no longer increases with increasing density. However, G_{ep} continues to increase with increasing density, and the temperature therefore rises.

TABLE 2

EQUILIBRIUM TEMPERATURE IN *H* II REGIONS

PARTICLE DENSITY (IN CM^{-3})		TEMPERATURE (IN ° K) FOR IONIZING RADIATION FROM			
n_p	n_i	Galaxy	O Star	B Star	A Star
10^{-2}	2×10^{-5}	6000	6800	4800	2800
10^{-2}	2×10^{-6}	11,000	12,000	9500	5800
1	2×10^{-3}		6900	5000	3000
1	2×10^{-4}		12,000	9500	5900
10^2	2×10^{-1}		7600	5700	3600
10^2	2×10^{-2}		13,000	10,000	6600

The observations of the general galactic emission by Struve and his co-workers[21] give evidence on the temperatures of *H* II regions. These observations show that the line [*O* II] λ 3727 is, on the average, about as strong as *Hα*. The excitation of λ 3727 requires 3.31 e.v. of energy, equivalent to an electron temperature of many thousand degrees. More quantitatively, from the equations given in Papers I and II, the ratio of intensities of *Hα* and λ 3727 can readily be expressed in terms of n_i/n_p, the collisional cross-section for excitation of *O* II, the electron temperature, and other parameters. By adopting extreme assumptions for the other quantities, a lower limit on the temperature can be obtained. In this way we find that even if $\sigma_{nA}(a)$ in equation (20) of Paper II is set equal to 10^{-17} per unit weight of the ground state, about the maximum value permitted by the conservation theorem, and if there is one *O* II ion to every thousand protons, the temperature is found to be about 7500°, which we may take as a lower limit for T in the observed *H* II regions.

According to Table 2, the computed temperatures for the standard composition are actually less than this lower limit in almost all cases. A small decrease in ion density from the standard composition, with a reduced value of n_i/n_p in the range 5×10^{-4} to 10^{-3}, would give good agreement between the theoretical temperatures and the lower limit found from observations. Alternatively, a further decrease by a factor of 2–4 in the

[20] D. H. Menzel and L. H. Aller, *Ap. J.*, **94**, 30, 1941.

[21] O. Struve and C. T. Elvey, *Ap. J.*, **88**, 364, 1938; **89**, 119, 1939; **89**, 517, 1939; O. Struve, C. T. Elvey, and W. Linke, *Ap. J.*, **90**, 301, 1939.

cross-section for collisional de-excitation would give the same agreement, but with the standard ratio of 2×10^{-3} for n_i/n_p. It may be noted that, if the collisional cross-section had not been reduced at the beginning of this paper, the computed temperatures for n_p equal to 1 and for the standard composition would range from 210° near an A star to 1200° near an O star.

To obtain an upper limit on T we note that the greatest temperature in Table 2 is 13,000°. This value is already based on a relatively low abundance of ions or on a very low excitation cross-section. Further marked decreases in either of these quantities seem unlikely. Moreover, it seems most improbable that cosmic rays can increase the temperature materially; even if G_{ec} were increased by a factor of 10^5, the upper limit found in Section III, this quantity would only just equal G_{ep}. While it is always possible that unknown sources of energy may increase T, we may tentatively adopt an upper limit of about 13,000° for the kinetic temperature of most *H* II regions.

The contributions of photoelectric grains to the energy gain were generally quite small and have been neglected in Table 2. Even for surface A, the value of G_{eg} is almost always less than G_{ep}, provided that T exceeds 4000° and that the ratio n_g/n_p does not exceed the standard value 10^{-12}. For example, to make G_{eg} equal to G_{ep} with the standard value of n_g/n_p and a kinetic temperature of 4000° requires[22] that the grains have the very high positive charge of 50 volts (γ about 100) to make collisions with electrons sufficiently frequent. With so high a charge, the wave length at the photoelectric threshold would be decreased to about 250 A! The energy density of such short-wave radiation in interstellar space is much too small to permit the maintenance of so high a charge. If n_g/n_p is increased to 10^{-10}, G_{eg} can exceed G_{ep} in a number of extreme cases, whose physical interest did not seem to warrant the computational labors required for their investigation.

b) TIME OF EQUILIBRIUM

It is natural to inquire not only as to the temperature in equilibrium but also as to the rate of approach to equilibrium. We shall define the time of approach to equilibrium, designated by t_E, by the equation

$$t_E = \frac{3nk(T - T_E)}{2n_e(L_e - G_e)}, \tag{2}$$

where n is the total density of particles of all sorts, T_E is the equilibrium temperature, and G_e and L_e are the sums of all the individual G's and L's; as usual, k is the Boltzmann constant, and n_e is the number of electrons per cubic centimeter. It will be noted that t_E is simply the excess kinetic energy per cubic centimeter of the interstellar medium divided by the net rate of loss of kinetic energy per cubic centimeter per second. When T is nearly equal to T_E, the numerator and denominator in equation (2) become proportional to each other, t_E is then constant with temperature, and the approach to equilibrium temperature will become exponential. When the deviation is large, however, t_E is a function of T.

Values of t_E, computed for four different values of T, are given in Table 3 for the standard composition and a low proton density. For different over-all densities the value of t_E is very nearly inversely proportional to n_p. Only at the highest densities and at temperatures of 50° and 500° do the values of t_E differ by more than 10 per cent from what is found on the assumption of strict inverse proportionality to the density. For lower values of n_i/n_p, the value of t_E will be proportionally greater at the highest temperatures but will be independent of n_i/n_p at the lowest temperatures. The values in Table 3 are computed for *H* II regions surrounding a B star, but the values obtained for other types of ionizing radiation do not usually differ by more than 20 per cent from the values in Table 3 and are always within a factor of 2 of these values.

[22] See eq. (57) of Paper I; in this equation the numerical factor 10^{-11} must be corrected to 10^{-10}.

The general behavior of the values in Table 3 is in accord with physical expectations. As T increases, the cross-section for interaction between electrons and either protons or ions goes down as $1/T$, thus increasing t_E. At the higher temperatures this effect is partially offset by the increased number of atomic energy levels which may be excited by the electrons.

It is evident from this table that the values of t_E are not very high even when the density is low and that for higher densities equilibrium will be reached relatively rapidly. For comparison it may be noted that an H II region around an O star requires 10^7 years to move through a distance about equal to its radius. We may conclude that, as a hot star moves through space, the region of ionized hydrogen around it is usually at a temperature not far from its equilibrium value. This conclusion may require some modification if turbulent motions within the medium are responsible for large heating effects, but it does not seem likely that the rate of heating from such a source can exceed the rate resulting from absorption of starlight.

TABLE 3

TIME FOR EQUILIBRIUM IN H II REGIONS

From Initial Temperature (° K)	Time (in Years) with $n_p = 10^{-2}$ Cm^{-3} and Standard Composition*	From Initial Temperature (° K)	Time (in Years) with $n_p = 10^{-2}$ Cm^{-3} and Standard Composition*
50	1.8×10^5	5000	1.4×10^6
500	7.5×10^5	50,000	1.7×10^6

* For other proton densities t_E is roughly proportional to $1/n_p$.

c) CHARGE ON THE GRAINS

Since G_{eg} was found to be unimportant in these regions, no detailed computations were made of the electrical charge on the grains. However, certain simple results are evident at once from the basic equations. For substance C the photoelectric emission vanishes, and the charge adjusts itself to equate the number of electrons captured per second to the corresponding number of positive ions captured. If the sticking probabilities ξ_e and ξ_i for electrons and positive ions, respectively, are equal to each other, then the results previously obtained[23] are applicable; the value of γ is 2.51, and the potential is $-2.2 \times (T/10{,}000°)$ volts. These potentials are quite moderate. If, however, the sticking probability ξ_i has the minimum value of 10^{-4} envisaged in Paper I and γ consequently rises to about 10, the charge now becomes $-8.6 \times (T/10{,}000°)$ volts on the basis of the equations given in Paper I. When the potential exceeds several volts, it is probable that free-field emission occurs, and thus an upper limit of about -3 volts may be taken for the charge; the importance of this free-field emission was first emphasized by van de Hulst.[13]

For surface A the photoemissivity is so high that the grains are likely to be charged to a very high positive potential, especially at close distances from stars of early type. For surface B, negative charges are to be expected for high atomic densities and weak radiation, while close to an early-type star moderate positive charges are likely; this result is similar to that obtained by Cernuschi.[24]

III. REGIONS OF NEUTRAL HYDROGEN

a) TEMPERATURES

Temperatures were computed for H I regions by the same methods as those used for H II regions. The situation was made somewhat more complicated by the increased number of processes which required consideration. In particular, the computation of G_{eg} for

[23] L. Spitzer, Jr., *Ap. J.*, **93**, 369, 1941.

[24] *Ap. J.*, **105**, 241, 1947.

surfaces A and B required a simultaneous solution of equations (52), (54), and (55) of Paper I for each of a number of temperatures. The solution of these equations for γ was obtained by a series of successive approximations. Fortunately, it was found that ξ_i, the neutralization probability for ions, had no important effect on G_{eg}, and thus the large range which Table 8 of Paper I exhibits for values of this quantity did not complicate the computations.

The results of these calculations are given in Table 4. For surface C the temperatures are all low, and at high densities are only 10°–20° higher than the internal grain temperature, T_g. In view of the importance of this result, let us examine carefully its physical basis. Two sources of energy gain, G_{He} and G_{ei}, and two sources of energy loss, L_{ei} and L_{Hg}, are dominant for surface C. At the lowest density, collisions of cosmic rays with neutral H atoms are largely responsible for the heating. As the density increases, G_{ei}

TABLE 4

EQUILIBRIUM TEMPERATURE IN H I REGIONS

PARTICLE DENSITY (IN CM^{-3})			TEMPERATURE (IN ° K) FOR GRAINS OF SURFACE		
n_H	n_i	n_g	A	B	C
10^{-2}	5×10^{-4}	10^{-14}	1310	1100	740
1	5×10^{-4}	10^{-12}	420	52.0	47.3
	5×10^{-3}	10^{-12}	1200	330	230
	5×10^{-4}	10^{-10}	450	105	34.9
10^2	5×10^{-2}	10^{-10}	56	43.0	42.6
	5×10^{-3}	10^{-10}	72	37.7	35.1
	5×10^{-2}	10^{-8}	202	34.5	32.4

increases, while G_{He} does not, and when n_H is 10^2, n_eG_{ei} exceeds n_HG_{He} in all cases. Most of the cooling results from inelastic electron-ion collisions when the composition is standard; but, for relatively low ion density and in a concentrated cloud, n_HL_{Hg} is about equal to n_eL_{ei}. The quantity L_{ea} is less than 1 per cent of L_{ei} because of the very large cross-section for encounters between an ion and a low-speed electron. For the situations considered, L_{eH} and G_{eH} were of no importance.

The increase of T with decreasing n_H, shown in Table 4, is readily explained. As the density changes, G_{He} is constant, while L_{ei} and L_{Hg} both decrease proportionally with the density.

Since both L_{ei} and G_{He} are somewhat uncertain, one may inquire as to the variation of temperature to be expected with possible variations in these two quantities. First, we consider changes in L_{ei}. At temperatures below 100°, L_{ei} is primarily the result of electron excitation of the low-lying level of C II. To obtain an upper limit on the temperature, we may set L_{ei} equal to zero, which gives T equal to about 190° for the standard composition and n_H equal to unity. If L_{ea} is also set equal to zero, T rises to about 280°. Within an H I cloud, however, the presence of H_2 molecules may be expected to keep T below these values. For example, if n_m/n_H is set equal to 0.1, T becomes about 60° when the composition is standard, L_{ei} is neglected, and n_H is 1 or higher. One may conclude that possible errors in the adopted value of L_{ei} do not modify the conclusion that in an H I cloud T is in the neighborhood of 60°.

Possible errors in the assumed value of G_{He} are more serious, since the low-energy end of the cosmic-ray spectrum is highly uncertain and G_{He} may exceed the assumed value of

4.1×10^{-30} erg/sec by several orders of magnitude. If H_2 molecules are present, however, very large increases in G_{Hc} will be required to increase T very materially. For example, if one H_2 molecule to every ten H atoms is added to the standard composition, and n_H is taken to be unity, G_{Hc} must be increased by a factor of 10^3 to make T equal to 200°; if n_H is taken as 10^2, G_{Hc} must be increased by 10^6 to give 200° for T. Such large increases seem improbable, since they would imply a dissipation of energy by cosmic rays that would be an appreciable fraction of the total stellar radiation. If G_{Hc} is increased by a factor of 10^6, for example, the average dissipation of energy per cubic parsec, with n_H set equal to 1, becomes $3 \times 10^{-3}\ L_\odot$ per cubic parsec. It would be difficult to account for the generation within the galaxy of such intense cosmic radiation. We may conclude that cosmic rays are not likely to yield temperatures much in excess of 200° within an H I cloud.

For surface B the temperatures shown in Table 4 tend to be somewhat higher than for surface C, especially at the lower densities. This results from the influence of G_{eg}, which becomes appreciable under these conditions. As with surface C, the temperatures tend to be greater at the lower densities. When the photoelectric efficiency is not too great and the charge on the grain relatively small as a result, the rate of photoemission of electrons from a grain will be nearly independent of the gas density. Thus G_{eg} behaves in much the same way as G_{Hc}, and T decreases with increasing n_H. In fact, when n_H is as great as 10^2, G_{eg} for surface B becomes less than $G_{ei} + n_H G_{Hc}/n_e$ and the temperatures are practically those found for surface C.

Loss of energy by molecules can be important at the temperatures reached for surface B. At the temperature of 105° shown in the fourth row of Table 4, L_{Hm} contributes half the total loss, with L_{Hg} and L_{ei} each contributing about one-fourth.

For the highly emitting surface A the trends seen with surface B become even more marked. Now G_{eg} is the dominant energy gain under all the conditions considered, except for the lowest density, where cosmic rays contribute two-thirds of the energy gain. The change of temperature with over-all density is now less marked, since the photoelectric emission gives the grain a very high charge and the limiting factor on the photoelectric emission is the number of electrons reaching the grain per second rather than the amount of radiation available.

The only previous analysis of kinetic temperature in H I regions is apparently that by Woolley.[25] In this work Woolley considers that free-free transitions of electrons on impact with ions provide the only source of energy loss in H I regions, and he finds a temperature of 1000°. Electron captures in excited states, which are neglected in his analysis, would raise T more nearly to the values found in H II regions. However, the neglect of the three main sources of energy loss considered here makes Woolley's results scarcely comparable to the present ones.

The depression of interstellar temperatures by H_2 molecules and by grains has already been noted by Hoyle and Lyttleton[26] and by Hoyle,[27] respectively. Excitation of the rotational states of H_2 was not considered, but formulae were given for essentially L_{em} (with an assumed spontaneous transition probability greater by a factor of 5×10^4 than the value adopted in Paper II) and for L_{Hg}. However, these authors were not primarily interested in the temperatures of the interstellar clouds observed within 1000 parsecs of the sun and have not pointed out the probable difference of temperature between H I and H II regions.

b) TIME OF EQUILIBRIUM

Equation (2) in Section II*b* may also be used to determine the time of approach to equilibrium in H I regions. In this case L_{Hg}, L_{Hm}, and G_{Hc} are frequently important, and,

[25] *M.N.*, **107**, 308, 1947.

[26] *Proc. Cambridge Phil. Soc.*, **35**, 405, 1939; **36**, 424, 1940.

[27] *M.N.*, **105**, 287, 1945.

as in equation (1), these quantities must be multiplied by n_H/n_e before they are combined with the various L_{ej}'s and G_{ej}'s. The values of t_E found are given in Table 5 for initial temperatures of 50°, 500°, and 5000°. Results are given for grains with the surface C only. The times found for the other surfaces are usually only slightly less than the values given. At $T = 5000°$, for example, the values of t_E for surface B are within 10 per cent of the values in Table 5, although at 50° the values are in some cases only one-fourth as great. For surface A the deviation is somewhat greater, but for $T = 5000°$ the times are usually within 20 per cent of the values for surface C.

It is evident from this table that, especially at low densities, the values of t_E are very long. If the region of low density was originally at a high temperature, it would scarcely have time to cool down to its equilibrium temperature during the age of the universe. At higher densities the times become much shorter and are much less than the million

TABLE 5

TIME FOR EQUILIBRIUM IN *H* I REGIONS WITH GRAINS OF SURFACE C

PARTICLE DENSITY (IN CM^{-3})			TIME IN YEARS FROM INITIAL TEMPERATURE		
n_H	n_i	n_g	$T = 50°$	$T = 500°$	$T = 5000°$
10^{-2}	5×10^{-6}	10^{-14}	1.1×10^{9}	1.2×10^{9}	2.1×10^{9}
1	5×10^{-4}	10^{-12}	1.2×10^{7}	1.1×10^{7}	1.9×10^{7}
	5×10^{-3}	10^{-12}	3.1×10^{6}	2.1×10^{6}	9.2×10^{7}
	5×10^{-4}	10^{-10}	4.3×10^{6}	1.3×10^{5}	1.8×10^{4}
10^{2}	5×10^{-2}	10^{-10}	9.2×10^{4}	1.8×10^{2}	1.8×10^{2}
	5×10^{-3}	10^{-10}	4.8×10^{6}	1.9×10^{4}	1.8×10^{2}
	5×10^{-2}	10^{-8}	4.3×10^{4}	1.8×10^{3}	1.8×10^{2}

years required for an interstellar cloud to move through a distance about equal to its diameter. The rapid approach to equilibrium when n_H equals 10^2 is largely the result of energy dissipation by H_2 molecules. If n_m is set equal to zero, when n_H is 10^2 and n_g is 10^{-10}, then for initial temperatures between 500° and 5000° t_E lies in the range from 10^5 to 10^6 years.

c) CHARGE ON THE GRAINS

As a result of the low temperatures found, the electrostatic potential of the grains becomes very low when photoelectric emission is weak. With surface C, for example, if ξ_i equals ξ_e, then γ equals 2.2; and when T equals 40°, the potential on the grain is only about 9×10^{-3} volts, corresponding to an average charge of less than 1 electron. Even if ξ_i is as low as 10^{-4}, the number of electrons computed for a grain of substance C in an *H* I region is only about 3. Obviously, the equations used to determine γ, which consider a uniform potential on the grain, no longer apply, except perhaps statistically, when the number of electrons per grain becomes so small.

For surfaces B and C photoelectric emission may produce an appreciable potential, especially at the low densities. Values of V, the potential of the grain in volts, were found as a by-product of the temperature calculations. These values are given in Table 6 for the equilibrium temperatures listed in Table 4. For comparison, values are also given for the potential of dielectric grains (surface C), computed for $\xi_i = \xi_e$. The values for surfaces A and B are mostly independent of ξ_i, the sticking probability for ions, since the metallic grains are not charged to a sufficiently great negative potential to make the number of collisions with ions as great as the number of collisions with electrons.

IV. Conclusions

The largely tentative nature of the present investigation should be remembered. The astronomical data on the radiation field and on the density of the interstellar medium are still quite incomplete and uncertain; numerical values of the physical parameters affecting the kinetic temperature are even more uncertain. In view of this situation, the computations summarized here have dealt with somewhat idealized and simplified situations. Evidently, the present results should be used only as an indication of general trends and not as a definite proof that certain specific kinetic temperatures may be expected in interstellar space.

Despite the uncertainty in all these numerical results, however, a large difference of temperature between *H* I and *H* II regions seems clearly evident. The observations of [*O* II] λ 3727 in *H* II regions indicate that the temperature of these regions must be at

TABLE 6

Electrostatic Potential of Grains

Particle Density (In Cm^{-3})			Potential (in Volts) for Surface		
n_H	n_i	n_g	A	B	C
10^{-2}	5×10^{-6}	10^{-14}	+10.2	+2.84	−0.16
1	5×10^{-4}	10^{-12}	+ 3.5	+0.016	−0.010
	5×10^{-6}	10^{-12}	+ 8.3	+0.37	−0.050
	5×10^{-4}	10^{-10}	+ 3.4	+0.020	−0.008
10^{2}	5×10^{-2}	10^{-10}	+ 0.13	−0.011	−0.009
	5×10^{-3}	10^{-10}	+ 0.81	−0.002	−0.008
	5×10^{-2}	10^{-8}	+ 0.22	−0.009	−0.007

least 7500° and may be somewhat higher. This result can be reconciled with theory either if (*a*) the ratio of *O*, *N*, and *C* ions to protons is somewhat less than 2×10^{-3}, possibly between 5×10^{-4} and 10^{-3}, or if (*b*) the cross-section for excitation of these ions by electron impact is even smaller than the reduced value adopted at the beginning of this paper. These changes are quite within the uncertainty of our present knowledge. While one may conclude that the temperatures of *H* II regions around early-type stars probably lie between 7500° and 13,000°, a more precise determination is not now possible.

The temperatures of *H* I regions are lower by a factor of about 100 than those of *H* II regions. When the hydrogen is neutral, cosmic rays provide most of the heating at low densities, while at higher densities capture of electrons by *C*, *Mg*, *S*, and *Fe* ions, with subsequent re-emission, makes the larger contribution. Both these sources of energy gain are relatively weak, unless cosmic rays of low energy are much more intense than has previously been assumed. On the other hand, there are three very efficient processes which tend to radiate away the kinetic energy of the assembly: electron excitation of the lowest excited levels of *C* II and *Si* II (and, at somewhat higher temperatures, of *Fe* II), inelastic collisions between *H* atoms and grains, and excitation of the low rotational levels of H_2 on impact with *H* atoms. At low densities, such as may be expected between clouds, these radiative processes are relatively ineffective, and equilibrium temperatures of 500° or more may be expected. In an *H* I cloud, where n_H is probably 10 or more, these three processes probably keep the temperature down to a value between 30° and 100°, with about 60° as the mean of the probabilities. On extreme assumptions, temperatures

as high as 200° are possible, but higher values seem very improbable if, as seems likely, H_2 molecules are abundant in an H I cloud. On the other hand, temperatures even less than 30° are possible in H I regions.

The times required to approach equilibrium temperatures are relatively short for H II regions and for dense H I regions where H_2 molecules are present. In between the clouds, where the density is much less, the times of equilibrium are considerably longer, and, if the hydrogen is neutral, it is doubtful whether equilibrium will be attained. The temperature of such rarefied regions will doubtless depend on the previous history of the intercloud gas. Material torn out of a dense, cool cloud will probably remain cool until hydrogen is ionized. Gases which once formed part of an H II region will probably remain hot, although the hydrogen will become neutral relatively soon if the ionizing radiation is cut off.

Finally, one must consider other factors which may, in principle, affect the temperature. Conduction is readily shown to be unimportant over regions several parsecs in size, even if the density is as low as 10^{-2} H atoms or protons per cubic centimeter. Heating produced by the random motions of the clouds will certainly be important in localized regions, as, for example, in two clouds which are colliding; but it seems doubtful whether this influence can increase the average cloud temperatures appreciably. If, as seems likely, the cloud motions result from temperature differences in the interstellar medium, then these motions obviously cannot much increase the average cloud temperature. If, on the other hand, turbulence produced by galactic rotation is the driving force for these motions, then the kinetic energy of galactic rotation is inadequate to maintain all the H I clouds at temperatures of some 200° for 10^9 years, since the radiation of energy by H_2 molecules at this temperature becomes very rapid. We may therefore conclude that these other factors apparently have no great effect on average interstellar temperatures.

The authors are much indebted to Mr. William Buscombe and Mr. John Schopp for assistance in the details of this work.

APPENDIX

Equipartition of Kinetic Energy

In a previous analysis[23] it was shown that equipartition of energy is established very rapidly between the electrons and ions of the interstellar gas and that the grains would also reach this equipartition in some 10^4–10^5 years. This conclusion is not affected by the low temperatures computed for H I regions, since at lower temperatures the times of relaxation and equipartition are, for the most part, even smaller than the values previously found.

Inelastic collisions were not considered in this earlier analysis, on the assumption that these are usually much less frequent than elastic collisions. For encounters between electrons and ions this assumption is certainly valid, and one may conclude that inelastic electron-ion encounters do not distort appreciably the Maxwellian velocity distribution of electrons. This same conclusion has already been reached by Bohm and Aller,[28] who analyzed in some detail the more favorable case in which electrons and protons outnumber by 1000 to 1 the ions producing inelastic impacts.

When H atoms are the dominant constituent of the interstellar gas, an important effect not previously considered may appear. Gains of kinetic energy are chiefly experienced by electrons; and, if the losses are experienced primarily by H atoms, the mean kinetic energy of these atoms will be less than that of the electrons. It is readily shown that, in any case, elastic collisions between electrons will establish a Maxwellian distribution for electron velocities, and, similarly, elastic collisions between H atoms will separately establish a Maxwellian velocity distribution for these atoms. As before, inelastic

[28] *Ap. J.*, **105**, 131, 1947.

collisions of all sorts are much less likely than these elastic collisions. Hence it is appropriate to define kinetic temperatures T_e and T_H for the electrons and H atoms separately. The difference between T_e and T_H is treated in this appendix. We discuss, first, the transfer of kinetic energy directly from electrons to H atoms, postponing until later the consideration of other atoms and ions present.

We let F_{eH} be the kinetic energy transferred from electrons to H atoms per electron per second. Evidently, in a steady state $n_e F_{eH}$ equals both the energy lost by H atoms per cubic centimeter in inelastic collisions and also the difference between the energy gained by electrons and the energy lost by these electrons in inelastic encounters. The gain of energy from encounters between cosmic rays and H atoms is, in this connection, a gain of kinetic energy by the free electrons produced in the encounters, not a gain of energy by the H atoms. Hence we have the equation

$$n_H G_{He} + n_e \left\{ \sum_j G_{ej} - \sum_j L_{ej} \right\} = n_e F_{eH} = n_H \sum_j L_{Hj} . \tag{3}$$

We compute F_{eH} on the reasonable assumption that the electron velocity, v_e, is much greater than the velocity, v_H, of the H atom. We also assume that the scattered electron wave has spherical symmetry, as measured in the reference frame in which the center of gravity of electron plus H atom is at rest. This assumption should be correct for the low temperatures of interest here, since the electron wave length is then several orders of magnitude larger than the H atom.

We let $\boldsymbol{V}_g$ be the velocity of the center of gravity, $\boldsymbol{v}_H$ and $\boldsymbol{v}'_H$ the velocities of the H atom before and after encounter, $\boldsymbol{u}_H$ and $\boldsymbol{u}'_H$ the same velocities relative to $\boldsymbol{V}_g$. Similar quantities with a subscript e refer to electron velocities. In a single collision the energy change of an H atom, denoted by ΔE_H, is given by

$$\Delta E_H = \tfrac{1}{2} m_H \{ (\boldsymbol{V}_g + \boldsymbol{u}'_H)^2 - (\boldsymbol{V}_g + \boldsymbol{u}_H)^2 \} . \tag{4}$$

Since the absolute value of $\boldsymbol{u}_H$ equals that of $\boldsymbol{u}'_H$ and since the distribution of $\boldsymbol{u}'_H$, like that of the scattered-electron velocity $\boldsymbol{u}'_e$, has spherical symmetry, most of the terms in equation (4) cancel out, and we have

$$\Delta E_H = - m_H \boldsymbol{V}_g \cdot \boldsymbol{u}_H . \tag{5}$$

The quantity F_{eH}, the total energy lost by an electron per second, on the average, in collisions of this sort, is given by the equation

$$F_{eH} = n_H \sigma_{eH} \overline{V \Delta E_H} , \tag{6}$$

where V is the relative velocity. The two bars denote averages, first over θ, the angle between $\boldsymbol{v}_e$ and $\boldsymbol{v}_H$, and, second, over the magnitudes of $\boldsymbol{v}_e$ and $\boldsymbol{v}_H$. To carry out the first average, we multiply equation (5) by V, express V, $\boldsymbol{V}_g$, and $\boldsymbol{u}_H$ in terms of $\boldsymbol{v}_e$ and $\boldsymbol{v}_H$, multiply by $\frac{1}{2} \sin \theta d\theta$, and integrate over θ, obtaining the equation

$$\overline{V \Delta E_H} = \frac{m_e m_H}{(m_e + m_H)^2} \int_0^\pi \tfrac{1}{2} \sin \theta \{ v_e^2 + v_H^2 - 2 v_e v_H \cos \theta \}^{1/2} \times \{ m_e v_e^2 - m_H v_H^2 + (m_H - m_e) v_e v_H \cos \theta \} d\theta . \tag{7}$$

To evaluate equation (7), we expand the square root in a series of ascending powers of $\cos \theta$. After multiplication by the other expression in the integrand, terms of order m_e/m_H

and v_H/v_e are neglected compared to unity. The integration over θ and the subsequent averages over v_e and v_H are all straightforward, and we find

$$F_{eH} = 8\left(\frac{2m_e k^3}{\pi}\right)^{1/2} \frac{\sigma_{eH} n_H T_e^{1/2}}{m_H}(T_e - T_H). \tag{8}$$

The value of the scattering cross-section σ_{eH} may be found from the Hartree field of an H atom for a free electron. In atomic units, the potential energy of a free electron, at a distance r from the nucleus of the atom, is given by $(1 + [1/r])\exp(-2r)$. For an electron whose kinetic energy corresponds to a kinetic temperature of 60°, the potential energy equals the kinetic at a distance of 2.3×10^{-8} cm, or at about four times the radius of an H atom. This value may be taken as the collision radius, yielding a value of 1.6×10^{-15} cm^2 for σ_{eH}. Inserting other numerical constants into equation (8), we have, finally,

$$F_{eH} = 3.0 \times 10^{-28} n_H T_e^{1/2}(T_e - T_H)\ \text{erg/sec}. \tag{9}$$

If we now substitute equation (9) in equation (3), it is possible to determine T_e and T_H separately. More simply, if a value of T_H is assumed, $T_e - T_H$ can be found directly. If we consider that L_{Hg} is the dominant source of energy loss, then equations (3) and (9) may be combined directly with equation (44) of Paper II to give

$$\frac{T_e - T_H}{T_H - T_g} = 3.1 \times 10^6 \frac{n_g}{n_e}\left(\frac{T_H}{T_e}\right)^{1/2}. \tag{10}$$

For the standard abundance, n_g/n_e in H I regions is 2×10^{-9}, and $T_e - T_H$ is less than 1 per cent of $T_H - T_g$. Thus, even if T_H rises to 200°, T_e will exceed T_H by only 1°.2. In a concentrated cloud, n_g/n_e rises to 2×10^{-7}, and $T_e - T_H$ becomes about equal to $T_H - T_g$. In this extreme case T_e may be about twice T_H if T_H much exceeds T_g.

Next we consider situations in which L_{Hm} is dominant. First, as an extreme case, we take T_H equal to 200°, the temperature obtained within a dense H I cloud if G_{Hc} is increased by 10^5 over the adopted value. If the standard composition is assumed and n_m is set equal to $0.1n_H$, T_e equals 420°. As the density is decreased, L_{Hm} falls off less rapidly than n_e, and the deviations from equipartition increase. If the relative composition is held constant, then, for n_H less than about 10, T_e is about 760° if T_H is 200°. In these extreme cases, with marked deviations from equipartition, the temperatures computed in Section III above will refer essentially to T_H rather than to T_e.

The effect of other atoms, specifically excluded so far, must now be taken into account. Other neutral atoms behave in the same way as H and have a negligible effect because of their relatively low abundance. Atomic ions, on the other hand, will bring T_H and T_e significantly closer together. As a result of the strong electrostatic interaction between ions and electrons at low temperatures, the kinetic temperature of these ions will be closely equal to T_e. The interaction of the ions with H atoms will then tend to increase T_H. It may be seen that encounters with ions will have quantitatively about the same effect on T_H as do encounters with electrons. There are about as many ions as electrons. While the relative velocity of an atom-ion collision is less than that of an atom-electron collision and the frequency of the atom-ion collisions consequently less, each collision with an ion is more effective in changing the kinetic energy of an H atom.

Numerical values of the rate at which an ion gains kinetic energy from H atoms may be determined from equation (8), provided that m_H and T_H replace m_e and T_e, while m_i and T_i (assumed to equal T_e) replace m_H and T_H. The chief numerical difference comes from replacing $\sigma_{eH} m_e^{1/2}/m_H$ by $\sigma_{iH} m_H^{1/2}/m_i$. However, even for C II, the lightest ion present in H I regions, $m_H^{1/2}/m_i$ is only 3.6 times $m_e^{1/2}/m_H$, and much of this increase may be offset by a smaller collision cross-section for atom-ion collisions. Evidently, the presence of

heavy ions decreases $T_e - T_H$ by perhaps half an order of magnitude from the value found when elastic electron-atom collisions provide the only source of energy gain for the H atoms.

Evidently, deviations from equipartition, while not negligible in all cases, are likely to be small, and we may conclude that under most conditions the kinetic temperatures of the different constituents of the interstellar gas are closely equal to each other. In H I regions, under certain rather unlikely conditions, it is possible that T_e may appreciably exceed T_H. Even in extreme situations it seems very improbable that T_e exceeds $2T_H$.

TARGET AREAS FOR THE COLLISIONAL EXCITATION OF NEBULAR LINES

L. H. ALLER
University of Michigan Observatory, Ann Arbor, Michigan
Received March 1, 1950

ABSTRACT

The theoretical target areas for inelastic collisions involving metastable and ground levels associated with the nebular lines appear to be in error. The densities of the *O* III ions responsible for the green nebular lines exceed values previously given by a factor of at least 3. Improved estimates of the abundance of *O* II and *O* III are given for a number of typical nebulae.

Many years ago, I. S. Bowen suggested that the forbidden lines observed in the spectra of novae, gaseous nebulae, and extended stellar envelopes were produced by inelastic collisions with electrons. Since then much observational evidence has been accumulated to substantiate this hypothesis.

A quantitative interpretation of the intensities of forbidden lines requires a knowledge not only of their transition probabilities but also of the target areas for their collisional excitation. Calculations of the latter parameter have been carried out by Hebb and Menzel for [*O* III];[1] by Yamanouchi, Inui, and Amemiya[2] for [*O* I]; by Marvin White and the writer for [*N* II];[3] and by the writer for [*O* II].[4] A considerable amount of theoretical work on the gaseous nebulae has been based on the calculations for *O* III.

Unfortunately, the theory tends to predict cross-sections which are too large. The situation has recently been reviewed by Bates, Fundaminsky, Massey, and Leech,[5] who find that the theory is capable of yielding satisfactory results when a change of electron spin is not involved. That is, reasonably satisfactory results are obtained for transitions such as *He* $1S^1-3^1S$, *Na* 3^2S-3^2D, etc.; but the theory yields cross-sections for such transitions as *He* I 1^1S-2^3S, *O* I $^3P-^1D$, etc., which may be in error by perhaps an order of magnitude.

The target areas for collisional excitation obey a conservation theorem due to Mott, Bohr, Peierls, and Placzek,[6] which may be written in the form

$$\Sigma \frac{\Omega}{2J_A+1} \leq (2l+1),$$

where Ω is the target parameter defined by Hebb and Menzel, J_A is the inner quantum number of the lower level, and l is the azimuthal quantum number of the partial wave that contributes the largest share to the cross-section. For the transitions of interest, $l = 1$. The summation is carried out over all the levels of the ground configuration.

This conservation theorem is of value only when the electrons of some particular

[1] *Ap. J.*, **92**, 408, 1940.

[2] *Proc. Physico-math. Soc. of Japan*, ser. 3, **22**, 848, 1940.

[3] Unpublished. The Ω-values for [*N* II] were about 0.46 those found for [*O* III].

[4] *Pub. A.S.P.*, **60**, 317, 1948. The Ω-value for the $^4S_{3/2}-^2D$ [*O* II] transition obtained by the conventional theory is actually about 50. The value given in the paper referred to contains a numerical error.

[5] *Proc. R. Soc. London, A* (in press). The writer is indebted to Dr. D. R. Bates for communicating these results in advance of publication, as well as for helpful comments on this paper.

[6] Mott and Massey, *The Theory of Atomic Collisions* (2d ed.; Oxford, 1949).

azimuthal quantum number give the dominant contribution to the cross-section. Essentially, the conservation theorem limits only the partial cross-sections. By "partial cross-section" we mean the contribution to the cross-section for a transition that arises from incident electrons of a given azimuthal quantum number. In exchange transitions, only one partial cross-section is appreciable, but for nonexchange transitions many partial cross-sections contribute, and the conservation theorem (though still true) is no longer useful.

Application of this theorem to Hebb and Menzel's target-area calculations shows that the values of Ω are at least two times too large and that, if the relative Ω's are to be preserved, we must divide the tabulated values by a factor of at least 3. Similarly, the Ω-value of about 50 found by the writer for the $^4S_{3/2}-{}^2D$ [O II] transition should be divided by about 5.

We may derive a lower limit for the oxygen abundance in the gaseous nebulae if we employ the upper limit to Ω. That is, we shall adopt $\Omega(^4S_{3/2}-{}^2D) = 10$ for O II and divide the Ω-values for O III by 3. With $A = 8.87\times10^{-8}$ for λ 3727, the revised equation

TABLE 1

ESTIMATED ABUNDANCE OF OXYGEN IONS IN PLANETARY NEBULAE

Nebula	N_e	T_e(°K)	$(1-\beta)$	$[I(3727)]/[I(N_1+N_2)]$	$[N(O\,II)]/[N(O\,III)]$	$N(O\,III)$	$[N(O\,II+O\,III)]/N(H)$
NGC 7027	5900	9600	0.97	0.0064	0.025	3.4	5.9×10^{-4}
NGC 6572	10,500	9000	.95	.0274	0.195	2.3	2.6
NGC 6826	4500	8200	.98	.0243	0.097	1.0	2.6
NGC 6543	11,700	6500	.93	.0395	0.52	6.2	8.0
IC 418	11,000	9700	.94	.83	5.4	0.21	1.2
NGC 7662	13,200	9900	.93	.0113	0.084	3.0	2.5
NGC 7009	20,400	8900	0.90	0.0128	0.16	3.4	2.0

XVI (6)[7] and equation XVIII (18), the ratio of O II to O III ions in their respective ground states is related to the intensity ratio of λ 3727 and the green nebular lines N_1N_2 by

$$\frac{N(O\,II)}{N(O\,III)} = 0.021\left[\frac{N_e}{\sqrt{T_e}}+\frac{104}{\Omega(^4S;\ ^2D)}\right]10^{4180/T_e}(1-\beta)\frac{I(3727)}{I(N_1+N_2)}.$$

Here N_e and T_e are, respectively, the electron density and the temperature; the definition of β according to equation XVI (7) must be modified for the new Ω.

Table 1 gives the designation of the nebulae, N_e and T_e adopted from XVIII, $(1-\beta)$, $[I(3727)]/[I(N_1+N_2)]$, the ratio $N(O\,II)/N(O\,III)$, $N(O\,III)$ adopted from equation XVI (5) corrected for the new value of Ω, and, finally, the ratio $[N(O\,II+O\,III)]/N(H)$. This ratio represents a lower limit to the oxygen/hydrogen abundance, since no allowance has been made for the distribution of oxygen atoms among other stages of ionization and since an upper limit of Ω has been used. The effect of the filamentary structure of the nebula is difficult to estimate.

The mean value of the O/H ratio 3.5×10^{-4} is in fair agreement with the results found for the atmospheres of Tau Scorpii[8] and 10 Lacertae[9] and with the result found by Bowen for the sun.[10] The revised target areas would appear to be correct within a factor of 2 or 3.

[7] Series of papers entitled "Physical Processes in Gaseous Nebulae" in the *Astrophysical Journal*. "Equation XVI (6)" refers to eq. (6) of Paper XVI, *Ap. J.*, **94**, 30, 1941; see also Paper XVIII, *ibid.*, **102**, 239, 1945.

[8] A. Unsöld, *Zs. f. Ap.*, **21**, 22, 229, 1941–1942.

[9] L. H. Aller, *Ap. J.*, **104**, 347, 1946.

[10] *Rev. Mod. Phys.*, **20**, 109, 1948.

THE VIBRATIONAL STABILITY OF WHITE DWARFS

P. J. LEDOUX* AND E. SAUVENIER-GOFFIN
Institut d'Astrophysique, Université de Liége
Received December 31, 1949

ABSTRACT

The condition of vibrational stability of white dwarf stars is established and studied in detail for the two main nuclear reactions which have been considered in connection with the generation of energy in these stars (carbon cycle and proton-proton reaction) when it takes place in the central region or in an external layer. It is shown that nuclear reactions would render the white dwarfs unstable except in a very special case, and hence it seems that the generation of energy in these stars must definitely be attributed to some other cause.

I. INTRODUCTION

The white dwarf stars constitute probably the most numerous class of stellar objects next to the main sequence. However, until now, they have been studied mainly from the point of view of pure hydrostatic equilibrium only, and it is useful to extend to them the other criteria of internal structure provided by the conditions of stability.

Some time ago A. B. Severny[1] touched upon the question of their dynamical stability but only in a formal way. Since, in this respect, the value $\gamma = \frac{4}{3}$ of the ratio of specific heats is critical for gaseous stars, while in a white dwarf, in which relativistic degeneracy develops, the value of Γ_P in the adiabatic relation $\delta P/P = \Gamma_P(\delta\rho/\rho)$ tends toward $\frac{4}{3}$, he concluded that the limit of dynamical stability would be approached at the same time as a state of complete relativistic degeneracy.

In a preceding paper[2] which will be cited as "Paper I" in the following, one of us has studied the dynamical stability of white dwarfs, starting from the exact equation of state. If a star is stable toward convection, it can be shown[3] that purely radial perturbations are the most dangerous for its dynamical stability, and hence, in this case, the study has been restricted to the fundamental mode of radial pulsation.

It was found that, instead of decreasing, the dynamical stability actually increases with the extent of the relativistic degenerate region. This can be understood easily on the basis of the first approximation for the frequency of pulsation σ given in that paper, namely,

$$\sigma = -\frac{\{\langle 3\bar{\Gamma}_P - 4\rangle\,\Omega}{I}, \tag{1}$$

the ratio of the moment of inertia I to the gravitational potential Ω tending toward zero more rapidly than $(3\bar{\Gamma}_P - 4)$, when the whole configuration approaches a state of complete relativistic degeneracy. These degenerate configurations are dynamically stable in all cases, and the limiting mass keeps a purely hydrostatic meaning. We are not concerned here with the possible effects of extra forces, such as centrifugal forces in rapidly rotating configurations or the effects of rotational instability,[4] and we shall limit our-

* Associé du Fonds National de la Recherche Scientifique.

[1] *C.R. Acad. Sci., U.R.S.S.*, **31**, No. 2, 109, 1941.

[2] E. Sauvenier-Goffin, *Ann. d'ap.*, **12**, 39, 1949.

[3] P. Ledoux, *Mém. Soc. R. Sci. Liége*, 4ème sér., Vol. **9**, No. 1, chap. iii, 1949.

[4] F. Hoyle, *M.N.*, **107**, 231, 1947.

selves, as in the previous paper, to spherical configurations with negligible rotation or none at all.

In this paper we wish to discuss the condition of vibrational stability, which seems particularly interesting because it involves the generation of energy in white dwarfs, a question which has been much debated recently. If it is attributed to nuclear reactions, many difficulties arise from the point of view of instantaneous hydrostatic equilibrium,[5] as well as from the point of view of past and future evolution.[6] However, in these aspects of the problem it is always possible to find a way out of the difficulties by adopting special abundances or a particular stratification of the elements. As far as vibrational stability is concerned, it is the form of the law of generation of energy which matters, and this cannot be varied at will.

II. FUNDAMENTAL EQUATIONS

We shall generally use Chandrasekhar's notations,[7] in which the mean electronic concentration, n, is expressed in terms of the temperature, T, and the variable $x = p_0/mc$, by

$$n = a x^3 \left[1 + \pi^2 \left(\frac{kT}{mc^2} \right)^2 \frac{2x^2+1}{2x^4} + \dots \right], \tag{2}$$

where

$$a = \frac{8\pi m^3 c^3}{3h^3}.$$

The density ρ is related to n and the mean molecular weight per electron, μ_e, by

$$\rho = n \mu_e m_H , \tag{3}$$

where m_H is the mass of the proton.

The pressure P can be written as

$$P = A f(x) \left[1 + 4\pi^2 \left(\frac{kT}{mc^2} \right)^2 \frac{x(x^2+1)^{1/2}}{f(x)} + \dots \right], \tag{4}$$

if

$$A = \frac{\pi m^4 c^5}{3h^3} \quad \text{and} \quad f(x) = x(2x^2-3)(x^2+1)^{1/2} + 3 \sinh^{-1} x . \tag{5}$$

In terms of the same variable, the internal energy E per unit volume is given by

$$E = A g(x) \left[1 + 4\pi^2 \left(\frac{kT}{mc^2} \right)^2 \frac{(3x^2+1)(x^2+1)^{1/2} - (2x^2+1)}{x g(x)} + \dots \right], \tag{6}$$

where

$$g(x) = 8x^3[(x^2+1)^{1/2} - 1] - f(x). \tag{7}$$

In all these expressions, the terms in T^2 are very small and are usually neglected.

If we denote by δr, the displacement of a small element of matter in the course of a perturbation and by primes the corresponding Eulerian variations, the equation of continuity can be written in the form

$$\rho' = -\rho \operatorname{div} \delta r - \delta r \cdot \operatorname{grad} \rho ; \tag{8}$$

[5] R. E. Marshak, *Ap. J.*, **92**, 321, 1940.

[6] A. Eddington, *M.N.*, **99**, 575, 1939; Hoyle, *op. cit.*, p. 253.

[7] S. Chandrasekhar, *An Introduction to the Study of Stellar Structure* (Chicago: University of Chicago Press, 1939), chaps. x and xi.

and the equation of conservation of energy per unit volume is

$$E' + (E+P)\operatorname{div}\delta\mathbf{r} + \delta\mathbf{r}\cdot\operatorname{grad}E = -\frac{i}{\sigma}[(\rho\epsilon)' - \operatorname{div}\mathbf{F}'], \tag{9}$$

where ϵ is the rate of generation of energy per unit mass and $\mathbf{F}$ is the total flux due to radiation and conduction.

For adiabatic pulsations the right-hand member of equation (9) cancels out, and it can easily be seen from Paper I and the preceding definitions that, neglecting small terms in T^2, the left-hand member expressed in terms of P' and ρ' reduces to

$$P' = \Gamma_P \frac{P}{\rho}\rho', \tag{10}$$

where

$$\Gamma_P = \frac{8x^3}{3(x^2+1)^{1/2}f(x)} \tag{11}$$

This corresponds to the fact that, to the same degree of approximation, matter inside a white dwarf can be considered as autobarotropic.

In that case it was shown in Paper I that the differential equation for adiabatic radial pulsations in terms of $\xi = \delta r/r$, can be written

$$F(\xi) \equiv \frac{d}{dr}\left(\Gamma_P P r^4 \frac{d\xi}{dr}\right) + \xi\left\{\sigma^2\rho r^4 + r^3\frac{d}{dr}[(3\Gamma_P - 4)P]\right\} = 0, \tag{12}$$

in perfect analogy to the case of gaseous stars,[8] which immediately justifies formula (1) for the frequency of the fundamental mode.

As Γ_P tends toward $\frac{5}{3}$ when x tends toward zero, equation (12) goes over continuously into the ordinary equation of radial pulsation for a monatomic gas, as it should, when we reach the nondegenerate fringe of the star. The solutions of equation (12), satisfying the boundary conditions,

$$\begin{aligned} \delta r &= 0 \quad \text{at} \quad r = 0, \\ P' + \delta\mathbf{r}\cdot\operatorname{grad}P &= 0 \quad \text{at} \quad r = R, \end{aligned} \tag{13}$$

form a complete set of orthogonal functions with respect to $\rho r^4 \delta r$.

For nonadiabatic pulsations we must use the complete equation of conservation of energy, and an extra term appears in equation (12), which becomes[9]

$$F(\xi) = -\frac{ir^3}{\sigma}\frac{d}{dr}\{(\Gamma_T - 1)[(\rho\epsilon)' - \operatorname{div}\mathbf{F}']\}, \tag{14}$$

where

$$\Gamma_T = \frac{4x^2+5}{3(x^2+1)}. \tag{15}$$

Physically, Γ_T relates the variations of temperature T' to the variations of density ρ' in the case of an adiabatic modification. Indeed, if, in equation (8) and in the left-hand member of equation (9) equaled to zero, we express ρ' and E' in terms of x' and T' and replace E and P by their values in equations (4) and (6), taking the terms in T^2 into consideration, we obtain

$$T' = (\Gamma_T - 1)\frac{T}{\rho}\rho' + \delta r\left[(\Gamma_T - 1)\frac{T}{\rho}\operatorname{grad}\rho - \operatorname{grad}T\right]. \tag{16}$$

[8] P. Ledoux and C. L. Pekeris, *Ap. J.*, **94**, 124, 1941.

[9] S. Rosseland, *The Pulsation Theory of Variable Stars* (Oxford: Clarenden Press, 1949), chap. ii.

Again Γ_T tends to $\frac{5}{3}$ when x tends to zero, so that the right-hand member of equation (14) also goes over continuously into the corresponding expression for monatomic gas, when we reach the gaseous envelope of the white dwarfs.

Using the orthogonality properties of the solutions of equation (12) and the perturbation method,[10] one finds, for the perturbation σ' of σ due to the second member of equation (14), the following expression:

$$\sigma' = \frac{1}{2i\sigma^2} \int_0^R \frac{d}{dr} \{ (\Gamma_T - 1) [(\rho\epsilon)' - \operatorname{div} \boldsymbol{F}'] \} \, r^3 \xi \, dr .$$

Hence the condition of vibrational stability is

$$\int_0^R \frac{d}{dr} \{ (\Gamma_T - 1) [(\rho\epsilon)' - \operatorname{div} \boldsymbol{F}'] \} \, r^3 \xi \, dr < 0 .$$

It is somewhat more practical to express this condition in Lagrangian co-ordinates, using $m(r)$ as an independent variable. After an integration by parts and denoting variations following the motion by δ, we have

$$\delta f = f' + \delta r \frac{df}{dr}, \tag{17}$$

and the condition of vibrational stability becomes

$$\int_0^M (\Gamma_T - 1) \frac{\delta\rho}{\rho} \, \delta \left[\epsilon - \frac{d(4\pi r^2 F)}{dm} \right] dm < 0 , \tag{18}$$

which is the form in which this condition will be applied in the following paragraph.

III. EXPLICIT EXPRESSIONS OF THE DIFFERENT QUANTITIES IN EQUATION (18) FOR DEGENERATE AND NONDEGENERATE MATTER

For the sake of simplicity we shall suppose that a white dwarf can be considered as composed of a large, completely degenerate core of mass M_d and a gaseous envelope.

We have to express $\delta\epsilon$, $\delta[d(4\pi r^2 F)/dm]$, etc., explicitly for degenerate and nondegenerate matter. The necessary algebra is much simplified by the property of ξ discovered in Paper I, where it was shown that, for all practical purposes, ξ can be considered a constant in a typical white dwarf. The special behavior of ξ, illustrated in Figure 1, results from the small central condensation of these configurations and the regular increase of Γ_P from the center toward the surface.

Treating ξ as a constant, equations (8) and (16), using the transformation (17), become

$$\frac{\delta\rho}{\rho} = -3\xi , \tag{19}$$

$$\frac{\delta T}{T} = (\Gamma_T - 1) \frac{\delta\rho}{\rho} = -(\Gamma_T - 1) 3\xi . \tag{20}$$

For nuclear reactions, ϵ can be written as

$$\epsilon = \epsilon_0 \rho T^\nu$$

and its variation is given by

$$\frac{\delta\epsilon}{\epsilon} = \frac{\delta\rho}{\rho} + \nu \frac{\delta T}{T} = -3\xi [1 + \nu(\Gamma_T - 1)] , \tag{21}$$

[10] Rosseland, *op. cit.*, chap. iv, § 2.

where Γ_r is given by equation (15) in the degenerate part and is equal to $\frac{4}{3}$ in the gaseous envelope.

The radiative flux, F_R, is given by

$$F_R = -\frac{4\pi c r^2}{\kappa_R}\frac{dp_R}{dm}, \tag{22}$$

where $p_R = \frac{1}{3}aT^4$ is the pressure of radiation.

But in the degenerate core the flux due to the electronic conductivity, λ, becomes very important, and we can define a coefficient of conductive opacity $\kappa_C = 4acT^3/3\rho\lambda$ such that the total flux becomes

$$F = F_R + F_C = -\frac{4\pi r^2 c}{\kappa}\frac{dp_R}{dm}, \tag{23}$$

where the total opacity, κ, is defined by $\kappa^{-1} = \kappa_C^{-1} + \kappa_R^{-1}$. Because of the different roles played by the conductivity in the core and the envelope, it seems best to compute the perturbation of F separately for each region.

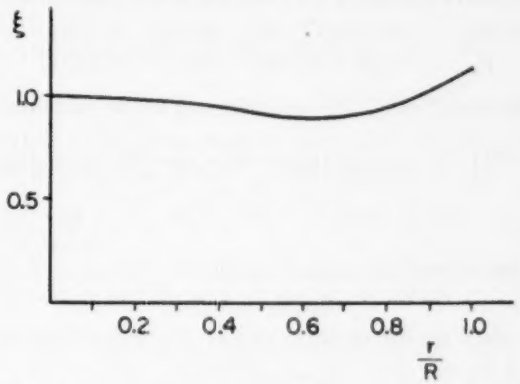

FIG. 1.—The variation in the amplitude of adiabatic pulsation of white dwarf star

a) DEGENERATE CORE

For this region the expressions given by Kothari[11] are quite sufficient for our purpose, and we can write them

$$\kappa_R = \alpha T^{-2} \quad \text{and} \quad \kappa_C = \frac{\alpha}{\beta}\frac{T^2}{\rho^2}\ln Q \tag{24}$$

and

$$F_C = \beta F_R \frac{\rho^2 T^{-4}}{\ln Q}, \tag{25}$$

where

$$Q = 1 + \vartheta\rho^{2/3}, \tag{26}$$

α, β, and ϑ being constants whose numerical values do not interest us at present.

From equation (22), using equations (19), (20), and (24) and the definition of p_R, we obtain, after some transformations,

$$\frac{\delta F_R}{F_R} = 2\xi\left[\frac{Tx}{(x^2+1)^2}\frac{dx}{dT} - \frac{2x^2+5}{x^2+1}\right]. \tag{27}$$

[11] *M.N.*, **13**, 61, 1932.

On the other hand, dividing the hydrostatic equation

$$\frac{dP}{dr} = \frac{8Ax^4}{(x^2+1)^{1/2}}\frac{dx}{dr} = -\frac{Gm(r)}{r^2}\rho$$

by equation (23), we get

$$\frac{dx}{dT} = \frac{2\pi acG}{3A}\frac{M}{L}\frac{T^3}{\kappa}\frac{(x^2+1)^{1/2}}{x^4}\frac{m(r)/M}{L(r)/L}, \tag{28}$$

where $L(r)$ is the total flux $4\pi r^2F$ across the sphere of radius r, L is the luminosity of the star, and M its total mass.

The variation of F_C, according to equation (25), is

$$\frac{\delta F_C}{F_C} = \frac{\delta F_R}{F_R} - 4\frac{\delta T}{T} + 2\frac{\delta\rho}{\rho}\left[1 + \frac{1-Q}{3Q\ln Q}\right],$$

which, on introduction of the values (19), (20), and (27), reduces to

$$\frac{\delta F_C}{F_C} = 2\xi\left[\frac{Tx}{(x^2+1)^2}\frac{dx}{dT} - \frac{3x^2+4}{x^2+1} - \frac{1-Q}{Q\ln Q}\right]. \tag{29}$$

Combining equations (27) and (29), we finally get, for the variation of the total flux,

$$\delta(4\pi r^2F) = 8\pi r^2F\xi\left[1 + \frac{Tx}{(x^2+1)^2}\frac{dx}{dT} - \frac{(3x^2+4)(\kappa_R/\kappa_C) + 2x^2 + 5}{(1+\kappa_R/\kappa_C)(x^2+1)} + \frac{(Q-1)(\kappa_R/\kappa_C)}{Q\ln Q(1+\kappa_R/\kappa_C)}\right], \tag{30}$$

where dx/dT has the value given in equation (28).

b) GASEOUS ENVELOPE

Here we shall adopt for the radiative opacity the general form of Kramer's law,

$$\kappa_R = \kappa_0\rho^n T^{-s}; \tag{31}$$

and, for the sake of generality, we shall still take into account the possible influence of conduction, again using Kothari's expression for F_c in nondegenerate matter,

$$F_C = \beta' F_R\frac{\rho^2 T^{-4}}{\ln S} \quad \text{or} \quad \kappa_C = \frac{\kappa_R}{\beta'\rho^2}T^4\ln S, \tag{32}$$

where

$$S = 1 + \vartheta' T^2\rho^{-2/3}. \tag{33}$$

Proceeding as before and taking $\Gamma_r = \gamma = \frac{5}{3}$ in equation (20), we have

$$\delta F_R = 2\xi F_R[1 + \tfrac{3}{2}n - (s+4)]; \tag{34}$$

and, after evaluating δF_C from equation (32), we finally obtain

$$\delta(4\pi r^2F) = 8\pi r^2F\xi\left[2 + \tfrac{3}{2}n - (s+4) + \frac{(\kappa_R/\kappa_C)[1 + (S-1)/S\ln S]}{1+\kappa_R/\kappa_C}\right]. \tag{35}$$

IV. APPLICATIONS

As we mentioned in the introduction, the question of the generation of energy in white dwarfs raises many difficulties. If thermonuclear reactions are adopted, the two following

cases have been considered. In the first one, the abundances of the elements, although particular, are uniform through the star, and, owing to the greater densities, the reactions take place mainly in the internal part of the degenerate core.[5] Depending on the presence or absence of carbon and nitrogen, the determining process will be the carbon cycle or the proton-proton reaction, although for the latter some uncertainty exists.

In the other case[12] the core is practically devoid of hydrogen, which is supposed to be concentrated in the gaseous envelope. The transition region is very narrow, and in it hydrogen and heavy elements occur simultaneously in rapidly varying proportions. This zone can be the seat of nuclear reactions such as the carbon cycle. If the abundances of C and N were everywhere extremely low, the proton-proton reaction could still be of interest in the transition region and at the base of the gaseous envelope. It is not our purpose here to discuss the origin of such a stratification, but, although there are serious difficulties to account for it either by gravitational separation or evolutionary exhaustion, it has, however, the advantage, from the point of view of instantaneous hydrostatic equilibrium, of introducing some quantitative agreement without resorting to anomalous abundances. These two cases will be discussed separately.

a) GENERATION OF ENERGY IN THE DEGENERATE CORE

The part of the integral in condition (18) depending on the generation of energy in which we introduce equations (19) and (21) reduces to

$$(3\xi)^2[\overline{(\Gamma_T-1)}+\nu\overline{(\Gamma_T-1)^2}]\int_0^{M_d}\epsilon_0 dm=(3\xi)^2[\overline{(\Gamma_T-1)}+\nu\overline{(\Gamma_T-1,^2]}L\,, \tag{36}$$

where the mean values are computed with respect to ϵ,

$$\overline{(\Gamma_T-1)}=\int_0^{M_d}(\Gamma_T-1)\epsilon\, dm\,, \qquad \text{etc.} \tag{37}$$

On the other hand, integrating the second term in condition (18) by parts and taking into account the boundary conditions at the center, we obtain

$$\int_0^M(\Gamma_T-1)\frac{d\,\delta(4\pi r^2F)}{dm}\frac{\delta\rho}{\rho}\,dm=-\tfrac{2}{3}[\delta(4\pi r^2F)\,3\xi]_M + 3\xi\int_0^M\delta(4\pi r^2F)\,d(\Gamma_T-1)\,,$$

or, since Γ_T is a constant in the gaseous envelope,

$$\int_0^M(\Gamma_T-1)\frac{d\,\delta(4\pi r^2F)}{dm}\frac{\delta\rho}{\rho}\,dm=-\tfrac{2}{3}[\delta(4\pi r^2F)\,3\xi]_M - 3\xi\int_0^{M_d}\delta(4\pi r^2F)\frac{2x\,dx}{3(x^2+1)^4}. \tag{38}$$

We must now introduce the appropriate values for $\delta(4\pi r^2F)$ in equation (38), i.e., expression (35), where (κ_R/κ_C) is negligible in the integrated part, and expression (30), where (κ_R/κ_C) and Q can be considered as very large compared to 1, in the last integral. Then, grouping expressions (36) and (38), the condition of vibrational stability for this case can be written

$$9\xi^2L\left\{\overline{(\Gamma_T-1)}+\nu\overline{(\Gamma_T-1)^2}+\tfrac{2}{5}[4+3n-2(s+4)] + \tfrac{4}{3}\int_0^{M_d}\frac{L(r)}{L}\frac{x\,dx}{3(x^2+1)^2}\left[\frac{Tx}{(x^2+1)^2}\frac{dx}{dT}-2-\frac{1}{x^2+1}+\frac{1}{\ln Q}\right]\right\}\leqslant 0\,. \tag{39}$$

[12] C. L. Critchfield, *Ap. J.*, **96**, 1, 1942; E. Schatzman, *Ann. d'ap.*, **8**, 143, 1945.

b) GENERATION OF ENERGY AT THE INTERFACE BETWEEN THE DEGENERATE CORE AND THE GASEOUS ENVELOPE

We will suppose that the generation of energy takes place in a thin layer at the base of the gaseous envelope. In that case the contribution of the generation of energy to condition (18) reduces to

$$\int_{M_d}^{M} \tfrac{2}{3}\,\delta\epsilon\,\frac{\delta\rho}{\rho}\,dm = 9\xi^2\tfrac{2}{3}\,[1+\tfrac{2}{3}\nu]L\,. \tag{40}$$

In equilibrium the degenerate core should be isothermal, since there is no generation of energy in it, and the equilibrium flux F in that region should be zero. During the pulsation there will appear a gradient of temperature equal to

$$\frac{d\,(T+\delta T)}{dm} = \frac{d\,\delta T}{dm} = -3\,\xi T\,\frac{d\Gamma_T}{dm}\,; \tag{41}$$

and, according to equation (23), the corresponding flux δF will be given by

$$\delta F = \frac{16\pi r^2 c}{\kappa}\,aT^4\xi\,\frac{d\Gamma_T}{dm} \tag{42}$$

or, since F is equal to zero,

$$\delta\,(4\pi r^2 F) = \frac{16\pi r^2 c\,aT^4\xi}{\kappa\rho}\,\frac{d\Gamma_T}{dr}\,. \tag{43}$$

One can easily prove that one recovers the same expression from the general equation (30) by keeping only the term containing the indeterminate product $F(dx/dT)$ and using equations (28) and (29) and the definition of Γ_T.

In the gaseous envelope, $\delta(4\pi r^2 F)$ is still given by equation (35). Integrating by parts the term depending on the flux in condition (18), we again obtain equation (38), since it can be shown that $\delta(4\pi r^2 F)$ is still continuous across the boundary of the degenerate core.

But now we must introduce expression (43) for $\delta(4\pi r^2 F)$ in the integral of equation (38), while the integrated part reduces to the same expressions as before, so that the condition of vibrational stability becomes

$$\xi^2 L\left[\,6n-4s-2+4\nu-\int_0^{M_d}\frac{48\pi^2 c\,a}{L}\,\frac{T^4 r^4}{\kappa\rho}\left(\frac{d\Gamma_T}{dr}\right)^2 dr\,\right] \leq 0\,. \tag{44}$$

The last term contributes to the stability of the star, but we shall see that it is practically negligible. The position of the generation of energy is not very critical either, provided that it is near enough to the surface so that the effective ratio of specific heats is close to its value $\frac{5}{3}$.

V. NUMERICAL RESULTS

The application of these formulae requires the use of a model, and we took for that purpose the model ($M = 1.95 \times 10^{33}$ gm, $L = 9.72 \times 10^{31}$ erg/sec, $R = 5.7 \times 10^{10}$ cm) computed by Marshak.[5] The corresponding values of Γ_T and some other of the expressions appearing in conditions (39) and (44) are collected in Table 1. The numerical value of ϑ in Q (eq. [26]) was taken equal to 3.10^{-3}, and κ in condition (44) reduces in practice to κ_C as given by equation (24), where $(\alpha/\beta) = 3.5 \times 10^{-6}$.

The numerical value of the integral in condition (39) turns out to be -0.17, while the integral in condition (44), taken with its sign, is of the order of -0.03. This shows that these integrals play only a secondary role as compared to the other terms; this is not

peculiar to this model but would remain true for all white dwarfs, because these integrals arise only from the rate of variation of Γ_T in the star, which is slight in any case.

Taking into account the fact that, for the distribution of temperature found by Marshak, ϵ varies in the star practically as ρ, the mean values of $(\Gamma_T - 1)$ and $(\Gamma_T - 1)^2$ are

$$\overline{\Gamma_T - 1} = 0.41 \quad \text{and} \quad \overline{(\Gamma_T - 1)^2} = 0.168 .$$

With these values and adopting for n and s the values corresponding to Kramer's law, $n = 1$, $s = 3.5$, conditions (39) and (44) give the following critical values, ν_c, of ν:

a) Generation of energy in the core:

$$\nu \leqslant (\nu_c)_1 = 9.5 . \tag{45}$$

TABLE 1

$m(r)/M$	x	ρ/ρ_c	$T\times 10^{-6}$	Γ_T	$2\pi/3(x^2+1)^2$	$L(r)/L$
0.000	2.425	1.000	15.20	1.3818	0.03416	0.000
.0045	2.409	0.980	15.20	1.3823	.03471	0.003
.0214	2.367	0.930	15.20	1.3838	.03620	0.022
.0562	2.297	0.850	15.20	1.3861	.03888	0.069
.111	2.205	0.752	15.20	1.3902	.04278	0.138
.184	2.094	0.644	15.18	1.3952	.04816	0.228
.272	1.971	0.537	15.16	1.4016	.05507	0.344
.370	1.839	0.436	15.14	1.4094	.06387	0.470
.471	1.702	0.346	15.11	1.4188	.07466	0.587
.569	1.563	0.268	15.07	1.4302	.08787	0.690
.662	1.425	0.203	15.03	1.4438	.1034	0.782
.745	1.291	0.151	14.98	1.4583	.1210	0.855
.817	1.158	0.109	14.91	1.4761	.1408	0.920
.875	1.029	0.0765	14.83	1.4954	.1618	0.958
.922	0.9039	0.0518	14.73	1.5168	.1825	0.980
.956	0.7801	0.0333	14.60	1.5408	.2010	0.986
.979	0.6571	0.0199	14.45	1.5662	.2137	0.990
.992	0.5293	0.0104	14.10	1.5937	.2158	1.000
0.999	0.3940	0.00429	13.60	1.6196	0.1982	1.000

b) Generation of energy in a shell close to the surface:

$$\nu \leqslant (\nu_c)_2 = 2.6 . \tag{46}$$

As the values $\overline{\Gamma_T - 1}$ and $\overline{(\Gamma_T - 1)^2}$ depend on the values reached by x toward the center of the star, they could vary with the mass of the star considered, and the value of $(\nu_c)_1$ would be a little smaller for smaller masses (x smaller at the center) and a little larger for larger masses (x larger at the center). The maximum value of $(\nu_c)_1$ is about 13 and corresponds to a configuration very close to the critical mass of Chandrasekhar. Otherwise, the integrals in conditions (39) and (44) being small, these critical values of ν_c will remain good approximations for practically all white dwarfs.

VI. THE EFFECTIVE VALUE ν_e OF THE EXPONENT OF THE TEMPERATURE IN THE LAW OF GENERATION OF ENERGY IN A PULSATING WHITE DWARF

If we consider a chain of nuclear reactions comprising n combinations and m disintegrations, the generation of energy per unit mass can be written

$$\epsilon = \frac{1}{\bar{m}} \left(\sum_{i=1}^{n} K_i x_p x_q N \epsilon_i + \sum_{j=1}^{m} \lambda_j x_j \epsilon_j \right), \tag{47}$$

where N is the total number of particles per unit volume and $\bar{m}$ is the average mass of a particle; x_p and x_q are the abundances by number of particles of kinds p and q involved in the i reaction and $K_i x_p x_q N^2$ is the number of these reactions per unit volume and unit time. The probability of disintegration of the j element is λ_j, and ϵ_i and ϵ_j are the corresponding energies liberated. The K_i's depend only on temperature, and during a pulsation they will vary according to the law

$$K_i = K_i^0\left(1 + \nu_i \frac{\delta T}{T}\, e^{i\sigma t}\right), \tag{48}$$

while the λ_j's are independent of temperature and remain constant. The variations of N can, with a very good approximation, be represented by

$$N = N_0\left(1 + \frac{\delta \rho}{\rho}\, e^{i\sigma t}\right). \tag{49}$$

Eddington pointed out that, if the abundances x_i do not remain in phase with the pulsation, this could introduce delays in the generation of energy which might affect considerably the stability of the star. S. Rosseland and G. Randers,[13] starting from the equations of continuity for each element involved in the chain and equation (49), studied the form of the solutions for the x_i's and stressed in particular the importance for this question of the ratio of the mean lives of the disintegrating elements to the period of pulsation.

Bethe[14] showed that, in the case of the carbon cycle, these effects would be negligible for ordinary stars, while in the case of the proton-proton reaction they would decrease or increase considerably the value of ν with respect to its hydrostatic value, according to whether the period of pulsation is smaller or larger than the mean life of Be^7.

For the model of Sirius B treated here, a period P of the order of 10 seconds was found in Paper I, and in a first approximation we can find the period for any other model by using the relation $P\sqrt{\bar{\rho}} = \text{Constant}$ where $\bar{\rho}$ is the mean density.

a) THE CARBON CYCLE

In this case, there are two radioactive disintegrations,

$$N^{13} \rightarrow C^{13} + \epsilon^+ \qquad \text{and} \qquad O^{15} \rightarrow N^{15} + \epsilon^+ ,$$

the mean lives of N^{13} and O^{15} being, respectively, of the order of 10 and 2 minutes. The mean life of the other elements can be obtained by multiplying the values given by Bethe[15] for the sun by a factor $(\rho x_H \tau^2 e^{-\tau})_\odot/(\rho x_H \tau^2 e^{-\tau})$, where x_H is the abundance of hydrogen and τ is the quantity defined by Bethe and is inversely proportional to $T^{1/3}$. As the generation of energy per unit mass is directly proportional to $\rho x_H \tau^2 e^{-\tau}$ and since it must be much less in a white dwarf than in the sun, one has to take abundances of hydrogen small enough to render the ratio $(\rho x_H \tau^2 e^{-\tau})_\odot/\rho x_H \tau^2 e^{-\tau})$ much greater than 1. Hence the mean lives of these elements will be longer in a white dwarf than in the sun.

Even if the reactions take place in a shallow layer near the surface, the mean lives of these elements will still be at least as long as in the sun, so that in all cases the abundances of C^{12}, C^{13}, N^{14}, and N^{15} can be treated as constant during periods of time long compared to the periods of pulsations.

As far as the two disintegrations are concerned, the energy liberated is so small that

[13] *Astrophysica Norvegica*, **3**, 71, 1933; cf. also S. Rosseland, *op. cit.*, chap. v, §§ 3, 4, 5.

[14] *Phys. Rev.*, **55**, 434, 1939.

[15] For corrections to the original values cf. H. A. Bethe, *Ap. J.*, **92**, 118, 1940, and W. A. Fowler and R. N. Hall, *Phys. Rev.*, **74**, 1558, 1948.

it does not matter much whether it is delayed or not with respect to the pulsation, and for all practical purposes we can neglect the second term in the right-hand member of equation (47). Denoting the rate of generation of energy in equilibrium by ϵ_0, this equation can then be written

$$\epsilon = \epsilon_0\left[1+\left(\frac{\epsilon_1+\epsilon_3+\epsilon_4+\epsilon_6}{\epsilon_1+\epsilon_2+\epsilon_3+\epsilon_4+\epsilon_5+\epsilon_6}\right)\frac{\delta\rho}{\rho}\,e^{i\omega t}+\left(\frac{\epsilon_1\nu_1+\epsilon_2\nu_2+\epsilon_4\nu_4+\epsilon_6\nu_6}{\epsilon_1+\epsilon_2+\epsilon_3+\epsilon_4+\epsilon_5+\epsilon_6}\right)\frac{\delta T}{T}\,e^{i\omega t}\right], \quad (50)$$

which is strictly correct when the period of pulsation is shorter than the mean lifetime of N^{13} and O^{15}, which is the case in white dwarfs. As we have already said, the energies ϵ_2 and ϵ_5 liberated by the disintegrations are so small that we can put the coefficient of $\delta\rho/\rho$ equal to 1.

Taking into account the variations of τ and ν with the range of temperatures to which the formula must apply and using the integrations of Marshak,[5] one finds for ν_ϵ, which is the coefficient of $\delta T/T$ in equation (50), the following values: for Sirius B, generation of energy in the central region, $\nu_\epsilon = 19$, and generation of energy in an external shell, $\nu_\epsilon = 22$; for 40 Eridani B, generation of energy in the central region, $\nu_\epsilon = 15$, and generation of energy in an external shell, $\nu_\epsilon = 22$.

The temperatures obtained by Marshak are undoubtedly too high, since they correspond to a negligible helium content, while one would normally expect a fairly high abundance of helium in a star having very little hydrogen left. Increasing the abundance of helium would decrease the temperature, and this, in turn, would again increase the values of ν_ϵ. It does not seem possible to imagine cases where ν_ϵ could be smaller than, say, the value given for the central region of 40 Eridani B.

b) THE PROTON-PROTON REACTION

In this case, since the mean life $\Lambda(Li^7)$ of Li^7 tends to be very short, the mean life $\Lambda(Be^7)$ of Be^7, from which Li^7 results by electron capture, plays a determining role in the evaluation of ν_ϵ.

The probability of capture of an electron by Be^7 in a white dwarf is proportional in a first approximation to

$$NW^2\left[1+\frac{g(x)}{4Wx^3}+\frac{1}{W^2}\left\{[(1+x^2)^{1/2}-1]^2-\frac{2}{5}x^2+\frac{f(x)}{4x^3}\right\}\right], \quad (51)$$

where $x = p_0/mc$ has the same meaning as before and $g(x)$ and $f(x)$ are the functions defined by equations (5) and (7) and tabulated by Chandrasekhar on page 361 of his book. The energy W is measured in units of mc^2, m being the rest-mass of the electron, and is equal to

$$W = \frac{1}{m}[m(Be^7) - m(Li^7)] + 1,$$

where $m(Be^7)$ and $m(Li^7)$ are the masses of the corresponding nuclei. The factor multiplying NW^2 in equation (51) can be taken equal to 1 in the external part of a white dwarf, where x is small; and for $x = 2$, 5, and 10 it takes, respectively, the values 2.3, 7, and 24. The ratio of the number of electrons, N, in a white dwarf poor in hydrogen to the number of electrons in the sun is given by

$$\frac{N}{N_\odot} = \frac{\rho}{\rho_\odot(1+x_H)_\odot}. \quad (52)$$

As Bethe gives 14 months for $\Lambda(Be^7)$ at the center of the sun, one easily computes from equations (51) and (52) that its value at the center of Sirius B is $\Lambda(Be^7) \simeq 65$

seconds. In the transition region between the degenerate core and the gaseous envelope $\Lambda(Be^7) \simeq 2$ days.

On the other hand, again using the model computed by Marshak, one finds $\Lambda(Li^7) = 60$ seconds, just as at the center of the sun, the corresponding quantity $(\rho x_H T^2 e^{-\tau})$ being about the same in both cases. If the generation of energy takes place in an external shell with a high abundance of hydrogen, one finds $\Lambda(Li^7) \simeq 90$ seconds.

The period of pulsation of Sirius B being of the order of 10 seconds, one finds by integrating the equations of continuity that the abundances x_1, x_2, x_4, x_5 of H, He^3, Be^7, and Li^7 can again be considered as constant and equal to their original values, while the abundance x_3 of H^2, which has an extremely short life—smaller than 1 second—is given by

$$x_2 = \frac{K_1^0 x_1}{K_2^0}\left[1 + (\nu_1 - \nu_2)\frac{\delta T}{T}\, e^{i\sigma t}\right]. \tag{53}$$

Introducing these abundances into the corresponding equation (47), one gets

$$\epsilon = \epsilon_0\left[1 + \left(\frac{\delta\rho}{\rho}\right) e^{i\sigma t} + \frac{(\epsilon_1+\epsilon_2)\nu_1 + \epsilon_3\nu_2 + \epsilon_5\nu_5}{(\epsilon_1+\epsilon_2+\epsilon_3+\epsilon_4+\epsilon_5)}\frac{\delta T}{T}\, e^{i\sigma t}\right]. \tag{54}$$

Using the appropriate values in the coefficient of $(\delta T/T)$, one finds, for the center of Sirius B,

$$\nu_e = 10.7\ .$$

The case of the external layer is similar, since the Λ's, except Λ_2, are still all larger than the period of pulsation.

In the case of 40 Eridani B, if we take for the temperature the values computed by Marshak, we find

$$\Lambda(Be^7) \simeq 20 \text{ minutes}\ , \qquad \Lambda(Li^7) \simeq \tfrac{1}{2} \text{ second}\ ,$$

while the period of pulsation is approximately equal to 40 seconds. Thus $\Lambda(Li^7)$ is now smaller than the period, and the abundance x_5 of Li^7 can no longer be treated as a constant but is given in a first approximation by

$$x_5 = x_5^0\left[1 - \nu_5\frac{\delta T}{T}\, e^{i\sigma t}\left(1 - \frac{2\pi i \Lambda Li^7}{P}\right)\right]. \tag{55}$$

Introducing expressions (53) and (55) into the corresponding equation (47) and treating the other abundances as constant, we obtain in this case

$$\epsilon = \epsilon_0\left\{1 + \frac{\delta\rho}{\rho}\, e^{i\sigma t} + \frac{\delta T}{T}\, e^{i\sigma t}\left[(\epsilon_1+\epsilon_2)\nu_1 + \epsilon_3\nu_2 + \epsilon_5\nu_5\frac{2\pi i \Lambda Li^7}{P}\right]\right\}. \tag{56}$$

The last term in the coefficient of $\delta T/T$ can be neglected in any case, since it is out of phase by 90° and cancels out in the course of a period. The value of ν_e is now much smaller and equal to 1.8.

In the external regions of 40 Eridani B, $\Lambda(Li^7)$ becomes much larger and of the order of 120 seconds, i.e., larger than the period of pulsation, and ϵ is again given by formula (54), ν_e again being of the order of 10–11.

We must notice, however, that, as we mentioned before, the temperatures given by Marshak are probably too high. A large abundance of helium would reduce the central

temperature of 40 Eridani B by a factor of the order of $\frac{1}{2}$, and this would bring back $A(Li^7)$ to a value greater than the period of pulsation and ν_e to a value of the order of 10–11. In Sirius B a large abundance of helium would also increase slightly the value of ν_e.

VII. CONCLUSIONS

We have collected the main results of the preceding discussion in Table 2. A comparison between the values of ν_e for the carbon cycle and the critical values ν_c shows immediately that this reaction cannot take place inside a white dwarf either at the center or in the external layers. The same applies for the proton-proton reaction, as far as the external layers are concerned. In the interior of Sirius B the value of ν_e and ν_c for this reaction are very close, and our computations are perhaps not precise enough to be absolutely sure of the sign of $(\nu_e - \nu_c)$. However, in any case, the margin of stability would be very small.

TABLE 2

VALUES OF ν_e AND ν_c

Star and Region of Generation of Energy	Effective Values of $\nu = \nu_e$ for the Carbon Cycle	Effective Values of $\nu = \nu_e$ for the Proton-Proton Reaction	Critical Values of $\nu = \nu_c$
Sirius B:			
Central region	19	10.7	9.5
External shell	22	11	2.6
40 Eridani B:			
Central region	15	1.8	9.5
External shell	22	11	2.6
40 Eridani B:			
Central region, large amount of helium	19	11	9.5

In 40 Eridani B we see that, if the helium content is negligible, the proton-proton reaction could, in fact, take place toward the center without endangering the stability. However, it seems likely that the helium abundance will be large, and, as we saw before, in that case the value of ν_e becomes again of the order of 10–11.

In the preceding discussion, when we referred to the proton-proton reaction, we always assumed that the Gamow-Teller selection rules were applicable. If one reverted to the primitive Fermi rules, the reaction would become less probable by a factor of the order of 10^6. In that case and if C and N were absent from the star, the necessary abundance of H to explain the generation of energy would turn out to be much larger and of the same order as in ordinary stars. But this, in turn, would reduce considerably the central temperature and also the density, so that the mean life of Li^7 would again become larger in all cases than the period of pulsation, and the corresponding values of ν_e would tend again to values of the order of 10–12, bringing about vibrational instability. The critical values of ν_c will change very little from one star to another, as the variable terms in equations (39) and (44) are very small.

One can also remark that the period of pulsation decreases as $(\bar{\rho})^{-1/2}$, while the mean life of Be^7 decreases as $(\bar{\rho})^{-1}$; and thus, if we go to white dwarfs of larger and larger densities, the mean life of Be^7 soon becomes smaller than the period of pulsation, and in that

case the value of ν_e for the proton-proton reaction is at least of the order of 11 or 12 in all cases. For instance, in the case of the white dwarf (AC 70°8247), taking the value of ρ given by S. Chandrasekhar,[16] one finds that $\Lambda(Be^7)$ is reduced to 1.5 seconds, while the period of pulsation is 3 seconds. Thus, altogether, it appears extremely unlikely that nuclear reactions could be the source of the energy radiated by white dwarfs.

[16] *Op. cit.*, p. 431.

HYDROGEN CONTENT AND ENERGY-PRODUCTIVE MECHANISM OF WHITE DWARFS

T. D. LEE
Department of Physics, University of Chicago*
Received January 9, 1950

ABSTRACT

The equilibrium states of white dwarf stars of arbitrary mass and chemical composition are discussed. An improved expression for electronic conductivity and free electron density in the intermediate degenerate state is derived. It is found that no appreciable amount of hydrogen can exist in any white dwarf star. The upper limit of hydrogen concentration (by weight) in the interior of a star having the mass of the sun is found to be 4×10^{-3} even in the absence of the carbon cycle. The corresponding value for stars of half the mass of the sun is 4.6×10^{-4}.

Investigations on stability show that a white dwarf star cannot live on the nuclear energy produced in its interior. The alternate mechanism of energy produced in the envelope is discussed. The equilibrium distribution of hydrogen in the envelope is also calculated. From this the observed fact of strong hydrogen lines in the spectrum of white dwarfs is explained.

It has been shown by R. E. Marshak,[1] by using the existing knowledge of thermonuclear processes and the experimental data on the mass and luminosity of Sirius B and 40 Eridani B, that no appreciable hydrogen content can exist in either star. The purpose of this paper is to generalize Marshak's result; to see whether an equilibrium state exists for a dwarf star of arbitrary mass and chemical composition; to investigate some different possible mechanisms of energy production of the dwarf stars; and, finally, to apply these results to known white dwarfs.

The expressions for various physical quantities, such as gas pressure, free electron density, and opacity, are given in Part I as functions of density, temperature, and chemical composition. The numerical values of some of these quantities are also calculated for the regions that will be of importance. In Part II the equilibrium solutions and the stability of a white dwarf star of arbitrary mass and hydrogen concentration are investigated, and the general conclusion about the upper limit of hydrogen content is reached. It is also proved that no stable white dwarf star can live on nuclear energy produced in its interior. In Part III, some possible mechanisms of energy production are discussed, especially that due to the hydrogen in the surface of a star. Also the distribution of hydrogen under the influence of the gravitational field is calculated in some detail. In the final part (IV), we shall discuss astronomical applications of the above results.

I. GAS PRESSURE; FREE ELECTRON DENSITY AND OPACITY

A. GAS PRESSURE AND FREE ELECTRON DENSITY

The total gas pressure, P, can be expressed as the sum of the partial pressure of the heavy particles and that of the free electrons:[2]

$$P = N_{\text{heavy}} kT + \frac{8\pi}{3}\left(\frac{2m_e}{h^2}\right)^{3/2} \int_0^\infty \frac{E^{3/2} dE}{1 + e^{(E-\mu)/kT}}, \tag{1}$$

where N_{heavy} is the total number of heavy particles per unit volume; μ, the Gibbs free

* Now at the Yerkes Observatory.

[1] *Ap. J.*, **92**, 321, 1940.

[2] Mayer and Mayer, *Statistical Mechanics* (New York: John Wiley & Sons, Inc., 1940), chap. xvi.

energy per electron; h, Planck's constant; k, Boltzmann's constant; T, the temperature of the gas; and m_e the mass of the electron.

The quantity μ is again related to N_e, the total number of free electrons per unit volume, by the relation[2]

$$4\pi\left(\frac{2m_e}{h^2}\right)^{3/2}\int_0^\infty \frac{E^{1/2}dE}{1+e^{(E-\mu)/kT}} = N_e. \tag{2}$$

In our calculations we shall make use of the mathematical tables of McDougall and Stoner;[3] the foregoing equations can be expressed in terms of their F-functions as follows:

$$P = N_{\text{heavy}}kT + \frac{8\pi}{3}\left(\frac{2m_e}{h^2}\right)^{3/2}(kT)^{5/2}F_{3/2}\left(\frac{\mu}{kT}\right) \tag{1'}$$

and

$$N_e = 4\pi\left(\frac{2m_e}{h^2}\right)^{3/2}(kT)^{3/2}F_{1/2}\left(\frac{\mu}{kT}\right), \tag{2'}$$

with

$$F_n(x) \equiv \int_0^\infty \frac{y^n dy}{1+e^{y-x}}. \tag{3}$$

A quite accurate expression for free electron density is necessary for the calculation of the gas pressure. This problem has been treated by various authors.[4] It is customary to neglect entirely the effect of "pressure ionization" when the gas is nondegenerate and to neglect the effect of temperature when the gas is degenerate. Owing to the wide range of density and temperature that will be covered by our subsequent calculations, this approximation is found to be unreliable in some regions.

Let A_i, Z_i, and X_i be, respectively, the atomic weight, charge, and relative abundance by weight of the chemical element i. The number of free electrons per nucleon contributed by that element will be denoted as η_i. We then have

$$N_e = \frac{\rho}{m_H}\sum_i \eta_i X_i \equiv \eta\,\frac{\rho}{m_H} \tag{4}$$

and

$$\eta_i A_i = Z_i - \sum_n \frac{2n^2}{1+e^{(E_n-\mu)/kT}}, \tag{5}$$

with ρ as the mass density; m_H, the mass of proton; η, the average number of free electrons per nucleon; and E_n the binding energy of the electron in the quantum state n.

Since the volume occupied by the atom is given by $(\eta_i A_i)/N_e$, the radius of the atom becomes approximately $R_i = [3(\eta_i A_i)/4\pi N_e]^{1/3}$. In equation (5) we use the approximation of summing over only those electronic orbits having their mean distances to the nucleus less than R_i because the rest of the orbits will not exist. In the expression of E_n, complete screened effect and unscreened effect are used, depending upon whether the orbits inside are filled or empty. For intermediate cases, both calculations are made. A fluctuation of about 2 per cent is observed in the final values of η and will be regarded as the uncertainty of our approximation. There would also be a depression of the lower limit of the energy of the free electron state due to the finite volume occupied by the atom.[5] However, this effect is found to be of no importance here.

Calculations are made by using equations (2), (4), and (5) for all components of

[3] *Phil. Trans. R. Soc. A*, **237**, 96, 1939.

[4] Strömgren, *Zs. f. Ap.*, **4**, 118, 1932; Marshak, *loc. cit.*

[5] P. M. Morse, *Ap. J.*, **92**, 27, 1940.

Russell mixture. The result for η as a function of density and temperature is plotted in Figure 1 for a pure Russell mixture. For $\rho > 10^4$ gm/cm^3, η becomes independent of temperature, and Marshak's[5] result will be used. The corresponding values of η for a mixture of hydrogen, helium, and Russell mixture can be obtained readily by using the fact that both hydrogen and helium can be regarded as completely ionized.

B. ELECTRONIC CONDUCTIVITY AND TOTAL OPACITY

The mechanism of energy transfer in white dwarfs is quite different from that in main-sequence stars. In the nondegenerate region the usual radiative transfer is the dominant factor, but the electronic conductivity becomes extremely important in the degenerate region. In fact, it transfers energy so fast that the main body of the star is practically isothermal. This was first pointed out by Marshak.[1] However, owing to some numerical errors in the calculation,[6] his expression of electronic conductivity is correct only in the extremely degenerate region. A corrected and improved expression of the electronic heat conductivity λ is derived[7] and is given by

$$\lambda = \frac{16 m_e}{3 h^3 e^4 I} k^5 T^4 \left[\frac{g_3 g_4 - g_5^2}{g_3}\right] \quad \text{if} \quad \frac{\mu}{kT} > 0 ,$$

$$\lambda = \frac{16 m_e}{3 h^3 e^4 I} k^5 T^4 \times \left[\frac{\frac{1}{3}\pi^2 (\mu/kT)^6 + \frac{1}{5}\pi^4 (\mu/kT)^4 + \frac{7}{15}\pi^6 (\mu/kT)^2 - (\frac{7}{15}\pi^4)^2 + I'}{(\mu/kT)^3 + (\mu/kT)\pi^2 + g_3}\right] \quad \text{if} \quad \frac{\mu}{kT} > 0 , \tag{6}$$

with

$$g_n = n! \sum_{r=1}^{\infty} (-1)^{r-1} \frac{e^{-r|\mu/kT|}}{r^n} ,$$

and

$$I = \frac{\rho}{m_H} \left\{ \sum_i \frac{X_i Z^2}{A_i} \left[1.183 + \tfrac{1}{2} \ln \left(\tfrac{2}{3} F_{2/3}\left[\frac{\mu}{kT}\right]\right) - \tfrac{5}{6} \ln \left(F_{1/2}\left[\frac{\mu}{kT}\right]\right)\right] + \frac{1}{3} \sum_i \frac{X_i Z_i}{A_i} \ln Z_i \right\} ,$$

$$I' = g_3 \left(\frac{\mu}{kT}\right)^5 + 2 g_4 \left(\frac{\mu}{kT}\right)^4 + (\tfrac{10}{3}\pi^2 g_3 + g_5)\left(\frac{\mu}{kT}\right)^3 + 4\pi^2 g_4 \left(\frac{\mu}{kT}\right)^2 + (\tfrac{7}{3}\pi^4 g_3 + \pi^2 g_5)\frac{\mu}{kT} + \tfrac{14}{15}\pi^4 g_4 + g_3 g_5 - g_4^2 .$$

It is more convenient to introduce the conductive opacity κ_c, defined by

$$\kappa_c = \frac{4 a c T^3}{3 \rho \lambda} , \tag{7}$$

where a is the Stefan-Boltzmann constant and c is the velocity of light. It should be noticed that $\kappa_c T$, thus defined, is a function of μ/kT only. The numerical values of $\kappa_c T$

[6] *Ann. New York Acad. Sci.*, **41**, 49, 1940.

[7] See Appendix I. The expression of λ in the relativistic case is also derived and will be of use in estimating the temperature gradient in the interior.

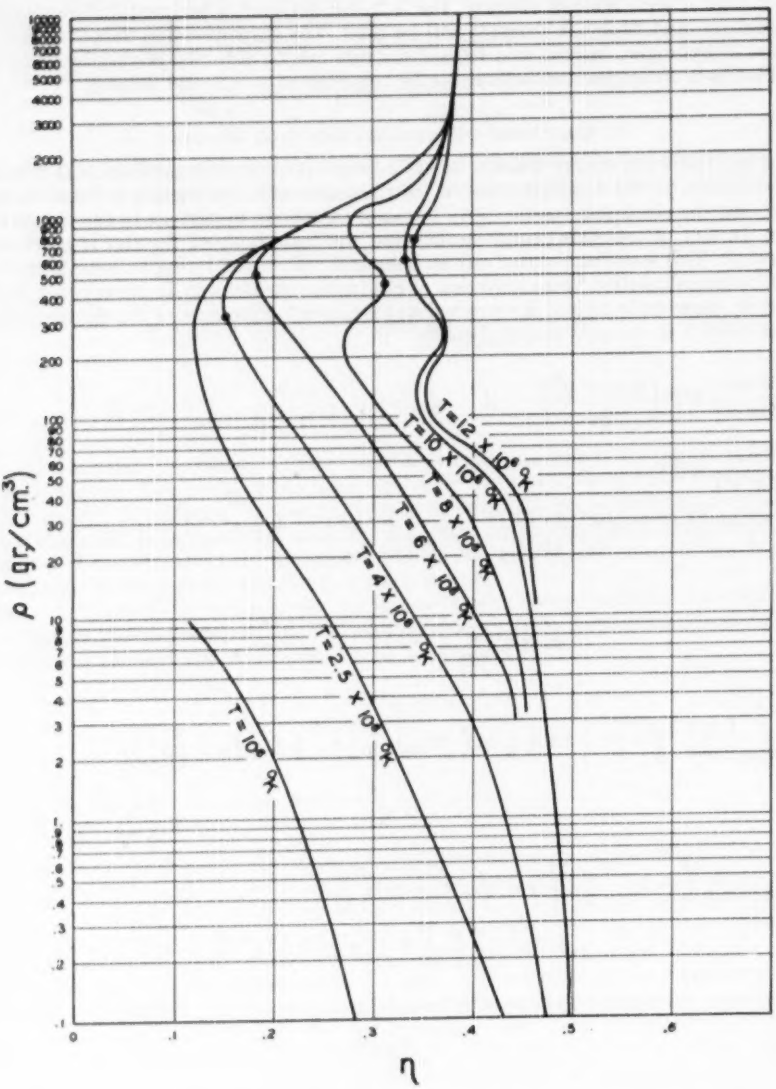

FIG. 1.—Free electron density η for pure Russell mixture. Dotted points denote $\frac{\mu}{KT} = 0$

for three different chemical compositions are tabulated in Table 1. The three different compositions, A, B, and C, are defined as follows:

$$\begin{aligned} A:&\quad X_H = 0\,, &&\quad X_{He} = 90 \text{ per cent}\,, &&\quad X_{\text{Russell}} = 10 \text{ per cent}\,;\\ B:&\quad X_H = 0\,, &&\quad X_{He} = 0\,, &&\quad X_{\text{Russell}} = 100 \text{ per cent}\,; \\ C:&\quad X_H = 90 \text{ per cent}\,, &&\quad X_{He} = 0\,, &&\quad X_{\text{Russell}} = 10 \text{ per cent}\,. \end{aligned} \tag{8}$$

These three compositions will be used later.

TABLE 1

CONDUCTIVE OPACITY

μ/kT	$T_\kappa(_c^A)$ (in 10^6 °K Cm^2/Gm)	$T_\kappa(_c^B)$	$T_\kappa(_c^C)$
− 3	3.99×10^4	1.83×10^5	3.80×10^4
− 2	1.23×10^4	5.74×10^4	1.16×10^4
− 1.5	6.37×10^3	3.00×10^4	5.80×10^3
− 1	4.41×10^3	2.09×10^4	4.01×10^3
− 0.5	2.61×10^3	1.25×10^4	2.42×10^3
0	1.54×10^3	7.40×10^3	1.40×10^3
0.5	627	3.11×10^3	580
1	593	2.93×10^3	545
1.5	375	1.86×10^3	342
2	255	1.27×10^3	232
3	126	635	114
4	68	348	61.9
5	40.3	205	36.3
6	25.4	133	23.4
7	16.9	89	15.6
8	12.1	61.9	10.8
9	8.71	44.8	7.83
10	6.52	33.6	5.86
11	4.96	25.5	4.45
12	3.86	19.9	3.46
13	3.09	15.9	2.77
14	2.49	12.8	2.23
15	2.03	10.5	1.82
16	1.68	8.70	1.51
17	1.41	7.27	1.26
18	1.19	6.14	1.07
19	1.01	5.23	0.91
20	0.87	4.50	0.78

The opacity κ_r due to radiative transfer has been calculated in great detail by various authors,[8] and the numerical table of P. M. Morse[9] will be used in our calculation. The energy transfer due to convection is, however, of no importance, as it can be shown[10] that dwarfs are always convectively stable. The total opacity of the gas, then, is

$$\kappa = \frac{\kappa_r \kappa_c}{\kappa_r + \kappa_c}\,. \tag{9}$$

[8] M. Stobbe, *Ann. d. Phys.*, **7**, 661, 1930; J. A. Gaunt, *Phil. Trans. R. Soc.*, *A*, **229**, 163, 1930; D. H. Menzel and C. H. Pekeris, *M.N.*, **96**, 77, 1935.

[9] *Loc. cit.*

[10] See Appendix II.

II. EQUILIBRIUM STATE OF DWARF STARS

We write the basic equations of equilibrium in the usual form:[11]

$$-\frac{dP}{dr}=\frac{GM\rho}{r^2}, \tag{10}$$

$$\frac{dM}{dr}=4\pi r^2\rho, \tag{11}$$

$$-\frac{dT}{dr}=\frac{3\kappa\rho L}{16\pi acr^2T^3}, \tag{12}$$

$$\frac{dL}{dr}=4\pi r^2\rho\epsilon, \tag{13}$$

with M as the total mass inside the radius r; L, the total energy flux at r; ϵ, the rate of energy produced per unit mass; G, the gravitational constant; P and κ as given in equations (1) and (9), respectively.

Let us consider a star of given mass and given uniform chemical composition.[12] We shall solve these equations by the perturbation method, regarding the solution of cold dwarf star[13] as the zeroth approximation. We arbitrarily assume a total luminosity of the star, and equations (10)–(13) will be integrated inward. The distribution of temperature and the amount of energy produced can then be obtained, and this should be consistent with the assumed luminosity if the star is in equilibrium. It will be shown in sections C and D that the temperature varies rapidly only in the envelope of the star, which contains only 1 per cent of its total mass; all the rest of the mass is practically isothermal. Hence, in finding the distribution of temperature, it is most convenient to treat the envelope and the interior separately.

C. ENVELOPE OF THE STAR

The mass of the envelope is set to be 1 per cent of that of the star. In solving these equations, we keep both M and L constant, since their variations will always be less than 1 per cent in the envelope. Equations (10) and (12) are integrated inward numerically for three different chemical compositions, A, B, and C, defined in equation (8), and for different values of L, starting from the outer radius given by a cold dwarf of the same mass and same uniform chemical composition. The results, for a star having the mass of the sun, are tabulated in Table 2, where r, T_0, and $(\mu/kT)_0$ are the corresponding values reached at the inside surface of the envelope; R is the total radius of the star; and $L_\odot$ the luminosity of the sun.

The distribution of ρ and T in the envelope for stars of different mass can be obtained by a simple transformation. From equations (10) and (12) we have

$$\frac{dP}{dT}=\frac{M}{L}\left(\tfrac{16}{3}\pi acG\right)\frac{T^3}{\kappa}$$

and

$$\frac{16\pi ac}{3}\int_0^T\frac{T^3}{\kappa\rho}\,dT=L\left(\frac{1}{r}-\frac{1}{R}\right).$$

[11] See S. Chandrasekhar, *An Introduction to the Study of Stellar Structure* (Chicago: University of Chicago Press, 1939), chap. v.

[12] It is true that under the strong gravitational field the equilibrium distribution of hydrogen and helium will not be uniform. However, owing to the high density, the diffusion rate in a white dwarf star is quite slow. For a star having the mass of the sun and $X_H=\frac{1}{2}$, the time required for gravitational separation is estimated to be $\tau\sim R^2v_{th}/GMd\sim 3\times 10^{11}$ years, where v_{th} is the thermal velocity of a proton, and d is the mean free path of a proton, taken to be $\sim 10^{-10}$ cm.

[13] Chandrasekhar, *op. cit.*, chap. xi.

Therefore, consider two stars of mass M, M' and luminosity L, L'. If we keep

$$\frac{M}{L}=\frac{M'}{L'}, \tag{14}$$

the distribution of density and temperature in these two stars, then, is connected by the relation:

$$\text{when} \quad T=T', \quad \text{then} \quad \rho=\rho', \quad \text{and} \quad M\left(\frac{1}{r}-\frac{1}{R}\right)=M'\left(\frac{1}{r'}-\frac{1}{R'}\right). \tag{15}$$

D. INTERIOR OF THE STAR

The remaining 99 per cent of the mass will be regarded as the interior. We shall now calculate the energy production of the star with given chemical composition and the temperature, T_0, at the outer surface of the interior. Only the formation of helium due to

TABLE 2

TEMPERATURE AND DEGREE OF DEGENERACY AT THE INNER SURFACE OF THE ENVELOPE

Chemical Composition	$L/L_\odot$	$(R-r)/R$	T_0 (° K)	$(\mu/kT)_0$	$\Delta T/T_0$
A	10^3	0.23	2.11×10^8	3.07	.....
A	1	.15	6.18×10^7	11.8	.....
A	10^{-2}	.12	1.36×10^7	51.0	0.004
A	10^{-4}	.11	2.55×10^6	27.1	.01
B	1	.15	8.70×10^7	8.4	.....
B	10^{-2}	.13	2.55×10^7	27.1	0.04
C	10^{-2}	.20	1.13×10^7	6.10	.....
C	10^{-4}	0.11	2.50×10^6	25.8	.....

proton-proton reaction will be considered, since this lower limit of energy production alone is sufficient for determining a small upper limit of the hydrogen content in dwarf stars. The energy production of this reaction has been calculated by Bethe and Critchfield,[14] using the Gamow-Teller selection rule for β-decay. It is

$$L_{(H,H)}=410\int(X_H\rho)^2(33.8T^{-1/3})^2e^{-33.8T^{-1/3}}dv \text{ erg/sec}, \tag{16}$$

with ρ expressed in grams per cubic centimeter and T in 10^6 °K, and v as the volume of the star in cubic centimeters. A more convenient form for the lower limit of energy production is

$$L_{(H,H)}>410\left(\frac{3}{4\pi R^3}\right)M_H^2(33.8T_0^{-1/3})^2e^{-33.8T_0^{-1/3}} \text{ erg/sec}, \tag{17}$$

where M_H is the total mass of hydrogen in the star.

If

$$kT\lesssim\frac{1}{2m_H}\left(\frac{3h^3}{8\pi}\frac{\rho}{m_H}X_H\right)^{2/3},$$

the proton gas will also become degenerate, and equation (16) will no longer hold. However, this will occur at a very low temperature ($T\sim1.5\times10^6$ °K if $X_H=10^{-2}$ for stars of $M=M_\odot$). It follows readily from the discussions in the next section that this effect is of no importance to us.

The variation of temperature in the interior can be estimated easily by using equations (12) and (16) and the solution of a cold dwarf. The results are shown in the last column of Table 2, where ΔT is the difference between the central temperature and T_0. For $L<10^{-2}L_\odot$, the interior is practically isothermal.

[14] *Phys. Rev.*, **54**, 250, 1938.

E. EQUILIBRIUM STATE AND STABILITY

The necessary condition for equilibrium is that

$$L_{(H,H)}(T_0) \leqslant L_0(T_0), \tag{18}$$

where $L_{(H,H)}$ is the energy production per second calculated from equation (17) by assuming a temperature T_0 at the outer surface of the interior; and L_0 is the luminosity assumed in the calculation of the envelope such that the temperature reached at the inner surface of the envelope is the same T_0.

In Figure 2 the solid curves represent the lower limit of energy production, given by

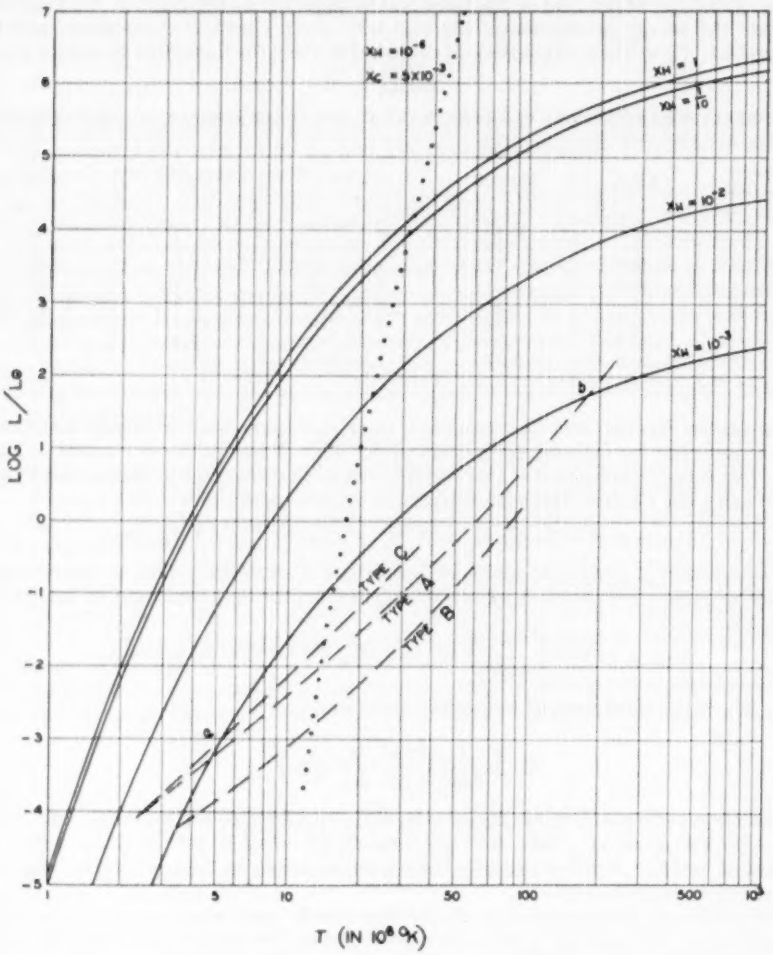

FIG. 2.—Solid curves represent energy production due to proton-proton reaction. Dotted curve represents energy production due to carbon cycle. Dashed curves are the results of integrations of the envelope (for $M = M_\odot$).

equation (17), as function of T_0 and X_H. The dashed curves represent L_0 as a function of T_0 and different chemical compositions. All these curves are calculated for a dwarf having the mass of the sun. From this figure we observe that no equilibrium state is possible if $X_H > 4 \times 10^{-3}$ and $10^{-4} < L/L_\odot < 10^3$. For $L > 10^3\ L_\odot$, the perturbation method breaks down because the temperature is so high that there will be hardly any degenerate region in the star. Even if an equilibrium state does exist near that region, the lifetime of such a state will be only about 10^5 years and will not correspond to any observed star. Also, for practical reasons, a star with total luminosity less than 10^{-4} times that of the sun will be regarded as dark and will escape observation. Hence, we reach the conclusion that *for any observed white dwarf star of mass $M_\odot$, the total mass of hydrogen must be less than $1.4 \times 10^{-2}\ M_\odot$*, where $M_\odot$ is the mass of the sun, and *the upper limit of the mass of hydrogen must be $4 \times 10^{-3}\ M_\odot$ if the hydrogen is distributed uniformly in that star.*

Using equations (14) and (15), a similar calculation is made for a star of mass $M = \frac{1}{2}\ M_\odot$, which gives the upper limit of X_H as 4.6×10^{-3}.

The intersecting point of these two curves indicates an equilibrium state of the dwarf living on proton-proton reaction. There are two kinds of intersecting points denoted by *a* and *b* in Figure 2. Type *b* can be discarded for the same arguments as those used in discarding the existence of any equilibrium solution for $L > 10^3\ L_\odot$. Type *a* occurs only if $X_H > 4 \times 10^{-3}$ (for $L > 10^{-4}\ L_\odot$ and $M = M_\odot$) and gives the star a luminosity comparable to that of the observed white dwarfs. From Table 1 it is found that the interior is practically isothermal near the region of temperature and luminosity. Suppose we increase the equilibrium value of T_0 by a positive amount δT_0; then, from Figure 2, the corresponding increase in the rate of energy production, $\delta L_{(H,H)}$, is found to be higher than the increase, δL_0, in the energy flow that can be carried away by the envelope. Hence the star becomes hotter and consequently unstable. Since this argument depends only on the slopes of these two curves, this instability holds for arbitrary distribution of $X_H \rho$ in the interior.

The problem of energy production due to the carbon cycle has been investigated by H. Bethe.[15] In Figure 2 we have also plotted the energy production due to the carbon cycle for $X_H = 10^{-6}$ and $X_c = 0.5$ per cent as a dotted curve. From the steepness of this curve, it is quite clear that the same argument of instability applies also in this case. We then reach another conclusion: *No stable white dwarf star can live on the nuclear energy produced in the interior*, although this is regarded as the correct mechanism of energy production for the main-sequence stars.

Marshak has also reached a similar conclusion by consideration of the lifetime of the star. He obtains an upper limit of $X_H = 2 \times 10^{-5}$ for Sirius B by assuming an envelope consisting only of Russell mixture and a concentration of carbon $X_c = 0.5$ per cent. In this case a short lifetime of 8×10^5 years is found. However, this argument is very dangerous, since the upper limit of X_H depends extremely sensitively on the chemical composition of the envelope. From Figure 2 it can be shown that X_H can be $\sim 10^{-4}$ for Sirius B if the composition of the envelope is of type *A*, and the corresponding lifetime will be $\sim 4 \times 10^9$ years for the same assumed value of X_c.

III. POSSIBLE MECHANISMS OF ENERGY PRODUCTION FOR DWARFS

As shown in Part II, a dwarf star cannot live on nuclear reactions in its interior. The alternative mechanisms will then be: (*a*) The star does not live on nuclear energy but, say, on gravitational contraction. (*b*) The star still lives on nuclear energy, however, produced only in the envelope.[16] Marshak[1] has considered the possibility of gravitational contraction and found 3×10^8 and 5×10^8 years as the lifetimes for Sirius B and 40

[15] *Phys. Rev.*, **55**, 434, 1939; *Ap. J.*, **92**, 118, 1940.

[16] This model was first proposed by E. Schatzman (*Ap. J.*, **107**, 110, 1948).

Eridani B, respectively. This is quite compatible with the known density of white dwarfs in space.

We will now discuss the alternative mechanism *b* in some detail. This mechanism requires that the hydrogen exist mainly only in the envelope, which is possible only if, owing to some evolutional reasons at the time of formation of the dwarf, the interior is already devoid of hydrogen. If this were not so, as mentioned in Part II, the slowness of the diffusion rate in the dense stars would always keep the star rather uniform in composition. For simplicity, we shall consider in the following discussions a star consisting only of hydrogen and helium.

F. DISTRIBUTION OF HYDROGEN AND HELIUM UNDER A GRAVITATIONAL FIELD

Let n_H, n_{He}, and n_e be the number of protons, helium nuclei, and electrons; g and E be the radial gravitational and electrical fields, respectively; e be the charge of proton, and P_e the partial pressure of electron gas given by equation (1). The basic equations are:

$$-\frac{d}{dr}(n_H kT) = n_H(m_H g + eE), \tag{19}$$

$$-\frac{d}{dr}(n_{He} kT) = n_{He}(4m_H g + 2eE), \tag{20}$$

$$-\frac{dP_e}{dr} = n_e(m_e g - eE), \tag{21}$$

$$\frac{1}{r^2}\frac{d}{dr}(r^2 E) = 4\pi(n_H + 2n_{He} - n_e)\, e, \tag{22}$$

$$\frac{1}{r^2}\frac{d}{dr}(r^2 g) = -4\pi[(n_H + 4n_{He})\, m_H + n_e m_e]G, \tag{23}$$

together with equations (12) and (13).

As $eE \sim mg$, we have, from equations (22) and (23),

$$\left|\frac{n_H + 2n_{He} - n_e}{n_H + 4n_{He}}\right| \sim \frac{Gm_H^2}{e^2} = 8 \times 10^{-37}. \tag{24}$$

In the subsequent treatments we neglect Gm_H^2/e^2 and m_e/m_H as compared to unity. These equations will now be solved in the nondegenerate region and the extremely degenerate region separately.

a) Nondegenerate region.—We will set $P_e = n_e kT$ and $\kappa = \kappa_r$ in equations (21) and (12). From equations (19), (20), (21), and (24), we obtain

$$eE = -\frac{n_H + 8n_{He}}{2n_H + 6n_{He}}\, m_H g. \tag{25}$$

Substituting back into equations (19) and (20), we have

$$-\frac{d}{dr}(n_H kT) = n_H m_H g\left(\frac{n_H - 2n_{He}}{2n_H + 6n_{He}}\right), \tag{26}$$

$$-\frac{d}{dr}(n_{He} kT) = n_{He} m_H g\left(\frac{6n_H + 8n_{He}}{2n_H + 6n_{He}}\right), \tag{27}$$

which leads to the equation

$$\frac{d(n_H T)}{d(n_{He} T)} = \frac{n_H}{n_{He}} \frac{n_H - 2n_{He}}{6n_H + 8n_{He}}. \tag{28}$$

Equation (2) can be interpreted to give

$$n_H^2 (n_H + 2n_{He}) n_{He}^{-1/2} T^{5/2} = B^{5/4}, \tag{29}$$

where B is an integrating constant.

It is more convenient to introduce the relative concentration defined by

$$v \equiv \frac{n_H}{n_{He}}. \tag{30}$$

We then have

$$\frac{dv}{dr} = \frac{5}{2} \frac{m_H g}{kT} v \left(\frac{v+2}{v+3} \right). \tag{31}$$

Using the expression of opacity of hydrogen and helium,[17] equation (12) becomes

$$-\frac{dT}{dr} = \frac{\pi e^6 h^2 n_e (n_H + 4n_{He}) L}{S(\infty) \sqrt{3} a c^2 (2\pi m_e)^{3/2} k^{3.5} r^2 T^{6.5}} \equiv A \frac{L}{r^2} \frac{n_e (n_H + 4n_{He})}{T^{6.5}}, \tag{32}$$

where $S(\infty)$ is the Strömgren function with the argument taken to be infinity. The Gaunt factor is taken to be unity.

Combining equations (29), (31), and (32) and setting $g = GM/r^2$, we have

$$\frac{dT}{dv} = -\left(\frac{2}{5} \frac{kA}{m_H G} \right) B \frac{L}{M} \frac{(v+4)(v+3)}{v^{13/5} (v+2)^{4/5}} \frac{1}{T^{7.5}}. \tag{33}$$

We may set L/M constant at the outer shell of the envelope. The relation between T and v is then given by

$$T^{8.5} = \left(\frac{17}{5} \frac{kA}{m_H G} \right) B \frac{L}{M} F(v), \tag{34}$$

where $F(v)$ is defined as

$$F(v) \equiv \int_v^\infty \frac{(v+4)(v+3)}{v^{13/5} (v+2)^{4/5}} dv, \tag{35}$$

and

$$F(v) = \tfrac{5}{2} v^{-2/5} (1 + \tfrac{54}{35} v^{-1} + \tfrac{46}{75} v^{-2} + \ldots) \qquad \text{if} \qquad v \gg 1,$$

$$F(v) = 5.83 + \frac{15}{2^{2/5} v^{8/5}} (1 + \tfrac{22}{45} v + \ldots) \qquad \text{if} \qquad v \ll 1.$$

For intermediate values of v, $F(v)$ is calculated numerically and is given by Table 3. The dependence of n_H, n_{He}, and T on r can be obtained from a single integration by substituting equations (29) and (34) in equation (32). It should be noticed that, at the outer shell of the envelope, $v \gg 1$, hence $T \propto (R-r)$; $n_H \propto (R-r)^{3.25}$; and $N_{He} \propto (R-r)^{24.5}$, i.e., n_{He} increases much faster than n_H as the depth of the shell $(R-r)$ increases. As $v \ll 1$, $n_{He} \propto T^{3.25}$ and $n_H \propto 1/T^{8.25/4}$, i.e., as the depth increases, n_{He} still keeps on increasing, but n_H will start to decrease. The decrease of the hydrogen concentration will become much more rapid when the degenerate region is reached.

b) Extremely degenerate region.—We will set T = Const. and neglect $(kT/\mu)^2$ as com-

[17] Chandrasekhar, *op. cit.*, chap. vii.

pared with unity. The distribution of hydrogen and helium will then be given by the usual Boltzmann distribution. This can be obtained by eliminating mg and eE between equations (19), (20), and (21). It then is

$$\frac{n_H^4}{n_{He}} = K e^{-2\mu/kT}, \tag{36}$$

where K is another constant of integration. Furthermore, the distribution of n_e is given by the solution of cold dwarf stars, from which the distribution of n_H and n_{He} can be found. It is evident that in this region n_H decreases extremely rapidly as r decreases. No simplified formula can be obtained for the intermediate region. However, one may extrapolate these two results and estimate the rough distribution of hydrogen and helium. We shall apply this method to Sirius B in Part IV and show that a total mass of hydrogen $\sim 10^{-3}\, M_\odot$ is sufficient to explain the observed luminosity. The corresponding lifetime is about 3×10^{10} years.

TABLE 3

THE FUNCTION $F(v)$

v	$F(v)$	v	$F(v)$	v	$F(v)$
0.20	62.5	1.40	4.76	3.40	2.02
0.40	22.6	1.80	3.65	3.80	1.84
0.60	13.3	2.20	2.99	4.20	1.69
0.80	9.17	2.60	2.50		
1.00	7.00	3.00	2.25		

IV. ASTRONOMICAL APPLICATIONS

G. RADII AND MASSES OF WHITE DWARFS

From the above discussions we can set[18] $\eta = \frac{1}{2}$ in the relation between the radius and the mass of a cold dwarf.[13] Then, if either of the quantities is known, we can determine the other quantity theoretically. From Chandrasekhar's result, the critical mass of the cold dwarf, then, is

$$M = 5.75\,\eta^2 M_\odot = 1.44 M_\odot . \tag{37}$$

The following examples will illustrate the application to the known white dwarfs.

a) Van Maanen No. 2.[13]—The radius of this star is determined quite accurately by parallax and spectral type and is found to be

$$R = 10^{-2.05} R_\odot , \tag{38}$$

where $R_\odot$ is the radius of the sun. We may then deduce its mass to be $0.9\, M_\odot$, which is within the errors of the old mass value determined from the red shift.

b) Procyon B.[19]—Here

$$M = 10^{-0.53} M_\odot . \tag{39}$$

Hence we may deduce

$$R = 8.6 \times 10^8 \text{ cm} , \tag{40}$$

which is also consistent with the experimental values of absolute visible magnitude and spectral type.

[18] It has been suggested that He^3 may be present in the interior of white dwarfs and consequently η can be greater than $\frac{1}{2}$. Apart from other improbabilities, this is quite impossible because, under the condition of white dwarfs, He^3 is "unstable" against capture of free electron (inverse process of β-decay).

[19] G. Kuiper, *Ap. J.*, **88**, 472, 1938.

II. ENVELOPE MODEL OF WHITE DWARFS

Since the white dwarfs have a different abundance in hydrogen as compared with the other stars, it is quite natural to assume that these dwarfs are really the end of some main-sequence stars after they have used up their hydrogen. The interior will then be devoid of hydrogen, and the hydrogen, if any, will distribute itself in the envelope under the influence of the gravitational field. For definiteness we consider Sirius B and assume that it contains only hydrogen and helium. The distribution of these two elements is calculated according to the method described in section F. The distributions in the non-degenerate and extremely degenerate regions are extrapolated, and the constants B and K of equations (29) and (36) are determined by the smooth joining of these two dis-

TABLE 4

DISTRIBUTION OF HYDROGEN AND HELIUM IN THE ENVELOPE OF SIRIUS B

$(R-r)$ in 10^8 Cm	ρ_H Gm/Cm³	ρ_{He} Gm/Cm³	ρ_H/ρ_{He}
0	0	0	∞*
10	330	.....	.....
20	6.4×10^3	.....	.....
30	1.2×10^6	.....	.....
40	1.9×10^8	5×10^8	3.8
50	5×10^8	4.9×10^8	0.1
52	850	5.5×10^8	1.5×10^{-3}

* At the outer atmosphere of the envelope, the Unsöld convective zone will become important, and the ratio ρ_H/ρ_{He} is really finite at $R = r$. This effect has been discussed recently by E. Schatzman (*Ap. J.*, **110**, 261, 1949).

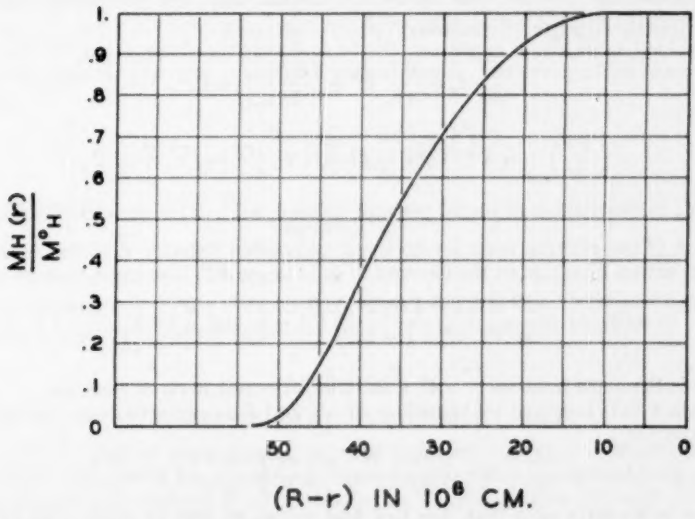

FIG. 3.—Distribution of hydrogen mass in Sirius B. $M_H(r)$ is the mass of hydrogen inside the radius r and M_H^0 the total mass of hydrogen in the star.

tributions and by requiring the total mass of hydrogen, M_H, to be compatible with the observed luminosity. The results are

$$M_H \simeq 10^{-3} M_\odot , \qquad T_0 \simeq 5 \times 10^6 \,^\circ\mathrm{K} , \tag{41}$$

determined from the observed luminosity and mass of Sirius B, which are

$$L = 10^{-2.52} L_\odot , \qquad M = 10^{-0.01} M_\odot . \tag{42}$$

Owing to the crudeness of this approximation method, the results cannot be trusted to more than order of magnitude. The lifetime of this model, then, is

$$\tau \simeq \frac{M_H E}{m_H L} \sim 3 \times 10^{10} \text{ years}, \tag{43}$$

where E is the energy evolved per proton and is taken as 10^{-5} ergs. The rough distributions of n_H and n_{H_e} are given by Table 4. From this table the experimental fact that only hydrogen lines are observed on the surface of white dwarfs is readily explained. The corresponding distribution of hydrogen mass is plotted in Figure 3.

In conclusion, the author wishes to express his gratitude to Professor E. Fermi for many helpful suggestions in various stages of this work, and to Professor S. Chandrasekhar for stimulating discussions. He is also much indebted to Professors Chandrasekhar and G. Kuiper for astronomical information.

APPENDIX I

Electronic Heat Conductivity

We shall only sketch the method used to obtain the electronic conductivity, since it is identical with the usual treatment of the same problem in metals.[20] Let dT/dx and F be the temperature gradient and the induced electric field. The Boltzmann equation for the distribution function of electrons $f(\vec{p}, x)$ is given as

$$\frac{\partial f}{\partial x} v_x + \frac{\partial f}{\partial p_x} eF + \left[\frac{\partial f}{\partial t}\right]_{\text{coll}} = 0 , \tag{44}$$

where

$$\left(\frac{\partial f}{\partial t}\right)_{\text{coll}} = \int [f(\vec{v}') - f(\vec{v})] N_A |\vec{v}| \sigma(\vec{v}', \vec{v}) \, d\Omega' ,$$

where N_A is the number of nuclei per unit volume; $\sigma(\vec{v}', \vec{v})$ is the cross-section for the transition of the electron from a velocity $\vec{v}$ to another velocity $\vec{v}'$ of the same magnitude but with a direction in the element of solid angle $d\Omega'$. The expression of σ[21] is

$$\sigma(\theta, v) = \frac{Z^2 e^4}{m^2 v^4} \frac{(1 - [v^2/c^2])}{(1 - \cos\theta)^2} \left(1 - \frac{v^2}{c^2} \sin^2 \frac{\theta}{2}\right) + 0\left(\frac{Z e^2}{\hbar c}\right)^2 , \tag{45}$$

where θ is the angle between $\vec{v}$ and $\vec{v}'$, and m is the rest mass of electron.

Equation (43) is solved by regarding dT/dx and F as perturbations. The first-order solution of f is

$$f = f_0 + v_x \frac{\partial f_0}{\partial E} \left[eF - \left(\frac{d\mu}{dT} + \frac{E - \mu}{T}\right) \frac{dT}{dx} \right] \frac{4\pi e^4 I}{m^2 v^3} \left(1 + \frac{v^2}{c^2}\right), \tag{46}$$

[20] Refer to Marshak's paper (*Ann. New York Acad. Sci.*, **41**, 49, 1940) for details of the formalism of this method.

[21] Mott, *Proc. R. Soc. London*, *A*, **135**, 454, 1932.

where

$$f_0 = \frac{2}{1 + e^{(E-\mu)/kT}} \tag{47}$$

and

$$2I = N_A Z^2 \int_{\theta_0}^{\pi} \frac{(1 - [v^2/c^2] \sin^2 [\theta/2])}{1 - \cos\theta} \sin\theta d\theta \simeq N_A Z^2 \ln \frac{2}{1 - \cos\theta_0} \tag{48}$$

with $\theta_0 \simeq \bar{\lambda}/a$ as the minimum scattering angle due to the finite radius, a, of the atom.[10] The quantities $\bar{\lambda}$ and a are given by the equations

$$\bar{\lambda} = \frac{\hbar}{p} \tag{49}$$

and

$$a \simeq \left(\frac{3Z}{4\pi N_e}\right)^{1/3}. \tag{50}$$

The expressions for particle current j and energy flow Q are

$$j = \int\int v_x \frac{d^3p}{h^3} \tag{51}$$

and

$$Q = \int\int v_x E \frac{d^3p}{h^3}. \tag{52}$$

For a steady state we require $j = 0$. If we substitute equations (46), (47), and (48) in equation (50), we may then express F in terms of dT/dx. Substitute this expression, together with equations (46), (47), and (48) again in equation (51). We shall make the approximation that in the expression (48) for I, p^2 will be taken as the square root of the average value of p^2 for electrons. Also, we shall take I outside the integration in equations (50) and (51), since it varies only logarithmically with the momentum. After a rather tedious but straightforward calculation, λ can be expressed in the form (6) for the nonrelativistic region. For the relativistic region (hence, extremely degenerate in white dwarfs),

$$\lambda = \frac{2\pi^2 (E_m^2 - m^2c^4)^3 k^2 T}{9h^3 e^4 E_m^2 c^2 I}, \tag{53}$$

which reduces to

$$\lambda = \frac{16\pi^2 k^2 T \mu^3 m}{9h^3 e^4 I}, \tag{54}$$

as given by equation (6) for the extremely degenerate but nonrelativistic region. E_m is the maximum energy, including the rest mass, of the degenerate electron.

APPENDIX II

Convective Stability of White Dwarfs

At the outer shell of the envelope, only the radiative opacity is of importance and is proportional to $\rho/T^{3.5}$ if the variation of the guillotine factor is neglected. Also, one may set the pressure proportional to ρT in this region. From equations (10) and (12) we have

$$\frac{d(\rho T)}{dT} \propto \frac{T^{3.5}}{\rho}, \tag{55}$$

which gives

$$\frac{d\ln T}{d\ln P}=\frac{1}{4.25} \tag{56}$$

at the surface of the star. As we approach the interior, the star becomes almost isothermal. The corresponding value of $d\ln T/d\ln P$ will be much less than 1/4.25. On the other hand, the adiabatic expansion of a mixture of free electrons and heavy particles, at all temperatures, gives

$$\left(\frac{d\ln T}{d\ln P}\right)_{\text{ad}}=\tfrac{2}{5} \tag{57}$$

if one neglects the effect of incomplete ionization. This can be seen by writing down the expressions of total energy, E, and pressure, P. They are

$$P=N_{\text{heavy}}kT+\frac{8\pi}{3}\left(\frac{2m_e}{h^2}\right)^{3/2}(kT)^{5/2}F_{3/2}\left(\frac{\mu}{kT}\right) \tag{1'}$$

and

$$E=\tfrac{3}{2}PV\,, \tag{58}$$

where $F_{3/2}(\mu/kT)$ is defined in equation (3). For adiabatic expansion we have

$$dE=-PdV\,, \tag{59}$$

which gives

$$\left(\frac{d\ln P}{d\ln \rho}\right)_{\text{ad}}=\tfrac{5}{3}\,. \tag{60}$$

Equation (58) can then be obtained readily by substituting equation (1′) in equation (60). It is then concluded that convection will not be set up in the case of white dwarf stars.

ON THE COMPOSITIONS AND STRUCTURES OF THE PLANETS

HARRISON BROWN
Institute for Nuclear Studies, University of Chicago
Received October 21, 1949

ABSTRACT

The observed physical and chemical characteristics of the planets can be explained in a reasonably satisfactory manner by assuming that they condensed from a medium possessing varying temperatures and densities but fairly uniform composition. Using as a basis for calculations our knowledge concerning the behavior of matter under extremely high pressures, the conclusion is drawn that the inner planets possess nearly identical composition, the differences in density between them being largely the result of compression effects.

Approximate models are derived for the major planets. It is found that Uranus, Neptune, Saturn, and Jupiter possess, respectively, 3.1, 3.7, 6.4, and 9.1 earthlike cores and that nearly 70 per cent of the mass of Saturn and 90 per cent of the mass of Jupiter is composed of helium-hydrogen.

I. INTRODUCTION

Many investigations and speculations have been made concerning the possible internal compositions and structures of the planets of our solar system. Limited in our knowledge as we are to but a few pertinent measurable planetary properties, such as mass, surface temperature, density, oblateness, and atmospheric composition, large numbers of unrelated artificial solutions are possible, and, indeed, many specific solutions have been proposed. Typical of the possible solutions for the major planets are the interesting and stimulating possibilities discussed by Wildt,[1] who finds that the measurable properties of Jupiter, for example, can be explained by using a three-shell model in which there is iron and stone of density 6 extending to 40 per cent of the planet's radius, ice of density 1.5 extending to 85 per cent, and a mixture of compressed hydrogen, helium, ammonia, and methane extending to the boundary. Reference is made also to the important discussion of Kuiper relating Wildt's models for the major planets to the observed atmospheric spectra.[2]

More data are available in the case of the earth than in the case of the other planets. In particular, seismic data are available which demonstrate the presence of a core of high density occupying approximately half the earth's diameter. For many decades it has been assumed that this core is composed of metallic iron. The choice of iron rather than any one of a number of other elements arises primarily from the assumption that, to a first approximation, the earth possesses the same composition as does gross meteoritic matter. Indeed, the analogy between the composition of the earth and that of meteoritic matter has persisted for about a century, fortified by such developments as the discovery of the seismic discontinuity of first order and the studies of V. M. Goldschmidt and others on the distribution of trace elements in meteorites and in the earth's crust.

More recently, Kuhn and Rittman[3] have made a novel proposal to the effect that the earth's interior is composed of highly compressed hydrogen rather than of metallic iron-nickel. This suggestion will be discussed in Section III.

Explanations of the specific differences in properties between the major planets, on the

[1] *Veröff. U.-Sternw. Göttingen*, No. 40, 1934; *Ap. J.*, **87**, 508, 1938; *Rev. Mod. Phys.*, **14**, 151, 1942; and *M.N.*, **107**, 84, 1947.

[2] G. P. Kuiper, *The Atmospheres of the Earth and Planets* (Chicago: University of Chicago Press, 1949), chap. xii.

[3] W. Kuhn and A. Rittman, *Geol. Rdsch.*, **32**, 215, 1941; W. Kuhn, *Naturwiss.*, **30**, 689, 1942.

one hand, and the terrestrial planets, on the other, have seldom been attempted, although it is usually stated that the major planets must possess substantial fractions, by weight, of gases. Within the class of terrestrial planets, little has been stated other than that they are all probably composed of metallic iron and rock in varying proportions. The substantial differences in density and oblateness between the earth and Mars have usually been attributed to a difference in composition, Mars being frequently referred to as nearly a "pure chondrite." Venus is usually stated to be intermediate between the earth and Mars in composition.

It is of interest to determine whether or not the differences in the observed properties of the planets can be explained on a common basis. If one can assume that the planets were formed at approximately the same time, a reasonable common basis for comparison would be the composition and physical properties of the medium from which the planets were formed. Weizsäcker[4] and ter Haar,[5] in their discussions of the origin of the solar system, have assumed that the planets were formed from a medium of uniform composition within which the relative abundances of the elements were identical with the relative abundances at present existing in the sun.[6]

In this paper an attempt will be made, on the basis of such an assumption, to see whether or not one can explain the observed chemical and physical properties of the individual planets.

II. THE CHEMICAL COMPOSITION OF THE PRE-PLANETARY MEDIUM

As a first approximation to the composition of the pre-planetary medium, we can assume the author's tables of elemental abundances,[7] based, in the cases of the major constituents, largely upon the work of A. Unsöld, V. M. Goldschmidt, J. Greenstein, and M. Harrison. Table 1 shows the derived abundances of the major constituents. As we are interested in the composition at the time of planet formation, the table must be corrected for changes due to thermonuclear reactions. We shall assume, in view of the fact that carbon and nitrogen are regenerated in the carbon cycle, that their abundances have not been appreciably altered. Oxygen and neon[8] are too heavy to react with protons at appreciable rates at the temperatures existing in the solar interior.[9] This leaves corrections to be applied to hydrogen and helium. The hydrogen correction is small. Assuming the present rate of energy liberation, it is estimated that the solar helium abundance has increased by approximately 10 per cent during the last two to three billion years.

The molecular composition of the medium at a given point will depend markedly upon the temperature and density, in addition to the elemental composition. For a density of 10^{16} atoms/cm^3, and a temperature of a few hundred degrees K, ter Haar[5] has roughly estimated various molecular ratios, which may be higher or lower than calculated, by factors of 10:

H	:	H_2	:	H_2O
1		0.1		10^{-4}

CH	:	CH_4	:	CN	:	HCN	:	C_2	:	CO	:	SiC
1		0.1		10^{-3}		10^{-4}		10^{-4}		10^{-4}		10^{-6}

[4] *Zs. f. Ap.*, **22**, 319, 1944.

[5] *Det. Kgl. dansk. Vid. Selsk., Mat.-fys. Medd.*, Vol. **25**, No. 3, 1948; and *Science*, **107**, 405, 1948.

[6] With the exception, of course, of those elements whose abundances have been appreciably changed as the result of thermonuclear reactions which have taken place in the solar interior since the planets were formed.

[7] H. Brown, *Rev. Mod. Phys.*, **21**, 625, 1949.

[8] The isotopes O^{18} and Ne^{20} would react slowly. The rates for the consumption of the less abundant isotopes O^{17} and Ne^{21} would be more rapid.

[9] H. A. Bethe, *Phys. Rev.*, **55**, 434, 1939.

NH_3	:	CN	:	HCN	:	NO
1		10^{-2}		10^{-3}		10^{-3}

H_2O	:	CO	:	O_2	:	NO	:	CO_2
1		10^{-2}		10^{-2}		10^{-2}		10^{-5}

In a medium possessing a composition given by Table 1, the metallic elements of high oxygen affinity (*Mg*, *Al*, *Si*, *Na*, *K*, *Ca*) would be present almost entirely in the form of oxides (or silicates). In localized regions of higher density, as, for example, in regions where gravitational capture is playing a role, the chemical forms of the elements of intermediate oxygen affinity would be determined by equilibria such as

$$H_2 + FeO \rightleftharpoons H_2O + Fe$$

or

$$H_2 + FeSiO_3 \rightleftharpoons H_2O + SiO_2 + Fe$$

which are frequently strongly temperature-dependent.

TABLE 1

ELEMENTAL ABUNDANCES
(Atoms per 10,000 Atoms of *Si*)

Z	Element	Abundance	Z	Element	Abundance
1	*H*	3.5×10^{8}	17	*Cl*	170
2	*He*	3.5×10^{7}	18	*A*	130
6	*C*	80,000	19	*K*	69.3 ± 7.5
7	*N*	160,000	20	*Ca*	670 ± 74
8	*O*	220,000	21	*Sc*	0.18
9	*F*	90	22	*Ti*	26.0 ± 9.0
10	*Ne*	40,000	23	*V*	2.5
11	*Na*	462 ± 36	24	*Cr*	95
12	*Mg*	8870 ± 250	25	*Mn*	77
13	*Al*	882 ± 81	26	*Fe*	18,300
14	*Si*	10,000	27	*Co*	99
15	*P*	130	28	*Ni*	1340
16	*S*	3500	29	*Cu*	4.6

From the point of view of completely formed chemical compounds, thermodynamically we can consider the medium to possess the composition shown in Table 2, where the compounds, together with their molecular weights and boiling points, are shown. It can be seen that the molecular species shown in Table 2 fall naturally into three distinct classes when one considers both ease of condensation and molecular weight: *Class I:* The metals and oxides. The major constituents of this class possess exceedingly high boiling points, as a result of which they would be the first substances to condense. *Class II:* Molecular species of intermediate boiling points and intermediate molecular weight (CH_4, NH_3, H_2O, *Ne*). *Class III:* Hydrogen and helium, neither of which can condense at temperatures existing within the orbit of Neptune. As the molecular-weight ratio of helium to hydrogen is large, we shall consider the elements separately as Classes III*a* and III*b*.

Table 3 shows the various planetary properties with which we shall be concerned in this discussion. A comparison of Table 2 with Table 3 is interesting, for we see that the planets may be divided into classes which correspond to the three classes of molecular species. In order of increasing mass we have, first, the terrestrial planets, all of which possess relatively high densities and which we may assume are composed of substances of

TABLE 2

ASSUMED CHEMICAL COMPOSITION OF THE PRE-PLANETARY MEDIUM

Class	Compound	Weight Abundance (Class I = 1)	Molecular Weight	Boiling Point (° K)
IIIb	H_2	180	2.0	20
IIIa	He	56	4.0	4
II	CH_4	0.6	16.0	112
	NH_3	1.2	17.0	240
	H_2O	1.7	18.0	373
	Ne	0.3	20.2	27
Total Class II		3.8		
I	Fe	0.40	55.84	~3300
	Ni	0.03	58.69	~3200
	FeO	0.05	71.84	High
	SiO_2	0.26	60.06	~2500
	MgO	0.15	40.32	>3100
	Σ	0.11		
Total Class I		1.0		

TABLE 3

PHYSICAL AND CHEMICAL PROPERTIES OF THE PLANETS*

PLANET	$M/M_\oplus$	ρ (GM/CM³)	OBLATENESS	ϵ/ϕ	KNOWN ATMOSPHERIC CONSTITUENTS†	
					Gas	Amount in Cm S.P.T.
Mercury	0.045?	4.1?	0.00			
Venus	0.82	4.9	0.00		CO_2	100,000
Earth	1.000	5.52	1/297	0.97	N_2	625,000
					O_2	168,000
					CO_2	220
					CH_4	1.7
Mars	0.108	3.96‡	1/192	1.14	CO_2	440
Jupiter	318.35	1.33	1/15.4	0.76	CH_4	15,000
					NH_3	700
Saturn	95.3	0.71	1/9.5	0.65	CH_4	35,000
Uranus	14.58	1.26	?§		CH_4	150,000
Neptune	17.26	2.2‖	?		CH_4	250,000
Pluto	0.93?	5.5?	?			

* Unless otherwise indicated, the figures are taken from Russell, Dugan, and Stewart, *Astronomy*, Vol. **1**, *The Solar System* (rev. ed.; Boston: Ginn & Co., 1945).

† G. P. Kuiper, *The Atmospheres of the Earth and Planets* (Chicago: University of Chicago Press, 1949), p. 326.

‡ Recalculated. See F. Whipple, *Earth, Moon, and Planets* (Philadelphia: Blakiston Co., 1941).

§ Dynamical and direct values for the oblateness of Uranus have been obtained ranging from 1/11 to 1/19. I am indebted to Mr. Daniel L. Harris III, of the Yerkes Observatory, for a valuable discussion of this question.

‖ This figure is the result of a recent redetermination of the radius of Neptune by Professor G. P. Kuiper, *Ap. J.*, **110**, 93, 1949.

Class I. We then have Uranus and Neptune associated with a fifteen fold increase in mass and a marked decrease in density, corresponding to the addition of the abundant compounds belonging to Class II. Following this we have Saturn associated with over a fivefold increase in mass and another appreciable decrease in density, corresponding to the addition of helium. The increase in mass upon going from Saturn to Jupiter may result from the addition of greater quantities of helium and perhaps hydrogen.

As a first approximation to a quantitative treatment, we shall assume the chemical compositions shown in Table 4 (the assumed ratios being based entirely upon observed elemental abundances) and then, through a study of the densities of substances as a function of pressure, attempt to see how the calculated models agree with those assumed.

We shall limit the discussion in this paper to the planets whose properties are fairly well known. Pluto is not discussed, nor has an analysis been made of the compositions and structures of the satellites.

TABLE 4

ASSUMED COMPOSITIONS OF THE PLANETS
(Relative Proportions of Compounds in Each Class
Based upon Observed Abundance Ratios)

Planet	Class I	Class II	Class III
Mercury	1	0	0
Venus	1	0	0
Earth	1	0	0
Mars	1	0	0
Jupiter	Small	Small	~1
Saturn	Small	Small	~1
Uranus	0.2	0.8	Small
Neptune	0.2	0.8	Small

III. THE MINOR PLANETS

A partial justification of the assumption that the planets were formed in a medium possessing fairly uniform composition can be obtained by comparing the concentrations of elements of Class I in meteorites with the relative abundances of the same elements in the solar atmosphere. Either meteorites resulted from the breakup of a relatively small planet, or they represent small fragments of condensed matter which escaped assimilation into a body of planetary size. In either case meteorites should represent a satisfactory sampling of the elements of Class I. If our assumptions as to the composition of the medium are correct, then the relative abundances of the elements of Class I in meteorites should correspond on a one-to-one basis with the relative abundances of the same elements in the solar atmosphere.[10]

A comparison of meteoritic abundances and solar abundances has been made by the author,[7] with results shown diagrammatically in Figure 1. The solar abundances are those determined by Unsöld[11] and are, in the best cases, reliable to within a factor of 2. The solar values have been normalized so that solar calcium equals meteoritic calcium. In spite of the rather large errors involved (primarily in the solar data), it can be seen that the agreement between the solar and the meteoritic values is remarkably linear, the linearity covering a range of about 10^6 in elemental concentrations.

In view of the agreement in composition between meteorites and the sun, we can as-

[10] Assuming, of course, that there is no fractionation of these elements between the solar atmosphere and the interior.

[11] *Zs. f. Ap.*, **21**, 1, 1941.

sume with fair certainty that the elements of Class I were fairly well mixed in the pre-planetary medium. As a result, we must expect the minor planets to be nearly alike in composition, their differing mean densities resulting from one or both of two effects: (1) gravitational compression or (2) equilibria of the type

$$H_2 + FeSiO_3 \rightleftharpoons Fe + SiO_2 + H_2O \,.$$

This equilibrium, which is temperature-sensitive, may determine the ratio of combined iron to metallic iron during the process of condensation and subsequent planet accretion.

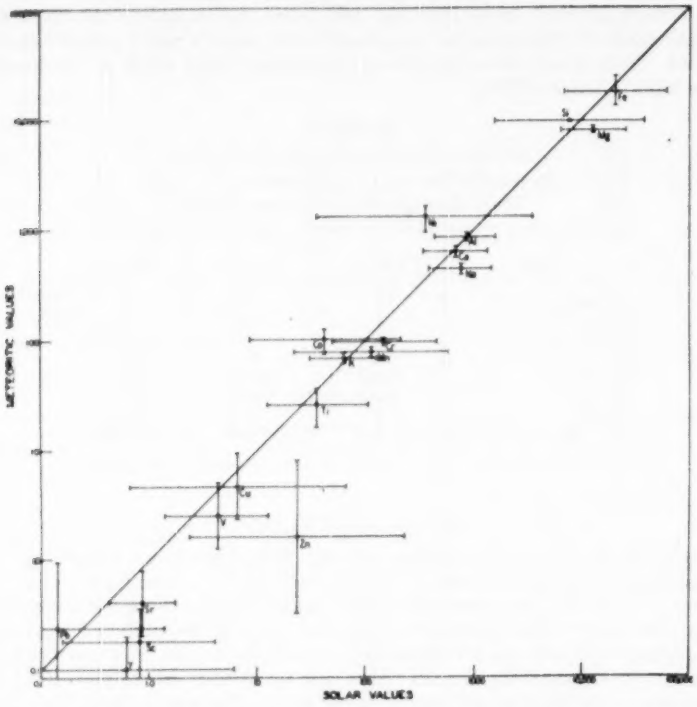

FIG. 1.—The abundances of elements in Class I in meteorites, compared with their abundances in the sun.

Considering the high abundance of iron, the shifting of the equilibrium either all the way to the left or all the way to the right would result in uncompressed density limits ranging from about 3.7 to 4.1.

Theoretical studies on the behavior of cold matter under very high pressures (higher than pressures obtainable in the laboratory and comparable to the internal pressures existing within the planets) demonstrate that gravitational compression is perhaps the major effect in determining the densities of the minor planets. Several investigators, notably Slater and Krutter,[12] Jensen,[13] and, more recently, Feynman, Metropolis, and Teller,[14] utilizing the Fermi-Thomas statistical atomic model, have made calculations of potential fields and charge densities in metals as a function of lattice spacing. Such calculations make possible the determination of pressure-volume relationships correspond-

[12] *Phys. Rev.*, **47**, 559, 1935. [13] *Zs. f. Phys.*, **111**, 373, 1938. [14] *Phys. Rev.*, **75**, 1561, 1949.

ing to various atomic numbers. Slater and Krutter carried through calculations for Z = 3, 11, and 29; Jensen for Z = 18, 36, and 54; Feynman, Metropolis, and Teller for Z = 6 and 92. The latter authors have summarized the data in a form which permits interpolation for additional Z-values.

The pressure-density relationships derived are valid only at pressures which are sufficiently high to obliterate the influence of the outer shell-structure of the atoms. For pressures intermediate between the upper limit of direct measurement (about 10^5 bars) and the region where the computations are reliable (in general, $P > 10^7$ bars) interpolation must be used. In general, this can be done by connecting the experimental curve with the theoretical curve by as smooth a curve as possible.

Jensen[13] found by an analysis of Bridgeman's data that the slope of the experimental pressure-density-curve for iron curves upward near the upper experimental limit, as required by theory. He further found that a smooth interpolation between the experimental and the theoretical curves is possible which runs through the pressure-density-curve for the core of the earth as determined by Bullen.[15]

For the purpose of determining the effects of pressure upon the densities of the terrestrial planets, we need concern ourselves with only two elements, iron and oxygen, the former because it represents approximately 30 per cent of the mass of the earth, the latter because it represents (owing to its large ionic radius) over 90 per cent of the volume of the mantle. Iron and oxygen together account for well over 90 per cent of the volume of the earth.

Figure 2 shows the pressure-density relationships for oxygen and iron (including the interpolations that will be assumed in this paper), together with the density of the silicate phase as determined from the oxygen compression and assuming a zero-pressure density of 3.2.

In case of the earth, we have the following criteria:

1. On the basis of seismic data, we assume a two-shell structure, with the shell boundary at about 0.55 the earth's radius. The core is assumed to consist of iron-nickel of zero-pressure density 7.8. The mantle is assumed to consist of silicates of zero-pressure density 3.2.

2. $4\pi \int_0^R \rho r^2 dr$ must equal the mass of the earth, where ρ is the density and r is the radius.

3. The acceleration of gravity at point b is

$$g_b = \frac{4\pi}{b^2} \int_0^b \rho r^2 d r .$$

4. The pressure at point b is

$$p_b = \int_b^R g \rho d r .$$

5. The density at point b must equal the density corresponding to p_b in Figure 2.

One can determine the solution which fits the criteria by successive approximations, utilizing graphical integration. When this is done, one finds a core-to-mantle weight ratio of 0.50 and a density-pressure distribution substantially in agreement with that determined by Bullen.[15] The uncompressed density of the earth on this basis is 4.0 gm/cc.

This density is very close to that of Mars. Remembering that the central pressure of Mars probably does not greatly exceed 2.6×10^6 atm., inspection of Figure 2 indicates that compression in this planet should be small. Thus, *to a first approximation, we may consider the elemental compositions of the earth and Mars to be nearly identical.*

The two-shell model with compression gives a mass distribution for the earth which

[15] *M.N., Geophys. Suppl.*, **3**, 395, 1936; and *Trans. Soc. New Zealand*, **67**, 122, 1937.

fits the observed value of the ratio of the oblateness, ϵ, to the centrifugal force-gravity ratio at the planet's equator. For a planet of homogeneous density, we have

$$\frac{\epsilon}{\phi} = 1.25.$$

For a planet with the mass concentrated at the center:

$$\frac{\epsilon}{\phi} = 0.50.$$

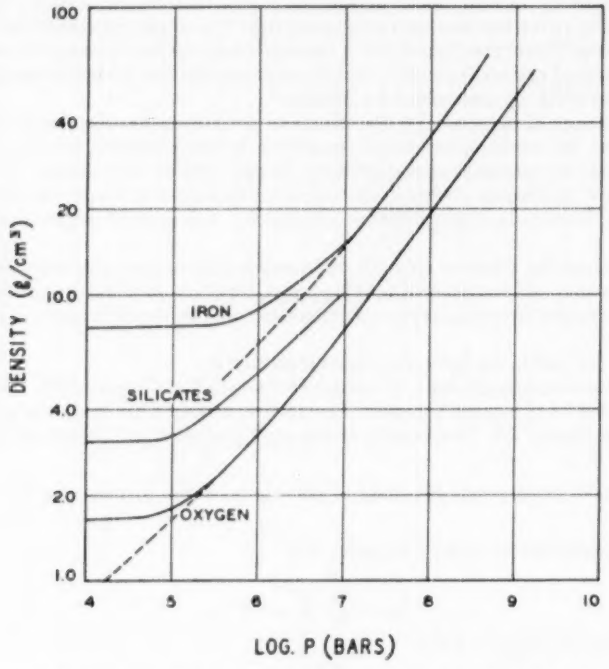

FIG. 2.—Estimated densities of iron, oxygen, and silicates as functions of pressure

For the earth and Mars we have

$$\left(\frac{\epsilon}{\phi}\right)_{\text{Earth}} = 0.97; \qquad \left(\frac{\epsilon}{\phi}\right)_{\text{Mars}} = 1.14.$$

If we assume (as our gross densities indicate) a two-shell structure for Mars similar to that of the earth, we calculate

$$\frac{\epsilon}{\phi} = 1.01,$$

which is higher than that of the earth because of the lower internal compression, yet considerably lower than the measured value. One would conclude that one or the other of two effects has operated to produce in Mars a more uniform density distribution than is

given by a two-shell model: (*a*) the metal phase and the silicate phase are perhaps not so completely separated as in the case of the earth; or (*b*) in the region of Mars the conditions might have been such as to shift the equilibrium

$$H_2 + F\,\epsilon SiO_3 \rightleftharpoons H_2O + SiO_2 + F\,\epsilon$$

more to the left relative to the equilibrium in the region of the earth. This would result in a lower metal-to-silicate ratio and consequent greater homogeneity. From the point of view of elemental composition, a shifting of the equilibrium to the left would result in a somewhat higher oxygen concentration in the planet, but the abundance ratios of the metals would remain the same.

For planets composed entirely of "earth-forming materials," i.e., metals and silicates in the proportions observed, one would expect the density increase with mass to become rapid above the mass where central pressures are greater than 10^6 bars. Indeed, we find that Venus, with a mass of 0.82 that of the earth, possesses a density of 4.9. One calculates, on the basis of the two-shell model, a density of 5.0, in reasonable agreement with observation. Unfortunately, the value of ϵ/ϕ for Venus is unknown.

The mass of Mercury is not known accurately, and as a result the quoted density of 4.1 is unreliable. One might predict on the above basis that the most probable value for the density of Mercury is 4.0. Depending upon the location of the iron silicate–metal equilibrium, the minimum density of Mercury should be 3.7 and the maximum density 4.1.

The moon, with the very low density of 3.34, does not even remotely fit into the above scheme. Clearly, the gross composition of the moon must differ widely from the gross composition of the minor planets and probably closely resembles the composition of metal-free silicate of low combined iron content.

Recently, Kuhn and Rittman[8] postulated that the earth's core is composed of hydrogen under very high pressures rather than of metallic iron-nickel. Their proposal was made because of the difficulty of finding a plausible explanation for the differentiation between metal and silicate which must have occurred. They argue that extensive original gravitational separation in the gaseous state must be disregarded and that conditions existing in the earth's interior during the early stages of its history would not permit liquid separation. Only limited diffusion and sinking velocities are permitted, which, they calculate, are too small to have brought about the observed segregation.

The problem as to how segregation took place is indeed a major one. But the difficulties brought about by the Kuhn and Rittman alternate hypothesis are of an even greater order of magnitude, as has been pointed out by Haalck,[16] Von Wolff,[17] Eucken,[18] and Kleber.[19] Aside from the major difficulty of understanding how solar material was effectively trapped in the center of the earth, it becomes most difficult to explain the mass-density relationship between the minor planets without making assumptions concerning the compressibility of matter which would appear to be beyond the realm of probability. In particular, the agreement between the composition of meteoritic matter and the composition of the solar atmosphere when the composition of the earth is assumed to be as described above (thus fixing the ratio of metal to silicate) makes it appear that the assumption of a hydrogen core creates far more difficulties than it remedies. Greater precision in the determination of the iron-silicon ratio in the sun would aid appreciably in finally settling the matter.

[16] *Zs. f. Geophys.*, **18**, 32, 1943.

[17] *Nova Acta Leopoldina*, **12**, No. 87, 383, 1943.

[18] *Naturwiss.*, **31**, 112, 1944.

[19] *Neues Jahrb. f. Min., Geol. u. Pal.*, Abt. A, Heft 5, p. 88, 1945–1948.

IV. URANUS AND NEPTUNE

If we are to explain the densities of planets which are considerably more massive than the earth, we must necessarily assume that substances lighter than earth-forming materials are present in considerable abundance. Consequently, before proceeding with a study of models, we must obtain some idea of the densities of these lighter substances at elevated pressures.

The temperatures of the major planets are above the critical temperatures of both hydrogen and helium and below the critical temperatures of methane, ammonia, and water. Therefore, we shall consider the densities of the former substances in the gaseous state, and the latter substances in the liquid or solid states. For the cases of hydrogen and helium we shall assume van der Waals behavior up to pressures of the order of 10^4 atm.

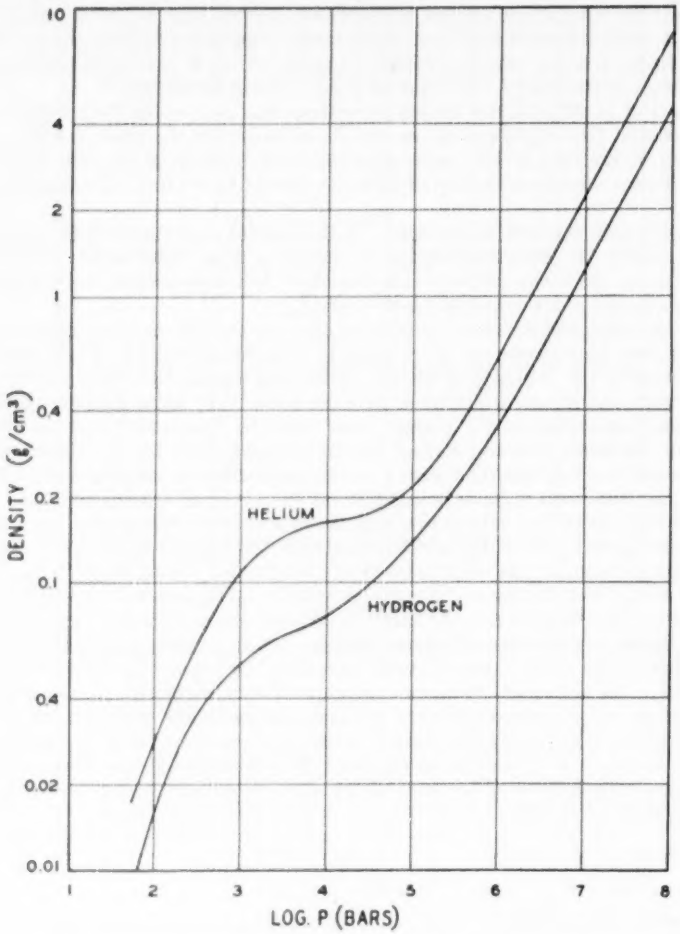

FIG. 3.—Estimated densities of hydrogen and helium as functions of pressure

and degenerate behavior above pressures of the order of 10^6 atm. For the pressure range of 10^5–10^6 atm., we shall assume behavior according to the very rough estimates of Kothari.[20] For a description of the behavior in the intermediate region, interpolation is employed. The results, calculated for a temperature of 140° K (approximately the surface temperature of Jupiter) are shown in Figure 3.

It is to be emphasized that the densities in the region of 10^5–10^6 bars may well be underestimates. For example, Wigner and Huntington[21] have estimated that metallic hydrogen of density 0.6 gm/cm³ might possibly be formed at pressures as low as 250,000

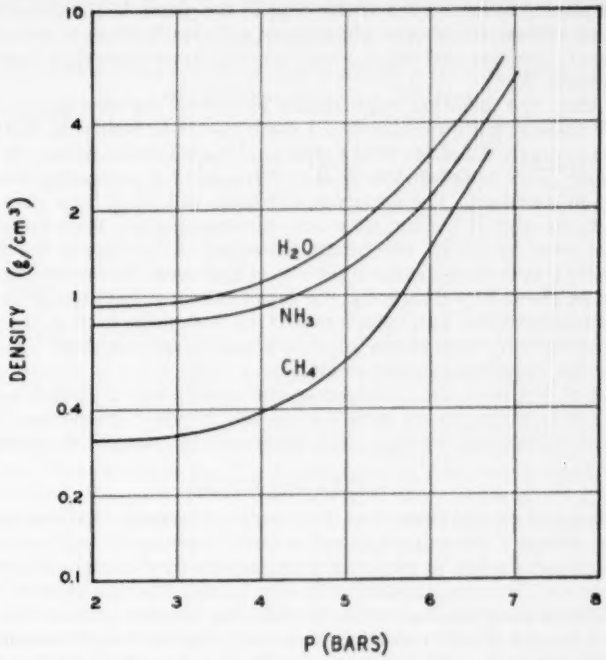

FIG. 4.—Estimated densities of methane, ammonia, and water as functions of pressure

bars. This seems unlikely, but it must be emphasized that the Kothari estimates are, if anything, too low.

The density functions for methane, ammonia, and water have been roughly estimated by combining the observed zero-pressure densities of those substances (liquid or solid), the density functions of carbon, nitrogen, and oxygen (as determined from the curves of Feynman, Metropolis, and Teller), and the density function of hydrogen as given above. Of course, at pressures where outer electron shells lose their identity, chemical compounds as such cease to have a meaning. In the completely degenerate state, for example, methane would consist of a gaseous mixture of ionized carbon, hydrogen, and electrons and would no longer resemble methane as the substance is commonly known. The estimated density functions for methane, ammonia, and water are shown in Figure 4. It

[20] *Proc. R. Soc. London, A*, **165**, 486, 1938; and *Proc. 31st I.S.C. Delhi*, pp. 12–31, 1944.

[21] *J. Chem. Phys.*, **3**, 764, 1935.

should be pointed out that the curve for water (solid) passes close to the observed density of 1.5 (ice VII) at a pressure of 40,000 bars, as determined experimentally by Bridgeman.[23]

From the density-curves it can be determined that a planet of the mass of Uranus or Neptune would possess a mean density of approximately 2.4, if it is composed only of substances belonging to Classes I and II in the ratios listed in Table 2. This density is slightly greater than the redetermined density of Neptune.[14] It is, however, considerably greater than the accepted density value of 1.26 for Uranus. In the case of Uranus, the addition of but a small quantity of hydrogen and helium is required (relative to the weight of the planet) to extend the visible edge of the planet to the observed diameter. For example, an extensive hydrogen atmosphere, sufficiently dense to extend the diameter of Neptune to the observed value, would amount to no more than 3 per cent of the mass of the planet.

We have, then, the following approximate picture of the structure of Uranus: An earthlike core possessing approximately 3.1 earth masses in which the metal of density 16–18 extends to nearly 0.2 of the total radius, and the silicate of density 9–10.5 extends to 0.3 the radius. This is surrounded by H_2O, NH_3, and CH_4 extending to slightly over 0.8 the radius of the planet. The density of this layer will range from about 0.32 at the surface to 7 at the edge of the earthlike core. Surrounding this is an extensive gaseous atmosphere of neon, hydrogen, and helium extending to the edge of the planet. If the atmosphere should be composed almost entirely of hydrogen, the pressure at the methane surface would be about 40,000 bars, and the density at the surface would be 0.1 gm/cm^3. The mass of the atmosphere would amount to 3 per cent of the mass of the planet. For a pure helium atmosphere, these values would be approximately doubled. The actual situation probably lies in between these two limits.

In the case of Neptune, the hydrogen-helium atmosphere is probably considerably less extensive, amounting to no more than a few hundred kilometers. The mass of Neptune's atmosphere must be very small relative to the mass of the planet.

V. SATURN AND JUPITER

It can be seen that planets larger than Neptune must possess considerable quantities of hydrogen and helium if their densities are to be in the range 0.7–1.4 gm/cm^3. We can consider Saturn and Jupiter to consist of cores possessing the same composition as the cores of Uranus and Neptune, together with added gases. If we consider helium to be the main constituent of the gaseous envelope surrounding Saturn's core, we have the following picture for the composition and structure of the planet: A core consisting of metal, silicates, water, ammonia, and methane contributes approximately 30 per cent of the mass of the planet and extends to a point which is approximately 0.4 the radius of the planet. This core, although of the same composition as Neptune, is considerably more dense ($\rho = 3.4$ gm/cm^3). The core is surrounded by a considerable weight of helium, representing about 70 per cent of the mass of the planet. The pressure at the methane surface amounts to somewhat over 4×10^6 bars, at which point the helium density is 1.6 gm/cm^3. The ratio ϵ/ϕ for Saturn, calculated on the basis of this model, is 0.7, which agrees fairly well with the observed ratio of 0.65.

The density of Jupiter can be reproduced only if we assume an even larger ratio of gases to core than is assumed in the case of Saturn. Indeed, we must assume that Jupiter consists of light gases to an extent of nearly 90 per cent by weight. A specific solution gives a Neptune-like core, approximately two and a half times the mass of Neptune and possessing a mean density of about 6 gm/cm^3. This core extends to about 0.3 the radius of the planet. The solution on the basis of the assumed helium and hydrogen compressibilities would give an atmosphere of helium extending to the boundary of the planet,

[23] *J. Chem. Phys.*, **5**, 964, 1937.

possessing a density at the base of 4.2 gm/cm³ and a pressure of 2.7×10^7 bars. The ratio ϵ/ϕ for Jupiter, calculated on the basis of this model, is 0.8, in satisfactory agreement with the observed value of 0.76.

It is to be noted that the solutions for Saturn and Jupiter permit of no preponderant quantities of hydrogen on either planet. If, as seems likely, our estimates of densities for these gases in the pressure range 10^6–10^7 bars are *underestimates*, then the solutions could permit "atmospheres" composed almost entirely of hydrogen. Aside from this feature of the solutions, the compositions outlined would remain essentially the same.

In Table 5 a summary is given of the results thus far discussed. The first and second

TABLE 5

THE COMPOSITIONS OF THE MAJOR PLANETS AND THEIR HELIUM FRACTIONATION FACTORS

Planet	Earth Cores (M/M_{Earth})	Uranus Cores (M/M_{Uranus})	Helium-Hydrogen (Per Cent by Weight)	Helium Fractionation Factor
Jupiter	9.1	2.8	87	1.7
Saturn	6.4	2.0	69	5.3
Uranus	3.2	1.0	6	180
Neptune	3.7	1.15	0.5	2300

columns, which compare the relative masses of the earthlike cores and the total solid-liquid cores of the major planets, indicate that these cores do not differ greatly one from the other in mass. To a first approximation, it appears that the major differences between the outer planets are due fundamentally to the differing quantities of helium-hydrogen present in each. If one assumes that the atmospheres of the major planets are composed primarily of helium, then one can calculate the "fractionation factor," i.e., the extent to which helium has been fractionated from the heavier elements during the process of planet formation. The helium fractionation factors are given in the fifth column. It can be seen that the fractionation factor is apparently strongly dependent upon the distance of the planet from the sun, as well as upon the size of the core.

It is to be emphasized that the solutions given for the major planets depend upon the following determined quantities or functions: (1) mass, (2) equations of state of substances involved, (3) relative abundances of Class I and Class II elements in the planet, and (4) mean density. Once these quantities are fixed, the proportions of the Class III elements present in the planet are uniquely determined, as is the oblateness function. Of the quantities used, the equations of state probably give rise to the largest errors in the final result. It seems clear that further progress in our knowledge of planet structure will depend upon further theoretical studies on the behavior of cold matter under extremely high pressures.

ON A RECENT PAPER ON RADIATIVE EQUILIBRIUM BY D. H. MENZEL AND H. K. SEN

IDA W. BUSBRIDGE
St. Hugh's College, Oxford, England
Received February 24, 1950

ABSTRACT

The mathematics of the paper by Menzel and Sen is examined and shown to be unsound, the results being correct only in form. It is shown that all the results are obtained correctly by means of the operational calculus.

1. *Introduction.*—In a recent paper,[1] D. H. Menzel and H. K. Sen have used a method depending on the operators D and D^{-1} to express Planck's function $B(\tau)$, at optical depth τ in a gray atmosphere, in the form

$$B(\tau) = a + b\tau + \int_0^1 \phi(y)\, e^{-\tau/y} dy\,. \tag{1.1}$$

In section 2 we shall examine the validity of their method, and we shall show that it is unsound mathematically. In fact, the function $\phi(y)$ obtained by Menzel and Sen does not exist for $0 \leqslant y \leqslant 1$. The form (1.1) is, however, correct, as has been shown by C. Mark[2] in his exact solution of Milne's problem. Because, in the second half of their paper, Menzel and Sen do not make any use of the explicit form of $\phi(y)$, all that part of their work is correct, though the method employed is somewhat artificial. In section 3 it will be shown that equivalent results are obtained simply and naturally from the operational form of Milne's first integral equation.

2. *Analysis of the method of Menzel and Sen.*—On writing

$$I^+ = I^+(\tau, \mu) = I(\tau, \mu) \qquad (0 \leqslant \mu \leqslant 1),$$

$$I^- = I^-(\tau, \mu) = I(\tau, \mu) \qquad (-1 \leqslant \mu \leqslant 0),$$

we have the well-known formulae

$$I^+ = e^{\tau/\mu} \int_\tau^\infty B(t)\, e^{-t/\mu} \frac{dt}{\mu} \tag{2.1}$$

and

$$I^- = -\, e^{\tau/\mu} \int_0^\tau B(t)\, e^{-t/\mu} \frac{dt}{\mu} \tag{2.2}$$

for the intensities of the outwardly and inwardly directed rays at the depth τ. Now Menzel and Sen write equation (2.1) in the form

$$I^+ = \frac{1}{1 - \mu D} B\,,$$

and we therefore have the operator equivalence

$$\frac{1}{1 - \mu D} \equiv e^{\tau/\mu} \int_\tau^\infty e^{-t/\mu} \ldots \frac{dt}{\mu}\,. \tag{2.3}$$

[1] *Ap. J.*, **110**, 1, 1949.

[2] *Phys. Rev.*, **72**, 558, 1947.

For functions which behave for large τ in the manner of $B(\tau)$, the integral involved in this operator will converge for $\mu > 0$ but not for $\mu < 0$. Hence, in writing (2.2) in the form

$$I^- = \frac{1}{1-\mu D} B - e^{\tau/\mu}\left[\frac{1}{1-\mu D} B\right]_{\tau=0},$$

the authors are expressing I^- as the difference of two nonconvergent integrals. This difficulty could be overcome if the two always remained together, but they are separated, and the nonexistent function

$$\left[\frac{1}{1-\mu D} B\right]_{\tau=0} \qquad (-1 \leqslant \mu \leqslant 0),$$

which the authors rewrite in the form

$$\left[\frac{1}{1+\mu D} B\right]_{\tau=0} \qquad (0 \leqslant \mu \leqslant 1)$$

plays an important part in their analysis. In fact, their function $\phi(y)$ in equation (1.1) is

$$\left\{\tfrac{1}{2} y \log \frac{1+y}{1-y} - 1\right\}^{-1}\left[\frac{1}{1+yD} B\right]_{\tau=0},$$

and this does not exist for $0 \leqslant y \leqslant 1$.

There is another point at which the analysis of Menzel and Sen breaks down. They make unquestioning use of the operational relation

$$F(D)\, e^{m\tau} = F(m)\, e^{m\tau} \tag{2.4}$$

and of its inverse,

$$\frac{1}{F(D)}\, e^{m\tau} = \frac{1}{F(m)}\, e^{m\tau}, \tag{2.5}$$

where

$$F(D) \equiv \frac{1}{2}\int_0^1 \left\{\frac{1}{1+\mu D} + \frac{1}{1-\mu D} - 2\right\} \ldots d\mu .$$

Now, by the equivalence (2.3),

$$F(D)\, e^{m\tau} = \frac{1}{2}\int_0^1 d\mu \left\{ e^{-\tau/\mu} \int_\tau^\infty e^{t[(1/\mu)+m]} \frac{dt}{-\mu} + e^{\tau/\mu} \int_\tau^\infty e^{t[m-(1/\mu)]} \frac{dt}{\mu} \right\} - e^{m\tau},$$

and the inner integrals both converge only if $m < -1/\mu$. Since this must be true for $0 < \mu < 1$, we can only have $m = -\infty$. Thus equation (2.4) is untrue and hence, also, equation (2.5).

3. *The solution by the operational calculus and some deductions from it.*—Let

$$b(s) = s\int_0^\infty B(t)\, e^{-st} dt \qquad [\Re(s) > 0]. \tag{3.1}$$

Then G. Placzek and W. Seidel[2] have shown that the operational form of Milne's first integral equation is

$$b(s)\, a(s) = \int_0^1 b(\mu^{-1}) \frac{\mu}{1-\mu s} d\mu \equiv g(s), \tag{3.2}$$

[2] *Phys. Rev.*, **72**, 550, 1947. This paper and the one by Mark (*loc. cit.*) concern the problem of neutron diffusion, and the notation therefore differs from that adopted above.

where

$$a(s) = \frac{1}{s^2}\left\{\log\frac{1+s}{1-s} - 2s\right\}, \tag{3.3}$$

and the logarithm is the principal branch of the function. Starting with equation (3.2) and using the inversion formula for the Laplace transform and the calculus of residues, Mark[4] has expressed $B(r)$ in the form (1.1) with

$$b = \tfrac{3}{4}F, \tag{3.4}$$

where F is the constant flux, and with

$$\phi(y) = -\frac{g(-1/y)}{4y\{(\frac{1}{2}y\log[1+y]/[1-y]-1)^2+\frac{1}{4}\pi^2y^2\}}, \tag{3.5}$$

$g(s)$ being given by equation (3.2).

Starting, now, with equation (1.1) and the correct function $\phi(y)$, we can substitute for $B(t)$ in equation (3.1), and we get

$$b(s) = a + bs^{-1} + \int_0^1 \phi(y)\frac{sy}{sy+1}\,dy, \tag{3.6}$$

a formula which holds, by analytic continuation, for $\Re(s) > -1$. Substituting from equation (3.6) in equation (3.2), we have

$$\left(\frac{1}{s}\log\frac{1+s}{1-s} - 2\right)\left\{\frac{a}{s} + \frac{b}{s^2} + \int_0^1 \phi(y)\frac{y}{sy+1}\,dy\right\}$$
$$- \int_0^1 \frac{\mu(a+b\mu)}{1-\mu s}\,d\mu - \int_0^1 \frac{\mu}{1-\mu s}\,d\mu \int_0^1 \phi(y)\frac{y}{y+\mu}\,dy = 0.$$

On inverting the order of integration in the repeated integral, this reduces to

$$\left(\frac{a}{s^2}+\frac{b}{s^3}\right)\log(1+s) - \frac{a}{s} - \frac{b}{s^2} + \frac{b}{2s} + \int_0^1 \frac{y^2\phi(y)}{sy+1}\log\left(1+\frac{1}{y}\right)dy$$
$$+ \left\{\frac{1}{s}\log(1+s) - 2\right\}\int_0^1 \phi(y)\frac{y}{sy+1}\,dy = 0, \tag{3.7}$$

a result which also holds for $\Re(s) > -1$. We can expand in the neighborhood of $s = 0$, and we get

$$(as+b)\sum_{\nu=-3}^{\infty}\frac{(-1)^{\nu-1}}{\nu}s^{\nu-3} + \left(-1 + \sum_{\nu=2}^{\infty}\frac{(-1)^{\nu-1}}{\nu}s^{\nu-1}\right)\sum_{\nu=0}^{\infty}(-1)^{\nu}s^{\nu}$$
$$\times \int_0^1 \phi(y)\,y^{\nu+1}dy + \sum_{\nu=0}^{\infty}(-1)^{\nu}s^{\nu}\int_0^1 \phi(y)\,y^{\nu+2}\log\left(1+\frac{1}{y}\right)dy - \tfrac{1}{2}a = 0.$$

On multiplying and equating to zero the powers of s, we obtain the equations

$$\int_0^1 \phi(y)\left\{y^2\log\left(1+\frac{1}{y}\right) - y\right\}dy = \tfrac{1}{2}a - \tfrac{1}{3}b, \tag{3.8}$$

$$\int_0^1 \phi(y)\left\{y^{n+1}\log\left(1+\frac{1}{y}\right) - y^n + \frac{y^{n-1}}{2} + \frac{y^{n-2}}{3} + \ldots + \frac{y}{n}\right\}dy = \frac{a}{n+1} - \frac{b}{n+2} \tag{3.9}$$

[4] *Loc. cit.* Equation (3.5) is only one of several forms for $\phi(y)$.

for $n = 2, 3, \ldots$. Finally, if we multiply equation (3.7) by s and let $s \to \infty$ along the positive real axis, we get

$$\int_0^1 \phi(y) \left\{ y \log\left(1+\frac{1}{y}\right) - 2 \right\} dy = a - \tfrac{1}{3} b . \tag{3.10}$$

Equations (3.8), (3.9), and (3.10), together with (3.4), are precisely equivalent to those from which Menzel and Sen obtain all their numerical results. Here they have arisen naturally out of equations (3.2) and (1.1).

The accuracy of the final part of the Menzel-Sen paper and, indeed, of any approximation to $B(\tau)$ of the form

$$B(\tau) = a + b\tau + a_2 K_2(\tau) + a_3 K_3(\tau) + \ldots \tag{3.11}$$

turns upon the possibility of expressing $\phi(y)$ in the form

$$\phi(y) = \sum_{r=2}^{\infty} a_r y^{r-2}, \tag{3.12}$$

since substitutions of this in equation (1.1) give equation (3.11). Now the denominator in equation (3.5) can be expanded in ascending powers of y, but the numerator is, by equation (3.2),

$$\int_0^1 b(y^{-1}) \frac{\mu}{y+\mu} \, d\mu , \tag{3.13}$$

and this cannot be expanded in a Taylor series near to $y = 0$ because the integrals

$$\int_0^1 \mu^{-n} b\left(\frac{1}{\mu}\right) d\mu \qquad (n = 1, 2, \ldots)$$

do not converge. Hence equation (3.12) cannot give an accurate representation of $\phi(y)$.

By substituting from equation (3.6) in equation (3.13), we get

$$a\left\{1 - y \log\left(1+\frac{1}{y}\right)\right\} + b\left\{\tfrac{1}{2} - y + y^2 \log\left(1+\frac{1}{y}\right)\right\} + \int_0^1 \int_0^1 \frac{x\mu\phi(x)}{(x+\mu)(\mu+y)} \, dx d\mu ;$$

and it is probable, therefore, that the addition of one or more terms of the form $y^k \log y$ ($k \geqslant 1$) to the right-hand side of equation (3.12) would give a better representation of $\phi(y)$. This would add to the right-hand side of equation (3.11) terms of the form $K_{k+2}^{(2)}(\tau)$, where

$$K_n^{(2)}(\tau) = \int_1^{\infty} \frac{e^{-\tau u}}{u^n} \log u \, du .$$

If we add to equation (3.12) the single term $-a_1 y \log y$, it is easily found that equation (3.11) would be replaced by

$$B(\tau) = a + b\tau + a_1 [\tau^2 K_1^{(2)}(\tau) - \tau K_2(\tau)] + a_2 K_2(\tau) + a_3 K_3(\tau) + \ldots ,$$

and the use of this is likely to give even more accurate results than the use of equation (3.11). The function $K_1^{(2)}(\tau)$ has been studied by H. C. van de Hulst.[5]

[5] *Ap. J.*, **107**, 220, appendix, 1948.

NOTES

BRIGHT LINES OF *Ca* II IN THE SPECTRUM OF RW COMAE BERENICES

RW Comae Berenices, with a period of only 0.237 day, is a typical W Ursae Majoris binary with two components of spectral type G2 each. Although the apparent magnitude of the system is 11.3 pg at maximum and 12.03 and 11.86 pg at the two minima, I observed the spectrum at the McDonald Observatory in January, 1950. With the dispersion used in this work, namely, 100 A/mm at λ 3933, the two components were not completely resolved during the elongations, but the lines are much broader than they are during the conjunctions. As is the case in other systems of the same type, the violet components of the double absorption lines seem to be the stronger, irrespective of whether they belong to the more massive or to the less massive star.

Of particular interest is the presence of a fairly strong emission line of *Ca* II, which is clearly visible in the center of a broad, blended absorption line, at each of the two conjunctions. Figure 1 illustrates this phenomenon. It is similar to the one recently found in the spectrum of W Ursae Majoris.[1] During the elongations, at phases near 0.25 and 0.75*P*, counted from the middle of the principal eclipse as zero, the emission lines are weak and difficult to discern. On some of my spectrograms they look complex in structure, and it is possible that both stars are accompanied by emitting *Ca* gases. In the case of W Ursae Majoris, the emission seemed to be associated with the more massive component of the system.

The presence of fairly strong emission lines of *Ca* II in normal G-type spectra is somewhat unusual. Their existence in two systems of the W Ursae Majoris type should probably be regarded as a symptom indicating the presence of a gaseous ring or tidal extension analogous to those inferred previously from the intensities of the absorption lines.

OTTO STRUVE

YERKES AND MCDONALD OBSERVATORIES
March 15, 1950

OCCASIONAL SPECTROGRAPHIC OBSERVATIONS OF ECLIPSING BINARIES*

This paper contains the results of radial-velocity measurements of occasional spectrograms obtained at the McDonald Observatory on the program of eclipsing binaries. Most of these stars were not sufficiently well observed to justify a complete orbit determination. Nevertheless, it was possible to obtain some information concerning the character of the spectra and the ranges of the velocity-curves. Table 1 contains the list of the stars. Table 2 gives the photometric elements which were used in determining the phases. Table 3 lists the radial velocities, and Table 4 gives the principal elements.

The eccentric binary DI Herculis was observed more completely by McKellar at Victoria.[1] The McDonald spectrograms agree closely with his results. We have made the values of K_1 and K_2 slightly larger than those derived by him. The eccentricity obtained

[1] *Pub. A.S.P.* (in press).

* *Contributions from the McDonald Observatory, University of Texas*, No. 189.

[1] *Pub. A.S.P.*, **61**, 159, 1949.

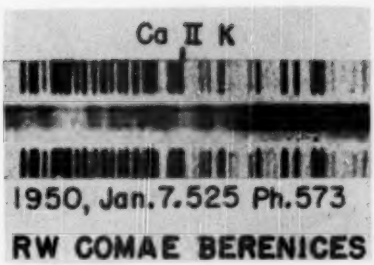

FIG. 1

TABLE 1

LIST OF STARS

No.	Star	Co-ordinates (1950.0)		Period (Days)	Mag.	Sp.	Remarks	No. of Spectrograms
		α	δ					
1	FO Ori	$5^h25^m32^s$	+ 3°35′.1	18.8	10	A3	One spectrum	7
2	DI Her	18 51 21	+24 12.9	10.6	8.5	A2	Two spectra	12
3	Y Cam	7 34 33	+76 11.6	3.31	11	A7 V	Metallic lines strong; one spectrum	4
4	FL Lyr	19 10 38	+46 14.2	2.18	9	G5	One spectrum	8
5	RZ Tau	4 33 43	+18 39.4	0.416	11	F0	W UMa type	7
6	UP eg	23 55 25	+15 40.5	0.375	10	F3	W UMa type	4
7	AB And	23 09 08	+36 37.3	0.332	10.5	G5	W UMa type	7
8	TW Cet	1 46 32	−21 08.2	0.317	10	G5	W UMa type	9

TABLE 2

PHOTOMETRIC ELEMENTS

No.	Star	Epoch JD	Period (Days)	Sources
1	FO Ori	2425503.540	18.80086	B. F. Whitney, *A.J.*, **53**, 13, 1947
2	DI Her	15182.732	10.550145	Jacchia, *Harvard Bull.*, No. 912, p. 18, February, 1940. Spectrographic orbit by A. McKellar in *Pub. A.S.P.*, **61**, 159, 1949
3	Y Cam	32288.317	3.30553	Kukarkin and Parenago, *Russian Catalogue of Variable Stars—Addendum*, 1949
4	FL Lyr	28034.327	2.17815081	E. J. Woodward, *Harvard Bull.*, No. 917, p. 7, December, 1943
5	RZ Tau	24031.9348	0.41567072	Oosterhoff, *B.A.N.*, **7**, 80, 1933
6	U Peg	30260.6790	0.37478214	J. B. Irwin, private communication
7	AB And	25497.48034	0.33188590	Oosterhoff, *B.A.N.*, **5**, 151, 1930
8	TW Cet	30656.504	0.316852	Zessewitsch, *Astr. Circ.* (Kasan), No. 29, p. 1, 1944

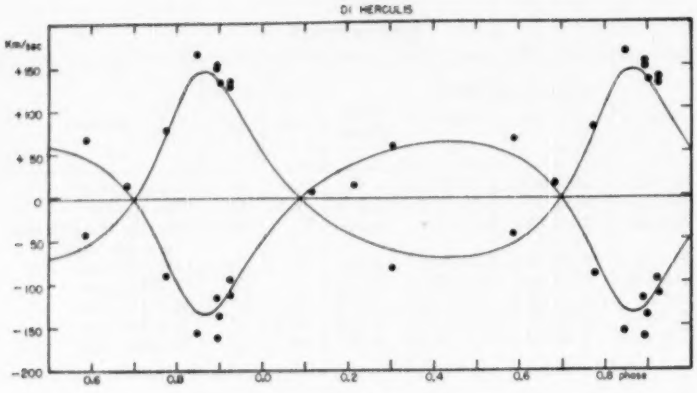
DI HERCULIS
Km/sec
+150
+100
+50
0
-50
-100
-150
-200
0.6
0.8
0.0
0.2
0.4
0.6
0.8 phase

FIG. 1

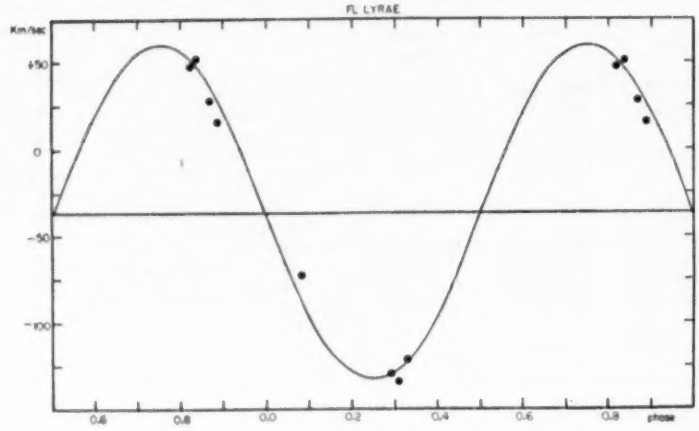
FL LYRAE
Km/sec
+50
0
-50
-100
0.6
0.8
0.0
0.2
0.4
0.6
0.8
phase

FIG. 2

TABLE 3

THE RADIAL VELOCITIES

No.	Star	Plate	Date (U.T.)	Phase		Radial Velocity (Km/Sec)	
				Days	Period	Comp. I	Comp. II
			1948				
1	FO Ori	Gf/2 11505	Dec. 7.360	0.582	0.031	+ 39	.....
		11527	12.415	5.637	.300	+ 28	.....
			1949				
		11567	Jan. 2.163	7.584	.403	0	.....
			1948				
		11532	Dec. 15.216	8.438	.449	− 13	.....
			1949				
		11581	Jan. 5.317	10.738	.571	+ 3	.....
			1948				
		11447	Nov. 30.411	12.434	.661	+ 1	.....
		11546	Dec. 21.335	14.557	.774	+ 20	.....
2	DI Her	CQ 7638	July 11.159	1.230	.117	.....	+ 5
		7641	12.152	2.223	.211	.....	+ 12
		7644	13.147	3.219	.305	− 83	+ 56
		7648	16.122	6.194	.587	− 44	+ 67
		7655	17.119	7.191	.682	.....	+ 14
		7661	18.120	8.192	.776	+ 78	− 92
		Gf/2 8227	Aug. 18.299	8.935	.847	+165	−157
		CQ 7679	July 19.353	9.425	.893	+153	−116
		7680	19.375	9.447	.895	+148	−161
		Gf/2 8145	Aug. 8.310	9.496	.900	+131	−136
		CQ 7697	July 30.215	9.737	.923	+134	− 98
		7698	30.241	9.763	.925	+127	−114
			1949				
3	Y Cam	Gf/2 11573	Jan. 3.417	0.244	.074	− 38	.....
			1948				
		11547	Dec. 21.455	0.504	.152	− 29	.....
		11519	9.418	1.689	.511	+ 13	.....
		11559	29.517	1.955	.591	+ 21	.....
4	FL Lyr	CQ 7654	July 16.450	0.177	.081	− 72	.....
		7729	Aug. 1.151	0.631	.290	−130	.....
		7730	1.193	0.673	.309	−133	.....
		7731	1.235	0.715	.328	−121	.....
		7710	July 31.123	1.781	.818	+ 48	.....
		7711	31.166	1.824	.837	+ 52	.....
		7715	31.232	1.890	.868	+ 28	.....
		7716	31.276	1.934	.888	+ 16	.....
5	RZ Tau	Gf/2 11364	Nov. 18.294	0.127	.306	−174	.....
		11506	Dec. 8.124	0.005	.012	.....	− 49
		11507	8.171	0.052	.125	+114	−128
		11508	8.214	0.095	.229	+ 77	.....
		11509	8.265	0.146	.351	+ 83	−192
		11511	8.360	0.241	.580	−178	+190
		11512	8.403	0.284	.683	− 59	+252
			1948				
6	U Peg	11523	Dec. 12.157	0.011	.029	.....	− 12
		11375	Nov. 19.111	0.201	.536	− 45	.....
		11376	19.152	0.242	.646	−113	+176
		11539	Dec. 19.188	0.296	.790	−159	+207
7	AB And	11450	1.085	0.329	.991	+ 2	.....
		11451	1.115	0.027	.081	− 39	.....
		11452	1.148	0.060	.180	.....	−290
		11453	1.181	0.093	.280	+ 79	−310
		11454	1.219	0.131	.395	+ 88	−232
		11455	1.260	0.172	.518	−134	+ 83
		11456	1.301	0.213	0.642	−148	+172

TABLE 3—*Continued*

No.	Star	Plate	Date (U.T.)	Phase		Radial Velocity (Km/Sec)	
				Days	Period	Comp. I	Comp. II
			1949				
8	TW Cet	*Gf*/2 12035	Nov. 19.303	0.005	0.016	− 24	.....
		12036	19.327	.029	.092	− 38	.....
		12027	19.097	.115	.363	− 69	.....
		12028	19.127	.145	.458	− 10	.....
		12029	19.160	.178	.562	+ 73	−123
		12031	19.207	.225	.710	+ 94	−230
		12032	19.232	.250	.789	+152	−230
		12033	19.256	.274	.865	+125	−123
		12034	19.280	0.298	0.941	+ 46	−114

TABLE 4

Orbital Elements

No.	Star	γ (Km/Sec)	K_1 (Km/Sec)	K_2 (Km/Sec)	$f(m)$ ($\odot = 1$)	m_1/m_2	$a_1 \sin i$ (Km)	$a_2 \sin i$ (Km)
1	FO Ori	+17	22	.....	0.021	.....	5.7×10^6	.....
2	DI Her*	− 2	116	108	1.4	0.93	16×10^6	15×10^6
3	Y Cam	0	35	.....	0.015	.....	1.6×10^6	.....
4	FL Lyr	−38	98	.....	0.21	.....	2.9×10^6	.....
5	RZ Tau	+ 5	135	250	0.11	1.85	0.77×10^6	1.4×10^6
6	U Peg	0	165	205	0.17	1.24	0.85×10^6	1.1×10^6
7	AB And	−45	165	265	0.15	1.61	0.75×10^6	1.2×10^6
8	TW Cet	+20	135	255	0.081	1.89	0.59×10^6	1.1×10^6

* $e = 0.37$.

by McKellar, namely, 0.37, and the longitudes of periastron, 344° and 164°, satisfy our observations, as does also the velocity of the center of mass, −2 km/sec.

Four of the stars are members of the W Ursae Majoris class. In AB Andromedae, RZ Tauri, and U Pegasi the more massive component is in front during the principal eclipse. In TW Ceti the opposite is true. Concerning this star little is known. The light-curve by Zessewitsch shows only one minimum. Hence we should perhaps not regard this system as a normal W Ursae Majoris star; the two components are approximately of the same intensity in our spectra. The average value of the mass ratio of these four systems is 1.65; this is not so extreme as the value of 2.0 found previously; but it is probable that additional material would tend to increase the mass ratios.

O. Struve
H. G. Horak
R. Canavaggia
V. Kourganoff
A. Colacevich

Yerkes and McDonald Observatories
February 25, 1950

A CHANGE IN THE SPECTRUM OF LAMBDA PAVONIS

In 1948, in the course of the color-gradient program of the Commonwealth Observatory,[1] the spectrum of the star λ Pavonis[2] was found to display strong emission lines. A note by S. C. B. Gascoigne[3] on July 28, 1948, states: ". . . There is no trace of absorption at $H\beta$, but at $H\gamma$ there is a definite emissive core superimposed more or less symmetrically on a broader absorption line." Previous references to λ Pavonis describe it as an early B star with wide (HD) or poor (Moore's *Catalogue of Radial Velocities*) lines, while Rimmer[4] classified it as B2s, its radial velocity (Lick) being $+20.4 \pm 1.9$ km/sec.[5]

A few slit spectrograms have been secured lately with the Wood-grating spectrograph attached to the Bosque Alegre reflector, giving a dispersion of about 42 A/mm. The spectral type, on the Yerkes system, is B2 III, in agreement with Gascoigne's estimation on plates taken by Rimmer in 1928.[2] The absorption lines are extremely weak, and those of *H* are the broadest ones. On our plates, $H\beta$ and $H\gamma$[6] show relatively sharp double emission of practically equal intensity, superposed upon a broad absorption line of a width of the order of 5 A at $H\gamma$. The higher members of the Balmer series appear only in absorption and show a complex structure which must arise from the fact that the absorption lines are affected by emission features not reaching the level of the neighboring continuous spectrum. The results obtained from the measurement of the Bosque Alegre material are given in Table 1. Spectrographic observations of the star will be continued.

TABLE 1

RADIAL VELOCITIES OF λ PAVONIS

Plate	Date	U.T.	Emulsion (Eastman)	Exposure Time (Minutes)	Radial Velocity (Km/Sec) from				Number of Measures
					He I*	*Mg* II	*H* Emission		
I 769.....	1949 Nov. 12	0:04	103*a*-F	15	+16	.....	−60	+107	3
801.....	Dec. 2	0:13	IIa-O	16	+15	− 5	−62	+ 88	2
808.....	Dec. 8	0:25	103*a*-F	20	+18	.....	−56	+ 72	2
1084.....	1950 Feb. 4	8:45	IIa-O	14	+12	−20	−74	+ 88	2

* The mean errors for each plate are ±7.0, ±7.8, ±4.6, and ±1.5, respectively.

I am greatly indebted to Dr. Jorge Landi Dessy for the two December, 1949, spectrograms, and to Mr. Julio Albarracín for assistance in the reduction of the plate measurements.

JORGE SAHADE

OBSERVATORIO ASTRONÓMICO
CÓRDOBA, ARGENTINA
March 2, 1950

[1] *M.N.*, **109**, 173, 1949.

[2] $\alpha = 18^h47^m6$; $\delta = -62°15'$ (1950.0). BS 7074 (4.42 mag.) = HD 173948 (Sp. B2) = MWC 963.

[3] *Observatory*, **69**, 30, 1949. The note is based on slitless spectrograms; dispersion 40 A/mm at $H\gamma$.

[4] *Mem. Commonwealth Solar Obs.*, No. 2, p. 36, 1930.

[5] *Pub. Lick Obs.*, **18**, 150, 1932. The quoted value is a mean of four plates.

[6] $H\alpha$ in emission is overexposed on our 103*a*-F spectrograms.

THE SPECTRUM OF COMET 1948l

The bright comet of 1948 (Comet 19481) was spectrographically observed at the Córdoba Observatory during the time that it was possible to do so with the available equipment and photographic supply, and this note reports on the spectral features shown by the obtained plates. Table 1 gives the details of the spectrographic material secured.

TABLE 1

THE SPECTROGRAPHIC MATERIAL

Plate	Date 1948 (November)	U.T.	Heliocentric Distance* r (A.U.)	Equivalent Slit Width (A)	Emulsion	Exp. Time (Min.)	Remarks
I 339	10	8:02	0.533	0.9	103*a*-O	55	1†
I 340	13	8:05	.618	1.1	103*a*-F	40	1
I 354	18	7:06	.748	1.5	103*a*-F	114	1
I 361	23	6:36	.871	1.5	103*a*-F	199	1
Pp 249	11	7:39	.561	.....	103*a*-O	24	2‡
Pp 250	12	7:44	.590	.....	103*a*-O	46	2
Pp 251	13	7:42	0.617	.....	103*a*-O	37	2

* I am indebted to Mr. Jorge Bobone for the data in this column. They were computed from his parabolic elements published on *Harvard Announcement Card*, No. 983.

† 1 = Slit spectrum of the comet's head.

‡ 2 = Objective-prism spectrum.

The slit spectrograms were taken with the Wood-grating spectrograph attached to the 154-cm reflecting telescope at the Bosque Alegre Astrophysical Station, which gives a dispersion of about 42 A/mm. The rest of the material was obtained at Córdoba with the 12.5-cm Sägmüller-Brashear camera and a 23° glass objective prism; its dispersion averages about 177 A/mm in the wave-length interval λλ 3800–4860.

Our slit spectrograms show a relatively strong reflected solar spectrum and some emission features, the most prominent of which being by far the *CN* band ($\Delta v = 0$) at about λ 3880. Table 2 lists the average measured wave lengths on the four plates and the estimated intensities on an arbitrary scale.

On the objective-prism plates the tail extends some 8° and shows the condensations due to CO^+ at about λλ 4010, 4260, 4540, and 4695 A. Figure 1 presents the distribution of intensities in the *CN* ($\Delta v = 0$) band on Plate I 339.

It is a pleasure to record my indebtedness to Dr. Ricardo Platzeck for turning over to me the spectrograms I 339 and 340 secured by him at Bosque Alegre and for making the microphotometer tracing shown in Figure 1 with the Zeiss microphotometer of the Physics Institute at La Plata. I am also indebted to Mr. Julio Albarracín for the reduction of the slit spectrograms and to Mr. Damián Canals Frau for assisting in the taking of the first two objective-prism plates.

JORGE SAHADE

OBSERVATORIO ASTRONÓMICO
CÓRDOBA, ARGENTINA
December 31, 1949

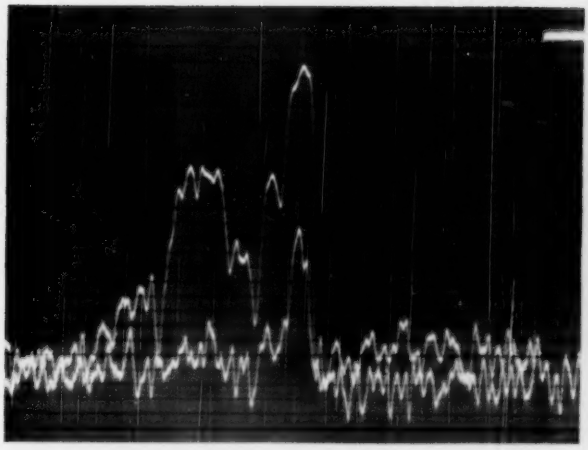

FIG. 1.—The distribution of intensities in the $C\mathcal{N}$ ($\Delta v = 0$) band of the spectrum of Comet 1948l on November 10.3347, 1948 (U.T.). On top there is the indication for total darkness and at the bottom for clear plate. The latter is distorted by the cometary emission features which extend beyond the region of the comparison spectra.

TABLE 2

THE SPECTRUM OF COMET 1948I

AVERAGE MEASURED WAVE LENGTH	ESTIMATED INTENSITIES*				IDENTIFICATIONS
	I 339	I 340	I 354	I 361	
3852.4	0	.....	.....	.....	
3855.6	1	0	.....	.....	
3858.2	1	1	.....	.....	
3859.6	1	.....	.....	.....	
3863.1	4	3	3	2	
3865.2	4	2+	1	1	
3867.4	4	3	1	4	CN ($\Delta v=0$)
3869.5	4	3	4	4	
3872.4	2	2	2	3	
3873.8	2	2	2	2	
3877.6	4	3	4	4‡	
3880.2	6	6	8	8	
3882.2	8	8	6	5	
4039.6	.....	.....	1−	1	
4043.8	.....	.....	1−	1	
4052.2	.....	0	1	2	
4061.4	.....	.....	1−	.....	CH_3†
4066.2	.....	.....	1−	.....	
4070.1	0	.....	0	0	
4074.0	0	.....	1−	1	
4214.9	3	.....	.....	.....	
4313.2	0+	.....	0	0+	
4677.5	3	.....	.....	.....	CN ($\Delta v=-1$)
4684.0	3	.....	1	.....	CH ($\Delta v=0$)
4689.7	0	.....	.....	.....	C_2 ($\Delta v=1$) except for the features at λλ 4690, 4706, and 4726, which are unidentified
4696.7	4	.....	2	0	
4705.9	0	.....	.....	.....	
4714.5	5	2	2	0	
4725.6	0	.....	.....	.....	
4736.6	5	2	2	1	
5165.0	.....	3	2+	1	C_2 ($\Delta v=0$)
5889.9	.....	3	.....	.....	Na (D_2)
5896.9	.....	1−	.....	.....	Na (D_1)

*"0" indicates a doubtful or an extremely faint line.

† This tentative identification by Herzberg (*Ap. J.*, **96**, 314, 1942) has been questioned by Monfils and Rosen (*Nature*, **164**, 713, 1949).

‡ Two lines?

ERRATA

Dr. D. M. Popper has called my attention to an error in the mass-functions of SW Lacertae (*Ap. J.*, **109**, 437, 1949, and *Proc. Nat. Acad. Sci.*, **35**, 161, 1949). The correct values are $0.95\odot$ and $0.81\odot$.

OTTO STRUVE

There are two errors in the atlas of white dwarfs (*Ap. J.*, **109**, 528, 1949); the field for h Per 1166 is upside down; also, *for* L 270-37 *read* L 270-137.

EDITOR

In *Ap. J.*, **110**, 405, 1949, the note on MWC 600, AR Pavonis, is in error. As I now understand it, Dr. E. Gaviola and Dr. Jorge Sahade agree that no M-type features have been observed in this spectrum. For a detailed description see Jorge Sahade, "The Spectrum of AR Pavonis," *Ap. J.*, **109**, 541, 1949.

PAUL W. MERRILL

In *Ap. J.*, **111**, 421, 1950, Table 2, *for* Pg_p of δ Ursae Majoris *read* 3.28 *instead of* 2.28. In Figure 4 (p. 422), and Figure 5 (p. 424), δ Ursae Majoris should be plotted on the bright blue-dwarf sequence at $M_{Pg_p} = +1.64$ and $+1.72$, respectively.

OLIN J. EGGEN